Four-Fermion Working Group Report

Martin Grünewald and Giampiero Passarino

E. Accomando , A. Ballestrero , P. Bambade , D. Bardin , W. Beenakker , F. Berends , E. Boos , A. Chapovsky , A. Denner , S. Dittmaier , M. Dubinin , J. B. Hansen, V. Ilyin , S. Jadach , Y. Kurihara , M. Kuroda , E. Maina , G. Montagna , M. Moretti , O. Nicrosini , M. Osmo , A. Pallavicini , C. Papadopoulos , H. Phillips , F. Piccinini , R. Pittau , W. Placzek , M. Roth , Y. Shimizu, M. Skrzypek , R. Tanaka , M. Verzocchi , D. Wackerot , B. F. L. Ward , Z. Wąs,

DRAFT

Contents

1. Introduction

This report is the result of an informal workshop that took place at CERN during the year 1999 with the goal of reviewing the progress made in Monte Carlo generators (hereafter MC) since the LEP 2 Yellow report. The main reason of this report was the need of having official statements before deciding on LEP 2 activities for year 2000.

At the beginning of the workshop the following goals were identified for the *Four-Fermion* sub-group:

a) Describe the new calculations, the improvements and the upgrading in the theoretical understanding and in the MC implementations.

b) Indicate where new contributions have changed previous predictions in the MC adopted by the collaborations. Why, how, how much.

c) In those cases where a substantial discrepancy has been registered and the physical origin has been understood, our goal should be to make recommendations on what to use.

d) In those cases where we have found incompleteness of the existing MC, but no complete improvement is available, we should be able to indicate a possible time scale for the solution and a sound estimate of the theoretical uncertainty.

The guideline determining our strategy was to take into proper account physical issues. Therefore, the experimental Collaborations have been asked to collect a list, process by process, with the level of the requested theoretical accuracy and with statements on the impact of new theoretical input.

A comment is needed here since, clearly, experiments look at and measure a lot of different processes, so that, for theoretical predictions, we have to manage with lots of different sets of cuts. At the beginning of our activities the four experiments have presented a list of recommendations that reflect different styles and different approaches. A related aspect is that the complete lists of observables considered by the LEP experiments vary greatly, ranging from a list with observables defined by simple phase-space cuts on four-fermion (+photon) level to full event-selection procedures. Nevertheless, during the workshop, an attempt has been made to come up, as much as possible, with some set of quasi-realistic cuts for each process. Therefore, we have collected processes and/or phase space regions where better theoretical predictions would be desirable. A weight has been given to the problems, according to their relevance/urgency.

Furthermore, the focus of activity in our sub-group has been on improving, when possible, the theoretical predictions for the relevant processes and/or phase space regions. All contributors have been asked to give, at least, a definite value for the theoretical uncertainty.

As a consequence of our strategy, we can now make a special consideration: the final output of the whole operation does not look as a mere collection of comparison tables but as a coherent attempt in assessing the theoretical uncertainty to be associated to any specific process.

The realm of theoretical uncertainty is often ill defined and, in order to reach a general consensus on it, one cannot be satisfied with some vague statement on overall agreement among different generators. Whenever differences are found, one has to make sure that they are due to physics, and not to some different input. So our project had to foresee a preliminar phase with a first technical benchmark. Once trivial bugs are found one can start digging into inevitable differences arising form different implementations of common theoretical wisdom.

In a vast majority of cases the main problem is represented by the inclusion of QED radiation. Therefore, one of the main goals of the workshop was: could we improve upon our treatment of QED radiation or give some safe estimate of the theoretical uncertainty associated with it?

For the sake of illustration we will consider some sort of basic reference table of four-fermion processes. It is an idealized common ground where, in principle, all theoretical predictions should be able to compare. More advanced setups could be accessible only to a limited number of generators, built for that specific purpose.

Perhaps, it will be useful to recall that the ultimate, perfect generator does not exist and, most likely, will never exist. Roughly speaking, generators belong to two, quite general, classes. Real generators, fully interfaced with hadronization and parton shower packages. Usually, they miss the fine points of the theoretical knowledge but represent an essential ingredient in dealing with the background and with the evaluation of the efficiency. They create the necessary bridge between raw data and subtracted (deconvoluted) data, e.g. those that are used to produce LEP averages.

At the other end of this cosmos we have those generators that are not really meant to generate events, although doable, but they rather show their power in dealing with the signal, furnishing the implementation of (almost) everything available in the literature.

On one thing all the participants in this workshop have found an immediate agreement: at this late stage in the life of LEP we do not need to experiment a new massive generation, we only need to know more about theoretical uncertainty, process by process and to make clear which generator can achieve that level of accuracy, under which configuration.

To proceed towards the final goal we shortly discuss our basic reference table. One should read it as summarizing our original manifesto and, after the following sections, it will be instructive to come back to it with critical eyes: not all the items below have found a satisfactory answer at the end of the workshop. This was, somehow, foreseeable but if you think carefully you will easily discover some important message also for those issues that remain unsolved. They cannot be solved in any reasonable time scale and the associated effect is a real source of uncertainty.

For all processes, radiative corrections and radiative photons in the final state should be considered, discussing energy and polar-angle spectra. Typical minimal requirements on photons are: energy $E_\gamma > 1$ GeV; polar angle $|\cos\theta_\gamma| < 0.985, 0.997, 0.9995$ depending on channel (see below); and minimal angle between photon and any charged final-state fermion $\xi > 5°$.

The following list contains a precision tag in $\%$. The accuracy of MC simulations should be better than the requested precision tag, i.e. the physics(!) uncertainty should be smaller and at worst the one indicated How much better is always left to the contributors; clearly, for benchmarking it is certainly advisable to use the maximum available precision.

- $WW - ZZ$ type signal:

1. $e^+e^- \to WW \to$ all (CC03). The full phase space is needed and the inclusive cross-section accuracy is 0.2%. The spectrum for the photon energy and the polar angle is needed ($|\cos\theta_\gamma| < 0.985\ (0.997)$).
2. $e^+e^- \to ZZ \to$ all (NC02). The full phase space is needed and the inclusive cross-section accuracy is 1%. The spectrum for the photon energy and the polar angle is needed ($|\cos\theta_\gamma| < 0.985\ (0.997)$).
3. $e^+e^- \to l\nu l\nu(\gamma)$ where all $\{e/\mu/\tau\} \otimes \{e/\mu/\tau\}$ combinations are requested with the following conditions: ($|\cos\theta_{l_1/l_2}| < 0.985$, $E_{l_1/l_2} > 5$ GeV, $M(l^+l^-) > 10\ (45)$ GeV (full and high-mass region). The inclusive cross-section accuracy is 4% for individual combination; the inclusive cross-section accuracy is 1% for the summed one; photon energy and polar angle spectrum ($|\cos\theta_\gamma| < 0.985\ (0.997)$).
4. $e^+e^- \to \overline{q}qe\nu(\gamma)$ (CC20), q-flavour blind, $|\cos\theta_e| < 0.985$, $E_e > 5$ GeV, $M(q\overline{q}) > 10\ (45)$ GeV (full and high-mass region); inclusive cross-section accuracy is 1% (5% for low-mass region); photon energy and polar angle spectrum ($|\cos\theta_\gamma| < 0.985\ (0.997)$).
5. $e^+e^- \to \overline{q}q\mu\nu(\gamma)$ and $e^+e^- \to \overline{q}q\tau\nu(\gamma)$ (incl. tau polarization in tau decay) (CC10), $|\cos\theta_{\mu/\tau}| < 0.985$, $E_{\mu/\tau} > 5$ GeV, $M(q\overline{q}) > 10\ (45)$ GeV (full and high-mass region), inclusive cross-section accuracy 1%. Photon energy and polar angle ($|\cos\theta_\gamma| < 0.985\ (0.997)$) spectrum.
6. $e^+e^- \to q\overline{q}q\overline{q}(\gamma)$, flavour blind, $bbq\overline{q}$, $bbbb$. At least two pairs with $M(q_i, q_j) > 10\ (45)$ GeV (full and high-mass region), inclusive cross-section accuracy 1%. photon energy and polar angle ($|\cos\theta_\gamma| < 0.985\ (0.997)$) spectrum.

7. $e^+e^- \to q\overline{q}l^+l^-(\gamma)$, q-flavour blind, heavy q-flavors, $l = e/\mu/\tau$, $|\cos\theta_{l_1}| < 0.985$, no cut on 2nd lepton (only one lepton tagged), $M(q\overline{q}) > 10$ (45) GeV (full and high-mass region), inclusive cross-section accuracy 2%. Photon energy and polar angle ($|\cos\theta_\gamma| < 0.985$ (0.997)) spectrum.
8. $e^+e^- \to q\overline{q}l^+l^-(\gamma)$, q-flavour blind, heavy q-flavors, $|\cos\theta_{l_1}|, |\cos\theta_{l_2}| < 0.985$ (both leptons tagged), full and high-mass regions: $M(l^+l^-) > 10$ (45) GeV, $M(q\overline{q}) > 10$ (45) GeV, inclusive cross-section accuracy 2%. Photon energy and polar angle ($|\cos\theta_\gamma| < 0.985$ (0.997)) spectrum.
9. $e^+e^- \to q\overline{q}e^+e^-(\gamma)$, q-flavour blind, heavy q-flavors, with one electron in the beam pipe, $|\cos\theta_e| > 0.997$, and one electron tagged, $|\cos\theta_e| < 0.985$, $M(q\overline{q}) > 10$ (45) GeV (full and high-mass region) . Photon energy and polar angle ($|\cos\theta_\gamma| < 0.985$ (0.997)) spectrum.
10. $e^+e^- \to q\overline{q}\nu\overline{\nu}(\gamma)$, q-flavour blind, heavy q-flavors, $M(q\overline{q}) > 10$ (45) GeV, inclusive cross-section accuracy 4% (10% for low-mass region). Photon energy and polar angle ($|\cos\theta_\gamma| < 0.985$ (0.997)) spectrum.
11. $e^+e^-l^+l^-L^+L^-(\gamma)$, $l^+l^-l^+l^-(\gamma)$ (all possible charged lepton flavour combinations): 3 or 4 leptons within acceptance $|\cos\theta| < 0.985$, $M(l^+l^-)$ and $M(L^+L^-) > 10$ (45) GeV (full and high-mass region). Photon energy and polar angle ($|\cos\theta_\gamma| < 0.985$ (0.997)) spectrum.

- single-W type signal:

1. $e^+e^- \to q\overline{q}e\nu(\gamma)$, $|\cos\theta_e| > 0.997$, either $M(q\overline{q}) > 45$ GeV or $E_{q_1}, E_{q_2} > 15$ GeV, inclusive cross-section accuracy 2%, photon energy and polar angle ($|\cos\theta_\gamma| < 0.997$ (0.9995)) spectrum
2. $e^+e^- \to e\nu e\nu(\gamma)$, $|\cos\theta_e| > 0.997$, $E_e > 15$ GeV, $|\cos\theta_e| < 0.7$ (0.95), inclusive cross-section accuracy 5%, photon energy and polar angle ($|\cos\theta_\gamma| < 0.997$ (0.9995)) spectrum.
3. $e^+e^- \to e\nu\mu\nu(\gamma)$ and $e^+e^- \to e\nu\tau\nu(\gamma)$, $|\cos\theta_e| > 0.997$, $E_{\mu/\tau} > 15$ GeV, $|\cos\theta_{\mu/\tau}| < 0.95$, inclusive cross-section accuracy 5%, photon energy and polar angle ($|\cos\theta_\gamma| < 0.997$ (0.9995)) spectrum.

The list above deserves already few words of comment:

For hadronic systems (NC or CC), there is usually a requirement of 45 GeV invariant mass (W and Z signal) or 10 GeV (background for other processes). Even lower invariant masses, down to 1 GeV, should be handled by the dedicated $\gamma\gamma$ subgroup. For leptons, there should be no problem to go down to even lower invariant masses or energies than listed above.

We consider as radiative events those events with photons where at least one photon passes the photon requirements listed above, and as non-radiative events those with no photon or only photons below the minimal photon requirements. In case of non-radiative and radiative events, the cross section and its accuracy is needed. In case of non-radiative events, this amounts to adding up virtual and soft radiative corrections. In case of radiative events, some distributions are needed in addition, in particular photon energy and polar angle, and photon angle with respect to the nearest charged final-state fermion.

1.1 Detailed Questions

In this section we elaborate in more detail on specific questions associated to specific processes, and give examples.

- **p_t ISR in WW and ZZ-dominated channels.**

The principle effects will be on the selection efficiency and on the differential distributions used for mass and TGC studies. The interest in photons is twofold: photons explicitly identified as such - usually at higher polar angles - and photons who simply create noticeable activity in the detector. The latter is, for example, important in single-W type analysis, therefore the photon angular range is extended to very low polar angles.

The single-W requires further specifications and it is better to. split this into several issues.

High mass hadronic final states (> 40 GeV). This is important for searches and TGC measurements. Assuming a cross section of 500 fb and an efficiency of 50% at the end of LEP 2 the statistical error on the cross section (per experiment) will be of the order of 10%. The goal for the theoretical uncertainty should be around 5%. One topic of investigation should be ISR: this process is dominated by t-channel diagrams, whereas the current MC program implement ISR assuming s-channel reactions.

A second issue is the treatment of the $\alpha_{\rm em}$ scale. Is it better to re-weight on a event by event basis? Or on a diagram basis?

In connection with the following point one of the outcomes of the workshop should be a recommendation on the mass cut which distinguishes the high mass (more reliable) from the low mass region, i.e. the lower value to which the 5% (or better) precision tag applies. The 5% precision requirement is also fine for the background estimation for Higgs searches.

The importance of ISR in this channel is threefold: (a) change in total cross-section due to normal radiative corrections, (b) change in event distributions used to make cuts which changes the fraction of the total that fall inside our cuts, (c) fraction of events with identified photons- this forms a background to some of the chargino searches where a detected gamma is required.

Since the single-W topology is defined as the one where a high mass object is found in the detector and the electron is not observed, we would like to know how the presence of p_t ISR changes the fraction of events where the electron gets *kicked* out of the beam-pipe, how the differential distributions are distorted for TGC studies and what the explicit hard photon rate is.

Low mass hadronic final states (< 40 GeV). This is mostly important for searches and should be studied in connection with the $\gamma\gamma$ working group, in particular for very low masses. One would like to trust the MC predictions down to 5-10 GeV invariant mass for the hadronic system. The required precision should be around 10%.

In the low hadronic mass region (5-60 GeV) the cross section measurement might reach (at the end of LEP 2) a precision around 5% (per experiment) (between 5 and 10% for the Z region, above 60 GeV). This implies that the theory prediction should be known better than 5%.

Topics which we would like to be discussed are: (a) t-channel ISR (same issue as in single W), (b) interference with $\gamma\gamma \to q\overline{q}$.

In conclusion we summarize some of the most important questions to be answered.

LEP is now quoting $1-2\%$ theoretical uncertainty (not changed since Yellow Report). Although no complete 1-loop $\mathcal{O}(\alpha)$ EW calculation exist (and will not in near future) for off-shell $e^+e^- \to WW \to 4$ f production, we wish the theoretical uncertainty to be below 1% (0.5% if possible) with justification. Also the uncertainties in CC03 $\to$ 4f corrections when measuring the WW cross section should be studied.

- WW (CC03) Questions:

1. Coulomb corrections: becoming less important, but which should be taken as default?
2. ISR, α/π (NLL) terms ($+0.7\%$ effect) can be taken into account as YFS form-factor. Should this be included? Which theoretical error should be assigned?
3. ISR non-universal correction for t-channel of $+0.4\%$. With which error?
4. Comparison of differential distributions among different MC generators with ISR/FSR on/off.

- General 4f Questions:

1. p_t effect of ISR/FSR ($d\sigma/dp_t$).
2. ISR/FSR implementation for $e+x$ final states.
3. Compare ISR; QEDPS v.s. YFS with p_t and establish uncertainty on them.
4. Compare FSR; QEDPS v.s. PHOTOS for $\mu\nu q\overline{q}$, $\mu\mu\nu_\mu\nu_\mu$.
5. Visible photon effect in the detector (efficiency change).

6. How to adopt FSR (prompt photon) for non-resonant $4\mathrm{f}$ diagrams.
7. Renormalization scheme and gauge invariance problem, establish theoretical uncertainty.

- Single-W questions:

1. ISR p_t effect for single W. New QEDPSt v.s. YFS v.s. SF v.s. etc, visible photon effect.
2. Which effective α_{QED}? (also for ZZ, $Z\gamma^*$, eeZ etc.) For the $\gamma - \gamma$ dominated final states like $e^+e^-q\overline{q}$ a running scale is usually implemented $alpha$ and one would very much like theoretical input as to the correctness of this prescription.
   This scale choice is a very significant problem as it has a 30% effect on the total cross-section for channels like $e^+e^-q\overline{q}$ when turning the running α on and off. This is also a particular concern for the measurement of the ZZ cross-section as here there is significant contribution from Zee even in the region where both $q\overline{q}$ and e^+e^- have mass within 10 GeV of the γ mass.
3. Multi-peripheral diagram: one should note the low momentum transfer in photon propagator. For $e\nu_e\mu\nu_\mu$ case, for example, muon is forward scattered with low energy, thus experimentally barely visible. For $e\nu_e\overline{q}q$ case, one quark goes forward, thus simulates mono-jet ($\nu\nu q\overline{q}$ is also the source of mono-jet).
4. Resolved photon effect for low invariant mass case (multi-peripheral diagrams). The estimate on uncertainty should be established. Use PDF like HERA if necessary?
5. $e^+e^-\nu_e\nu_e$: it would be extremely interesting if one can generate this channel without cut and compare among different generators (total cross section is not so large), one also should be realistic. Some cut like at least one visible $e^\pm$ could be applied.

- ZZ (NC02/NC08) Questions:

1. Which effective α_{QED} for ZZ? For $Z\gamma^*$, the situation is worse since the running QED α would be largely different between low invariant mass and high mass cases.
2. Low Q^2 γ^* (ZZ) fragmentation for invariant mass below 12 GeV. How to take into account resonances?

- Zee / $Z\nu\nu$ Questions:

1. ISR and its p_t effect for $e^+e^-l^+l^-$ and $e^+e^-\nu\bar{\nu}$ (similar to $e\nu W$).

- Two-photon collision processes - Questions:

1. Double counting problem $|4\mathrm{f} - \gamma\gamma|^2$, how to avoid it? - proposal; $4\mathrm{f}$ MC subtract diagrams of Multi-peripheral (and Bremsstrahlung), and use PHOT02 for these. The $4\mathrm{f}$ MC naturally includes $e^+e^-l^+l^-$ final states. It is not practical to generate hard processes (CC03, NC02 etc.) and two photon process together since the cross sections are different by three order of magnitude. There is a possibility to separate Multi-peripheral and Bremsstrahlung type graphs from others. Kinematics and cuts to be applied to these t-channel processes are so different from s-channel.

- Miscellaneous Questions and Wishes:

1. $\mathcal{O}(\alpha)$ calculation
2. Inclusion of quadruple-gauge-boson vertex with anomalous quartic gauge couplings.
3. Anomalous NC couplings - anomalous $\gamma\gamma Z$, γZZ and ZZZ vertices.
4. Non-factorizable (i.e. non-naive) QCD corrections to $\overline{q}q\overline{q}q$ and $\overline{q}ql\nu$ final state, do they affect angular distributions? This seems to be a problem between the pure ew phase and QCD parton-shower.

- Technical wishes:

1. Easy access to matrix elements for re-weighting purposes including anomalous couplings everywhere (Subroutine for initialization with masses and couplings, subroutine for event-by-event calculation based on four-vector kinematics of fermions and photons).
2. Faster event generation of weight=1 events for detector simulation.
3. Event mix in $4\mathrm{f}$ (eg $\overline{q}qe\nu$ summing all quark flavors and charge modes).
4. Non-trivial CKM matrix.
5. More cuts in phase-space sampling to implement the ZZ signal definition: Upper cuts on $M(\overline{f}f)$, $M(\overline{f}f)$ cuts in.or.on the three combinations (12)(34) (13)(24) (14)(23).

The results, which are presented in this Report, are based on several different approaches and on comparisons of their numerical predictions. The findings of the Report are based on the following computer codes:
`CompHEP`, `grc4f`, `KORALW/YFSWW/YFSZZ`, `NEXTCALIBUR`, `RacoonWW`, `SWAP`, `WPHACT`, `WRAP` and `WTO`.

2. Input Parameter Set

An important set of numbers to be considered concerns CC03 $\mathcal{O}(\alpha)$ predictions (to some extent also NC02). Once radiative corrections are switched on, the question of Renormalization Scheme (RS) and of Input Parameter Set (IPS) becomes relevant. One should use the following input parameters, in any calculation:

$$\begin{aligned} M_Z &= 91.1867\,\mathrm{GeV}, \quad 1/\alpha(0) = 137.0359895, \\ G_F &= 1.16637\,10^{-5}\,\mathrm{GeV}^{-2}. \end{aligned} \tag{1}$$

As far as masses are concerned one should use:

Leptons: PDG values, i.e.

$$\begin{aligned} m_e &= 0.51099907\,\mathrm{MeV}, \quad m_\mu = 105.658389\,\mathrm{MeV}, \\ m_\tau &= 1.77705\,\mathrm{GeV}. \end{aligned} \tag{2}$$

Quarks: for light quarks one should make a distinction; for phase space:

$$\begin{aligned} &m_u = 5\,\mathrm{MeV}, \qquad m_d = 10\,\mathrm{MeV}, \\ &\text{only relevant for single} - W, \end{aligned} \tag{3}$$

while, in principle, they should *not* be used in deriving $\alpha_{\mathrm{QED}}(s)$ from $\alpha_{\mathrm{QED}}(0)$. Here the recommendations is as follows: an important issue concerns the evaluation of α_{QED} at the mass of the Z.

There is an agreement in our community on using the following strategy. Define

$$\alpha(M_Z) = \frac{\alpha(0)}{1 - \Delta\alpha^{(5)}(M_Z) - \Delta_{\mathrm{top}}(M_Z) - \Delta_{\mathrm{top}}^{\alpha\alpha_S}(M_Z)}\,, \tag{4}$$

where one has $\Delta\alpha^{(5)}(M_Z) = \Delta\alpha_{\mathrm{lept}} + \Delta\alpha^{(5)}_{\mathrm{had}}$. The input parameter should be $\Delta\alpha^{(5)}_{\mathrm{had}}$, as it is the contribution with the largest uncertainty, while the calculation of the top contributions to $\Delta\alpha$ is left for the code. This should become common to all codes.

Codes should include, for $\Delta\alpha_{\mathrm{lept}}$, the recently computed $\mathcal{O}(\alpha^3)$ terms of [1] and use as default $\Delta\alpha^{(5)}_{\mathrm{had}} = 0.0280398$, taken from [2]. Using the default one obtains $1/\alpha^{(5)}(M_Z) = 128.877$, to which one must add the $t\overline{t}$ contribution and the $\mathcal{O}(\alpha\alpha_S)$ correction induced by the $t\overline{t}$ loop with gluon exchange, [3].

Therefore, light quark masses should *not* appear in the evaluation of $\alpha_{\rm QED}(M_Z)$ and one should end up with

$$\begin{aligned} 1/\alpha(M_Z) &= 128.887, \\ \text{for} \quad & M_Z = 91.1867\,GeV, \quad m_t = 175\,\mathrm{GeV}, \\ & M_H = 150\,\mathrm{GeV}, \quad \alpha_S(M_Z) = 0.119. \end{aligned} \tag{5}$$

Furthermore, one should use

$$\alpha_S(M_Z) = 0.119, \quad M_H = 150\,\mathrm{GeV}, \quad M_W = 80.350\,\mathrm{GeV}. \tag{6}$$

The quantities Γ_Z, Γ_W should be understood as computed in the minimal standard model, i.e. $\Gamma_Z = 2.49471\,\mathrm{GeV}$ for our IPS. Now we come to the most important point, what to do with IPS in the presence of radiative corrections. In principle, all RS and all IPS are equally good and accepted, and differences are true estimates of some component of the theoretical uncertainty. However, we want to make sure that differences are not due to technical precision. The IPS that we want to specify is over-complete, let us repeat,

M_H [GeV]	m_t [GeV]
100	170.03
150	174.17
180	176.14
250	179.90

Table 1: m_t as a function of M_H.

$$\begin{aligned} G_F &= 1.16637\,10^{-5}\,\mathrm{GeV}^{-2}, \qquad 1/\alpha(M_Z) = 128.887, \\ M_Z &= 91.1867\,\mathrm{GeV}, \quad M_W = 80.350\,\mathrm{GeV}, \\ \alpha_S(M_Z) &= 0.119, \quad M_H = 150\,\mathrm{GeV}. \end{aligned} \tag{7}$$

Clearly, once radiative correction are on, $s_\theta = s_\theta^{\rm xxx-scheme}$ and we don't care anymore since enough radiative corrections should be included to make all schemes equivalent to $\mathcal{O}(\alpha)$. Thus, for $\mathcal{O}(\alpha)$ numbers s_θ drops out. Perhaps we should give the highest marks to schemes where M_W is in the IPS; after all, experiments measure M_W at LEP 2 and any scheme where M_W is not a primary quantity in the IPS is as bad as a scheme for LEP 1 where M_Z is a derived quantity.

Nevertheless, we can use the over-completeness of the present IPS to set some internal consistency: it is a good idea to have an over-complete set of IPS, nevertheless consistent, so that everybody can make his favourite choice of the RS. Since we include values for $\alpha(M_Z)$ and for G_F we can, as well, fine-tune the numbers so that the internal relations hold, to the best of our knowledge. The recommendation, in this case, is as follows:

- write down your favorite equation

$$f\,(M_Z, M_W, m_t, M_H, \alpha_S(M_Z), \alpha(0), G_F) = 0, \tag{8}$$

  keep everything fixed but m_t which, in turn, is derived as a solution of the consistency equation (for OMS this involves typically Δr). Even this solution is RS-dependent but variation should be minimal, sort of irrelevant. For instance, one could use the following result (derived from `TOPAZ0`):

$$m_t = 174.17\,\mathrm{GeV} \quad \textbf{Default for CC03}\ \mathcal{O}(\alpha)\,. \tag{9}$$

  With $M_W = 80.350\,GeV$ and $M_H = 150\,\mathrm{GeV}$ we are in a lucky situation, m_t doesn't change too much.

For more solutions, we refer to Tab.(1).

3. The CC03 cross section

In order to extract the WW signal from the full set of $\mathrm{e}^+\mathrm{e}^- \to 4f$ processes, the CC03 cross section was introduced and discussed in [4]. In lowest order, this cross section is simply based on the three WW signal diagrams with the full four-particle kinematics with off-shell W bosons. Compared to the full set of diagrams, the CC03 subset depends only trivially on the final state and allows to combine all channels easily. However, since the CC03 cross section is based on a subset of diagrams, it is gauge-dependent and usually defined in the 't Hooft–Feynman gauge. While the CC03 cross section is not an observable, it is nevertheless a useful quantity at LEP2 energies where it can be classified as a pseudo-observable. It contains the interesting physics, such as the non-abelian couplings and the sensitivity of the total cross section to M_W near the W-pair threshold. The goal of this common definition is to be able to combine the different final state measurements from different experiments so that the new theoretical calculations can be checked with data at a level better than 1%. Note, however, that the CC03 cross section will become very problematic at linear-collider energies, where the background diagrams and the gauge dependences are much larger.

The double-pole approximation (DPA) of the lowest-order cross section emerges from the CC03 diagrams upon projecting the W-boson momenta in the matrix element to their on-shell values. This means that the DPA is based on the residue of the double resonance, which is a gauge-invariant quantity, because it is directly related to the sub-processes of on-shell W-pair production and on-shell W decay. In contrast to the CC03 cross section, the DPA is theoretically well-defined. The price to be paid for this is the exclusion of the threshold region, where the DPA is not valid. On the other hand, the DPA provides a convenient framework for the inclusion of radiative corrections.

It is worth summarizing the status of the WW cross-section prior to the 2000 Winter Conferences. Nominally, any $\mathrm{e}^+\mathrm{e}^- \to \mathrm{WW} \to 4f$ is a tree level calculation where one could try the LEP 1 exercise of including, in a reasonable way, as much as possible of the universal corrections by constructing an improved Born approximation (hereafter IBA). This is the way the data have been analyzed so far, mostly with the help of `GENTLE`. Experimenters have compared `GENTLE` and `grc4f` for CC03. When one puts the same input parameters, renormalization scheme, etc, a technical agreement at the 0.1% level is found. This is not enough, we wish the theoretical uncertainty to be below 1% (0.5% seems possible) with justification.

Indeed, we have clear indications that non-universal electroweak corrections for WW(CC03) cross-section are not small and even larger than the experimental LEP accuracy. `GENTLE` will produce a CC03 cross-section, typically in the G_F-scheme, with universal ISR QED and non-universal ISR/FSR QED corrections, implemented with the so called current splitting-technique. The corresponding curve has been used for the definition of the Standard Model prediction with a $\pm 2\%$ systematic error assigned to it. Note that, in `GENTLE`, the non-universal ISR correction with current splitting technique reads as $+0.4\%$ effect at LEP 2.

Recently, a new electroweak $\mathcal{O}(\alpha)$ CC03 cross-section has become available, in the framework of DPA, showing a result that is between -1% and -1.5% smaller than the CC03 cross section from `GENTLE`. This is a big effect since the combined experimental accuracy of LEP experiments is of the same magnitude. It is, therefore, of the upmost importance to understand the structure of a DPA-corrected CC03 cross-section.

4. Dealing with unstable particles

The main purpose of this report is to qualify as a reference handbook for precision experiments at LEP 2 energies. As such, the report is essentially devoted to describe the state-of-the-art in the predictions of the MC adopted by the experimental Collaborations, with particular emphasis on reaching a reliable estimate of the Standard Model background to searches.

Nevertheless, most of our *technical* problems originate from the complications naturally pertaining to the gauge structure of the theory and to the presence of unstable particles. As an interlude, we would like to summarize the nominal essence of the theoretical basis of all our generators. In this respect one should remember that the new theoretical ideas were fully developed also as a consequence of a previous workshop on WW-physics and, in turn, many generators have profited from the most recent theoretical development. Furthermore, this Section will be a natural place where to add some consideration about the fine points in the DPA-procedure.

Four-fermion production processes, with or without radiative corrections, all involve fermions in the initial and final state and unstable gauge bosons as intermediate particles. Sometimes a photon is also present in the final state. If complete sets of graphs contributing to a given process are taken into account, the associated matrix elements are in principle gauge-invariant, i.e. they are independent of gauge fixing and respect Ward identities. This is, however, not guaranteed for incomplete sets of graphs like the ones corresponding to the off-shell W-pair production process (CC03). Indeed this process has been found to violate the $SU(2)$ Ward identities [26].

In addition, the unstable gauge bosons that appear as intermediate particles can give rise to poles $1/(p^2 - M^2)$ in physical observables if they are treated as stable particles. In view of the high precision of the LEP2 experiments, the proper treatment of these unstable particles has become a demanding exercise, since on-shell approximations are simply not good enough anymore. A proper treatment of unstable particles requires the re-summation of the corresponding self-energies to all orders. In this way the singularities originating from the poles in the on-shell propagators are regularized by the imaginary parts contained in the self-energies, which are closely related to the decay widths (Γ) of the unstable particles. The perturbative re-summation itself involves a simple geometric series and is therefore easy to perform. However, this simple procedure harbours the serious risk of breaking gauge invariance. Gauge invariance is guaranteed order by order in perturbation theory. Unfortunately one takes into account only part of the higher-order terms by re-summing the self-energies. This results in a mixing of different orders of perturbation theory and thereby jeopardizes gauge invariance, even if the self-energies themselves are extracted in a gauge-invariant way. Apart from being theoretically unacceptable, gauge-breaking effects can also lead to large errors in the MC predictions. At LEP2 energies this problem occurs in the reactions $e^+e^- \to e^-\bar{\nu}_e u\bar{d},\ e^+\nu_e\bar{u}d$ for forward-scattered beam particles [27].

Based on this observation, it is clear that a truly gauge-invariant scheme is required for the treatment of unstable particles. It should be stressed, however, that any such scheme is arbitrary to a greater or lesser extent: since the Dyson summation must necessarily be taken to all orders of perturbation theory, and we are not able to compute the complete set of *all* Feynman diagrams to *all* orders, the various schemes differ even if they lead to formally gauge-invariant results. Bearing this in mind, we need besides gauge invariance some physical motivation for choosing a particular scheme. In this context two options can be mentioned. Either one can try to *subtract* gauge-violating terms or one can try to *add* gauge-restoring terms to the calculation.

The first option is the so-called *pole scheme* [28]. In this scheme one decomposes the complete amplitude by expanding around the poles. As the physically observable residues of the poles are gauge-invariant, gauge invariance is not broken if the finite width is taken into account in the pole terms $\propto 1/(p^2 - M^2)$. In reactions with multiple unstable-particle resonances it is rather awkward to perform the complete pole-scheme expansion with all its subtleties in the treatment of the off-shell phase space [29]. Therefore one usually approximates the expansion by retaining only the terms with the highest degree of resonance. This approximation is called the leading-pole approximation and is closely related to on-shell production and decay of the unstable particles. The accuracy of the approximation is typically $\mathcal{O}(\Gamma/M)$, making it a suitable tool for calculating *radiative corrections*, since in that case the errors are further suppressed by powers of the coupling constant [29]. Since diagrams with a lower degree of resonance do not feature in the leading-pole approximation, it is not an adequate approach for describing lowest-order reactions. So, for lowest-order reactions one needs an alternative approach.

The second option is based on the fundamentally different philosophy of trying to determine and include the minimal set of Feynman diagrams that is necessary for compensating the gauge violation caused by the self-energy graphs. This is obviously the theoretically most satisfying solution, but it may cause an increase in the complexity of the matrix elements and consequently a slowing down of the numerical calculations. Two methods have been developed along these lines. First of all, for the gauge bosons we are guided by the observation that the *lowest-order* decay widths are exclusively given by the imaginary parts of the fermion loops in the one-loop self-energies. It is therefore natural to perform a Dyson summation of these fermionic one-loop self-energies and to include the other possible one-particle-irreducible fermionic one-loop corrections (*fermion-loop scheme*) [27, 30, 31, 32]. For the *lowest-order* LEP2 process $e^+e^- \to 4f$ this amounts to adding the fermionic corrections to the triple gauge-boson vertex. The complete set of fermionic contributions forms a manifestly gauge-invariant subset, since it involves the closed subset of all $\mathcal{O}([N_c^f\alpha/\pi]^n)$ contributions (with N_c^f denoting the colour degeneracy of fermion f). Moreover, it obeys all Ward identities exactly, even with re-summed propagators [31]. The limitation of the fermion-loop scheme lies in the fact that it does not apply to particles that also have bosonic decay modes, which in turn disqualifies it as a candidate for handling radiative corrections. Moreover, the inclusion of a full-fledged set of one-loop corrections in a lowest-order amplitude tends to over-complicate things for reactions like $e^+e^- \to 4f\gamma$.

Recently a novel non-diagrammatic technique has been proposed for arbitrary *tree-level* reactions, involving all possible unstable particles and an unspecified amount of stable external particles [33]. By using gauge-invariant non-local effective Lagrangians, it is possible to generate the self-energy effects in the propagators as well as the required gauge-restoring terms in the multi-particle (3-point, 4-point, etc.) interactions. In this way the full set of Ward identities can be solved, while keeping the gauge-restoring terms to a minimum. At present the first MC implementation of this new method in an existing program, HELAC [34], is in progress. Hence, its full potential is still under scrutiny.

5. The leading-pole approximation

As mentioned above, the pole scheme consists in decomposing the complete amplitude by expanding around the poles of the unstable particles. The residues in this expansion are physically observable and therefore gauge-invariant. The pole-scheme expansion can be viewed as a gauge-invariant prescription for performing an expansion in powers of Γ/M. It should be noted that there is no unique definition of the residues. Their calculation involves a mapping of off-shell matrix elements with off-shell kinematics on on-resonance matrix elements with restricted kinematics. This mapping, however, is not unambiguously fixed. After all, it involves more than just the invariant masses of the unstable particles and one thus has to specify the variables that have to be kept fixed in the mapping. The resulting implementation dependence manifests itself in differences of sub-leading nature, e.g. $\mathcal{O}(\Gamma/M)$ suppressed deviations in the leading pole-scheme residue. In special regions of phase space, where the matrix elements vary rapidly, the implementation dependence can take noticeable proportions. This happens in particular near phase-space boundaries, like thresholds.

In order to make these statements a bit more transparent, we sketch the pole-scheme method for a single unstable particle. In this case the Dyson re-summed lowest-order matrix element is given by

$$\begin{aligned}\mathcal{M}^{\infty} &= \frac{W(p^2,\omega)}{p^2-\tilde{M}^2}\sum_{n=0}^{\infty}\left(\frac{-\tilde{\Sigma}(p^2)}{p^2-\tilde{M}^2}\right)^n = \frac{W(p^2,\omega)}{p^2-\tilde{M}^2+\tilde{\Sigma}(p^2)} \\ &= \frac{W(M^2,\omega)}{p^2-M^2}\,\frac{1}{Z(M^2)} + \left[\frac{W(p^2,\omega)}{p^2-\tilde{M}^2+\tilde{\Sigma}(p^2)} - \frac{W(M^2,\omega)}{p^2-M^2}\,\frac{1}{Z(M^2)}\right], \qquad (10)\end{aligned}$$

where $\tilde{\Sigma}(p^2)$ is the unrenormalized self-energy of the unstable particle with momentum p and unrenormalized mass $\tilde{M}$. The renormalized quantity M^2 is the pole in the complex p^2 plane, whereas $Z(M^2)$ denotes the wave-function factor:

$$M^2 - \tilde{M}^2 + \tilde{\Sigma}(M^2) = 0, \qquad Z(M^2) = 1 + \tilde{\Sigma}'(M^2). \qquad (11)$$

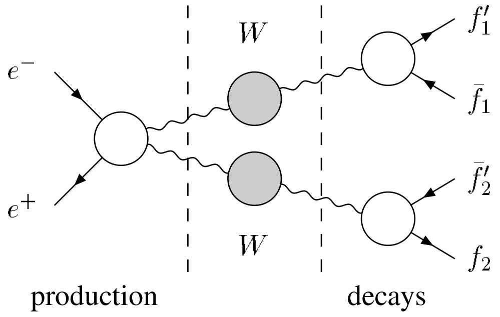

Fig. 1: The generic structure of the factorizable W-pair contributions. The shaded circles indicate the Breit–Wigner resonances, whereas the open circles denote the Green functions for the production and decay sub-processes up to $\mathcal{O}(\alpha)$ precision.

The first term in the last expression of Eq. (10) represents the single-pole residue, which is closely related to on-shell production and decay of the unstable particle. The second term between the square brackets has no pole and can be expanded in powers of $p^2 - M^2$. The argument ω denotes the dependence on the other variables, i.e. the implementation dependence. After all, the unstable particle is always accompanied by other particles in the production and decay stages. For instance, consider the LEP1 reaction $e^+e^- \to \bar{f}f$. In the mapping $p_Z^2 \to M^2$ one can either keep $t = (p_{e^-} - p_f)^2 = -p_Z^2(1 - \cos\theta)/2$ fixed or $\cos\theta$. In the former mapping $\cos\theta_{\text{pole}}$ is obtained from the on-shell relation $\cos\theta_{\text{pole}} = 1 + 2t/M^2$, whereas in the latter mapping $t_{\text{pole}} = -M^2(1-\cos\theta)/2$. It may be that a particular mapping leads to an unphysical point in the on-shell phase space. In the present example t_{pole} will always be physical when $\cos\theta$ is kept fixed in the mapping. However, since $|\cos\theta_{\text{pole}}| > 1$ for $t < -\text{Re}M^2$, it is clear that mappings with fixed Mandelstam variables harbour the potential risk of producing such unphysical phase-space points.[1] This can have repercussions on the convergence of the pole-scheme expansion. Therefore it is recommended to use implementations that are free of unphysical on-shell phase-space points.

The at present only workable approach for evaluating the radiative corrections to resonance-pair-production processes, like W-pair production, involves the so-called leading-pole approximation (LPA). This approximation restricts the complete pole-scheme expansion to the term with the highest degree of resonance. In the case of W-pair production only the double-pole residues are hence considered. This is usually referred to as the double-pole approximation (DPA). The intrinsic error associated with this procedure is $\alpha\Gamma_W/(\pi M_W) \lesssim 0.1\%$, except far off resonance, where the pole-scheme expansion cannot be viewed as an effective expansion in powers of Γ/M, and close to phase-space boundaries, where the DPA cannot be trusted to produce the dominant contributions. In the latter situations also the implementation dependence of the double-pole residues can lead to enhanced errors. Close to the nominal (on-shell) W-pair threshold, for instance, the intrinsic error is effectively enhanced by a factor $M_W/(\sqrt{s} - 2M_W) \equiv M_W/\Delta E$. In view of this it is wise to apply the DPA only if the energy is several Γ_W above the threshold.

In the DPA one can identify two types of contributions. One type comprises all diagrams that are strictly reducible at both unstable W-boson lines (see Fig. 1). These corrections are therefore called factorizable and can be attributed unambiguously either to the production of the W-boson pair or to one of the subsequent decays. The second type consists of all diagrams in which the production and/or decay sub-processes are not independent and which therefore do not seem to have two overall W propagators as factors (see Fig. 2). We refer to these effects as non-factorizable corrections.[2] In the DPA the non-

[1] In the resonance region, $|p_Z^2 - M^2| \ll |M^2|$, the unphysical on-shell phase-space points occur near the edge of the off-shell phase space, since $t < -\text{Re}M^2$ requires $\cos\theta \approx -1$.

[2] It should be noted that the exact split-up between factorizable and non-factorizable radiative corrections requires a precise (gauge-invariant) definition. We will come back to this point.

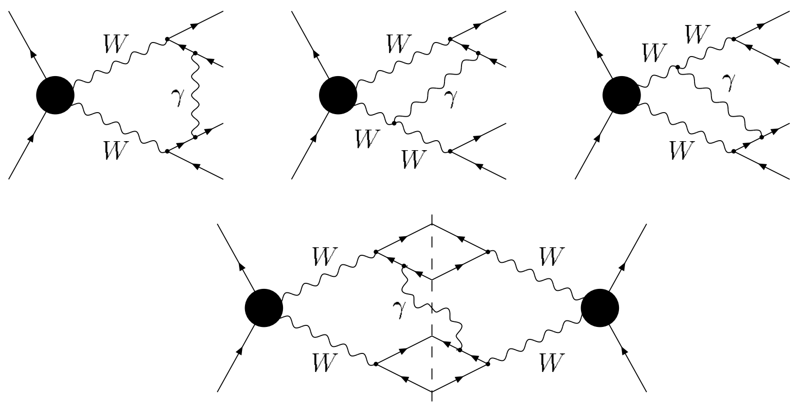

Fig. 2: Examples for virtual (top) and real (bottom) non-factorizable corrections to W-pair production. The black circles denote the lowest-order Green functions for the production of the virtual W-boson pair.

factorizable corrections arise exclusively from the exchange or emission of photons with $E_\gamma \lesssim \mathcal{O}(\Gamma_W)$ [35]. Hard photons as well as massive-particle exchanges do not lead to double-resonant contributions. The physical picture behind all of this is that in the DPA the W-pair process can be viewed as consisting of several sub-processes: the production of the W-boson pair, the propagation of the W bosons, and the subsequent decay of the unstable W bosons. The production and decay are hard sub-processes, which occur on a relatively short time interval, $\mathcal{O}(1/M_W)$. They are in general distinguishable as they are well separated by a relatively big propagation interval, $\mathcal{O}(1/\Gamma_W)$. Consequently, the corresponding amplitudes have certain factorization properties. The same holds for the radiative corrections to the sub-processes. The only way the various stages can be interconnected is via the radiation of soft photons with energy of $\mathcal{O}(\Gamma_W)$. These photons induce relatively long range interactions and thereby allow the various sub-processes to communicate with each other.

As is clear from the above-given discussion of the DPA, a specific prescription has to be given for the calculation of the DPA residues. Or, in other words, we have to fix the implementation of the mapping of the full off-shell phase space on the kinematically restricted (on-resonance) one. Two strategies have been adopted in the literature [29, 36]. One can opt to always extract pure double-pole residues [29]. This means in particular that after the integration over decay kinematics and invariant masses has been performed the on-shell cross-section should be recovered. Alternatively, one can decide to exclude the off-shell phase space from the mapping and apply the residue only to the matrix elements [36]. We will come back to the conceptual and numerical differences between these two implementation strategies in the detailed discussion of the DPA programs. At this point we merely note that the numerical differences can serve as an estimate of the theoretical uncertainty of the DPA procedure.

In the rest of this section we will explain those aspects of the DPA procedure that are common to both implementation methods. To this end we focus on the lowest-order reaction

$$e^+(q_1)\,e^-(q_2) \to W^+(p_1)\,W^-(p_2) \to \bar{f}_1(k_1) f_1'(k_1')\, f_2(k_2) \bar{f}_2'(k_2'), \tag{12}$$

involving only those diagrams that contain as factors the Breit–Wigner propagators for the W^+ and W^- bosons. Here $\bar{f}_1$ and f_1' are the decay products of the W^+ boson, and f_2 and $\bar{f}_2'$ those of the W^- boson. It should be noted that a large part of the radiative corrections in DPA to this reaction can be treated in a way similar to the lowest-order case, which is therefore a good starting point. The amplitude for process (12) takes the form

$$\mathcal{M} = \sum_{\lambda_1,\lambda_2} \Pi_{\lambda_1\lambda_2}(M_1, M_2)\,\frac{\Delta^{(+)}_{\lambda_1}(M_1)}{D_1}\,\frac{\Delta^{(-)}_{\lambda_2}(M_2)}{D_2}\,, \tag{13}$$

where any dependence on the helicities of the initial- and final-state fermions has been suppressed, and

$$D_i = M_i^2 - M_W^2 + iM_W\Gamma_W, \qquad M_i^2 = (k_i + k_i')^2. \tag{14}$$

The quantities $\Delta^{(+)}_{\lambda_1}(M_1)$ and $\Delta^{(-)}_{\lambda_2}(M_2)$ are the off-shell W-decay amplitudes for specific spin-polarization states λ_1 (for the W^+) and λ_2 (for the W^-), with $\lambda_i = (-1, 0, +1)$. The off-shell W-pair production amplitude $\Pi_{\lambda_1\lambda_2}(M_1, M_2)$ depends on the invariant fermion-pair masses M_i and on the polarizations λ_i of the virtual W bosons. In the limit $M_i \to M_W$ the amplitudes Π and $\Delta^{(\pm)}$ go over into the on-shell production and decay amplitudes.

In the cross-section the above factorization leads to

$$\sum_{\text{fermion helicities}} |\mathcal{M}|^2 \;=\; \sum_{\lambda_1,\lambda_2,\lambda_1',\lambda_2'} \mathcal{P}_{[\lambda_1\lambda_2][\lambda_1'\lambda_2']}(M_1, M_2)\, \frac{\mathcal{D}_{\lambda_1\lambda_1'}(M_1)}{|D_1|^2}\, \frac{\mathcal{D}_{\lambda_2\lambda_2'}(M_2)}{|D_2|^2}. \tag{15}$$

In Eq. (15) the production part is given by a 9×9 density matrix

$$\mathcal{P}_{[\lambda_1\lambda_2][\lambda_1'\lambda_2']}(M_1, M_2) \;=\; \sum_{e^\pm \text{ helicities}} \Pi_{\lambda_1\lambda_2}(M_1, M_2)\, \Pi^*_{\lambda_1'\lambda_2'}(M_1, M_2). \tag{16}$$

Similarly the decay part is governed by 3×3 density matrices

$$\mathcal{D}_{\lambda_i\lambda_i'}(M_i) \;=\; \sum_{\text{fermion helicities}} \Delta_{\lambda_i}(M_i)\, \Delta^*_{\lambda_i'}(M_i), \tag{17}$$

where the summation is performed over the helicities of the final-state fermions.

It is clear that Eq. (16) is closely related to the absolute square of the matrix element for stable unpolarized W-pair production. In that case the cross-section contains the trace of the above density matrix

$$\textbf{Tr}\, \mathcal{P}(M_W, M_W) = \sum_{\lambda_1,\lambda_2} \mathcal{P}_{[\lambda_1\lambda_2][\lambda_1\lambda_2]}(M_W, M_W) \;=\; \sum_{\text{all polarizations}} |\Pi_{\lambda_1\lambda_2}(M_W, M_W)|^2. \tag{18}$$

The decay of an unpolarized on-shell W boson is determined by

$$\textbf{Tr}\, \mathcal{D}(M_W) = \sum_{\lambda_i} \mathcal{D}_{\lambda_i\lambda_i}(M_W) \;=\; \sum_{\text{all polarizations}} |\Delta_{\lambda_i}(M_W)|^2. \tag{19}$$

Note, however, that also the off-diagonal elements of $\mathcal{P}(M_W, M_W)$ and $\mathcal{D}(M_W)$ are required for determining Eq. (15) in the limit $M_i \to M_W$.

As a next step it is useful to describe the kinematics of process (12) in a factorized way, i.e. using the invariant masses M_1 and M_2 of the fermion pairs. The differential cross-section takes the form

$$d\sigma = \frac{1}{2s}\sum |\mathcal{M}|^2\, d\Gamma_{4f} = \frac{1}{2s}\sum |\mathcal{M}|^2\, d\Gamma_{\text{pr}} \cdot d\Gamma^+_{\text{dec}} \cdot d\Gamma^-_{\text{dec}} \cdot \frac{dM_1^2}{2\pi} \cdot \frac{dM_2^2}{2\pi}, \tag{20}$$

where $d\Gamma_{4f}$ indicates the complete four-fermion phase-space factor and $s = (q_1 + q_2)^2$ the centre-of-mass energy squared. The phase-space factors for the production and decay sub-processes, $d\Gamma_{\text{pr}}$ and $d\Gamma^\pm_{\text{dec}}$, read

$$\begin{aligned}
d\Gamma_{\text{pr}} &= \frac{1}{(2\pi)^2}\, \delta(q_1 + q_2 - p_1 - p_2)\, \frac{d\vec{p}_1}{2p_{10}}\, \frac{d\vec{p}_2}{2p_{20}}, \\
d\Gamma^+_{\text{dec}} &= \frac{1}{(2\pi)^2}\, \delta(p_1 - k_1 - k_1')\, \frac{d\vec{k}_1}{2k_{10}}\, \frac{d\vec{k}_1'}{2k_{10}'}, \\
d\Gamma^-_{\text{dec}} &= \frac{1}{(2\pi)^2}\, \delta(p_2 - k_2 - k_2')\, \frac{d\vec{k}_2}{2k_{20}}\, \frac{d\vec{k}_2'}{2k_{20}'}.
\end{aligned} \tag{21}$$

When the factorized form for $\sum|\mathcal{M}|^2$ is inserted one obtains

$$
\begin{aligned}
d\sigma &= \frac{1}{2s}\sum_{\lambda_1,\lambda_2,\lambda_1',\lambda_2'} \mathcal{P}_{[\lambda_1\lambda_2][\lambda_1'\lambda_2']}(M_1,M_2)\, d\Gamma_{\rm pr} \times \mathcal{D}_{\lambda_1\lambda_1'}(M_1)\, d\Gamma^+_{\rm dec} \times \mathcal{D}_{\lambda_2\lambda_2'}(M_2)\, d\Gamma^-_{\rm dec} \times \\
&\quad \times \frac{1}{2\pi}\frac{dM_1^2}{|D_1|^2} \times \frac{1}{2\pi}\frac{dM_2^2}{|D_2|^2},
\end{aligned} \tag{22}
$$

which is the common starting point for any of the DPA implementations.

6. Radiative corrections in double-pole approximation

A full calculation of the complete electroweak $\mathcal{O}(\alpha)$ corrections to $\mathrm{e^+e^-} \to 4f(+\gamma)$ for all four-fermion final states is beyond present possibilities. While the real bremsstrahlung corrections induced by $\mathrm{e^+e^-} \to 4f\gamma$ are known exactly [5, 48, 7], there are severe technical and conceptual problems with the virtual corrections to four-fermion production. Fortunately, the full account of the $\mathcal{O}(\alpha)$ corrections is not needed at the level of accuracy demanded by LEP2. For W-pair-mediated processes, $\mathrm{e^+e^-} \to \mathrm{WW} \to 4f$, the required accuracy of predictions is of the order of 0.5% for integrated quantities. At this level, the corrections to W-pair production can be treated in the double-pole approximation, or DPA. In regions of phase space where two resonant W bosons do not dominate the cross sections, such as in the WW-threshold region or in the single-W domain, the DPA is, of course, not valid and one should resort to other approximations as the Weizsäcker-Williams for single-W.

Since only diagrams with two nearly resonant W bosons are relevant for the DPA,the number of graphs is reduced considerably, and a generic treatment of all four-fermion final states is possible. Obviously all diagrams that appear for the pair production and the decay of on-shell W bosons are also relevant for the pole expansion in the DPA. Since such contributions involve a product of two independent Breit–Wigner factors for the W resonances, they are called *factorizable* corrections. However, there exist also doubly-resonant corrections in which the production and decay sub-processes do not proceed independently. Power counting reveals that such corrections are only doubly-resonant if the particle that is exchanged by the sub-processes is a low-energetic photon. Owing to the complicated off-shell behaviour of these corrections, they are called *non-factorizable*.

While the definition of the DPA is straightforward for the virtual corrections, it is problematic for the real corrections. The problem is due to the momentum carried away by photon radiation. The invariant masses of the W bosons in contributions in which the photon is emitted in the W-pair production sub-process differ from those where the photon is emitted in the W-decay sub-processes. The corresponding Breit–Wigner resonances overlap if the energy of the emitted photon is of the order of Γ_{W}. It is not obvious how to define the DPA for such photons. Therefore, the results based on a DPA for the real corrections have to be treated with some caution.

According to the above classification, there are four categories of contributions to $\mathcal{O}(\alpha)$ corrections in DPA: factorizable and non-factorizable ones both for virtual and real corrections. In the following the salient features of those four parts are described.

The sum of virtual and real non-factorizable corrections has been calculated in Refs. [108, 16, 17][3]. To obtain the virtual non-factorizable corrections alone, some supplements are needed [18]. The sum of virtual and real non-factorizable corrections is IR-finite and can be discussed separately. It is been shown in Ref. [19] that this sum vanishes if the invariant masses of both W bosons are integrated over, i.e. in particular that the full non-factorizable correction to the total cross section is zero in DPA. In Refs. [16, 17] the full non-factorizable corrections have also been discussed numerically. They vanish on top of the double resonance and are of the order of 1% in its vicinity. The shift in the W invariant-mass distributions

[3]The original result of the older calculation [108] does not agree with the two more recent results [16, 17], which are in mutual agreement. As known from the authors of Ref. [108], their corrected results also agree with the ones of Refs. [16, 17].

is only of the order of a few MeV. These results can be reproduced by a simple approximation [20] based on the so called screened Coulomb ansatz. However, it is important to note that all these numerical results on non-factorizable corrections are based on the DPA for real corrections and have been obtained in idealized treatment of phase space, namely the assumption that the W-boson momenta can be reconstructed from the fermion momenta alone, i.e. without photon recombination. It is not clear how these results change in physical situations with photon recombination.

Having summarized the general features of the DPA-approximation we turn to discuss the complete $\mathcal{O}(\alpha)$ radiative corrections to process (12) in the context of the DPA. As mentioned before, the most economic way of calculating the radiative corrections up to $\mathcal{O}(\alpha)$ precision involves the DPA. In this approximation all virtual corrections can be classified into two groups: factorizable and non-factorizable corrections. As discussed above, the real-photon corrections can also be classified in factorizable and non-factorizable corrections, although the various regimes for the photon energy require some special attention.

6.01 Virtual corrections

As a first step we discuss how to separate the virtual corrections into a sum of factorizable and non-factorizable virtual corrections. The diagrammatic split-up according to reducible and irreducible W-boson lines is an illustrative way of understanding the different nature of the two classes of corrections, but since the double-resonant diagrams are not gauge-invariant by themselves the precise split-up needs to be defined properly.

We can make use of the fact that there are effectively two scales in the problem: M_W and Γ_W. Let us now consider virtual corrections coming from photons with different energies:

- soft photons, $E_\gamma \ll \Gamma_W$,
- semi-soft photons, $E_\gamma = \mathcal{O}(\Gamma_W)$,
- hard photons, $\Gamma_W \ll E_\gamma = \mathcal{O}(M_W)$.

Only soft and semi-soft photons contribute to both factorizable and non-factorizable corrections. The latter being defined to describe interactions between different stages of the off-shell process. The reason for this is that only these photons can induce relatively long-range interactions and thereby allow the various sub-processes, which are separated by a propagation interval of $\mathcal{O}(1/\Gamma_W)$, to communicate with each other. Virtual corrections involving the exchange of hard photons or massive particles contribute exclusively to the factorizable corrections. In view of the short range of the interactions induced by these particles, their contribution to the non-factorizable corrections are suppressed by at least $\mathcal{O}(\Gamma_W/M_W)$.

As hard photons contribute to the factorizable corrections only, we merely need to define a split-up for soft and semi-soft photons. It is impossible to do this in a consistent gauge-invariant way on the basis of diagrams. In Ref. [29] it was shown that only part of particular diagrams should be attributed to the non-factorizable corrections, the rest being of factorizable nature. The complete set of non-factorizable corrections was obtained by collecting all terms that contain the ratios $D_i/[D_i \pm 2kp_i]$, where k denotes the momentum of the (semi-)soft photon. The so-defined non-factorizable corrections read

$$\mathcal{M}_{\text{nf}}^{\text{virt}} = i\mathcal{M}_{\text{DPA}}^{0} \int \frac{d^4k}{(2\pi)^4[k^2+io]} \Big[(\mathcal{J}_0^\mu + \mathcal{J}_\oplus^\mu)\mathcal{J}_{+,\,\mu} + (\mathcal{J}_0^\mu + \mathcal{J}_\ominus^\mu)\mathcal{J}_{-,\,\mu} + \mathcal{J}_+^\mu \mathcal{J}_{-,\,\mu} \Big], \tag{23}$$

which contains the gauge-invariant currents

$$\mathcal{J}_0^\mu = e\left[\frac{p_1^\mu}{kp_1+io} + \frac{p_2^\mu}{-kp_2+io}\right],$$

$$\mathcal{J}_\oplus^\mu = -\,e\left[\frac{q_1^\mu}{kq_1+io} - \frac{q_2^\mu}{kq_2+io}\right], \quad \mathcal{J}_\ominus^\mu = +\,e\left[\frac{q_1^\mu}{-kq_1+io} - \frac{q_2^\mu}{-kq_2+io}\right] \tag{24}$$

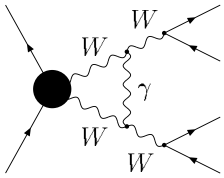

Fig. 3: The Coulomb graph, contributing to both factorizable and non-factorizable corrections.

for photon emission from the production stage of the process, and

$$\begin{aligned} \mathcal{J}_{+}^{\mu} &= -e\left[\frac{p_1^{\mu}}{kp_1+io}+Q_{f_1}\frac{k_1^{\mu}}{kk_1+io}-Q_{f_1'}\frac{k_1'^{\,\mu}}{kk_1'+io}\right]\frac{D_1}{D_1+2kp_1}, \\ \mathcal{J}_{-}^{\mu} &= -e\left[\frac{p_2^{\mu}}{-kp_2+io}+Q_{f_2}\frac{k_2^{\mu}}{-kk_2+io}-Q_{f_2'}\frac{k_2'^{\,\mu}}{-kk_2'+io}\right]\frac{D_2}{D_2-2kp_2} \end{aligned} \tag{25}$$

for photon emission from the decay stages of the process. Here $\mathcal{M}^0_{\rm DPA}$ is the lowest-order matrix element in DPA and Q_f stands for the charge of fermion f in units of e. After having defined the gauge-invariant currents, the $+io$ terms can be dropped from D_1+2kp_1 and D_2-2kp_2, since ${\rm Im}D_i > 0$. Note the difference in the sign of the io parts appearing in the currents $\mathcal{J}_{\ominus}$ and $\mathcal{J}_{\oplus}$. These signs actually determine which interference terms give rise to a non-vanishing non-factorizable contribution after virtual and real-photon corrections have been added. As a result of such considerations only a very limited subset of 'final-state' interferences survives [29, 40, 39]: the virtual corrections corresponding to Figs. 2 and 3 as well as the associated real-photon corrections. Since Eq. (23) contains (at least) all contributions from diagrams with irreducible W-boson lines, it can be viewed as a gauge-invariant extension of the set of W-irreducible diagrams.

The virtual factorizable corrections consist of all hard contributions and the left-over part of the semi-soft ones. The so-defined factorizable corrections have the nice feature that they can be expressed in terms of corrections to on-shell sub-processes, i.e. the production of two on-shell W bosons and their subsequent on-shell decays. The corresponding matrix element can be expressed in the same way as described at lowest-order:

$$\mathcal{M}^{\rm virt}_{\rm fact} = \sum_{\lambda_1,\lambda_2}\Pi_{\lambda_1\lambda_2}(M_1,M_2)\,\frac{\Delta^{(+)}_{\lambda_1}(M_1)}{D_1}\,\frac{\Delta^{(-)}_{\lambda_2}(M_2)}{D_2}. \tag{26}$$

Here two of the amplitudes are taken at lowest order, whereas the remaining one contains all possible one-loop contributions, including the W wave-function factors that appear in Eq. (10). In this way the well-known on-shell radiative corrections to the production and decay of pairs of W bosons [37]–[38] appear as basic building blocks of the factorizable corrections.[4] In the semi-soft limit the virtual factorizable corrections to the production stage, contained in Π, will cancel against the corresponding real-photon corrections. Non-vanishing contributions from Π occur as soon as the k^2 terms in the propagators cannot be neglected anymore. An example of this is the factorizable correction from the Coulomb graph Fig. 3. For the on-shell (factorizable) part of the Coulomb effect photons with momenta $k_0=\mathcal{O}(\Delta E)$ and $|\vec{k}| = \mathcal{O}(\sqrt{M_W\Delta E}\,)$ are important [41], i.e. k^2 cannot be neglected in the propagators of the unstable particles. Since we stay well away from the W-pair threshold ($\Delta E \equiv \sqrt{s}-2M_W \gg \Gamma_W$), this situation occurs outside the realm of the semi-soft photons. This fits nicely into the picture of the production stage being a hard subprocess, governed by relatively short time scales as compared with the much longer time scales required for the non-factorizable corrections, which interconnect the different sub-processes.

[4] Note that the complete density matrix is required in this case, in contrast to the pure on-shell calculation which involves the trace of the density matrix only.

6.02 Real-photon radiation

In this subsection we discuss the aspects of real-photon radiation in the DPA. To this end we consider the process

$$e^+(q_1)\, e^-(q_2) \to W^+(p_1)\, W^-(p_2)\, [\gamma(k)] \to \bar{f}_1(k_1) f_1'(k_1')\, f_2(k_2) \bar{f}_2'(k_2')\, \gamma(k), \tag{27}$$

where in the intermediate state there may or may not be a photon. We will show how to extract the gauge-invariant double-pole residues in different situations. The exact cross-section for process (27) can be written in the following form

$$d\sigma = \frac{1}{2s}|\mathcal{M}_\gamma|^2 d\Gamma_{4f\gamma} = \frac{1}{2s}\left[2\mathrm{Re}\Big(\mathcal{M}_0\mathcal{M}_+^* + \mathcal{M}_0\mathcal{M}_-^* + \mathcal{M}_+\mathcal{M}_-^*\Big) + |\mathcal{M}_0|^2 + |\mathcal{M}_+|^2 + |\mathcal{M}_-|^2\right] d\Gamma_{4f\gamma}, \tag{28}$$

where $d\Gamma_{4f\gamma}$ indicates the complete five-particle phase-space factor, and the matrix elements $\mathcal{M}_0$ and $\mathcal{M}_\pm$ correspond to the diagrams where the photon is attached to the production or decay stage of the three W-pair diagrams, respectively. This split-up can be achieved with the help of the partial-fraction decomposition

$$\frac{1}{D_i(D_i + 2pk)} = \frac{1}{2pk}\left(\frac{1}{D_i} - \frac{1}{D_i + 2pk}\right). \tag{29}$$

Each contribution to the cross-section can be written in terms of polarization density matrices, which originate from the amplitudes

$$\mathcal{M}_0 = \Pi_\gamma(M_1, M_2)\, \frac{\Delta^{(+)}(M_1)}{D_1}\, \frac{\Delta^{(-)}(M_2)}{D_2}\,, \tag{30}$$

$$\mathcal{M}_+ = \Pi(M_{1\gamma}, M_2)\, \frac{\Delta_\gamma^{(+)}(M_{1\gamma})}{D_{1\gamma}}\, \frac{\Delta^{(-)}(M_2)}{D_2}\,, \tag{31}$$

$$\mathcal{M}_- = \Pi(M_1, M_{2\gamma})\, \frac{\Delta^{(+)}(M_1)}{D_1}\, \frac{\Delta_\gamma^{(-)}(M_{2\gamma})}{D_{2\gamma}}\,, \tag{32}$$

where all polarization indices for the W bosons and the photon have been suppressed, and

$$D_{i\gamma} = D_i + 2kk_i + 2kk_i', \quad M_{i\gamma}^2 = M_i^2 + 2kk_i + 2kk_i', \quad M_i^2 = (k_i + k_i')^2. \tag{33}$$

The matrix elements Π_γ and $\Delta_\gamma^{(\pm)}$ describe the production and decay of the W bosons accompanied by the radiation of a photon. The matrix elements without subscript γ have been introduced in Eq. (13).

In the calculation of the Born matrix element and virtual corrections only two poles could be identified in the amplitudes, originating from the Breit–Wigner propagators $1/D_i$. The pole-scheme expansion was performed around these two poles. In contrast, the bremsstrahlung matrix element has four in general different poles, originating from the four Breit–Wigner propagators $1/D_i$ and $1/D_{i\gamma}$. As mentioned above, the matrix element can be rewritten as a sum of three matrix elements ($\mathcal{M}_0, \mathcal{M}_+, \mathcal{M}_-$), each of which only contain two Breit–Wigner propagators. For these three individual matrix elements the pole-scheme expansion is fixed, as before, to an expansion around the corresponding two poles. However, when calculating cross-sections [see Eq. (28)] the mapping of the five-particle phase space introduces a new type of ambiguity. The interference terms in Eq. (28) involve two different double-pole expansions simultaneously. As such there is no natural choice for the phase-space mapping in those cases. In Ref. [29] it was shown that the resulting ambiguity (implementation dependence) will not have significant repercussions on the quality of the DPA calculation.

Let us return now to the three earlier-defined regimes for the photon energy:

- for hard photons [$E_\gamma \gg \Gamma_W$] the Breit–Wigner poles of the W-boson resonances before and after photon radiation are well separated in phase space (see $M^2_{i\gamma}$ and M^2_i defined above). As a result, the interference terms in Eq. (28) can be neglected. This leads to three *distinct* regions of on-shell contributions, where the photon can be assigned unambiguously to the W-pair-production subprocess or to one of the two decays. This assignment is determined by the pair of invariant masses (out of M^2_i and $M^2_{i\gamma}$) that is in the M^2_W region. Therefore, the double-pole residue can be expressed as the sum of the three on-shell contributions without increasing the intrinsic error of the DPA. Note that in the same way it is also possible to experimentally assign the photon to one of the sub-processes, since misassignment errors are suppressed, assuming for convenience that all final-state momenta can ideally be measured.
- for semi-soft photons [$E_\gamma = \mathcal{O}(\Gamma_W)$] the Breit–Wigner poles are relatively close together in phase space, resulting in a substantial overlap of the line shapes. The assignment of the photon is now subject to larger errors. Moreover, since the interference terms in Eq. (28) cannot be neglected, a proper prescription for calculating the DPA residues (i.e. the phase-space mapping) is required [29].
- for soft photons [$E_\gamma \ll \Gamma_W$] the Breit–Wigner poles are on top of each other, resulting in a pole-scheme expansion that is identical to the one without the photon.

Let us first consider the hard-photon regime in more detail. Due to the fact that the poles are well separated in the hard-photon regime, it is clear that the interference terms are suppressed and can be neglected:

$$d\sigma = \frac{1}{2s}\Big[|\mathcal{M}_0|^2 + |\mathcal{M}_+|^2 + |\mathcal{M}_-|^2\Big]d\Gamma_{4f\gamma}. \tag{34}$$

Note that each of the three terms has two poles, originating from two resonant propagators. However, these poles are different for different terms. The phase-space factor can be rewritten in three equivalent ways. The first is

$$d\Gamma_{4f\gamma} = d\Gamma^\gamma_0 = d\Gamma^\gamma_{\text{pr}} \cdot d\Gamma^+_{\text{dec}} \cdot d\Gamma^-_{\text{dec}} \cdot \frac{dM_1^2}{2\pi} \cdot \frac{dM_2^2}{2\pi}, \tag{35}$$

with

$$d\Gamma^\gamma_{\text{pr}} = \frac{1}{(2\pi)^2}\,\delta(q_1+q_2-p_1-p_2-k)\,\frac{d\vec{p}_1}{2p_{10}}\,\frac{d\vec{p}_2}{2p_{20}}\,\frac{d\vec{k}}{(2\pi)^3 2k_0}. \tag{36}$$

The two others are

$$d\Gamma_{4f\gamma} = d\Gamma^\gamma_+ = d\Gamma_{\text{pr}} \cdot d\Gamma^{+\gamma}_{\text{dec}} \cdot d\Gamma^-_{\text{dec}} \cdot \frac{dM_{1\gamma}^2}{2\pi} \cdot \frac{dM_2^2}{2\pi}, \tag{37}$$

with

$$d\Gamma^{+\gamma}_{\text{dec}} = \frac{1}{(2\pi)^2}\,\delta(p_1-k_1-k_1'-k)\,\frac{d\vec{k}_1}{2k_{10}}\,\frac{d\vec{k}_1'}{2k_{10}'}\,\frac{d\vec{k}}{(2\pi)^3 2k_0}, \tag{38}$$

and a similar expression for $d\Gamma^\gamma_-$. The phase-space factors $d\Gamma_{\text{pr}}$ and $d\Gamma^\pm_{\text{dec}}$ are just the lowest-order ones. The cross-section can then be written in the following equivalent form

$$d\sigma = \frac{1}{2s}\Big[|\mathcal{M}_0|^2\,d\Gamma^\gamma_0 + |\mathcal{M}_+|^2\,d\Gamma^\gamma_+ + |\mathcal{M}_-|^2\,d\Gamma^\gamma_-\Big]. \tag{39}$$

In order to extract gauge-invariant quantities, the DPA limit should be taken. This amounts to taking the limit $p^2_{1,2} \to M^2_W$, using a particular prescription for mapping the full off-shell phase space on the kinematically restricted on-resonance one. Note however that $p_{1,2}$ can be different according to the δ-functions in the decay parts of the different phase-space factors. To be specific, the production term $|\mathcal{M}_0|^2$ has poles at $p_i^2 = M_i^2 = M_W^2$, $|\mathcal{M}_+|^2$ has poles at $p_1^2 = M^2_{1\gamma} = M^2_W$ and $p_2^2 = M_2^2 = M_W^2$, and $|\mathcal{M}_-|^2$ has poles at $p_1^2 = M_1^2 = M_W^2$ and $p_2^2 = M^2_{2\gamma} = M^2_W$.

We complete our survey of the different photon-energy regimes by considering semi-soft and soft photons. The split-up of factorizable and non-factorizable real-photon corrections proceeds in the same way as described in the previous subsection for virtual corrections. The result reads in semi-soft approximation

$$d\sigma = \frac{1}{2s}|\mathcal{M}_\gamma|^2 d\Gamma_{4f\gamma} \approx -\, d\sigma^0_{\rm DPA}\frac{d\vec{k}}{(2\pi)^3 2k_0}\left[2{\rm Re}\Big(\mathcal{I}^\mu_0\mathcal{I}^*_{+,\,\mu}+\mathcal{I}^\mu_0\mathcal{I}^*_{-,\,\mu}+\mathcal{I}^\mu_+\mathcal{I}^*_{-,\,\mu}\Big)+|\mathcal{I}^2_0|+|\mathcal{I}^2_+|+|\mathcal{I}^2_-|\right]. \tag{40}$$

The gauge-invariant currents $\mathcal{I}_0$ and $\mathcal{I}_\pm$ are given by

$$\begin{aligned}
\mathcal{I}^\mu_0 &= e\left[\frac{p_1^\mu}{kp_1}-\frac{p_2^\mu}{kp_2}-\frac{q_1^\mu}{kq_1}+\frac{q_2^\mu}{kq_2}\right],\\
\mathcal{I}^\mu_+ &= -\,e\left[\frac{p_1^\mu}{kp_1}+Q_{f_1}\frac{k_1^\mu}{kk_1}-Q_{f_1'}\frac{k_1'^{\,\mu}}{kk_1'}\right]\frac{D_1}{D_1+2kp_1},\\
\mathcal{I}^\mu_- &= +\,e\left[\frac{p_2^\mu}{kp_2}+Q_{f_2}\frac{k_2^\mu}{kk_2}-Q_{f_2'}\frac{k_2'^{\,\mu}}{kk_2'}\right]\frac{D_2}{D_2+2kp_2}.
\end{aligned} \tag{41}$$

The first three interference terms in Eq. (40) correspond to the real non-factorizable corrections. The last three squared terms in Eq. (40) belong to the factorizable real-photon corrections. They constitute the semi-soft limit of Eq. (39).

6.1 Intrinsic ambiguities and reliability of the double-pole approximation

A naive estimate for the intrinsic uncertainty of the DPA is given by $(\alpha/\pi)\times(\Gamma_{\rm W}/M_W)\times\log(\cdots)\lesssim 0.5\%$, which accounts for the relative size of the neglected corrections to background diagrams, including possible logarithmic enhancements. However, this estimate can fail whenever small scales play an essential role in the cross section. As mentioned above, this is definitely the case near the W-pair threshold and in the single-W region.

Whether the naive estimate is reliable for the emission of semi-soft photons, where $E_\gamma\sim\Gamma_{\rm W}$, is not clear a priori. Only a detailed numerical comparison between the DPA and the exact calculation of $4f+\gamma$ production can answer this question. Note that this issue is also closely related to the impact of non-factorizable corrections, since the definition of real non-factorizable corrections implicitly assumes a treatment of $4f+\gamma$ production in DPA. Thus, the question about the size of non-factorizable corrections should always be discussed in connection with the more general question about the quality of treating photon radiation within DPA.

An improved assessment of the theoretical uncertainty can be obtained by varying predictions within the intrinsic freedom of the followed approach for the DPA. For instance, any kind of DPA makes use of an on-shell projection of the off-shell four-fermion phase space to the phase space with on-shell W bosons. The difference between different on-shell projections is part of the theoretical uncertainty of the DPA approach and should be considered in predictions.

Besides the matrix element, the DPA can also be applied to the phase space. While this further approximation is not needed in a generator, it is useful in a semi-analytic approach. Moreover, it can help to assess the intrinsic ambiguity of the DPA.

It is a fact of life that questions of principle are sometimes of scarce practical relevance. CC03 contains gauge-invariance-breaking terms but what is their numerical impact at LEP 2 energies? It is quite a known fact that, when computed in the 't Hooft-Feynman gauge, they are unimportant. At least they are for the WW total cross-section – the signal – and we can verify this statement by comparing the gauge-dependent CC03 with the full gauge-invariant cross-section (CC11 for instance) including background diagrams. There is a general agreement, dating from the '95 workshop that the difference is less than 0.2% at LEP 2 energies.

It is bizarre that one can render the Born CC03 diagrams gauge-invariant at the prize of large numerical variations; it is enough if to project the kinematics onto the on-shell phase space, while keeping

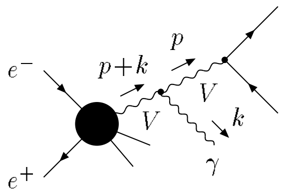

Fig. 4: Photon radiation from an unstable particle V. Virtualities: $s_V = p^2$ and $s'_V = (p+k)^2$.

the off-shellness in the Breit-Wigner propagators. However, this changes the cross-section by several per cent! At the Born level, therefore, one can accept a non-gauge-invariant CC03 cross-section (at least in the 't Hooft-Feynman gauge) as a reasonable quantity at LEP 2 energies. For higher energies one should be more careful.

The same phenomenon will occur when we include radiative corrections and we would like to add some comment on the DPA procedure, in particular on the arbitrariness introduced by projecting the kinematics.

For high enough energies, any process $e^+e^- \to VV$ will be a dominant source of fermion pairs due to the double resonant enhancement and hence CC03(NC02) well be a good approximation to the total cross-section for four-fermion production. Thus, for example, to calculate the cross-section $e^+e^- \to VV$ one proceeds as described above; one calculates the matrix element for $e^+e^- \to VV \to 4f$ and extract the part resonant in the invariant masses of the pairs, k_+^2, k_-^2. The general matrix element takes the form

$$\mathcal{M}\left(\dots, k_+, k_-, \dots\right) = \sum_i M_i\left(\dots, k_+, k_-, \dots\right)\, A_i\left(\dots, k_+^2, k_-^2\right), \tag{42}$$

where the M_i contain the spinor and Lorentz tensor structure of the matrix element, e.g. they have the external fermionic wave-functions attached. The A_i are Lorentz scalars that depends on the invariants of the problem and become non-trivial and difficult to compute when higher order corrections are included. One way of looking at the DPA-procedure is to say that the resonant part is extracted from the A_i, by Laurent expansion. The external particle wave functions should not be affected by the process hence the kinematics of the problem should be left unchanged because the final state integrations involve only the fermions, stable on-shell particles. The gauge nature of the theory is intimately connected with the A_i not with kinematics. This is hardly a surprise, even in Born CC03 two calculations performed in two different gauges differ by single resonant terms.

6.11 Remarks on DPA corrections to inclusive-photon distributions

The DPA corrections to inclusive-photon distributions depend in a very sensitive way on how the four-particle phase space is parametrized, or, in other words, on the way the distributions are defined after the photon has been integrated out. This statement sounds obvious, but nevertheless deserves some special attention.

In particular the invariant-mass distributions (W line shapes) are affected. In reactions with two resonances the invariant masses have to be defined from the decay products. Depending on the precise definition of the invariant masses different sources of large Breit–Wigner distortions can be identified [42], in contrast to the situation at LEP1 where only initial-state radiation (ISR) can cause such distortions. In Ref. [42] it has been shown that also final-state radiation (FSR) can induce distortions. This is a general property of resonance-pair reactions, irrespective of the adopted scheme for implementing the finite-width effects. The only decisive factor for the distortion to take place is whether the virtuality of the unstable particle is defined with (s'_V) or without (s_V) the radiated photon (see Fig. 4). Upon integration over the photon momentum, the former definition (cf $M_{i\gamma}^2$ defined in Sec. 6.02) is free of large FSR effects from the V-decay system. It can only receive large corrections from the other (production or *decay*) stages of the process. The latter definition (cf M_i^2 defined in Sec. 6.02), however, does give rise to large FSR effects from the *V-decay system*. In contrast to the LEP1 case, where the ISR-corrected line shape receives contributions from effectively *lower* Z-boson virtualities, the s_V line shape receives contributions from effectively *higher* virtualities s'_V of the unstable particle. As was argued above, only sufficiently hard photons ($E_\gamma \gg \Gamma_V$) can be properly assigned to one of the on-shell production or decay stages of the process in the DPA. For semi-soft photons [$E_\gamma = \mathcal{O}(\Gamma_V)$], however, the assignment lacks a solid motivation and an invariant-mass definition in terms of the decay products without the photon seems more natural. As was pointed out in Ref. [42], exactly these semi-soft photons are responsible for the FSR-induced distortion effects. The hard FSR photons move the virtuality s'_V of the unstable particle far off resonance for near-resonance s_V values, resulting in a suppressed contribution to the s_V line shape. This picture fits in nicely with the negligible overlap of the three on-shell double-pole contributions for hard photons, discussed above. The reason why the FSR distortions can be rather large lies in the fact that the final-state collinear singularities [$\propto \frac{\alpha}{\pi} Q_f^2 \log(m_f^2/M_V^2) \log(\Gamma_V/M_V)$] do not vanish, even not for fully inclusive photons. After all, a fixed value of s_V makes it impossible to sum over all degenerate final states by a mere integration over the photon momentum. So the KLN theorem does not apply in this case.

In Ref. [43] these FSR distortion effects have been investigated in detail for realistic event-selection procedures, resulting in shifts in the measurement of the W-boson mass of the order of 20 MeV.

When considering pure angular inclusive-photon distributions, one should integrate over the photon phase space *and* the invariant masses M_i^2. After integrating out both invariant masses the non-factorizable corrections will vanish, which is a typical feature of the non-factorizable interference effects [35].

6.2 Double-pole approximations in practice

For LEP2 energies three different groups[5] have formulated versions of a DPA for $\mathrm{e^+e^-} \to \mathrm{WW} \to 4f(+\gamma)$. While Beenakker, Berends and Chapovsky [22], called BBC in the following, formulated a semi-analytic DPA, the other two groups implemented variants of the DPA in the event generators `YFSWW` [23, 24] and `RacoonWW` [18, 109]. The basic features of these different implementations are summarized in the following.

6.21 The `YFSWW` approach

`YFSWW`: $\mathcal{O}(\alpha)$ correction to $\mathrm{e^+e^-} \to \mathrm{W^+W^-}$, leading-log corrections to W decays via PHOTOS and branching ratios, YFS exponentiation for ISR and photon emission from W-bosons, off-shell Coulomb singularity, no non-factorizable corrections, no W spin correlations

6.22 The BBC approach

BBC: full semi-analytical DPA (with non-factorizable corrections and W spin correlations), on-shell Coulomb singularity, no physical photon recombination, unphysical angles (angles are defined differently for initial- and final-state radiation)

6.23 The `RacoonWW` approach

`RacoonWW` [18, 109] treats the virtual $\mathcal{O}(\alpha)$ corrections to $\mathrm{e^+e^-} \to \mathrm{WW} \to 4f$ in DPA. No further approximations beyond the pole expansion of the matrix element are made, i.e. non-factorizable corrections are included, and W-spin correlations are respected. The off-shell Coulomb singularity is part of the virtual corrections. The real $\mathcal{O}(\alpha)$ corrections are based on the full $4f + \gamma$ matrix element (of the CC11 class), so that the full kinematics is supported also for photon radiation. All matrix elements are based on

[5] Another DPA has been discussed in Ref. [21] for linear-collider energies.

massless fermions, and fermion masses are introduced only for collinear photon emission that is inclusive within a (small) finite cone for each fermion. Thus, a photon collinear to an outgoing fermion has to be recombined with the corresponding fermion, and a photon close to the beams has to be considered as invisible. Initial-state radiation beyond $\mathcal{O}(\alpha)$ is treated in the structure-function approach, including soft-photon exponentiation and leading-log contributions in $\mathcal{O}(\alpha^2)$.

7. The fermion-loop and non-local approaches

As was mentioned above, the alternative to *subtracting* sub-leading gauge-violating terms is to *add* gauge-restoring terms to the calculation. In order to do this, one has to add to the amplitude those terms that are needed for satisfying the Ward identities. This is not easy to do in general. The following observation helps. The very fact that the perturbative amplitudes require re-summation of the self-energies indicates that either the perturbative expansion parameter (coupling constant) is not the proper one, or alternatively that the quantity that is expanded (i.e. the lowest-order Lagrangian of the Standard Model) is not the best choice. This observation leads one to consider first the one-loop corrected effective potential of the Standard Model before doing Born calculations, in order to avoid Dyson re-summation of the self-energies.

For the discussion of the fermion-loop and non-local approaches it is therefore worthwhile to first have a closer look at the origin of the gauge-invariance problem associated with the re-summation of self-energies. To this end we consider the simple example of an unbroken non-abelian $SU(N)$ gauge theory with fermions and subsequently integrate out these fermions.

First we fix our notation and introduce some conventions. The $SU(N)$ generators in the fundamental representation are denoted by T^a with $a = 1, \cdots, N^2-1$. They are normalized according to $\mathrm{Tr}\,(\mathrm{T}^a\mathrm{T}^b) = \delta^{ab}/2$ and obey the commutation relation $\left[\mathrm{T}^a, \mathrm{T}^b\right] = i f^{abc}\,\mathrm{T}^c$. In the adjoint representation the generators F^a are given by $(\mathrm{F}^a)^{bc} = -i f^{abc}$. The Lagrangian of the unbroken $SU(N)$ gauge theory with fermions can be written as

$$\mathcal{L}(x) = -\frac{1}{2}\,\mathrm{Tr}\left[\boldsymbol{F}_{\mu\nu}(x)\,\boldsymbol{F}^{\mu\nu}(x)\right] + \bar{\psi}(x)\,(i\,\not{D} - m)\,\psi(x), \tag{43}$$

with

$$\boldsymbol{F}_{\mu\nu} \equiv \mathrm{T}^a F^a_{\mu\nu} = \frac{i}{g}\,[D_\mu, D_\nu], \qquad D_\mu = \partial_\mu - ig\,\mathrm{T}^a A^a_\mu \equiv \partial_\mu - ig\boldsymbol{A}_\mu. \tag{44}$$

Here ψ is a fermionic N-plet in the fundamental representation of $SU(N)$ and A^a_μ are the (N^2-1) non-abelian $SU(N)$ gauge fields, which form a multiplet in the adjoint representation. The Lagrangian (43) is invariant under the $SU(N)$ gauge transformations

$$\psi(x) \to \psi'(x) = \mathrm{G}(x)\,\psi(x),$$

$$\boldsymbol{A}_\mu(x) \to \boldsymbol{A}'_\mu(x) = \mathrm{G}(x)\,\boldsymbol{A}_\mu(x)\,\mathrm{G}^{-1}(x) + \frac{i}{g}\,\mathrm{G}(x)\left[\partial_\mu \mathrm{G}^{-1}(x)\right], \tag{45}$$

with the $SU(N)$ group element defined as $\mathrm{G}(x) = \exp[ig\,\mathrm{T}^a\theta^a(x)]$. The covariant derivative D_μ and field strength $\boldsymbol{F}_{\mu\nu}$ both transform in the adjoint representation

$$D_\mu \to \mathrm{G}(x)\,D_\mu\,\mathrm{G}^{-1}(x), \qquad \boldsymbol{F}_{\mu\nu}(x) \to \mathrm{G}(x)\,\boldsymbol{F}_{\mu\nu}(x)\,\mathrm{G}^{-1}(x). \tag{46}$$

Since the Lagrangian is quadratic in the fermion fields, one can integrate them out exactly in the functional integral. The resulting effective action is then given by

$$i\,S_{\text{eff}}[J] = i\int d^4x\,\left\{-\frac{1}{2}\,\mathrm{Tr}\left[\boldsymbol{F}_{\mu\nu}(x)\,\boldsymbol{F}^{\mu\nu}(x)\right] + J^a_\mu(x)\,A^{a,\mu}(x)\right\} + \mathrm{Tr}\left[\ln(-\not{D} - i\,m)\right], \tag{47}$$

with $J^a_\mu(x)$ denoting the gauge-field sources. The trace on the right-hand side has to be taken in group, spinor, and coordinate space. As a next step one can expand the effective action in terms of the coupling constant

$$\begin{aligned}\mathrm{Tr}\Big[\ln(-\not{D} - i\,m)\Big] &= \mathrm{Tr}\Big[\ln(-\not{\partial} - i\,m)\Big] + \mathrm{Tr}\Big[\ln\Big(1 + \frac{g}{i\,\not{\partial} - m}\,\not{\boldsymbol{A}}\Big)\Big] \\ &= \mathrm{Tr}\Big[\ln(-\not{\partial} - i\,m)\Big] + \sum_{n=1}^{\infty}\frac{(-1)^{n-1}}{n}\,\mathrm{Tr}\Big[\Big(\frac{g}{i\,\not{\partial} - m}\,\not{\boldsymbol{A}}\Big)^n\Big]. \qquad (48)\end{aligned}$$

Note that the left-hand side of Eq. (48) is gauge-invariant as a result of the trace-log operation. In contrast, the separate terms of the expansion on the right-hand side are not gauge-invariant. This is due to the fact that, unlike in the abelian case, the non-abelian gauge transformation (45) mixes different powers of the gauge field A_μ in Eq. (48). Thus, if one truncates the series on the right-hand side of Eq. (48) one will in general break gauge invariance. From Eq. (48) it is also clear that the fermionic part of the effective action induces higher-order interactions between the gauge bosons.

What are these higher-order interactions? Let us consider the quadratic gauge-field contribution

$$-\frac{1}{2}\,\mathrm{Tr}\Big[\Big(\frac{g}{i\,\not{\partial} - m}\,\not{\boldsymbol{A}}\Big)^2\Big] = -\frac{1}{2}\int d^4x\, d^4y\,\mathrm{Tr}\Big[O(x,y)\,O(y,x)\Big], \qquad (49)$$

where

$$O(x,y) = g\,S_{\mathrm{F}}^{(0)}(x-y)\,\not{\boldsymbol{A}}(y) \qquad (50)$$

and $i\,S_{\mathrm{F}}^{(0)}(x-y) = <0\,|\,T(\psi(x)\,\bar{\psi}(y))\,|\,0>_{\mathrm{free}}$ is the free fermion propagator. The trace on the right-hand side of Eq. (49) has to be taken in group and spinor space. A quick glance at this quadratic gauge-field contribution reveals that it is just the one-loop self-energy of the gauge boson induced by a fermion loop. In the same way, the higher-order terms $\sim g^n A^n$ in Eq. (48) are just the fermion-loop contributions to the n-point gauge-boson vertices.

One can truncate the expansion in Eq. (48) at $n = 2$, thus taking into account only the gauge-boson self-energy term and neglecting the fermion-loop contributions to the higher-point gauge-boson vertices. This is evidently the simplest procedure for performing the Dyson re-summation of the fermion-loop self-energies. However, as was pointed out above, truncation of Eq. (48) at any finite order in g in general breaks gauge invariance. This leads to the important observation that, *although the re-summed fermion-loop self-energies are gauge-independent by themselves, the re-summation is nevertheless responsible for gauge-breaking effects in the higher-point gauge-boson interactions through its inherent mixed-order nature*. Another way of understanding this is provided by the gauge-boson Ward identities. Since the once-contracted n-point gauge-boson vertex can be expressed in terms of $(n-1)$-point vertices, it is clear that gauge invariance is violated if the self-energies are re-summed without adding the necessary compensating terms to the higher-point vertices.

An alternative is to keep all the terms in Eq. (48). Then the matrix elements derived from the effective action will be gauge-invariant. Keeping all the terms means that we will have to take into account not only the fermion-loop self-energy in the propagator, but also all the possible fermion-loop contributions to the higher-point gauge-boson vertices. This is exactly the prescription of the fermion-loop scheme (FLS) [27, 30, 31, 32]. Although the FLS guarantees gauge invariance of the matrix elements, it has disadvantages as well. Its general applicability is limited to those situations where non-fermionic particles can effectively be discarded in the self-energies, as is for instance the case for Γ_W and Γ_Z at lowest order. Another disadvantage is that in the FLS one is forced to do the loop calculations, even when calculating lowest-order quantities. For example, the calculation of the tree-level matrix element for the process $e^+e^- \to 4f\gamma$ involves a four-point gauge-boson interaction, which has to be corrected by fermion loops in the FLS. This overcomplicates an otherwise lowest-order calculation.

It is clear that the FLS provides more than we actually need. It does not only provide gauge invariance for the Dyson re-summed matrix elements at a given order in the coupling constant, but it also takes into account all fermion-loop corrections at that given order. In the vicinity of unstable particle resonances the imaginary parts of the fermion-loop self-energies are effectively enhanced by $\mathcal{O}(1/g^2)$ with respect to the other fermion-loop corrections. Therefore, what is really needed is only a minimal subset of the non-enhanced contributions such that gauge invariance is restored. In a sense one is looking for a minimal solution of a system of Ward identities. The FLS provides a solution, but this solution is far from minimal and is only practical for particles that decay exclusively into fermions. Since the decay of unstable particles is a physical phenomenon, it seems likely that there exists a simpler and more natural method for constructing a solution to a system of Ward identities, without an explicit reference to fermions. This is precisely the philosophy behind the non-local approach [33]. This approach consists in using gauge-invariant non-local effective Lagrangians for generating both the self-energy effects in the propagators and the required gauge-restoring terms in the higher-point interactions. In this way the full set of Ward identities can be solved, while keeping the gauge-restoring terms to a minimum.

7.1 The fermion-loop scheme

The Fermion-Loop scheme developed in [27] and refined in [31] makes the approximation of neglecting all masses for the incoming and outgoing fermions in the processes $e^+e^- \to n$ fermions.

It is possible, however, to give the construction of a complete, massive-massive, Fermion-Loop scheme (MFL), i.e., a scheme for incorporating the finite-width effects in the theoretical predictions for tree-level, LEP 2 and beyond, processes [44].

One can work in the 't Hooft-Feynman gauge and create all relevant building blocks, namely the vector-vector, vector-scalar and scalar-scalar transitions of the theory, all of them one-loop re-summed. The loops, entering the scheme, contains fermions and, as done before in [31], we allow for a non-zero top quark mass inside loops. There is a very simple relation between re-summed transitions and running parameters, since Dyson re-summation is most easily expressed in terms of running coupling constants and running sinuses.

In the MFL generalization, it is particularly convenient to introduce additional running quantities. They are the running masses of the vector bosons, $M_0^2(p^2) = M^2(p^2)/c^2(p^2)$, formally connected to the location of the W and Z complex poles. After introducing these running masses, it is straightforward to prove that all $\mathcal{S}$-matrix elements of the theory assume a very simple structure. Coupling constants, sinuses and masses are promoted to running quantities and the $\mathcal{S}$-matrix elements retain their Born-like structure, with running parameters instead of bare ones, and vector-scalar or scalar-scalar transitions disappear if we employ unitary-gauge–like vector boson propagators where the masses appearing in the denominator of propagators are the running ones.

The renormalization of ultraviolet divergences can be easily extended to the MFL-scheme by showing that all ultraviolet divergent parts of the one-loop vertices, γWW, $\gamma W\phi$, $\gamma\phi W$ and $\gamma\phi\phi$ for instance, are proportional to the lowest order part. Therefore, the only combinations that appear are of the form $1/g^2 + VVV$ vertex or $M^2/g^2 + VV\phi$ vertex etc. All of them are, by construction, ultraviolet finite.

Equipped with the generalization of the Fermion-Loop scheme, one can prove the fully-massive U(1) Ward identity which guarantees that it exists a correct treatment of the single-W processes. As a by-product of the method, the cross-section for single-W production automatically evaluates all channels at the right scale, without having to use ad hoc re-scalings and avoiding the approximation of a unique scale for all terms contributing to the cross-section.

The generalization of the Fermion-Loop scheme goes beyond its, most obvious, application to single-W processes and allows for a gauge invariant treatment of all $e^+e^- \to n$ fermion processes with a correct evaluation of the relevant scales. Therefore, the MFL-scheme can be applied to several other processes like $e^+e^- \to Z\gamma^*$ and, in general to all $e^+e^- \to 6$ fermion processes, with the inclusion of top quarks.

7.2 The non-local approach

The main idea of the non-local approach is to rearrange the series on the right-hand side of Eq. (48) in such a way that each term becomes gauge-invariant by itself. Subsequent truncation of the series at a given term is then allowed. It is possible to approximate Eq. (48) by means of an effective Lagrangian in such a way that the resulting effective action has the following properties:

- it generates the Dyson re-summed transverse gauge-boson self-energy in the propagator. This means that it contributes to the gauge-boson two-point function. Hence, the effective lagrangian should depend at least on two gauge-boson fields.
- the Dyson re-summed self-energy is in general not a constant, but rather a function dependent on the interaction between the gauge-bosons and the fermions. This means that the effective Lagrangian should in general be non-local (bi-local) in the gauge fields. Thus the gauge fields should be taken at two different space–time points.
- it is gauge-invariant. As such the effective Lagrangian should have the form of an infinite tower of gauge fields.

For the gauging procedure of the non-local Lagrangians we will need a special ingredient, the *path-ordered exponential*, which is defined as

$$U(x,y) = U^{\dagger}(y,x) \;=\; \mathrm{P}\exp\left[-\,ig\int\limits_{x}^{y} \boldsymbol{A}_{\mu}(\omega)\,d\omega^{\mu}\right] \tag{51}$$

Here $d\omega^{\mu}$ is the element of integration along some path $\Omega(x,y)$ that connects the points x and y [6]. The so-defined path-ordered exponential transforms as

$$U(x,y) \to \mathrm{G}(x)\,U(x,y)\,\mathrm{G}^{-1}(y) \tag{52}$$

under the $SU(N)$ gauge transformations. It hence carries the gauge transformation from one space-time point to the other.

For a $SU(N)$ Yang–Mills theory the non-local action with the above-described properties takes the form

$$\mathcal{S}_{\mathrm{NL}} = -\,\frac{1}{2}\int d^4x\, d^4y\, \Sigma_{\mathrm{NL}}(x-y)\,\mathrm{Tr}\left[U(y,x)\,\boldsymbol{F}_{\mu\nu}(x)\,U(x,y)\,\boldsymbol{F}^{\mu\nu}(y)\right] \equiv \int d^4x\, d^4y\,\mathcal{L}_{\mathrm{NL}}(x,y), \tag{53}$$

with $\mathcal{L}_{\mathrm{NL}}(x,y)$ the non-local effective Lagrangian. As required, the action contains bilinear gauge-boson interactions. The induced infinite tower of higher-point gauge-boson interactions, which are also of progressively higher order in the coupling constant g, is needed for restoring gauge invariance.

It is important to stress at this point that this term in the effective action should not be understood as a new fundamental interaction. It is generated by radiative corrections. From the point of view of general properties of non-local Lagrangians, the non-local coefficient $\Sigma_{\mathrm{NL}}(x-y)$ is arbitrary. In practice, however, it is fixed by the explicit interaction between the gauge-bosons and the fermions in the underlying fundamental theory. In our simple example this connection is simply given by Eq. (48).

Let us now derive the two-point function as an example of the Feynman rules generated by Eq. (53):

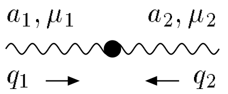

$$:\; i\,\Sigma^{a_1a_2,\,\mu_1\mu_2}(x_1,x_2) = \left.\frac{i\,\delta^2(\mathcal{S}_{\mathrm{L}}+\mathcal{S}_{\mathrm{NL}})}{\delta A^{a_1}_{\mu_1}(x_1)\,\delta A^{a_2}_{\mu_2}(x_2)}\right|_{A=0}, \tag{54}$$

[6] In principle we are free to choose this particular path. This freedom is just one out of the many freedoms that characterize the treatment of unstable particles (as mentioned earlier). It just reflects the fact that in a perturbative expansion one is free to pick up additional higher-order contributions, since the answer at any given (truncated) order will not be changed by such additional terms

where the local action $\mathcal{S}_{\rm L}$ follows from the gauge-boson term in Eq. (43). The Fourier transform of this two-point function can be calculated in a straightforward way, since the path-ordered exponentials are effectively unity. The result reads

$$i\,\tilde{\Sigma}^{a_1a_2,\,\mu_1\mu_2}(q_1,q_2) = i\,\delta^{a_1a_2}\Big(q_1^{\mu}q_1^{\nu} - q_1^2 g^{\mu\nu}\Big)\,\Big[1+\tilde{\Sigma}_{\rm NL}(q_1^2)\Big]\,(2\pi)^4\,\delta^{(4)}(q_1+q_2). \tag{55}$$

Note that this two-point interaction is transverse, as it should be for an unbroken theory. The non-local coefficient acts as a (dimensionless) correction to the transverse free gauge-boson propagator. So, exactly what is needed for the Dyson re-summation of the gauge-boson self-energies. The infinite tower of gauge-restoring higher-point gauge-boson interactions are provided by the gauge-boson fields present in both $\boldsymbol{F}_{\mu\nu}$ and the path-ordered exponential occurring in Eq. (53). For explicit Feynman rules we refer to Ref. [33].

Although the above-described non-local procedure provides a gauge-invariant framework for performing the Dyson re-summation of the gauge-boson self-energies, we want to stress that it is not unique. We have seen above that the FLS provides a different solution of the system of gauge-boson Ward identities. In the context of non-local effective Lagrangians it is always possible to add additional towers of gauge-boson interactions that start with three-point interactions and therefore do not influence the Dyson re-summation of the gauge-boson self-energies.

In the light of the discussion presented in Sect. 7., we rearrange the series on the right-hand side of Eq. (48) according to gauge-invariant towers of gauge-boson interactions labelled by the minimum number of gauge bosons that are involved in the non-local interaction. Effectively this constitutes an expansion in powers of the coupling constant g, since a higher minimum number of particles in the interaction is equivalent to a higher minimum order in g. In order to achieve minimality we have truncated this series at the lowest effective order. This should not be viewed as some *ad hoc* recipe, but rather as a systematic expansion of the effective potential.

Up to now we have seen how the non-local effective Lagrangian method works for unstable gauge bosons in a simple $SU(N)$ gauge theory with fermions. In the Standard Model there are different types of unstable particles: the top-quark, the massive gauge-bosons, the Higgs boson. In Ref. [33] it was shown how to extend the above-described method in such a way that it allows the description of all the unstable particles in terms of bi-local effective Lagrangians.

8. Results for the CC03 cross-section, σ_{WW}

As mentioned before, an electroweak $\mathcal{O}(\alpha)$ CC03 cross-section is available, showing a result that is between -1% and -1.5% smaller than the old CC03 cross-section predicted with GENTLE. This is a big effect since the combined experimental accuracy of LEP experiments is of the same magnitude. It is, therefore, of the upmost importance to discuss the numerical predictions for the DPA-corrected CC03 cross-section. Therefore, in this Section, we present numerical results and also an accurate description of the comparisons between different approaches, YFSWW, BBC and RacoonWW. By comparing different calculations one can numerically check the quality of the DPA for CC03.

8.1 CC03 with RacoonWW

Authors

Ansgar Denner	ansgar.denner@psi.ch
Stefan Dittmaier	stefan.dittmaier@cern.ch
Markus Roth	markus.roth@itp.uni-leipzig.de
Doreen Wackeroth	dow@pas.rochester.edu

8.11 General description

The program RacoonWW [45] evaluates cross sections and differential distributions for the reactions $\mathrm{e^+e^-} \to 4\mathrm{f}$ and $\mathrm{e^+e^-} \to 4\mathrm{f} + \gamma$ for all four-fermion final states. For the W-pair mediated channels $\mathrm{e^+e^-} \to \mathrm{WW} \to 4\mathrm{f}(+\gamma)$ the full virtual $\mathcal{O}(\alpha)$ corrections are taken into account in double-pole approximation (DPA), while for the corresponding real corrections the full $4\mathrm{f}+\gamma$ matrix elements are used. Beyond $\mathcal{O}(\alpha)$, leading-logarithmic corrections from initial-state radiation (ISR) are included via structure functions. Since the matrix elements are calculated as helicity amplitudes, any helicity configuration can be studied. For tree-level predictions of $4\mathrm{f}$ and $4\mathrm{f}+\gamma$ production, contributions of subsets of diagrams, such as CC03, can be selected. The phase-space integration is performed by the multi-channel Monte Carlo technique, thus allowing for the implementation of general experimental cuts and photon recombination procedures. The program produces weighted events.

8.12 Features of the program

- **Lowest order:** the full matrix elements for all $4\mathrm{f}$ final states are included, and the contribution of the CC03 matrix elements or of other subsets of diagrams is provided as an option. All external fermions are assumed to be massless.
- **Virtual $\mathcal{O}(\alpha)$ corrections:** the full one-loop corrections are included in DPA, i.e. all factorizable corrections [110] and non-factorizable corrections [47]. In this way, full W-spin correlations are taken into account.
- **Real corrections — $4\mathrm{f}+\gamma$ production**: the cross sections are based on the full matrix-element calculation [48] for all $4\mathrm{f}+\gamma$ final states with massless fermions. If the process $\mathrm{e^+e^-} \to 4f+\gamma$ is investigated with a separable photon, i.e. if the photon is neither soft nor collinear to a charged fermion, all $4\mathrm{f}+\gamma$ final states are possible, and subsets of diagrams can be chosen as options (e.g. boson-pair production diagrams, QCD background diagrams). If the real corrections to $\mathrm{e^+e^-} \to \mathrm{WW} \to 4f$ are calculated, the full $4\mathrm{f}+\gamma$ matrix elements for the CC11 class[7] are taken, i.e. photon radiation from background diagrams is partially included. The treatment of fermion-mass singularities is described below.
- **ISR:** higher-order ISR is implemented via structure functions for the incoming electron and positron. The structure functions used are those of Ref. [49] with the 'BETA' choice and the explicit β^3 terms omitted, i.e. the collinear-soft leading logarithms are exponentiated. If the $\mathcal{O}(\alpha)$

[7] The CC11 class is the smallest gauge-invariant subset of diagrams for $\mathrm{e^+e^-} \to 4f$ that contains all graphs with two resonant W bosons; in this class only those background diagrams are missing that are peculiar to $\mathrm{e^\pm}$, ν_e, $\bar\nu_\mathrm{e}$, or $f\bar f$ pairs in the final state.

corrections to $\mathrm{e^+e^-} \to \mathrm{WW} \to 4f$ are included, the $\mathcal{O}(\alpha)$ contributions already contained in the structure functions are subtracted, in order to avoid double counting, and the full CC11 Born matrix elements are used in the convolution.

- **Treatment of collinear photons:** the program is only applicable to observables that involve no mass-singular contributions from the final state. These mass singularities cancel if all photons collinear to a charged final-state fermion are combined with this fermion. The recombination procedure is controlled by recombination cuts, i.e. photon emission angles and photon energies, or invariant masses of photon–fermion pairs. Specifically, first the charged fermion that is closest to the photon according to these criteria (emission angle or invariant mass) is selected, and secondly the photon is recombined with this fermion if it is within the recombination cuts for a final-state fermion and discarded for an initial-state fermion. The mass singularities that remain from collinear photon emission off initial-state electron or positron [i.e. the $(\alpha \ln m_{\mathrm{e}})^n$ terms] are included in the structure functions.
  Depending on the choice of the user, the cancellation of collinear singularities is performed within the phase-space slicing method or within the subtraction formalism of Ref. [50]. In both cases, care is taken in avoiding mismatch between the singularities of the virtual and the real corrections, which is non-trivial owing to the application of the DPA to the virtual corrections only.
- **Coulomb singularity:** within DPA it is fully included in the $\mathcal{O}(\alpha)$ corrections. The full off-shell behaviour of the singularity as described in Ref. [47] can be switched on as an option.
- **Finite gauge-boson widths:** in the tree-level processes $\mathrm{e^+e^-} \to 4\mathrm{f}, 4\mathrm{f}+\gamma$ several options are included, such as fixed-width, running-width, and complex-mass scheme [48]. If $\mathcal{O}(\alpha)$ corrections are taken into account the fixed width is automatically used.
- **Cuts:** since each event is completely specified, in principle any conceivable phase-space cut can be implemented. However, since all fermions are taken to be massless, singularities can occur in photon-exchange channels, rendering cuts unavoidable. In particular, if a charged fermion–antifermion pair is produced, a lower cut on its invariant mass has to be specified, or if a final-state electron or positron is present, cuts on its minimal angle to the beam and its minimal energy are required. For calculations based on restricted sets of diagrams, not all cuts are necessary; in particular, no cut at all is needed for the CC03 diagrams.
  Note that some of the cuts specified in the input are applied already during the generation of the events, i.e. in the calculation of the outgoing momenta from the random numbers. Otherwise, many generated events would be rejected later, since the events are predominantly sampled near those regions of phase-space regions where the matrix element becomes even singular and which therefore have to be excluded. Additional, more complicated cuts can be implemented after the event generation.
- **QCD contributions:** gluon-exchange contributions can be switched on in the tree-level processes $\mathrm{e^+e^-} \to 4\mathrm{f}, 4\mathrm{f}+\gamma$. Gluon-emission processes $\mathrm{e^+e^-} \to 4\mathrm{f}+g$ can be calculated for the CC11 class of $4\mathrm{f}$ final states.
  For the QCD corrections to $\mathrm{e^+e^-} \to \mathrm{WW} \to 4f$, one can choose between the naive QCD factors of $(1+\alpha_{\mathrm{s}}/\pi)$ per hadronically decaying W boson and the full $\mathcal{O}(\alpha_{\mathrm{s}})$ corrections in DPA. The full calculation is performed in the same way as the photonic parts of the $\mathcal{O}(\alpha)$ corrections.
- **IBA:** the program includes, as an option, an improved Born approximation (IBA) [51], which involves the leading ISR logarithms, the running of the electromagnetic coupling, corrections associated with the ρ parameter, and the Coulomb singularity.
- **Subsets of diagrams:** As already mentioned, for lowest-order predictions of $\mathrm{e^+e^-} \to 4f, 4\mathrm{f}+\gamma$ there is the possibility to select subsets of diagrams, such as those including the pair production of W, Z, Z/γ^*, or $\mathrm{W}/\mathrm{Z}/\gamma^*$ bosons. Furthermore, all diagrams corresponding to the CC11 process class can be selected.

- **Intrinsic ambiguities:** the accuracy of the DPA can be studied by changing the DPA within its intrinsic ambiguities. For instance, the user can choose between different on-shell projections for the DPA of the virtual corrections. Moreover, rearrangement of the singular parts between virtual and real corrections are only fixed up to non-singular terms; this leads to differences beyond the accuracy of the DPA owing to the asymmetric treatment of the virtual and the real corrections. The phase-space slicing and subtraction method themselves represent different rearrangements; the user can additionally choose different versions within these methods. Furthermore, various input-parameter schemes can be used.

8.13 Planned extensions

- Non-standard triple and quartic gauge-boson couplings
- Leading universal corrections to $\mathrm{e^+e^-} \to 4\mathrm{f} + \gamma$

8.14 Program layout

`RacoonWW` consists of two nearly independent Monte Carlo programs: one uses phase-space slicing and the other the subtraction method of Ref. [50]. Only the main control program, the routines for photon recombination and phase-space cuts, and the calculation of the matrix elements are commonly used.

The numerical integration is performed with the multi-channel Monte Carlo technique [52] and adaptive weight optimization [53]. The mappings for the phase-space integration, called channels, are chosen in such a way that for each diagram a phase-space mapping exists with a Jacobian that widely cancels all propagators of the squared diagram.

The program starts by reading an input file and defining the physical parameters from this input. Thereafter, all sub-programs are initialized, and all input parameters are written into an output file.

In the main integration loop several phase-space points and their weights are calculated from the random numbers, using either the phase-space slicing or the subtraction method; these results are stored in a common block. The different weights originate from the $4\mathrm{f}$ process including the lowest order as well as the virtual $\mathcal{O}(\alpha)$ correction, from the $4\mathrm{f} + \gamma$ process for separable photons, from the $4\mathrm{f}$ process including $\mathcal{O}(\alpha)$ ISR (where the momentum of one of the incoming $\mathrm{e}^\pm$ is reduced), and from the $4\mathrm{f}$ process including ISR beyond $\mathcal{O}(\alpha)$ (where the energies of both initial-state particles are reduced). For the subtraction method, additional weights appear for the subtraction terms, which cancel the singularities of the $4\mathrm{f} + \gamma$ cross section in the soft or collinear limits. Note that the weights in general are not positive definite if radiative corrections are included.

The individual weights are determined in the following way: first, the momenta of the incoming $\mathrm{e}^\pm$ are generated. A channel is randomly chosen with probability α_i. The α_i are called a-priori weights and are optimized several times during the whole calculation, such that channels of more important diagrams are preferred (adaptive optimization). The momenta of the final-state particles are calculated from the random numbers with the phase-space generator of the chosen channel. After that, the photon recombination procedure is performed if a real photon is involved. Finally, the separation cuts are applied. If the event is excluded by cuts, it is rejected. If not, the corresponding weight is calculated from the matrix element, the structure function, the subtraction terms, the a-priori weights α_i, and from the Jacobians of all phase-space mappings (channels).

During the integration loop several histograms are filled. At the end, the cross section, the estimated statistical error, and the results for the distributions are given.

8.15 Input parameters/schemes

`RacoonWW` needs the following input parameters:

$$\alpha(0), \alpha(M_\mathrm{Z}), G_\mu, \alpha_\mathrm{s},$$

$$
\begin{aligned}
&M_{\mathrm{W}}, M_{\mathrm{Z}}, M_{\mathrm{H}}, \Gamma_{\mathrm{W}}, \Gamma_{\mathrm{Z}}, \\
&m_f, \quad f = \mathrm{e}, \mu, \tau, \mathrm{u}, \mathrm{c}, \mathrm{t}, \mathrm{d}, \mathrm{s}, \mathrm{b}.
\end{aligned} \tag{56}
$$

The weak mixing angle is fixed by $c_{\mathrm{w}}^2 = 1 - s_{\mathrm{w}}^2 = M_{\mathrm{W}}^2/M_{\mathrm{Z}}^2$, and the quark-mixing matrix is set to unity. The masses of external fermions are consistently set to zero where possible. While the masses of the final-state fermions appear only as regulators, the mass singular logarithms of ISR depend on m_{e}. The user can choose between the externally fixed W width Γ_{W} and an internally calculated value including electroweak and/or QCD one-loop radiative corrections.

The parameter set (56) is over-complete. The program supports three different input schemes, fixing the independent parameters:

- G_μ scheme (*recommended*): tree-level fixed by $G_\mu, M_{\mathrm{W}}, M_{\mathrm{Z}}$.
  There is no sizeable dependence of electroweak corrections on light-fermion masses other than m_{e}.
  The relative $\mathcal{O}(\alpha)$ corrections are calculated with $\alpha(0)$.
- $\alpha(M_{\mathrm{Z}})$ scheme: tree-level fixed by $\alpha(M_{\mathrm{Z}}), M_{\mathrm{W}}, M_{\mathrm{Z}}$.
  There is no sizeable dependence of electroweak corrections on light-fermion masses other than m_{e}.
  The relative $\mathcal{O}(\alpha)$ corrections are calculated with $\alpha(0)$.
- $\alpha(0)$ scheme: tree-level fixed by $\alpha(0), M_{\mathrm{W}}, M_{\mathrm{Z}}$.
  Electroweak corrections depend sizably on all light-fermion masses m_f upon charge renormalization, i.e. light-quark masses should be tuned to reproduce the correct running electromagnetic coupling $\alpha(M_{\mathrm{Z}})$. This scheme misses important universal two-loop corrections.

Besides the input data of (56), the following has to be specified in the input file

- name of output file
- number of events
- centre-of-mass energy
- input parameter scheme (see above)
- W-boson width: fixed input or calculated including electroweak and/or QCD one-loop radiative corrections
- final state: specific 4f state
- set of diagrams for tree-level processes: all diagrams or specific selections like CC03

For $\mathrm{e^+e^-} \to \mathrm{WW} \to 4f(+\gamma)$ including corrections the following options are provided in addition:

- $\mathcal{O}(\alpha)$ corrections: yes, no, or IBA
- treatment of mass and IR singularities: phase-space slicing or subtraction method
- photon recombination: different procedures possible
- ISR beyond $\mathcal{O}(\alpha)$ via structure functions: yes or no
- treatment of Coulomb singularity: full off-shell or on-shell
- QCD corrections: no correction, naive $\mathcal{O}(\alpha_{\mathrm{s}})$ factors, or full $\mathcal{O}(\alpha_{\mathrm{s}})$ in DPA

For $\mathrm{e^+e^-} \to 4f + \gamma$ with a separable photon or the tree-level process $\mathrm{e^+e^-} \to 4f$ the following option exists:

- finite gauge-boson widths: constant widths, running widths, or complex-mass scheme

Finally, the phase-space cuts have to be specified in either case. As a standard set of cuts the ADLO cuts are provided. Alternatively general cuts can be defined by the user.

8.16 Output

The output file of `RacoonWW` contains the input parameters, the process, and the chosen options. The cross section, its estimated statistical error, and results for various distributions are given. The generated phase-space points and the corresponding weights are made available via a common block.

8.17 Availability

The code is available from the authors upon request.

8.18 Numerical results

Here we will show some of the predictions from `RacoonWW`, mostly distributions where four different configurations are compared.

full Born: full Born without radiative corrections;

best full Born: full Born + with radiative corrections including ISR beyond $\mathcal{O}(\alpha)$, i.e. soft photon exponentiation, LL $\mathcal{O}(\alpha^2)$ plus naive QCD;

CC03 Born: CC03 Born without radiative corrections;

best CC03 Born: CC03 Born + with radiative corrections including ISR beyond $\mathcal{O}(\alpha)$, i.e. soft photon exponentiation, LL $\mathcal{O}(\alpha^2)$ plus naive QCD.

However, we start with a prediction for the total cross-section, shown in Tab.(2) The given errors are purely statistical. In all figures we report distributions for three processes, $\mu\nu_\mu\tau\nu_\tau$, $ud\mu\nu_\mu$ and $udcs$. In Fig. 5 we show the $M(W^-)$ invariant mass distribution for CC03 Born; in this case *bare* and *calo* are the same. Once radiative corrections are inserted in DPA-approximation, the three distributions are given in Fig. 6 In Fig. 7 we show the effect of radiative corrections by computing the ratio between Best-CC03-Born bare- and calo-mass distributions and the Born one. Although the numerical errors are large, away from the peak region, around it we have a clean evidence of the effects of radiative corrections lowering the line-shape of approximately $2\%(5\%)$ for bare(calo) distributions. In Fig. 8 we show the full Born, without radiative corrections, i.e. the invariant mass distributions constructed from all diagrams without a restriction to CC03. In the same figure we present also the ratio full-Born/CC03. Although the numerical errors are large this plot confirms the goodness of the CC03 approximation in describing the WW cross-section at LEP 2 energies. In Fig. 10 we show the ratio best-full-Born/CC03 for both the bare and the calo W^- mass ditributions, showing not only the inclusion of radiative corrections but also the effect of the background diagrams.

$\sqrt{s}$ [GeV]	lept.	semi-lept.	hadr.	total
172.1	142.088(71)	442.50(36)	1376.14(67)	12.0934(76)
182.7	180.697(89)	562.22(28)	1749.48(86)	15.3708(76)
188.6	190.882(96)	594.31(55)	1848.07(92)	16.2420(111)
191.6	194.271(118)	604.12(31)	1880.19(94)	16.5187(85)
195.5	197.320(123)	614.11(31)	1911.45(97)	16.7910(88)
199.5	199.497(103)	620.53(33)	1931.28(99)	16.9670(89)
201.6	200.200(104)	622.65(33)	1937.94(100)	17.0254(89)

Table 2: Cross-sections [fb] for $e^+e^- \to W^+W^-$ from `RacoonWW`.

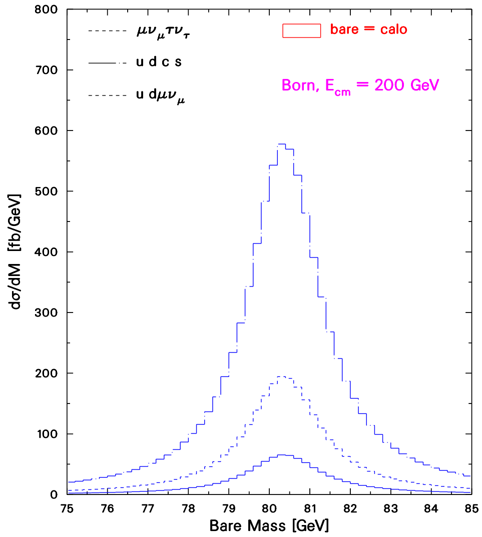

Fig. 5: Bare = calo mass distributions for CC03 Born from `RacoonWW`.

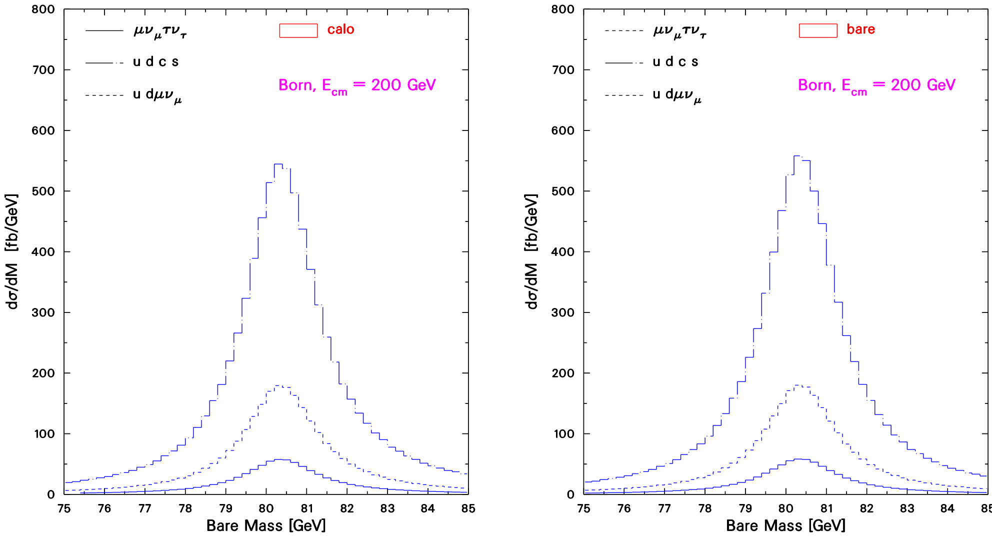

Fig. 6: Bare and calo mass distributions for Best-CC03-Born from `RacoonWW`.

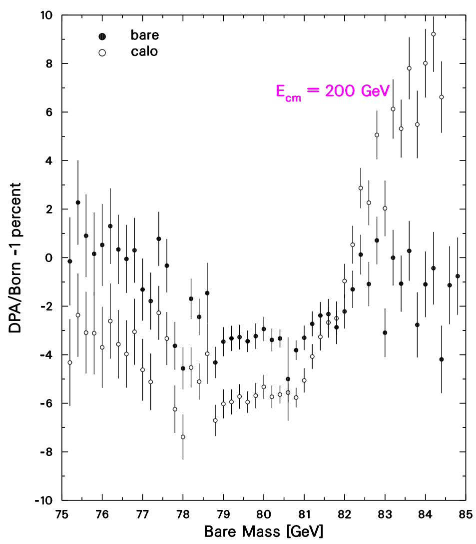

Fig. 7: The ratio Best-CC03-Born / Born for bare and calo mass distributions from `RacoonWW` for the process $udsc$.

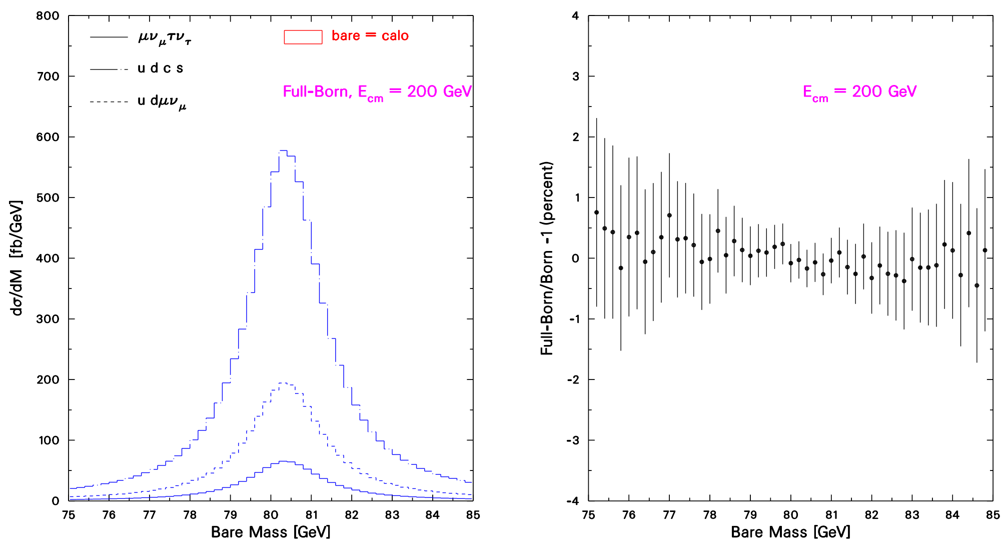

Fig. 8: Bare = calo mass distributions for full-Born from `RacoonWW`. The ratio full-Born/CC03 is also shown for the process $udcs$.

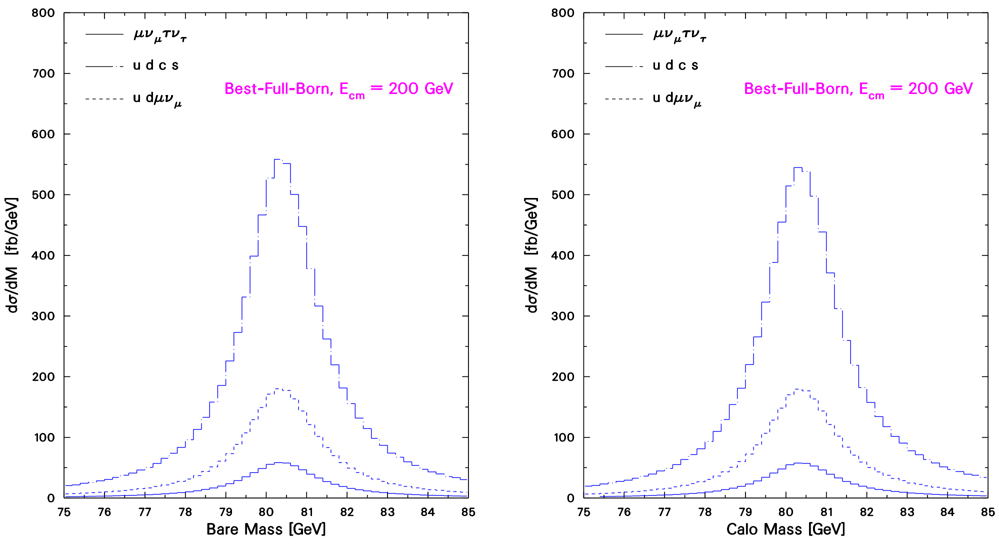

Fig. 9: Bare and calo mass distributions for best-full-Born from `RacoonWW`.

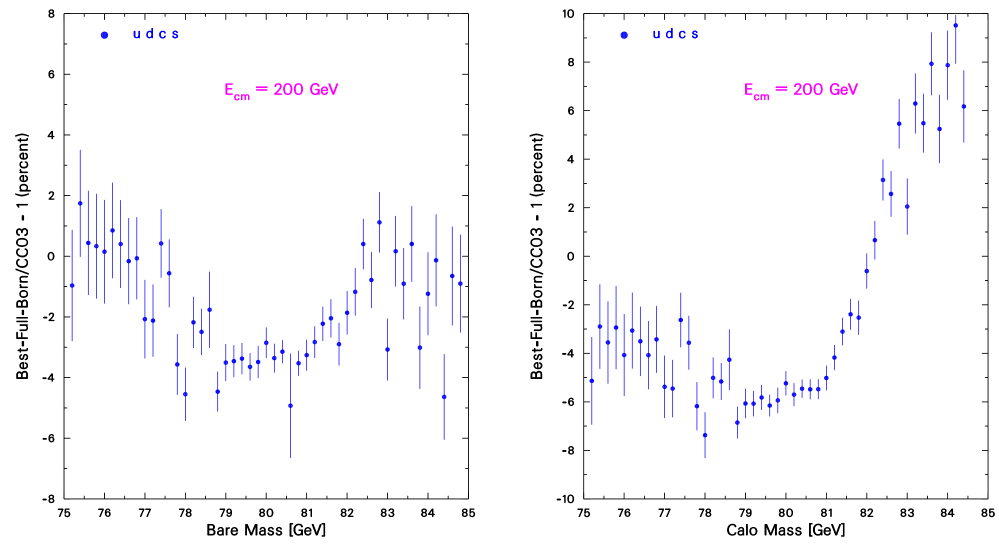

Fig. 10: Bare and calo mass ratio best-full-Born/CC03 from `RacoonWW`.

8.2 CC03 with `KORALW/YFSWW`

Authors

S. Jadach
W. Placzek
M. Skrzypek
B. Ward
Z. Was

8.21 General Description

The program evaluates the the double resonant process $e^+e^- \to W^+W^- \to 4f$ in the presence of multiple photon radiation using Monte Carlo event generator techniques. The theoretical formulation is based, in the leading pole approximation (LPA), on the exact $\mathcal{O}(\alpha)_{prod}$ YFS exponentiation, with $\mathcal{O}(\alpha)$ corrections (both weak and QED) to the production process taken from Ref. [142], combined with $\mathcal{O}(\alpha^3)$ LL ISR corrections in the YFS scheme and with FSR implemented in the $\mathcal{O}(\alpha^2)$ LL approximation using PHOTOS [143]. The calculation is fully gauge invariant. The Monte Carlo algorithm used to realize the YFS exponentiation is based on the YFS3 algorithm presented in Ref. [144] and in Ref. [145]. This algorithm is now described in detail in Ref. [146]. In this way, we achieve an event-by-event realization of our calculation in which arbitrary detector cuts are possible and in which infrared singularities are cancelled to all orders in α. A detailed description of our work can be found in Refs. [155, 148, 149].

8.22 Features of the Program

The code is a complete Monte Carlo event generator and gives for each event the final particle four-momenta for the entire $4f + n\gamma$ final state over the entire phase space for each final state particle. The events may be weighted or unweighted, as it is more or less convenient for the user accordingly. The code features two realizations of the LPA, which are described in Refs. [155, 148, 149] wherein we also discuss their respective relative merits. The accuracy of the combined result from YFSWW3 1.13 and our all 4-fermion process MC KoralW 1.42 [150] as presented in Ref. [149] is expected to be below 0.5% for the total cross section when all tests are finished. These tests are currently in progress.

8.23 How does the code work

The operation of the code is entirely analogous to that of the MC's YFS3 and YFS2 in Refs. [144, 152]. A crude distribution based on the primitive Born level distribution and the most dominant part of the YFS form factors that can be treated analytically is used to generate a background population of events. The weight for these events is then computed by standard rejection techniques involving the ratio of the complete distribution and the crude distribution. As the user wishes, these weights may be either used directly with the events, which have the four-momenta of all final state particles available, or they may be accepted/rejected against a maximal weight WTMAX to produce unweighted events via again standard MC methods. Standard final statistics of the run are provided, such as statistical error analysis, total cross sections, etc. The total phase space for the process is always active in the code.

8.24 Description of output

The program prints certain control outputs. The most important output of the program is the series of Monte Carlo events. The total cross section in pb is available for arbitrary cuts in the same standard way as it is for YFS3 and YFS2, i.e. the user may impose arbitrary detector cuts by the usual rejection methods.

Availability

The program is available from the authors via e-mail. The program is currently posted on `WWW` at `http://enigma.phys.utk.edu` as well as on `anonymous ftp` at `enigma.phys.utk.edu` in the form of a `tar.gz` file in the `/pub/YFSWW/` directory together with all relevant papers and documentation in postscript.

8.25 Numerical results

Channel	Born	Best
$ud\overline{s}\overline{c}$	1.96325(37)	1.59365(86)
$ud\overline{d}\overline{u}$	1.96369(41)	1.59572(71)
$u\overline{d}\mu^-\overline{\nu}_\mu$	0.65441(14)	0.53901(22)
$u\overline{d}e^-\overline{\nu}_e$	0.65458(12)	0.53899(23)
$\mu^-\overline{\nu}_\mu\tau^+\nu_\tau$	0.21809(4)	0.18193(7)
all WW channels	17.66681(351)	15.49161(618)

Table 3: Cross-sections [fb] for $e^+e^- \to W^+W^-$ from `YFSWW` at $\sqrt{s} = 183$ GeV.

Channel	Born	Best
$ud\overline{s}\overline{c}$	2.03231(39)	1.68293(93)
$ud\overline{d}\overline{u}$	2.03285(40)	1.68565(76)
$u\overline{d}\mu^-\overline{\nu}_\mu$	0.67756(14)	0.56931(24)
$u\overline{d}e^-\overline{\nu}_e$	0.67756(14)	0.56931(24)
$\mu^-\overline{\nu}_\mu\tau^+\nu_\tau$	0.22573(4)	0.19220(8)
all WW channels	18.29266(354)	16.36329(694)

Table 4: Cross-sections [fb] for $e^+e^- \to W^+W^-$ from `YFSWW` at $\sqrt{s} = 189$ GeV.

`KORALW` has multiple-options in presence multi-photonic events. It can define distributions for

1. visible γ (radiative);
2. all photons, i.e. no cuts, in which case one can take only a) the most energetic photon to determine energy and angles (*hardest*), b) the sum (*sum*).

8.3 WW-pairs with `GRACE`

Authors

Y. Kurihara
M. Kuroda
Y. Shimizu

Channel	Born	Best
$u\overline{d}s\overline{c}$	2.06691(40)	1.75725(96)
$u\overline{d}d\overline{u}$	2.06737(41)	1.76065(82)
$u\overline{d}\mu^-\overline{\nu}_\mu$	0.68899(16)	0.59440(26)
$u\overline{d}e^-\overline{\nu}_e$	0.68913(13)	0.59444(27)
$\mu^-\overline{\nu}_\mu\tau^+\nu_\tau$	0.22957(5)	0.20065(9)
all WW channels	18.59649(383)	17.09010(771)

Table 5: Cross-sections [fb] for $e^+e^- \to W^+W^-$ from `YFSWW` at $\sqrt{s} = 200$ GeV.

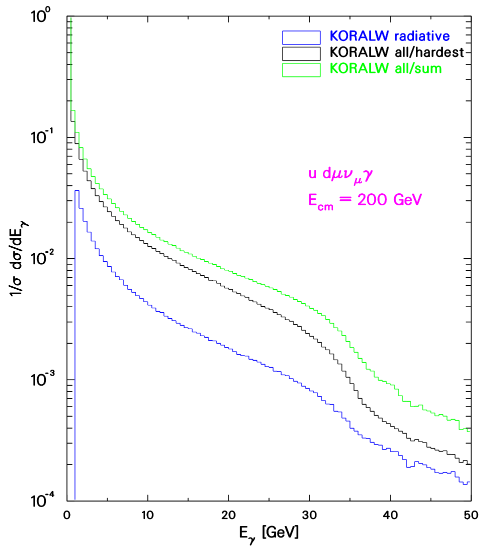

Fig. 11: `KORALW` E_γ spectra for $u\overline{d}\mu^-\overline{\nu}_\mu\gamma$.

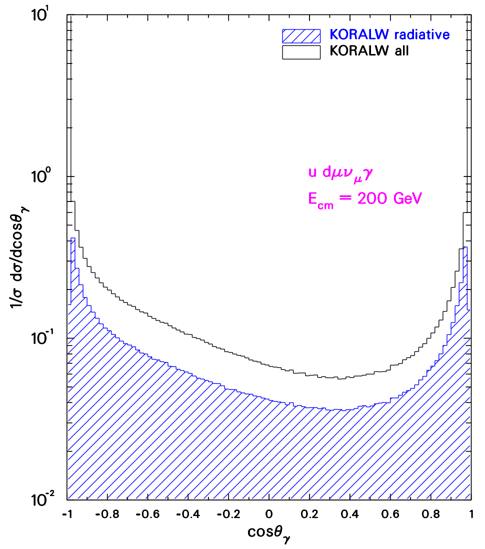

Fig. 12: KORALW $\cos\theta_\gamma$ spectra for $u\overline{d}\mu^-\overline{\nu}_\mu\gamma$.

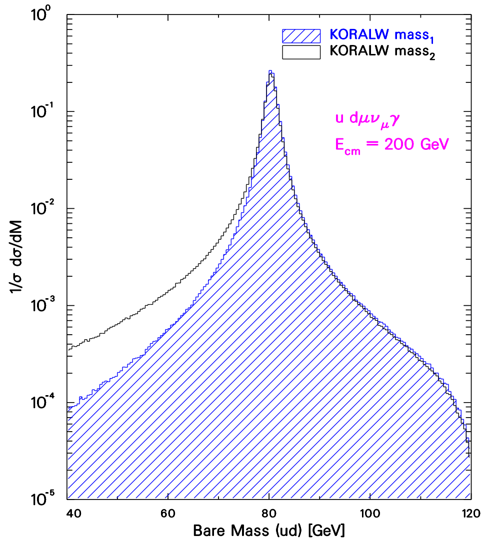

Fig. 13: KORALW *bare* M spectra for $u\overline{d}\mu^-\overline{\nu}_\mu\gamma$.

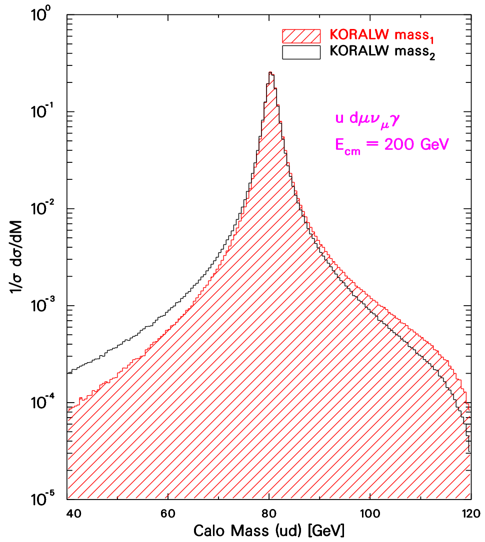

Fig. 14: KORALW *calo* M spectra for $u\overline{d}\mu^-\overline{\nu}_\mu\gamma$.

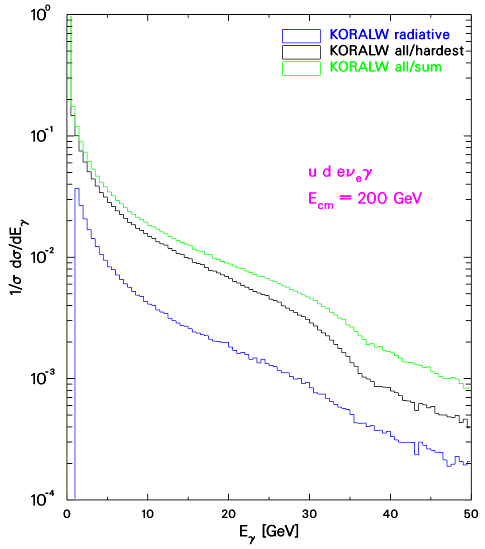

Fig. 15: KORALW E_γ spectra for $u\overline{d}e^-\overline{\nu}_e\gamma$.

8.31 Introduction

Four-fermion production, $e^+e^- \to 4\mathrm{fermions}$, in general, does not only proceed via the production and subsequent decay of a W-boson pair. Additional contributions are present that involve only a single W pole, or no pole at all (cf. e.g. [158]). With respect to W-pair production, such contributions form a non-doubly-resonant background. It is expected that by applying suitable experimental cuts on the invariant masses of the produced fermion pairs, one may be able to eliminate such background contributions to a large extent when comparing theoretical predictions with experimental data.

Since our interest at LEP2 is the production of W, it is natural to use the amplitudes for on-mass-shell production and decay. The propagation of the decaying W boson will be taken care of by Breit-Wigner denominators with constant width. This corresponds to the double-pole approximation (DPA) which consists of expanding the amplitude around the W pole and using only the double pole part for $e^+e^- \to W^+W^- \to$ 4 fermions[159, 160, 161].

In one-loop order the helicity amplitudes of the process $e^+(\sigma_+)e^-(\sigma_-) \to W^+_{\lambda_+}(f_1(\tau_1)\bar{f}_2(\bar{\tau}_2))$ $W^-_{\lambda_-}(f_4(\tau_4)\bar{f}_3(\bar{\tau}_3))$ are given in DPA by

$$\mathcal{H}(\sigma_+,\sigma_-;\tau_1,\bar{\tau}_2;\tau_4,\bar{\tau}_3) = \sum_{\lambda_+,\lambda_-} \frac{\mathcal{H}(e^+(\sigma_+)e^-(\sigma_-) \to W^+_{\lambda_+}(f_1(\tau_1)\bar{f}_2(\bar{\tau}_2))W^-_{\lambda_-}(f_4(\tau_4)\bar{f}_3(\bar{\tau}_3)))}{K_+K_-}, \tag{57}$$

where $\sigma_\pm$ is the positron(electron) helicity, $\lambda_\pm$ is the helicity of $W^\pm$, and $\tau_i(\bar{\tau}_i)$ are helicities of the final fermions (antifermions). The explicit form of the numerator of (57) is given by

$$\begin{aligned}
&\mathcal{H}(e^+(\sigma_+)e^-(\sigma_-) \to W^+_{\lambda_+}(f_1(\tau_1)\bar{f}_2(\bar{\tau}_2))W^-_{\lambda_-}(f_4(\tau_4)\bar{f}_3(\bar{\tau}_3))) \qquad (58)\\
&= +\mathcal{H}^{e^+e^-\to W^+W^-}_{Born}(\sigma_+,\sigma_-;\lambda_+,\lambda_-)\mathcal{H}^{W^+\to f_1\bar{f}_2}_{Born}(\lambda_+;\tau_1,\bar{\tau}_2)\mathcal{H}^{W^-\to f_3\bar{f}_4}_{Born}(\lambda_-;\tau_4,\bar{\tau}_3)\\
&\quad +\delta\mathcal{H}^{e^+e^-\to W^+W^-}(\sigma_+,\sigma_-;\lambda_+,\lambda_-)\mathcal{H}^{W^+\to f_1\bar{f}_2}_{Born}(\lambda_+;\tau_1,\bar{\tau}_2)\mathcal{H}^{W^-\to f_3\bar{f}_4}_{Born}(\lambda_-;\tau_4,\bar{\tau}_3)\\
&\quad +\mathcal{H}^{e^+e^-\to W^+W^-}_{Born}(\sigma_+,\sigma_-;\lambda_+,\lambda_-)\delta\mathcal{H}^{W^+\to f_1\bar{f}_2}(\lambda_+;\tau_1,\bar{\tau}_2)\mathcal{H}^{W^-\to f_3\bar{f}_4}_{Born}(\lambda_-;\tau_4,\bar{\tau}_3)\\
&\quad +\mathcal{H}^{e^+e^-\to W^+W^-}_{Born}(\sigma_+,\sigma_-;\lambda_+,\lambda_-)\mathcal{H}^{W^+\to f_1\bar{f}_2}_{Born}(\lambda_+;\tau_1,\bar{\tau}_2)\delta\mathcal{H}^{W^-\to f_3\bar{f}_4}(\lambda_-;\tau_4,\bar{\tau}_3),
\end{aligned}$$

and

$$K_\pm \equiv k^2_\pm - M^2_W + iM_W\Gamma_W, \tag{59}$$

where $\sqrt{k^2_\pm}$ is the invariant mass of the fermion pair. All the helicity amplitudes appearing in (58) are evaluated on the mass-shell of the $W^\pm$-bosons. The first line corresponds to the Born amplitude, while the second to the fourth line represent the one-loop corrections to the production and the $W^\pm$-decay subprocesses. The spin correlation is fully taken into account in the formulation (57).

In the spirit of the DPA the range of the integration over the fermion-pair masses squared, $k^2_\pm$, is to be restricted in order to sufficiently reduce non-double-resonance four-fermion production. While too small an integration range will strongly reduce event rates, too large a range will increase background. We find that the five-Γ_W choice

$$|\sqrt{k^2_\pm} - M_W| \lesssim 5\Gamma_W, \tag{60}$$

constitutes a reasonable compromise.

For simplicity we consider the final state $(u\bar{d})(\bar{c}s)$. In section 2 the tree-level cross section is evaluated in the DPA and the quality of DPA is investigated. The cross section including radiative corrections is discussed in section 3. More detailed result will be published separately [162].

Line	$\sqrt{s}$	184 GeV	189 GeV	200 GeV
1	$\sigma(e^+e^- \to W^+W^-)$	19.924(2)	19.365(2)	19.412(2)
	Zero width approximation			
2	$\sigma \times BR(W^+ \to u\bar{d})BR(W^- \to \bar{c}s)$	2.1138(2)	2.1516(2)	2.1569(2)
	Breit-Wigner, full four-fermion phase space			
3	$\sigma(e^+e^- \to W^+(\to u\bar{d})W^-(\to \bar{c}s))$	2.0254(8)	2.0686(8)	2.0839(8)
4	$\sigma(e^+e^- \to u\bar{d}\bar{c}s)$	1.978(1)	2.032(1)	2.068(1)
5	Difference Δ in %	2.4	1.8	0.7
	Breit-Wigner, restricted phase space, $\lvert\sqrt{k_\pm^2} - M_W\rvert < 5\Gamma_W$			
6	$\sigma(e^+e^- \to W^+(\to u\bar{d})W^-(\to \bar{c}s))$	1.8447(8)	1.8797(8)	1.8867(8)
7	$\sigma(e^+e^- \to u\bar{d}\bar{c}s)$	1.842(1)	1.879(1)	1.888(1)
8	Difference Δ in %	0.2	0.1	-0.1

Table 6: Tree-level total Born cross section for W^+W^- mediated four-fermion production compared with the full four-fermion production including background for different phase space cuts.

8.32 Born cross section

In order to see quantitatively the effect of the cut on the invariant mass of fermion pair, we compare the results of tree-level calculations for $e^+e^- \to W^+W^- \to u\bar{d}\bar{c}s$ with the results for $e^+e^- \to u\bar{d}\bar{c}s$ based on the full set of diagrams (CC11) contribution to the reaction. We use the following input parameters.

$$M_W = 80.35, \qquad M_Z = 91.1867, \qquad M_H = 150 (\text{in GeV}). \tag{61}$$

For the evaluation of the tree-level cross section, we use the effective coupling α_{G_F}

$$\alpha_{G_F} = \frac{\sqrt{2} G_F M_W^2 s_W^2}{\pi}, \tag{62}$$

and the corresponding tree-level width,

$$\Gamma_W = \frac{3}{4} \frac{\sqrt{2} G_F M_W^3}{\pi}. \tag{63}$$

Our numerical results are given in Table 1. For simplicity the fermion masses are neglected. Line 1 gives the the cross sections for W-pair production. Line 2 corresponds to the zero-width approximation,

$$\frac{M_W \Gamma_W}{|k_\pm^2 - M_W^2 + i M_W \Gamma_W|^2} BR \to \pi \delta(k_\pm^2 - M_W^2) \cdot BR. \tag{64}$$

with $BR = 1/3$ for $W^+ \to u\bar{d}$ and $W^- \to \bar{c}s$. Line 3 and 6 are evaluated by DPA, while line 4 and 7 are the result of the exact CC11 cross section computed by GRACE[163].

Line 3 and 4 show the result of the full phase space integration. The difference between line 2 and 3 is larger at LEP2 energies than at collider energies of $\sqrt{s} = 500$-1000GeV [164]. In the zero width approximation the integration region of the four-fermion-pair invariant masses is extended from its physical phase space to the region ranging from minus infinity to plus infinity, thereby including unphysical phase space. At low energies, the physical phase space of four-fermion-pair invariant mass is much smaller than at high energies and consequently, the zero width approximation becomes less accurate at low energies.

The difference between the results of line 3 and of line 4, arising from the non-doubly resonant contribution, is as large as a couple of percent. At low energies of LEP2 the result of DPA cross section based on the CC03 diagrams presented in line 3 is larger than the CC11 cross section of line 4. This trend flips at higher energies and at collider energies, CC11 cross section is larger than the DPA cross section [164].

Finally, enhancing the relative contribution of the $W^{\pm}$ resonances by imposing a cut (60) on the masses of the fermion-pairs, $\sqrt{k_{\pm}^2}$, we can substantially reduce the background contribution, as shown in line 6 and 7. The difference between line 6 and 7, indicated in line 8, is indeed of order 0.1 percent.

The above observation strongly supports the idea of using the DPA combined with the cut (60) on the invariant mass of the fermion-pair for the investigation of the W-pair production at LEP2.

Next we have compared our result of line 3 and 4 with those given by Denner et al, [165]. Since they have used the experimental value

$$\Gamma_W = 2.08699\mathrm{GeV}, \tag{65}$$

even for the evaluation of the tree-level cross section, the direct comparison is not possible. Our numerical result of the cross section computed by using Γ_W given by (65) becomes

$$\sigma(e^+e^- \to W^+(\to u\bar{d})W^-(\to \bar{c}s)) = \begin{cases} 1.9387(8) & \sqrt{s} = 184, \\ 1.9802(8) & \sqrt{s} = 189, \\ 1.9951(8) & \sqrt{s} = 200. \end{cases} \tag{66}$$

$$\sigma(e^+e^- \to u\bar{d}\bar{c}s) = \begin{cases} 1.892(1) & \sqrt{s} = 184, \\ 1.944(1) & \sqrt{s} = 189, \\ 1.979(1) & \sqrt{s} = 200. \end{cases} \tag{67}$$

The cross section $\sigma(e^+e^- \to u\bar{d}\bar{c}s)$ agrees well with the result full(Born) presented in [165]. Concerning the cross section $\sigma(e^+e^- \to W^+(\to u\bar{d})W^-(\to \bar{c}s))$, we note that in ref.[165], the CC03 cross section, called as CC03(Born) is not evaluated by the DPA but in the 't Hooft-Feynman gauge. It is not much meaningful, therefore, to compare our result (66) with the gauge-dependent quantity. A naive comparison, if allowed, shows that their result evaluated in 't Hooft-Feynman gauge is about 1 to 2% smaller than ours.

8.33 Order α corrections

In the calculation of the cross section including $\mathcal{O}(\alpha)$ radiative corrections, we have used not α_{G_F} but $\alpha = 1/137.035989$ everywhere including the Born amplitudes, and also the experimental value for the W-boson width given in (65). In the computation we have regulated the infrared singularity by giving photon a small mass as regulator. Changing the soft-photon energy cut, k_c from 0.1 to 1 GeV, we have checked the stability of the total cross section against the variation of k_c.

The total cross section including virtual corrections and photon radiation is evaluated by the DPA with the cut on the invariant mass of fermion- pair given in (60). The result is given in Table 2, together with the Born cross section and the percentage radiative corrections

$$\Delta = \frac{\sigma(Born) - \sigma(Born + \mathcal{O}(\alpha))}{\sigma(Born)}. \tag{68}$$

We observe substantially large radiative corrections. The dominant part of the radiative correction comes, however, from the hard photon radiation.

In order to compare our result with those given in ref.[165], we have integrated the cross section over the whole phase space. The result at $\sqrt{s} = 200$ GeV becomes

$$\sigma(no\ cut) = 1.778\, pb \tag{69}$$

which is about 1% larger than the result of ref.[165]. The difference of our amplitude and theirs lies in the treatment of non-factorizable corrections and correspondingly of the interference terms in the hard photon

$\sqrt{s}$	Born	Including order α	Δ in %
184	1.8447	1.512	-18.0
189	1.8797	1.564	-16.8
200	1.8867	1.610	-14.7

Table 7: The total cross section for $e^+e^- \to (u\bar{d})(\bar{c}s)$ in DPA. The second column is the Born cross section and third column is our result including order α corrections. The fourth column shows the percentage radiative corrections Δ defined by (68).

radiation. Although we have used the DPA in the calculation of hard photon radiation, a full interference among the diagrams in which photon is radiated from the different subprocesses is considered in ref.[165] by computing the hard photon radiation exactly. Since the non-factorizable correction is expected to be small due to the cancellation when integrated over the whole phase space, we expect the difference comes dominantly from the different treatment of the hard photon radiation part.

8.34 Conclusion

The total cross section of the process $e^+e^- \to (u\bar{d})(\bar{c}s)$ mediated via W-pair production is evaluated based on the double pole approximation (DPA) up to $\mathcal{O}(\alpha)$. The results are compared with those given in ref.[165], in which the same process is evaluated in a slightly different approach and approximation. At one-loop level the difference between the two groups is about 1%.

A detailed comparison with the exact calculations has shown that the DPA is a very good approximation once combined with the cut on the invariant mass of fermion-pairs because the most of the background is suppressed. Naturally, ultimate justification of the DPA must wait for the completion of the exact calculation of the four-fermion production cross sections including full radiative corrections.

8.4 Comparison between RacoonWW and BBC results

Authors

RacoonWW Ansgar Denner
Stefan Dittmaier
Markus Roth
Doreen Wackeroth

BBC F.Berends
W.Beenakker
A.Chapovsky

In this section we compare the Monte Carlo generator RacoonWW [45, 109] with the semi-analytical benchmark program [?] of Berends, Beenakker and Chapovsky, called BBC in the following. The numerical comparison has been done for the leptonic channel $\mathrm{e^+e^-} \to \nu_\mu\mu^+\tau^-\bar{\nu}_\tau$ and the input parameters of Ref. [?]. As explained in more detail below, in this section the RacoonWW results are not calculated with the preferred options, but rather in a setup as close as possible to the BBC approach.

The two programs include the complete electroweak $\mathcal{O}(\alpha)$ corrections to $\mathrm{e^+e^-} \to \mathrm{WW} \to 4f(+\gamma)$, both including the non-factorizable corrections and W-spin correlations, which at present is only possible within the DPA formalism. Although both programs use the DPA, nevertheless there are differences between these two calculations. One is technical, the usual difference between a flexible Monte Carlo calculation, which is also meant for experimental use, and a more rigid semi-analytical one, which was constructed as a benchmark for future calculations. The other difference is in the implementation of the DPA. The BBC calculation adheres strictly to DPA definitions, so also the phase space and photon emission are taken in DPA. In RacoonWW the matrix elements for virtual corrections are calculated in the DPA, but the exact off-shell phase space is used. For real photon radiation the DPA is not used. Instead all Born diagrams for $\mathrm{e^+e^-} \to 4f\gamma$ (including the background) are taken into account and the finite width is introduced in the fixed-width scheme. Formally this procedure is not gauge-invariant, but it has been checked numerically with a gauge-invariant calculation (complex-mass scheme). The matching between the virtual and real corrections, which is necessary in order to cancel the IR and mass singularities, is done in such a way that the leading-logarithmic corrections arising from ISR are taken into account exactly, i.e. not in DPA. By comparing the two calculations one can numerically check the quality of the DPA for real-photon radiation. The expected differences between both approaches are formally of the relative order $\mathcal{O}(\Gamma_\mathrm{W}/\Delta E)$, with $\Delta E = \sqrt{s} - 2M_\mathrm{W}$ near the W-pair production threshold.

The differences in the approaches have important consequences. With RacoonWW predictions can be obtained for general cuts and physically relevant situations. The fact that the masses of the final-state fermions are neglected restricts the applicability of the program to those observables that are free of mass singularities connected to the final state. This means, in particular, that collinear photons have to be combined with the corresponding fermions. This combination depends on the experimental situation, which in turn depends on the type of final state. The semi-analytical approach is of course less flexible for implementing the experimental cuts. In the benchmark BBC calculation some of the integrations were performed analytically in order to speed up the numerical evaluations. For instance, the invariant-mass distributions were treated differently from observables where the invariant masses have been integrated over. This is not a requirement in general in the DPA if one is prepared to do more of the integrations numerically. On the other hand, a treatment of mass-singular observables, i.e. ones without photon recombination, can be easily performed in the semi-analytical approach.

For the total cross section, the differences between the two approaches should be of the naively expected DPA accuracy of $\mathcal{O}(\Gamma_W/\Delta E)$ relative to the $\mathcal{O}(\alpha)$ correction. In Figure 16 we show the prediction of BBC as points with errorbars and the prediction of RacoonWW as a curve together with errorbars for some points. All errorbars are purely statistical. As shown in Figure 16, both calculations agree very well above $185\,\mathrm{GeV}$. Below this energy the differences in the implementation of the DPA become

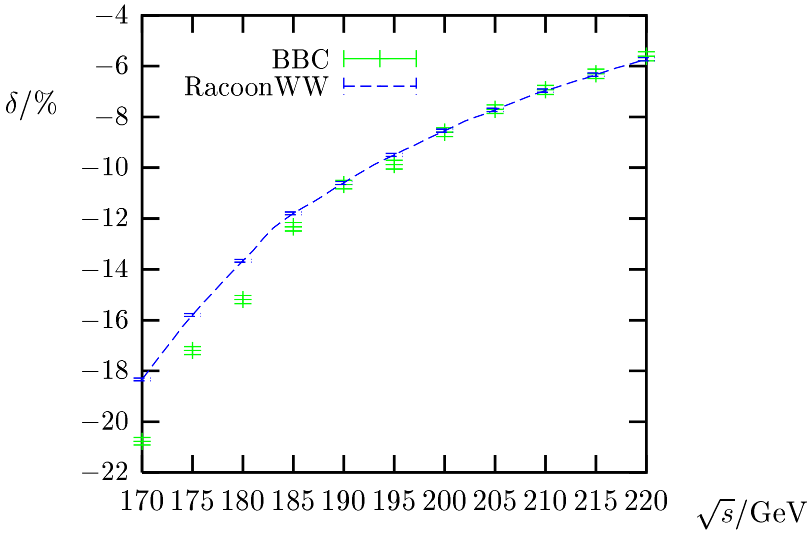

Fig. 16: Relative $\mathcal{O}(\alpha)$ corrections to the total cross section of $e^+e^- \to \nu_\mu\mu^+\tau^-\bar{\nu}_\tau$

visible, in agreement with the expected relative error of $\mathcal{O}(\Gamma_W/\Delta E)$. The main effect originates probably from the different treatment of the $\mathcal{O}(\alpha)$ ISR and the phase space. While `BBC` treat the complete $\mathcal{O}(\alpha)$ correction (including ISR) in DPA and use the on-shell phase space consistently, in `RacoonWW`[8] the universal leading-log part of the $\mathcal{O}(\alpha)$ ISR correction is applied to the *full CC11* cross section, and the off-shell phase space is used throughout. Below about $170\,\mathrm{GeV}$ the DPA cannot be trusted any more for both virtual corrections and real-photon radiation, since the kinetic energy of the W bosons becomes of the order of the W width.

For angular and energy distributions unavoidable differences arise from the definition of the phase-space variables in the presence of photon recombination. When defining the momenta of the W bosons for angular distributions, `BBC` chooses to assign the photon to one of the production/decay subprocesses. If the detected photon is hard, $E_\gamma \gg \Gamma_W$, then this is theoretically possible. The error in the assignment is suppressed by $\mathcal{O}(\Gamma_W/\Delta E)$. If the detected photon is semi-soft, $E_\gamma \sim \Gamma_W$, then it is impossible to assign it to any of the subprocesses, but as the photon momentum is much smaller than the W-boson momentum, the error associated with this procedure is suppressed by the same relative $\mathcal{O}(\Gamma_W/\Delta E)$. The angles are then determined from the resulting W-momenta and the original fermion momenta. In `RacoonWW`, all angles are defined from the fermion momenta after eventual photon recombination. To this end, the invariant masses of the photon with each of the charged initial- or final-state fermions are calulated. If the smallest of these invariant masses is smaller than M_{rec} and the fermion corresponding to this invariant mass is a final-state particle, the photon is recombined with this fermion. The two different angle definitions lead to a redistribution of events in the angular distributions, which arises, in particular, from hard photon emission.

The relative corrections to the distributions in the cosines of the production angle, $\theta_{\mathrm{W}} = \angle(\mathrm{e}^+, \mathrm{W}^+)$, and the decay angle, $\theta_{\mu\mathrm{W}} = \angle(\mu^+, \mathrm{W}^+)$, are compared for $\sqrt{s} = 184\,\mathrm{GeV}$ in Figure 8.4. The results of `BBC` are again shown as points with errorbars. The results of `RacoonWW` are plotted as histograms for two different photon recombination cuts $M_{\mathrm{rec}} = 5\,\mathrm{GeV}$ or $25\,\mathrm{GeV}$. The relative corrections in the two recombination schemes differ at the level of $0.5 - -1\%$ for large angles, where the cross section is small. The deviations between `BBC` and `RacoonWW` are somewhat larger but of the same order of magnitude. A repetition of the analysis at $\sqrt{s} = 250\,\mathrm{GeV}$ has shown that the deviations at large angles

[8] The exponentiation of ISR has been switched off in `RacoonWW` for this comparison, the on-shell Coulomb singularity has been used and no naive QCD corrections are included. Moreover, the lowest-order cross section used for normalization is calculated in DPA with on-shell phase space. This allows to compare directly the relative corrections of both approaches.

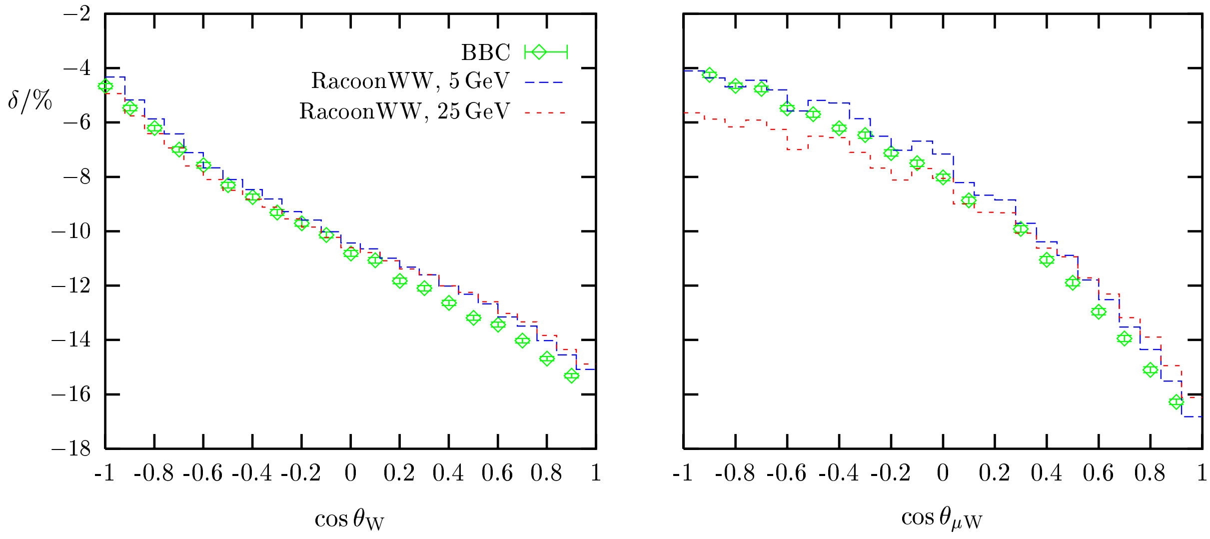

grow with increasing centre-of-mass energy, since also the hard-photon redistribution effects grow with energy.

Invariant-mass distributions depend crucially on the treatment of the real photons. Since this is fundamentally different in `RacoonWW` and `BBC`, it does not make sense to compare these distributions between the two programs. Specifically, `BBC` define the W invariant masses from the fermion momenta only (*bare* or muon-like) which make them sensitive to the collinear mass singularities. In `RacoonWW`, the photons are always recombined with the fermions (*calorimetric* or electron-like). The actual mass shifts crucially depend on the experimental setup. They are of the order of several $10\,\mathrm{MeV}$ and negative for the bare procedure. In the calorimetric treatment these mass shifts are reduced and can even become positive depending on the recombination procedure.

9. Theoretical uncertainty for CC03

From an experimental point of view CC03 occupies a special position. In CC03, LEP(ADLO) can now test the theory below its old uncertainty of $\pm 2\%$. Thus `RacoonWW/YFSWW` had been a hot topic around. Here we give a quantitative statement on the theoretical precision for DPA-approximation.

Estimating the theoretical uncertainty of the DPA with `RacoonWW`

All existing calculations of electroweak corrections to $\mathrm{e^+e^-} \to \mathrm{WW} \to 4f$ are based on the double-pole approximation (DPA). A naive estimate of the accuracy of this approach yields $(\alpha/\pi) \times \log(\ldots) \times \Gamma_{\mathrm{W}}/M_{\mathrm{W}}$, where $\Gamma_{\mathrm{W}}/M_{\mathrm{W}}$ is the generic accuracy of the DPA, α/π results from considering one-loop corrections, and $\log(\ldots)$ represents leading logarithms or other possible enhancement factors in the corrections. This naive estimate suggests that the DPA has an uncertainty of some 0.1%. Note, however, that this estimate can fail whenever small scales become relevant. In particular near the W-pair threshold, the estimate should be replaced by $(\alpha/\pi) \times \log(\ldots) \times \Gamma_{\mathrm{W}}/(\sqrt{s} - 2M_{\mathrm{W}})$.

In order to investigate the accuracy of the DPA quantitatively, a number of tests have been performed with `RacoonWW`. The implementation of the DPA has been modified within the formal level of $\alpha\Gamma_{\mathrm{W}}/M_{\mathrm{W}}$, and the obtained results have been compared. Note that in `RacoonWW` only the virtual corrections are treated in DPA, while real photon emission is based on the full $\mathrm{e^+e^-} \to 4f\gamma$ matrix element with the exact five-particle phase space. Thus, only the $2 \to 4$ part is effected by the following modifications. Specifically, three types of uncertainties have been considered (see Ref. [45] for details):

- Different on-shell projections:
  In order to define a DPA one has to specify a projection of the physical momenta to a set of momenta for on-shell W-pair production and decay[9]. This can be done in an obvious way by fixing the direction of one of the W bosons and of one of the final-state fermions originating from either W boson in the CM frame of the incoming $\mathrm{e^+e^-}$ pair. The default in `RacoonWW` is to fix the directions of the momenta of the fermions (not of the anti-fermions) resulting from the $\mathrm{W^+}$ and $\mathrm{W^-}$ decays (*def*). A different projection is obtained by fixing the direction of the anti-fermion from the $\mathrm{W^+}$ decay (*proj*) instead of the fermion direction.
- Treatment of soft photons:
  In `RacoonWW`, the virtual photon contribution is treated in DPA, while real photon radiation is fully taken into account. These two contributions have to be matched in such a way that IR and mass singularities cancel. This requirement only fixes the universal, singular parts, but leaves some freedom to treat non-universal, non-singular contributions in DPA or not. For instance, in the branch of `RacoonWW` that employs the subtraction method of Ref. [50], the endpoint contributions of the subtraction functions are calculated in DPA and added to the virtual photon contribution as default. As an option, `RacoonWW` allows to treat also the universal (IR-sensitive) part of the virtual photon contribution off-shell by extracting an U(1)-invariant factor à la YFS [117] from the virtual photon contribution and adding it to the real photon contribution, i.e. this soft+virtual part of the photonic correction is treated off shell (*eik*). The two described treatments only differ by terms of the form $(\alpha/\pi) \times \pi^2 \times \mathcal{O}(1)$ which are either multiplied with the DPA (*def*) or with the full off-shell Born cross sections (*eik*).
- On-shell versus off-shell Coulomb singularity:
  The Coulomb singularity is (up to higher orders) fully contained in the virtual $\mathcal{O}(\alpha)$ correction in DPA. Performing the on-shell projection to the full virtual correction leads to the on-shell Coulomb singularity. However, since the Coulomb singularity is an important correction in the LEP 2 energy range and is also known beyond DPA, `RacoonWW` includes this extra off-shell Coulomb correction as default. Switching the extra off-shell parts of the Coulomb correction off (*Coul*), yields an effect of the order of the accuracy of the DPA.

[9] This option only illustrates the effect of different on-shell projections in the four-particle phase space; if real photonic corrections are treated in DPA the impact of different projections may be larger.

	def	proj	eik	Coul
σ/pb	570.56(46)	570.47(46)	570.47(46)	571.30(46)
$\delta/\%$	0	-0.02	-0.02	0.13

Table 8: RacoonWW predictions for the total cross section of

In the following table and figures the total cross section and various distributions have been compared for the different versions of the DPA defined above. The results have been obtained using the LEP 2 input parameter set and the following set of separation and recombination cuts:

1. All photons within a cone of $5°$ around the beams are treated as invisible, i.e. their momenta are disregarded when calculating angles, energies, and invariant masses.
2. Next, the invariant masses of the photon with each of the charged final-state fermions are calculated. If the smallest one is smaller than a certain cutoff M_{rec} or if the energy of the photon is smaller than $1\,\mathrm{GeV}$, the photon is combined with the corresponding fermion, i.e. the momenta of the photon and the fermion are added and associated with the momentum of the fermion, and the photon is discarded.
3. Finally, all events are discarded in which one of the final-state fermions is within a cone of $10°$ around the beams. No other cuts are applied.

The recombination cut is chosen to be $M_{\mathrm{rec}} = 25\,\mathrm{GeV}$. As default, we take the RacoonWW results of Section **??** for the process $\mathrm{e^+e^-} \to \mathrm{u\bar{d}}\mu^-\bar{\nu}_\mu(\gamma)$ at $\sqrt{s} = 200\,\mathrm{GeV}$, which are based on the above input. The only differences are that the naive QCD factors and ISR corrections beyond $\mathcal{O}(\alpha)$ are not included in the results of this section.

ref to Section comparison wi YFSWW

The results for the total cross section are shown in Table 8. Note that these cross sections are calculated with the above cuts. We find relative differences at the level of 0.1–0.2%. As expected, the prediction that is based on the on-shell Coulomb correction is somewhat higher than the exact off-shell treatment, since off-shell effects screen the positive Coulomb singularity.

In Figures 17 and 18 we show the differences of the *proj*, *eik*, and *Coul* modifications to the default version of the DPA for some distributions. For the distribution in the W-production angle θ_{W^+} and in the W-decay angle $\theta_{\mathrm{W}^+\mu^+}$ (see Figure 17) the relative differences are of the order of 0.1–0.3% for all angles, which is of the expected order for the intrinsic DPA uncertainty. For the μ-energy distribution, shown in the l.h.s. of Figure 18, the differences are typically of the same order, as long as E_μ is in the range for W-pair production, which is $20.2\,\mathrm{GeV} < E_\mu < 79.8\,\mathrm{GeV}$ at $\sqrt{s} = 200\,\mathrm{GeV}$. Outside this region, the four-fermion process is not dominated by the W-pair diagrams, and the DPA is not reliable anymore, which is also indicated by large intrinsic ambiguities. The r.h.s. of Figure 18 shows the DPA uncertainties for the $\mathrm{d\bar{u}}$ invariant-mass distribution. Within a window of $2\Gamma_{\mathrm{W}}$ around the W resonance the relative differences between the considered modifications are also at the level of 0.1–0.3%. The differences grow with the distance from the resonance point.

The discussed results illustrate that the intrinsic ambiguities of the DPA, as applied in RacoonWW, are at the level of a few per mil, whenever resonant W-pair production dominates the considered observable.

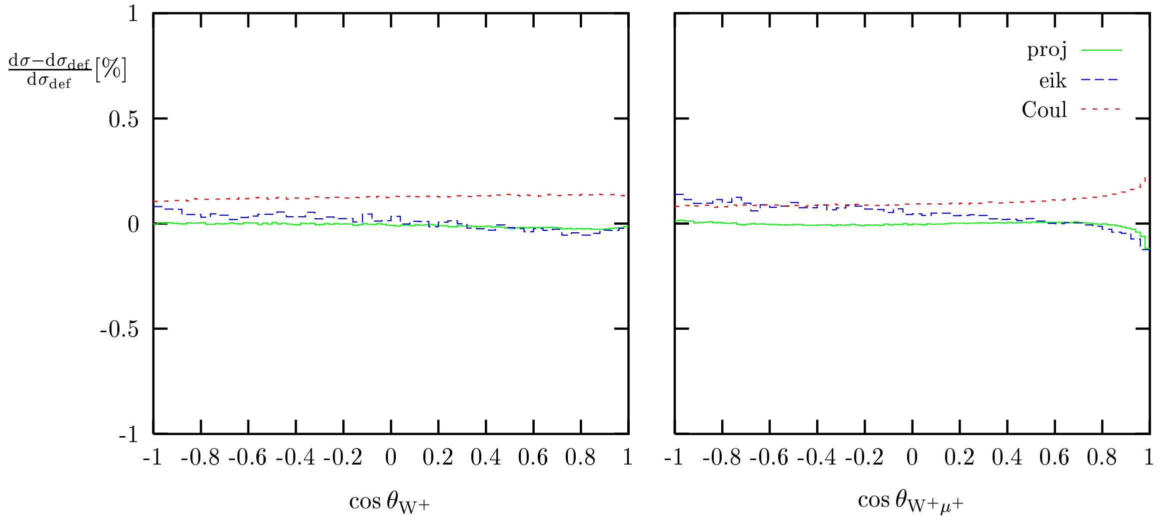

Fig. 17: Theoretical uncertainty within the DPA for distributions in the W-production and W-decay angles

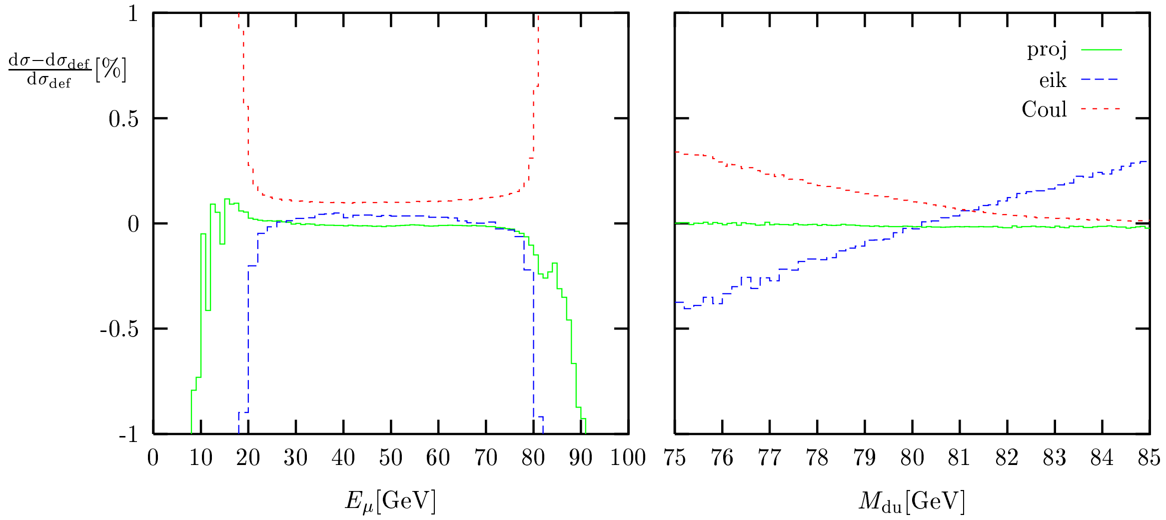

Fig. 18: Theoretical uncertainty within the DPA for distributions in

10. Four fermions plus a visible photon.

The class of processes that are investigated at LEP 2 are, in decreasing order of importance, $e^+e^- \to W^+W^- \to 4\,\mathrm{f}$, single-$W$ production, Z-boson-pair production, single-Z production. LEP 2 and also future linear colliders will allow us to study a new class of processes, $e^+e^- \to 4\mathrm{f} + \gamma$.

The physical interest of the latter is twofold. They can be used to obtain informations on the quartic gauge-boson couplings and include the production processes of three gauge-bosons, $W^+W^-\gamma$, $ZZ\gamma$ and $Z\gamma\gamma$. In this case the photon is visible by definition and we term the corresponding process *radiative*, i.e. we consider as radiative events those events with photons where at least one photon passes the experimental photon requirements. For instance $E_\gamma > 1\,$GeV, $\cos\theta_\gamma < 0.985(0.997)$ and $\theta_{f-\gamma} > 5^\circ$.

Note that for all final states, the invariant mass needs a more precise definition in case radiative photons are present in the event. From a calculational point of view, there is always a minimal invariant mass (energy and separation angle) below which photons are not *resolved*. Thus we need to specify fermion-photon invariant mass or fermion-photon energies and separation angles,

- below which the the photon are combined with the fermion and
- above which the photons are not included in the mass calculation.

A *bare* mass would set these cuts rather tight, excluding photons from the $f\overline{f}$ mass, a *calo* mass would set the separation cuts looser. Theorists like cuts on $M(\gamma - \mathrm{nearest}\, f)$. Experimentalists like cuts on energies and angles.

In the following we list both **TH-cuts** and **EXP-cuts**. Experiments agree with one conclusion, i.e. they prefer the angles, but if nothing can be produced then they would accept invariant masses.

TH cuts :
bare $M(\overline{f}f + (\gamma))$ including photons if $M(f+\gamma) < 5\,$GeV,
calo $M(\overline{f}f + (\gamma))$ including photons if $M(f+\gamma) < 25\,$GeV.

EXP-cuts :
bare : $M(\overline{f}_1 f_2 + (\gamma))$, photons less than 1 GeV or less than 1° away from f_1 or f_2 are included;
calo : $M(\bar{l}_1 l_2 + (\gamma))$, photons less than 1 GeV or less than 10° away from charged leptons are included,
$M(\overline{q}_1 q_2 + (\gamma))$, photons less than 1 GeV or less than 25° away from quarks $q_1 q_2$ are included, which takes at least the major difference between fermions - quarks versus leptons - into account.

These definitions serve for benchmarking distributions, not so much to mimic an actual experimental strategy, which is of course fermion dependent. In other words this is an approximation to the experimental side: if the fermion is a muon, they can separate even 0° opening angles. In addition, for identified photons we still may or may not choose to recombine the photon with the fermion.

Furthermore, $e^+e^- \to 4\mathrm{f}+\gamma$ id an important building block for the radiative corrections to the Born process $e^+e^- \to 4\,\mathrm{f}$, hence non-radiative events are those with no photon or only photons below the minimal photon requirements. In case of non-radiative events, this amounts to adding up virtual and soft radiative corrections. The effect of $\mathcal{O}\,(\alpha)$ QED corrections very often amounts to several percent, mostly originating from collinear photon radiation off highly energetic particles and from virtual photon exchange. For initial state radiation, for instance, we have three types of corrections, a) $\mathcal{O}\,(\alpha/\pi\,\ln(m_e/Q))$ with $Q \gg m_e$ being the typical scale at which the process occur, b) $\mathcal{O}\,(\alpha/\pi)$ from hard photons that must, nevertheless, be included for a 1% precision tag, c) leading $\mathcal{O}\,(\alpha^2)$, or higher corrections that becomes relevant for a precision tag below the 1% thresholds.

Owing to the fact that a theoretical prediction with a typical accuracy of some fraction of a percent must include all QED corrections, we face the complexity of it. Handling the singularities of the squared matrix element represents a formidable task; in any bremsstrahlung process the integrand blows up for arbitrary small photon energies and similar problems arise from collinear emission off the charged particles.

A general comment about this section is that technical precision is not a problem anymore. When tuned to the same IPS and renormalization schemes, all codes are equivalent, as far as technical precision is concerned. Most of the results, however, concern $WW(ZZ)$-like cuts and only one example is shown for single-W cuts.

10.1 $4f+\gamma$ with `RacoonWW`

Authors

Ansgar Denner	ansgar.denner@psi.ch
Stefan Dittmaier	stefan.dittmaier@cern.ch
Markus Roth	markus.roth@itp.uni-leipzig.de
Doreen Wackeroth	dow@pas.rochester.edu

10.11 General description

The program `RacoonWW` [45] evaluates cross-sections and differential distributions for the reactions $\mathrm{e}^+\mathrm{e}^- \to 4f$ and $\mathrm{e}^+\mathrm{e}^- \to 4f+\gamma$ for all four-fermion final states. The long write-up has already been presented.

10.2 $4f+\gamma$ with `PHEGAS/HELAC`

Authors

C. Papadopoulos

Nothing available yet.

10.3 $4f+\gamma$ with `WRAP`

Authors

G. Montagna
M. Moretti
O. Nicrosini
M. Osmo
F. Piccinini

10.31 Description of the Method.

Contributions of the Pavia/`ALPHA` group to the subject of four fermions plus gamma final states are summarized.

10.32 Hard-scattering matrix element

The exact tree-level matrix elements for the processes with four fermions plus a visible photon in the final state are computed by means of the `ALPHA` algorithm [70]. At present, the processes which can be mediated by two W-bosons (CC processes) or by two Z-bosons (NC processes) are accounted for. The effect of finite fermion masses is taken into account exactly both in the kinematics and dynamics. The contribution of anomalous *trilinear* gauge couplings can be also simulated, after having implemented in `ALPHA` and cross-checked the parameterization in terms of Δk_γ, λ_γ, δ_Z, Δk_Z and λ_Z of refs. [135, 72]. The genuinely anomalous *quartic* gauge boson couplings, involving at least one photon and relevant for this process at tree-level, are also included, according to the parameterization of ref. [111]. Final cross-checks on anomalous quartic couplings are in progress. The fixed-width scheme is adopted as gauge-restoring approach, as motivated in comparison with other gauge-invariance-preserving schemes in ref. [112].

10.33 Radiative corrections

The phenomenologically relevant Leading Log (LL) QED radiative corrections, due to initial-state radiation (ISR), are implemented via the Structure Function (SF) formalism [74], according to the two following options:

- collinear SF $D(x,s)$;
- p_t-dependent SF $\tilde{D}(x,\cos\vartheta_\gamma;s)$, i.e. a combination of the collinear SF $D(x,s)$ with an angular factor for photon radiation inspired by the leading behaviour $1/(p\cdot k)$ [113, 114].

In fact, as discussed in detail in refs. [114, 115], due to the presence of an observed photon in the final state, the treatment of ISR in terms of collinear SF turns out to be inadequate because affected by double counting between the pre-emission photons (described by the SF) and the observed one (described by the hard-scattering matrix element). By keeping under control also the transverse degrees of freedom of ISR, as allowed by p_t-dependent SF, it is possible to remove the double-counting effects, following the procedure for the calculation of the QED corrected cross-section discussed in ref. [114, 115], i.e.

$$\sigma_{QED}^{4f+1\gamma} = \int dx_1 dx_2 dc_\gamma^{(1)} dc_\gamma^{(2)}\, \tilde{D}(x_1, c_\gamma^{(1)}; s)\tilde{D}(x_2, c_\gamma^{(2)}; s)\Theta(\mathrm{cuts})d\sigma^{4f+1\gamma}\,, \tag{70}$$

where $c_\gamma^{(i)} \equiv \cos\vartheta_\gamma^{(i)}$, $i=1,2$. According to eq. (70), an *equivalent* photon is generated for each colliding lepton and accepted as a higher-order ISR contribution if:

- the energy of the equivalent photon is below the threshold for the observed photon E_γ^{min}, for arbitrary angles; or
- the angle of the equivalent photon is outside the angular acceptance for the observed photons, for arbitrary energies.

Within the angular acceptance of the detected photon, the cross-section is evaluated by means of the exact matrix element for the processes $e^+e^- \to 4f+\gamma$. Therefore, eq. (70) applies to the signature of four fermions plus exactly one photon in the final state, corrected by the effects of undetected soft and/or collinear ISR. The Q^2-scale entering the QED SF is fixed to be $Q^2 = s$.

10.34 Computational tool

The theoretical features sketched above have been implemented into a massive MonteCarlo (MC) program, named `WRAP` (`W` `R`adiative process with `A`lpha & `P`avia). The multi-channel importance sampling technique is employed to perform the phase-space integration, paying particular attention to the infrared and collinear peaking structures due to photon emission. The code supports realistic event selections and can be employed either as a cross-section calculator or as a true event generator.

10.35 Results Obtained

Results obtained in our study can be summarized as follows:

- critical analysis of the effect of ISR (see Fig. 19, Fig. 20, Fig. 21);
- study of the impact of finite fermion masses (see Fig. 22);
- tuned comparisons with the predictions of other codes, especially with `RACOONWW` (see Sec. 10.5).

ISR. The impact of ISR via collinear SF on the $4f+\gamma$ integrated cross-section of the CC10 final state $\mu^-\ \overline{\nu}_\mu\ u\ \overline{d}\ \gamma$ is shown in Fig. 19 and Fig. 20, as a function of the LEP2 c.m. energy (Fig. 19) and of the photon energy threshold at $\sqrt{s} = 192$ GeV (Fig. 20). Fig. 19 shows that ISR in the collinear approximation reduces the Born cross-section between 16-12% in the c.m. range 180-190 GeV and at the 10% level close to 200 GeV, for the considered photon separation cuts. In particular, at $\sqrt{s} = 192$ GeV the reduction factor as due to ISR is 12-13%, almost independent of the photon detection threshold, as shown in Fig. 20. In order to better understand the uncertainty associated to the implementation of ISR in $4f+\gamma$ processes, a comparison between the effects of ISR via collinear SF and p_t-dependent SF, respectively,

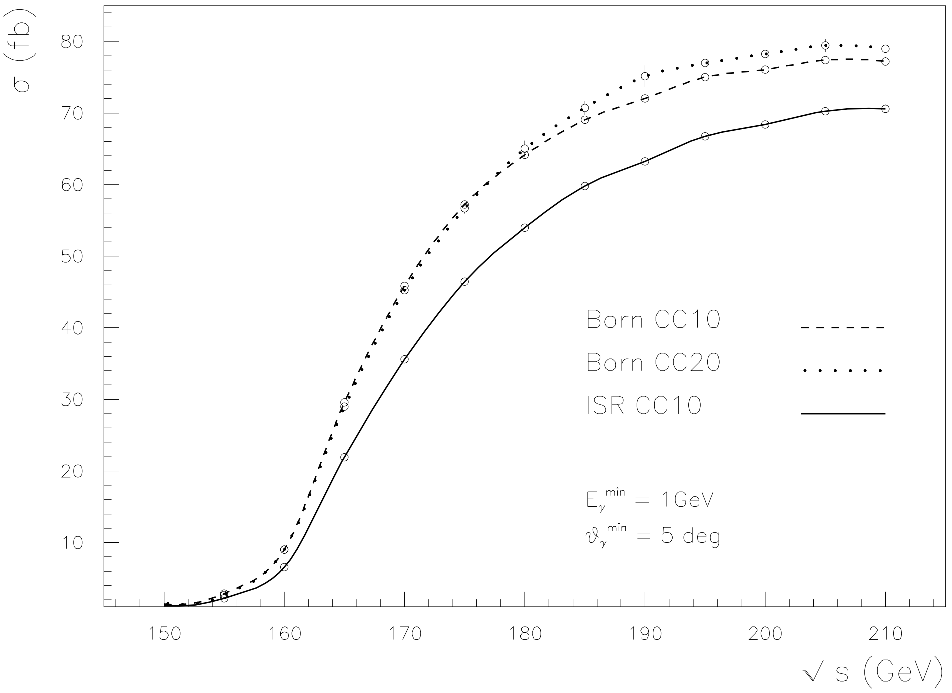

Fig. 19: The effect of ISR, simulated by collinear SF, on the integrated cross section of the CC10 final state $\mu^- \ \overline{\nu}_\mu \ u \ \overline{d} \ \gamma$ as a function of the LEP2 c.m. energy. The Born cross-section for the CC20 final state $e^- \ \overline{\nu}_e \ u \ \overline{d} \ \gamma$ is also shown.

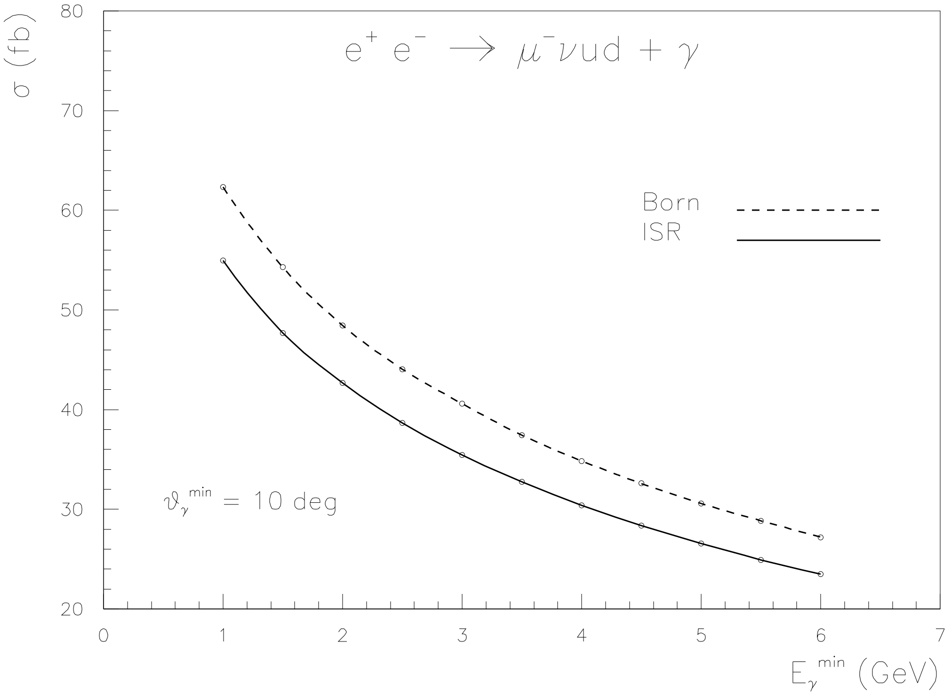

Fig. 20: The effect of ISR via collinear SF to the cross-section of the CC10 final state $\mu^- \ \overline{\nu}_\mu \ u \ \overline{d} \ \gamma$, as a function of the minimum energy of the observed photon, at 192 GeV.

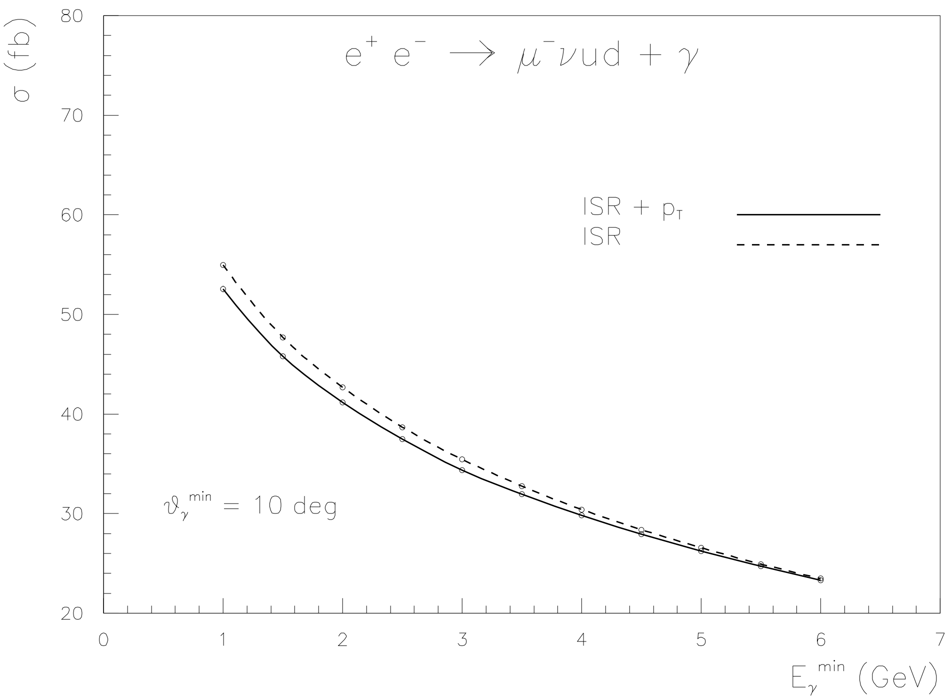

Fig. 21: Comparison between the effects of ISR via collinear SF (dashed line) and p_t-dependent SF (solid line), respectively, for the cross section of the the CC10 final state $\mu^- \; \overline{\nu}_\mu \; u \; \overline{d} \; \gamma$, as a function of the minimum energy of the observed photon, at 192 GeV.

is shown in Fig. 21 for the cross section of the the CC10 final state $\mu^- \; \overline{\nu}_\mu \; u \; \overline{d} \; \gamma$, as a function of the minimum energy of the observed photon, at $\sqrt{s} = 192$ GeV. As can be seen, the two prescriptions for ISR can differ at 5% level for E_γ^{min} close to 1-2 GeV, while the difference becomes smaller and smaller as E_γ^{min} increases. In general, the difference between collinear and p_t-dependent SF is stronger near the soft and collinear regions, as a priori expected, and it gives an estimate of the size of the double-counting effect at the level of ISR. *Fermion masses.* In Fig. 22 a comparison between the cross-section for the final state $\mu^- \; \overline{\nu}_\mu \; c \; \overline{s} \; \gamma$ in the massless approximation is compared with the same cross-section in the presence of finite masses for the final state fermions. The mass values and cuts used are: $m_\mu = 0.105$ GeV, $m_s = 0.3$ GeV, $m_c = 1.55$ GeV, with $M_{cs} \geq 3$ GeV. The mass effects are of the order of 1%, almost independent of realistic photon separation cuts.

10.36 Estimate of TU

In order to provide an estimate of TU associated to QED radiation in $4f$ processes, it would be important to compare the predictions of an exact $4f + \gamma$ matrix elements with a Parton Shower dressing of the corresponding $4\mathrm{f}$ final state.

`WRAP` has tried to estimate the theoretical uncertainty in $4\mathrm{f} + \gamma$ processes coming from variations in the renormalization scheme. The selected process is $e^+e^- \to u\bar{d}\mu^-\bar{\nu}_m u\gamma$ with the cuts used in the tuned comparisons. The following two schemes have been adopted:

$$
\begin{aligned}
I)s^2 &= 1 - \frac{M_W^2}{M_Z^2}, \quad alpha = \frac{4\,sqrt2\,G_F M_W^2 s^2}{4\,\pi}, \quad g^2 = 4\,\pi\,\frac{\alpha}{s^2}, \\
II)s^2 &= \frac{\pi\alpha(2M_W)}{/}\sqrt{2}G_F M_W^2, \quad g^2 = 4\sqrt{2}G_F M_W^2, \quad \text{with } \alpha(2M_W) = 128.07.
\end{aligned}
\tag{71}
$$

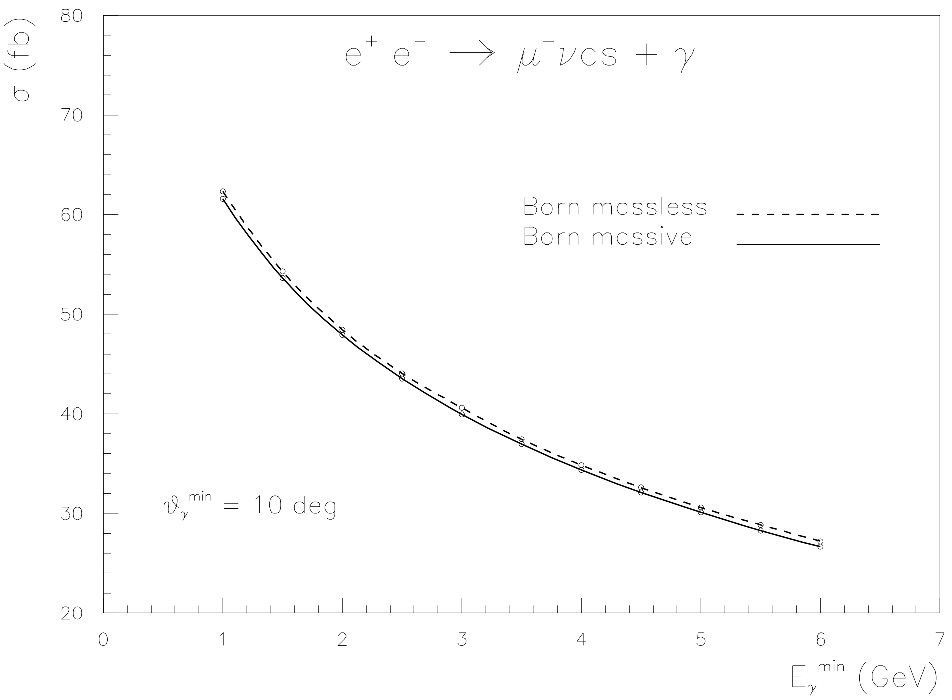

Fig. 22: The effect of fermion masses on the cross section of the CC10 final state $\mu^- \ \overline{\nu}_\mu \ c \ \overline{s} \ \gamma$, as a function of the minimum energy of the observed photon, at 192 GeV.

The cross section is always rescaled by the factor $\alpha(0)/\alpha$ in order to take into account of the scale $\alpha(0)$ for the emitted real photon. The results are shown in Tab.(9).

$\sqrt{s}$ [GeV]	cross section [fb]	δ
200 (I)	75.750(29) fb	
200 (II)	75.887(29) fb	0.18%
189 (I)	71.889(25) fb	
189 (II)	71.997(25) fb	0.15%
183 (I)	67.238(22) fb	
183 (II)	67.324(22) fb	0.13%

Table 9: Estimate of TU according to `WRAP`.

10.4 Recommendations

As shown by our analysis, ISR needs to be taken into account in programs for a realistic analysis of $4f+\gamma$ final states. Furthermore, in order to avoid double-counting between pre-emission and matrix-element radiation, the implementation of QED corrections in computational tools for $4f+\gamma$ processes should rely upon methods, such PS, YFS or p_t-dependent SF, able to keep under control photon p_t effects. Effects due to finite fermion masses can become important at the percent level for small photon-charged fermion separation cuts.

10.5 Available Comparisons

A first set of comparisons between the predictions of `WRAP` and those of other independent codes, namely `CompHEP, GRACE` and `RACOONWW`, is available as documented.

This comparison covers integrated cross-sections and various differential distributions, essentially for a CC10 final state. Discrepancies observed at that stage are mainly to be ascribed to non-tuned comparisons. In fact, a detailed tuned comparison between `WRAP` and `RACOONWW` presently shows a beautiful agreement for several distributions and final states. Additional results from `PHEGAS/HELAC` are also included in the comparison.

Input parameters and cuts used to carry out this tuned comparison correspond to those of the 4f proposal (in the approximation of massless fermions). In particular, the photon cuts are: $E_\gamma^{min} = 1$ GeV, $|\cos\vartheta_\gamma| < 0.985$, at $\sqrt{s} = 200$ GeV. In the `RACOONWW-WRAP` comparison, the following processes have been considered:

- $\mu\,\overline{\nu}_\mu\, u\,\overline{d}\,\gamma$
- $e^-\,\overline{\nu}_e\, u\,\overline{d}\,\gamma$
- $\mu\,\overline{\nu}_\mu\,\tau^+\,\nu_\tau\,\gamma$
- $e^-\,\overline{\nu}_e\,\tau^+\,\nu_\tau\,\gamma$
- $s\,\bar{c}\,u\,\overline{d}\,\gamma$

The observables studied are:

- integrated cross-sections;
- E_γ distribution in the range [0, 50] GeV, 100 bins, $d\sigma/dE$ [fb/GeV];
- $\cos\vartheta_\gamma$ in the range [-1, 1], 100 bins $d\sigma/d\cos\vartheta_\gamma$ [fb];
- opening angle $\vartheta_{f\gamma}$ between photon and the nearest charged final-state fermion in the range [0°, $180°$], 100 bins, $d\sigma/d\theta_{\gamma f}$ [fb];
- $M_{u\bar{d}}$, $M_{\tau^+\nu_\tau}$ invariant mass in the range [40, 120] GeV, 160 bins, $d\sigma/dM$ [fb/GeV];
- $M_{u\bar{d}}$, $M_{\tau^+\nu_\tau}$ invariant mass in the range [75, 85] GeV, 100 bins, $d\sigma/dM$ [fb/GeV];
- $M_{e^-\bar{\nu}_e}$ for the process $e^-\,\overline{\nu}_e\,\tau^+\,\nu_\tau\,\gamma$ in the range [40, 120] GeV, 160 bins, $d\sigma/dM$ [fb/GeV];
- $M_{e^-\bar{\nu}_e}$ for the process $e^-\,\overline{\nu}_e\,\tau^+\,\nu_\tau\,\gamma$ in the range [75, 85] GeV, 100 bins, $d\sigma/dM$ [fb/GeV];

All the observables are calculated for $\sqrt{s} = 200$ GeV in the fixed width scheme. The input parameters are:

- $\alpha(0) = 1/137.0359895$,
- $G_F = 0.1166370 \times 10^{-4}\,\mathrm{GeV}^{-2}$,
- $M_W = 80.35$ GeV,
- $M_Z = 91.1867$ GeV,
- $\Gamma_W = 2.04277$ GeV,
- $\Gamma_Z = 2.49471$ GeV,
- $s_\theta^2 = 1 - \frac{M_W^2}{M_Z^2}$,
- $\alpha = \frac{\sqrt{2}G_F}{\pi}\,M_W^2\,s_\theta^2$.

The squared matrix element is multiplied by $\alpha(0)/\alpha$ to take exactly into account of the scale of the real photon. The applied cuts are:

- common to all processes: $E_\gamma > 1$ GeV, $|\cos(\theta(\gamma,\mathrm{beam})| < 0.985$, $\theta(\gamma,\mathrm{f}) > 5°$, f = charged fermion.
- for $ud\mu\nu_\mu$ and $ude\nu_e$: $M(ud) > 10$ GeV $|\cos\theta(\mathrm{l},\mathrm{beam})| < 0.985$ $E_\mathrm{l} > 5$ GeV, where l is a charged lepton,

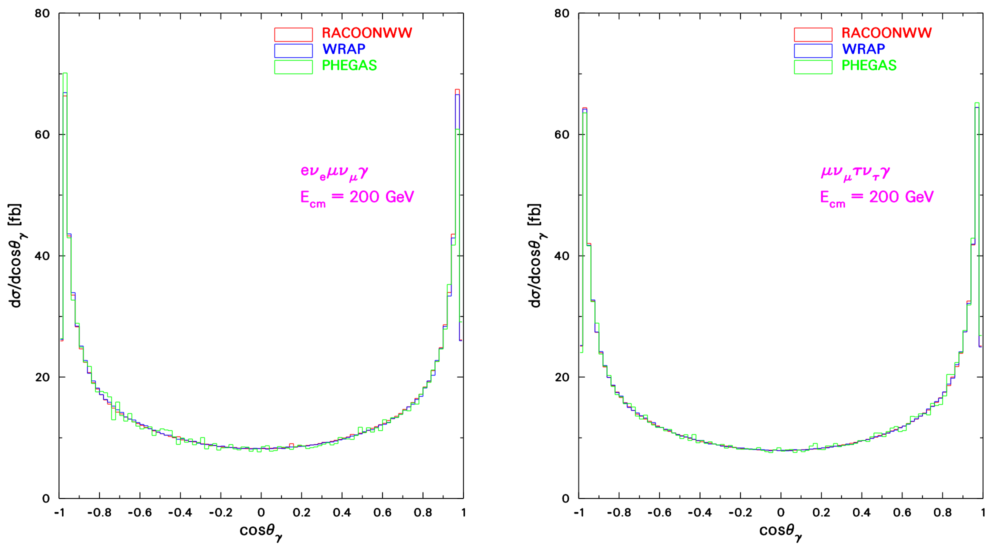

Fig. 23: $\cos\vartheta_\gamma$ distribution for the processes $\nu_\mu\mu^+e^-\overline{\nu}_e$ and $\nu_\mu\mu^+\tau^-\overline{\nu}_\tau$.

- for $\tau\nu_\tau\mu\nu_\mu$ and $\tau\nu_\tau e\nu_e$: $|\cos\theta(\mathrm{l},\mathrm{beam})| < 0.985$, $E_\mathrm{l} > 5\,\mathrm{GeV}$, $M(l^+l^-) > 10\,\mathrm{GeV}$,
- for $udcs$: at least two pairs with $M(q_iq_j) > 10\,\mathrm{GeV}$.

The total cross-sections are reported in Fig. 10 where the differences between `WRAP` and `RacoonWW` are around 0.1%, signalling perfect technical agreement. Results from `PHEGAS/HELAC` register, in general, a 0.5% difference although the MC error is ten times larger. Next we consider the angular distribution,

Process	`WRAP`	`RacoonWW`	`PHEGAS/HELAC`
$u\overline{d}\mu^-\overline{\nu}_\mu$	75.732(22)	75.647(44)	76.200(350)
$u\overline{d}e^-\overline{\nu}_e$	78.249(43)	78.224(47)	78.140(423)
$\nu_\mu\mu^+\tau^-\overline{\nu}_\tau$	28.263(9)	28.266(17)	28.359(111)
$\nu_\mu\mu^+e^-\overline{\nu}_e$	29.304(19)	29.276(17)	29.185(154)
$u\overline{d}s\overline{c}$	199.63(10)	199.60(11)	200.48(81)

Table 10: Comparison between `WRAP`, `RacoonWW` and `PHEGAS/HELAC` for a sample of total cross-sections (fb).

i.e. the $\cos\vartheta_\gamma$ distribution in the range [-1, 1], as reported in Figs. 23–25. By comparing two different codes with a *tuned* comparison we get a rough estimate of the associated theoretical uncertainty. In Fig. 26 we plot the difference `WRAP/RacoonWW` - 1 in percent for the $\cos\vartheta_\gamma$ distribution for the processes $\nu_\mu\mu^+e^-\overline{\nu}_e$. The E_γ distribution in the range [1, 50] GeV is shown for various processes in Figs. 27–29. Note that virtual corrections are not included, therefore, the photon spectrum starts at some lower boundary of 1 Gev. In Fig. 26 we plot the difference `WRAP/RacoonWW` - 1 in percent for the E_γ distribution for the processes $u\overline{d}\mu^-\overline{\nu}_\mu$. Deviations are of the order of 1% for soft photons and tends to deteriorate for harder ones, although in the same region the technical precision of the two codes becomes considerably less.

In Fig. 31 we show the $\theta(\gamma,\mathrm{charged fermion})$ distribution. In the same figure we show the percentage deviation between the two predictions. The most interesting region occurs for small angles, i.e.

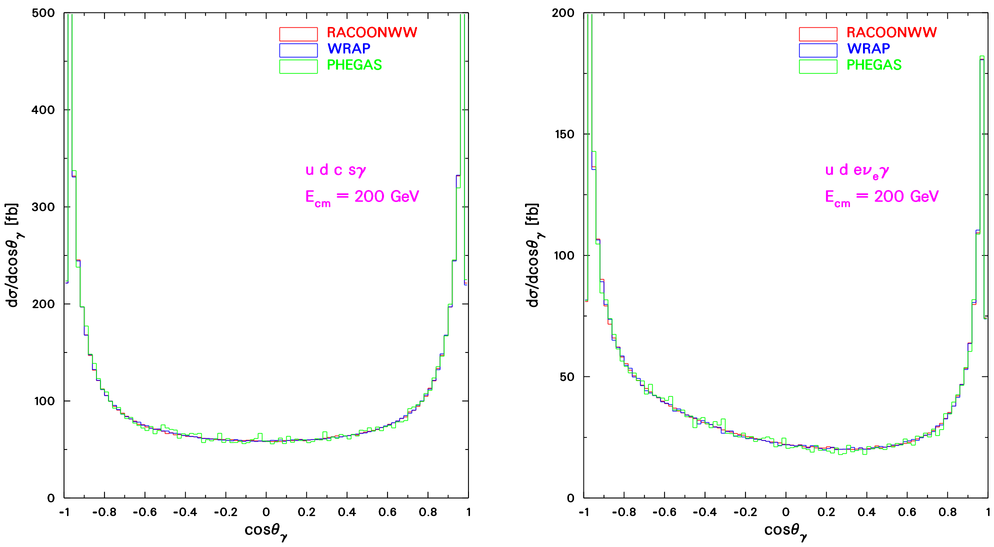

Fig. 24: $\cos\vartheta_\gamma$ distribution for the processes $u\overline{d}s\overline{c}$ and $u\overline{d}e^-\overline{\nu}_e$.

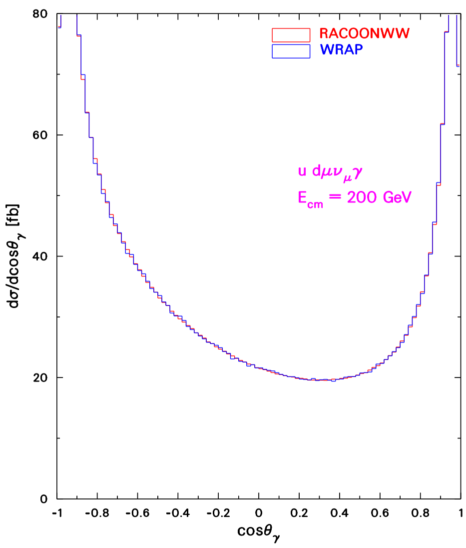

Fig. 25: $\cos\vartheta_\gamma$ distribution for the processes $u\overline{d}s\overline{c}$ and $u\overline{d}\mu^-\overline{\nu}_\mu$.

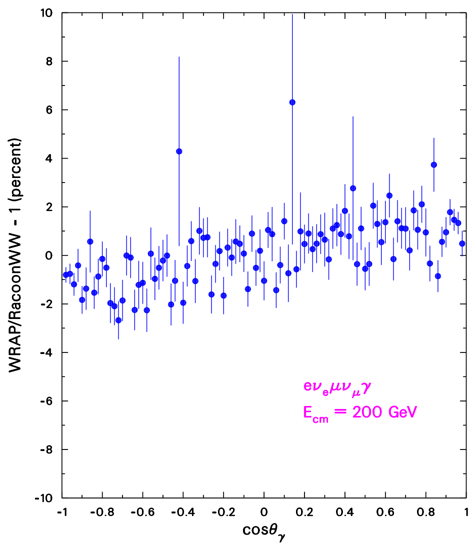

Fig. 26: The ratio WRAP/RacoonWW for the $\cos\vartheta_\gamma$ distribution in the processes $\nu_\mu\mu^+e^-\overline{\nu}_e$.

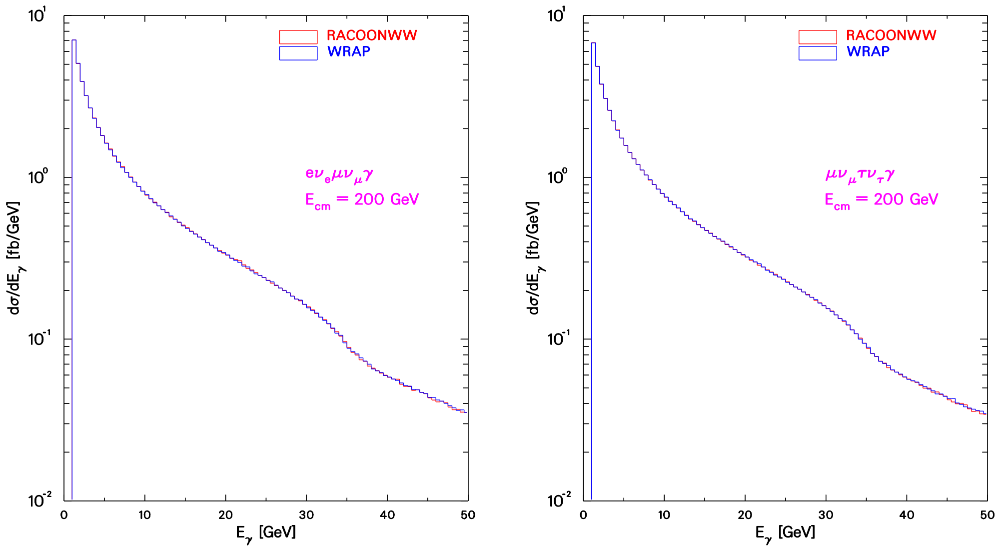

Fig. 27: E_γ distribution for the processes $\nu_\mu\mu^+e^-\overline{\nu}_e$ and $\nu_\mu\mu^+\tau^-\overline{\nu}_\tau$.

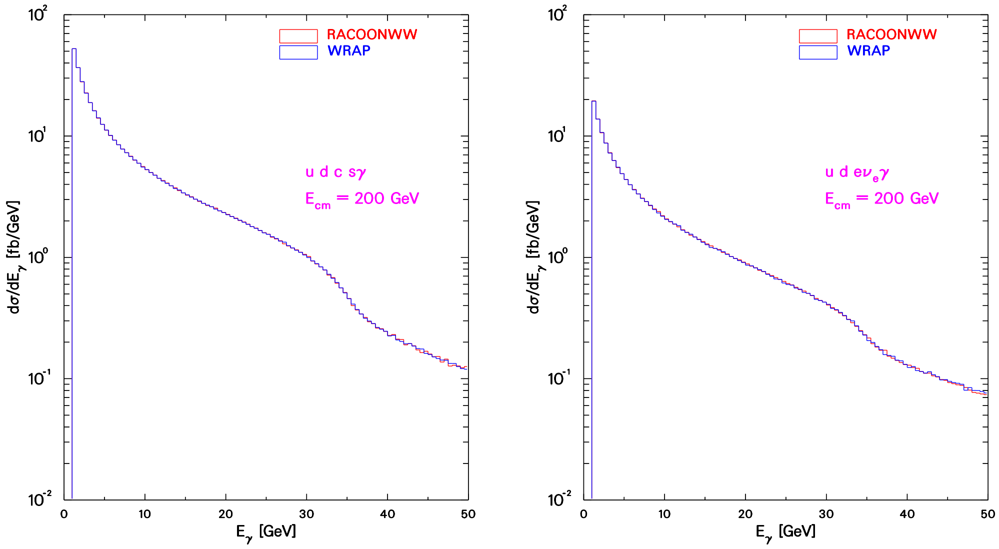

Fig. 28: E_γ distribution for the processes $u\overline{d}s\overline{c}$ and $u\overline{d}e^-\overline{\nu}_e$.

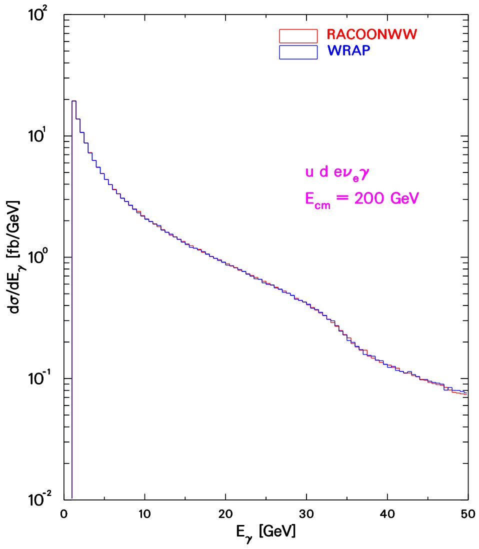

Fig. 29: E_γ distribution for the processes $u\overline{d}s\overline{c}$ and $u\overline{d}\mu^-\overline{\nu}_\mu$.

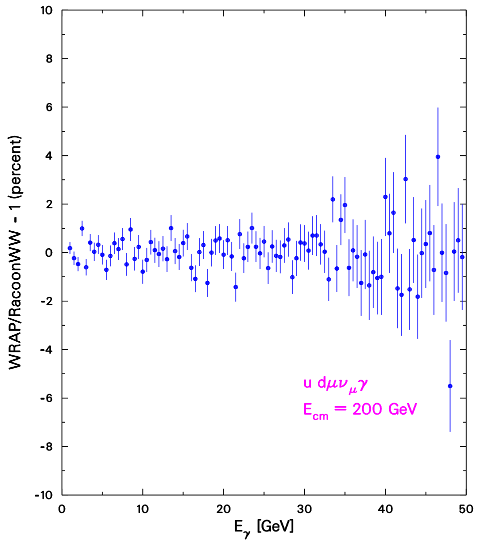

Fig. 30: The ratio WRAP/RacoonWW for the E_γ distribution in the processes $u\overline{d}\mu^-\overline{\nu}_\mu$.

towards the collinear region, where a reasonable agreement is registered, of the order of few percent. The agreement deteriorates for larger separation between the photon and the charged particles. However, in this region the cross-section is a factor of magnitude lower. Note that the peculiar behavior of the distribution towards $0°$ is only due to the fact that the third bin is between $3.6°$ and $5.4°$ with a cut at $5°$. Here we have the results of the tuned comparison between WRAP and RACOONWW concerning the bare masses for the following processes:

1. $u\overline{d}\mu^-\overline{\nu}_\mu$,
2. $u\overline{d}e^-\overline{\nu}_e$,
3. $\nu_\mu\mu^+\tau^-\overline{\nu}_\tau$,
4. $\nu_\mu\mu^+e^-\overline{\nu}_e$,
5. $u\overline{d}s\overline{c}$.

The distributions cover the bare W^- and W^+ invariant masses ($d\sigma/dM$ [fb/GeV]) in the two ranges:

1. 75-85 GeV with 100 bins
2. 40-120 GeV with 160 bins

Input parameters and cuts are stated above. Results for all channels and for the W^--distribution are shown in Fig. 32 where we also show percentage deviations for the process $u\overline{d}s\overline{c}$. In Fig. 33 we give the corresponding W^+-distribution, where also PHEGAS is included. In Fig. 34 we show the ratio between the W^+ and the W^- mass distributions.

10.6 On-shell W boson approximation for $e^+e^- \to \gamma\mu\bar{\nu}_\mu u\bar{d}$

Authors

E. Boos
M. Dubinin
V. Ilyin

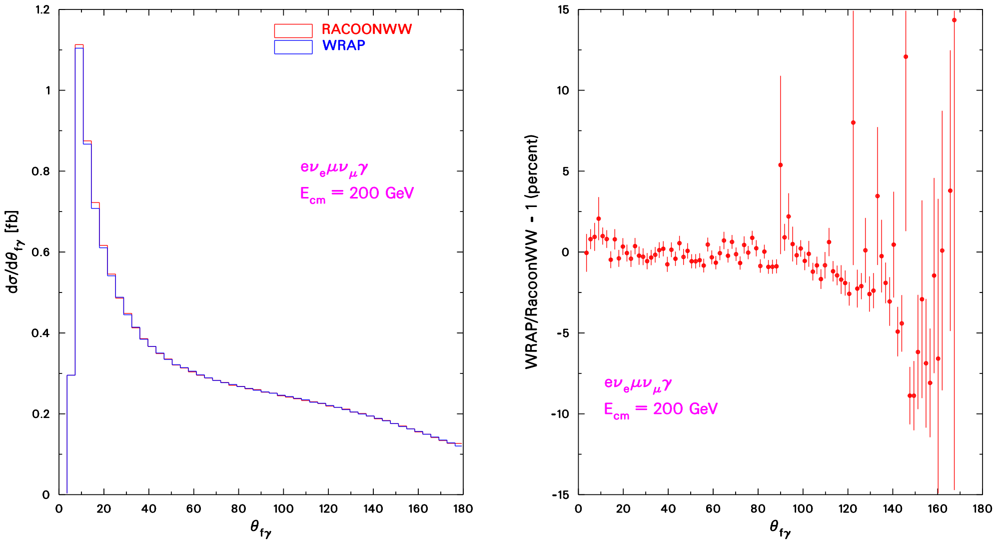

Fig. 31: The prediction from WRAP --RacoonWW for the $\theta(\gamma, \mathrm{charged fermion})$ distribution in the processes $e\nu_e\mu^-\overline{\nu}_\mu$. The ratio WRAP/RacoonWW is also shown.

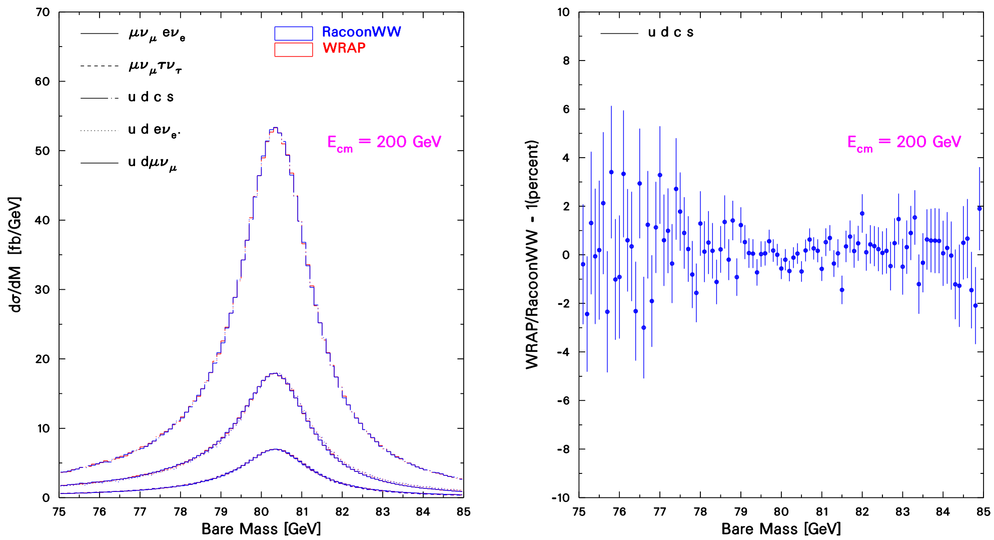

Fig. 32: Bare W^- mass distributions and percentage deviations between WRAP and RacoonWW for one specific example, $u\overline{d}s\overline{c}$.

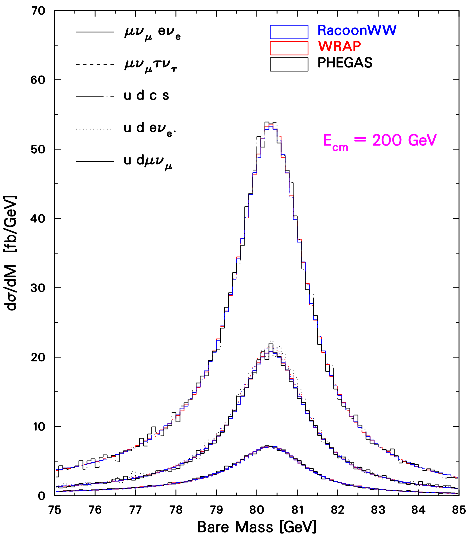

Fig. 33: Bare W^+ mass distributions from `WRAP`, `RacoonWW` and `PHEGAS`.

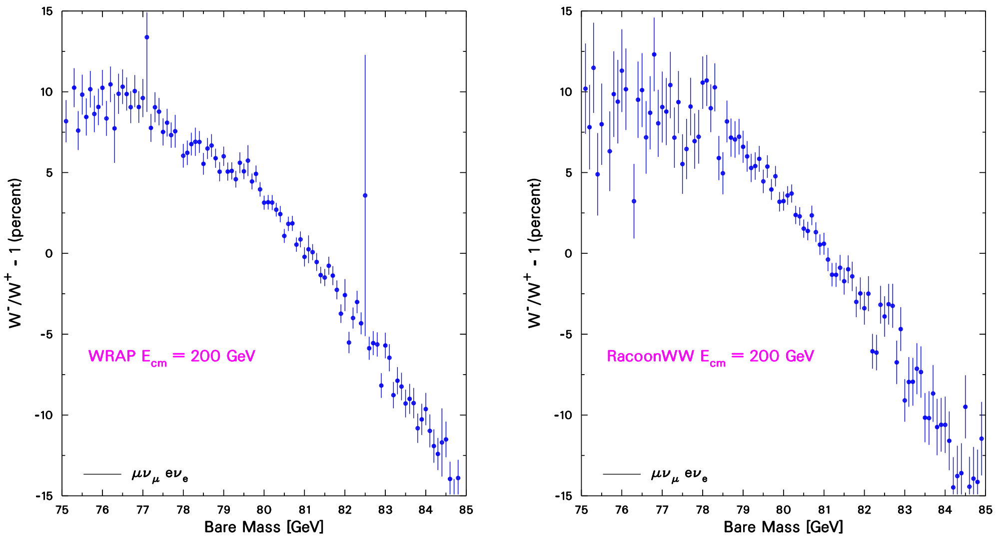

Fig. 34: Ratio W^-/W^+ mass distributions from `WRAP` and `RacoonWW` for one specific example.

In the $2 \to 4$ approximation of the on-shell W boson $e^+e^- \to \gamma\mu\bar{\nu}_\mu W^+$ for the $2 \to 5$ process $e^+e^- \to \gamma\mu\bar{\nu}_\mu u\bar{d}$ the number of diagrams is much smaller (31 for the 4-body and 71 for the 5-body final state). It is interesting to find out if a simpler on-shell W approximation reproduces with enough likelihood the total rate and distributions given by the exact $2 \to 5$ tree level amplitude. CompHEP [118] squared diagrams technique applied to the 5-body state (2556 squared diagrams) leads to a rather tedious and CPU time consuming computations, so the possibility to describe quantitatively the 5-body distributions of radiative events by some trivial change of the normalization in the 4-body results looks attractive.

We calculated the cross section of the process $e^+e^- \to \gamma\mu\bar{\nu}_\mu W^+$ multiplied by a factor given by the following on-shell W isotropic decay to $u\bar{d}$. Vectors of the u, $\bar{d}$ quarks momenta generated randomly in the rest frame of the W were boosted to the e^+e^- c.m.s., where the standard kinematical cuts

$$E_\gamma \geq 1 \text{ GeV}, \qquad E_\mu \geq 5 \text{ GeV},$$
$$|\cos\theta_{\gamma e}| \leq 0.985, \qquad |\cos\theta_{\mu e}| \leq 0.985, \qquad \theta_{\gamma,\mu},\, \theta_{\gamma,u},\, \theta_{\gamma,\bar{d}} \geq 5^\circ$$

were introduced. Such a scheme of calculation is based on the well-known approximation of infinitely small W width $M_W\Gamma_{tot}/[(M^2_{u\bar{d}} - M^2_W)^2 + M^2_W\Gamma^2_{tot}] \Rightarrow \pi\,\delta(M^2_{u\bar{d}} - M^2_W)$ and have been widely used for the simulation of the 3- and 4-body final states in many generators. The `PYTHIA` generator [119] follows generally the same scheme, but the W decay products invariant mass is distributed according to the Breit-Wigner and gamma radiation from quarks can be switched on in the approximation of final state shower.

The total rate of the $\sigma(e^+e^- \to \gamma\mu\bar{\nu}_\mu W^+)$ Br$(W^+ \to u\bar{d})$ is equal to $49.4(2)$ fb to be compared with the exact $2 \to 5$ result $69.1(9)$ fb. Missing contribution of the omitted diagrams, especially from the phase space regions near the collinear and infrared poles of the photons radiated from the initial state and the u, d quarks leads to substantial underestimate of the rate. Distributions in the photonic energy and transverse momentum, calculated in the infinitely small W width approximation, reproduce qualitatively correctly the exact $2 \to 5$ results (see upper plots in Fig. **??**). Peaks of the forward and back-scatterd photons (Fig. **??**), radiated from the initial e^+, e^-, are much stronger underestimated than the photon distribution in the central rapidity region. Distributions in the quark energy and transverse momentum (upper plots in Fig. **??**) are rather different in the exact and approximate calculation. For the exact calculation the quark energy spectrum more rapidly decreases than for the approximation where the photon radiation from quarks is not accounted for. Transverse momentum distribution is underestimated for all p_T greater than 20 GeV. In the exact 5-body consideration the W boson is created in a rather well defined polarization state, so our approximation of an isotropic on-shell W decay may be unsatisfactory for angular variables. Large difference of the distributions in the photon-fermion (muon or quark) angle (lower plot in Fid.1) is caused by a simple combinatorial reason. *Calo* jet-jet mass (lower plot in Fig. **??**) contains the unresolved photon radiated from the initial state or from the muon, so only $M_{u\bar{d}\gamma} \geq M_W$ is possible.

It follows that in the case of four fermion events with radiative photon the approximation of the on-shell W isotropic decay does not, generally speaking, satisfactorily describe both the total rate and the full set of final particle distributions.

10.7 $4\text{f} + \gamma$ with `NEXTCALIBUR`

Authors

F.A.Berends
C. G. Papadopoulos
R.Pittau

In this Sections we show illustrative results for the processes $e^+e^- \to \mu^-\mu^+u\bar{u}$ (ZZ signal), $e^+e^- \to \mu^-\bar{\nu}_\mu u\bar{d}(\gamma)$ (WW signal) and $e^+e^- \to e^-\bar{\nu}_e u\bar{d}(\gamma)$ (single-W signal).

We used the set of cuts specified in the proposal at $\sqrt{s} = 200$ GeV, all diagrams and fermion masses included. The distributions are the energy and the $\cos\theta$ (with respect to the incoming e^+) of the most energetic photon (100 bins from $0 < E_\gamma < 50$ GeV and $-1 < \cos_\theta < 1$). Three or four values of cross section (in pb) are shown. The first value corresponds to radiative plus non-radiative events (within the specified separation cuts for the generated photons), the second one to non-radiative events and the third one to radiative events. In some cases, we also include a fourth entry that represents the small fraction of radiative events with 2 photons.

Some comments are in order for the process $e^+e^- \to e^-\bar{\nu}_e u\bar{d}(\gamma)$ (CC20). To generate ISR, we used Structure Functions with two different scales for the two incoming fermions ($q_+^2 = s$ and $q_-^2 = |t|$), as described previously. Also, rather than using our Modified Fermion Loop approach, we rescaled, event by event, by a factor $(\frac{\alpha(t)}{\alpha_{G_F}})^2$. Note, however, that the recipe of using Structure Functions with a proper choice of scales is not enough to determine without ambiguity the pattern of the radiation in t-channel dominated processes. The reason is that, when $|t| = q^2 \sim m_e^2$, the Structure Function approach fails and one has to introduce a cut-off value for $|t|$, below which only non-radiative events from the corresponding leg are generated. To produce numbers for run n. 1 we used a cut-off value of $|t| = 100\ m_e^2$. To estimate the sensitivity of the result to that choice, we run again the program with a cut-off value of $|t| = e\ m_e^2 = 2.71828\ m_e^2$. The results is reported as run n. 2. As a reference, we report two more results, namely numbers obtained by running CC20 with both ISR scales equal to s, but keeping the rescaling $(\frac{\alpha(t)}{\alpha_{G_F}})^2$ (run n. 3), and numbers with both ISR scales equal to s and without $(\frac{\alpha(t)}{\alpha_{G_F}})^2$ rescaling (run n. 4).

Finally, to check the sensitivity of the distributions to the chosen form of Structure Function, we run again the processes $e^+e^- \to \mu^-\mu^+u\bar{u}(\gamma)$ and $e^+e^- \to e^-\bar{\nu}_e u\bar{d}(\gamma)$ with a slightly different implementation of the sub-leading terms, without observing any significant deviation with respect to the previous results.

Process: $e^+(1)e^-(2) \to \mu^-(3)\mu^+(4)u(5)\overline{u}(6)$.

- Here $M(34) > 10\,\mathrm{GeV}$ and $M(56) > 10\,\mathrm{GeV}$.
- Separation cuts for the photons: $E_gamma > 1\,\mathrm{GeV}, |\cos\theta_gamma| < 0.985$.
- Cross-sections are shown in Tab.(11).

Type	Cross-section
σ_{tot}	16.070(12)
σ_{nrad}	15.530(12)
σ_{rad}	0.5402(30)
σ_{drad}	0.0180(5)

Table 11: Cross-sections in fb from NEXTCALIBUR

Process: $e^+(1)e^-(2) \to \mu^-(3)\overline{\nu}_\mu(4)u(5)\overline{d}(6)$.

- Here $M(56) > 10\,\mathrm{GeV}$.
- Separation cuts for the photons: $E_gamma > 1\,\mathrm{GeV}, |\cos\theta_gamma| < 0.985$.
- Cross-sections are shown in Tab.(12).

Process: $e^+(1)e^-(2) \to e^-(3)\overline{\nu}_e(4)u(5)\overline{d}(6)$.

- Cut of on $|t| = 100\,m_e^2$ in the e^- Structure Function;

- $M(56) > 45\,\mathrm{GeV}$, no energy cut;
- Separation cuts for the photons: $E_gamma > 1\,\mathrm{GeV}, |\cos\theta_gamma| < 0.997$
- Cross-sections are shown in Tab.(13).

- Cut of on $|t| = 2.71828\,m_e^2$ in the e^- Structure Function;
- $M(56) > 45\,\mathrm{GeV}$, no energy cut;
- Separation cuts for the photons: $E_gamma > 1\,\mathrm{GeV}, |\cos\theta_gamma| < 0.997$
- Cross-sections are shown in Tab.(14).

Process: $e^+(1)e^-(2) \to e^-(3)\overline{\nu}_e(4)u(5)\overline{d}(6)$.

- Both ISR scales = s, with $(\alpha(t)/\alpha_{G_F})^2$ rescaling;
- $M(56) > 45\,\mathrm{GeV}$, no energy cut.
- Separation cuts for the photons: $E_gamma > 1\,\mathrm{GeV}, |\cos\theta_gamma| < 0.997$.
- Cross-sections are shown in Tab.(15).

Process: $e^+(1)e^-(2) \to e^-(3)\overline{\nu}_e(4)u(5)\overline{d}(6)$.

- Both ISR scales = s, without $(\alpha(t)/\alpha_{G_F})^2$ rescaling;
- $M(56) > 45\,\mathrm{GeV}$, no energy cut.
- Separation cuts for the photons: $E_gamma > 1\,\mathrm{GeV}, |\cos\theta_gamma| < 0.997$.
- Cross-sections are shown in Tab.(16).

10.8 $4\mathrm{f} + \gamma$ with GRACE

Authors

Y. Kurihara
M. Kuroda
Y. Shimizu

In this Section we present results from GRACE for the $4\mathrm{f} + \gamma$ processes with W-pair and single-W cuts.

Parameters and cuts used are the same as those of the WRAP and RacoonWW collaborations, except that we used α_{G_F} for all vertices. When GRACE numbers are be compared with the others one should multiply by a factor $\alpha(0)/\alpha_{G_F}$.

The differential cross sections are normalized to the total cross section instead of unity. If you simply summed up each bin without multiplying a bin-width, you can get the total cross section.

To check the calculations, the following tests have been performed for the processes $e^+e^- \to \mu\overline{\nu}_\mu u\overline{d}\gamma$ at $\sqrt{s} = 200\,\mathrm{GeV}$:

- Gauge parameter independence check; the amplitude generated by GRACE keeps gauge parameters in covariant gauge. We numerically checked that the amplitude is independent of gauge parameters at several phase-space points. With the quadratic precision calculations, it is confirmed that the amplitude does not depend on the gauge parameter at order of 10^{-30}.
- Ward Identity check; when the polarization vector of the external photon is replaced by their for-momentum, the amplitude must be zero due to Ward-Identity. We have checked it numerically at several phase-space points. After the replacement the amplitude is at order of 10^{-60} with the quadratic precision calculations.
- Soft photon check; the cross-sections with soft-photon emission can be easily calculated by non-radiation cross-section and the soft-photon emission function. We have calculated the soft-photon emission cross-section by two methods;

Type	Cross-section
$\sigma_{\rm tot}$	614.65(60)
$\sigma_{\rm nrad}$	595.00(59)
$\sigma_{\rm rad}$	19.65(13)
$\sigma_{\rm drad}$	0.56(2)

Table 12: Cross-sections in fb from NEXTCALIBUR

Type	Cross-section
$\sigma_{\rm tot}$	103.88(27)
$\sigma_{\rm nrad}$	100.05(29)
$\sigma_{\rm rad}$	3.83(3)
$\sigma_{\rm drad}$	0.118(4)

Table 13: Cross-sections in fb from NEXTCALIBUR

Type	Cross-section
$\sigma_{\rm tot}$	104.32(63)
$\sigma_{\rm nrad}$	100.16(54)
$\sigma_{\rm rad}$	4.16(33)

Table 14: Cross-sections in fb from NEXTCALIBUR

Type	Cross-section
$\sigma_{\rm tot}$	100.55(19)
$\sigma_{\rm nrad}$	96.75(19)
$\sigma_{\rm rad}$	3.80(4)

Table 15: Cross-sections in fb from NEXTCALIBUR

Type	Cross-section
$\sigma_{\rm tot}$	106.56(20)
$\sigma_{\rm nrad}$	102.53(20)
$\sigma_{\rm rad}$	4.03(4)

Table 16: Cross-sections in fb from NEXTCALIBUR

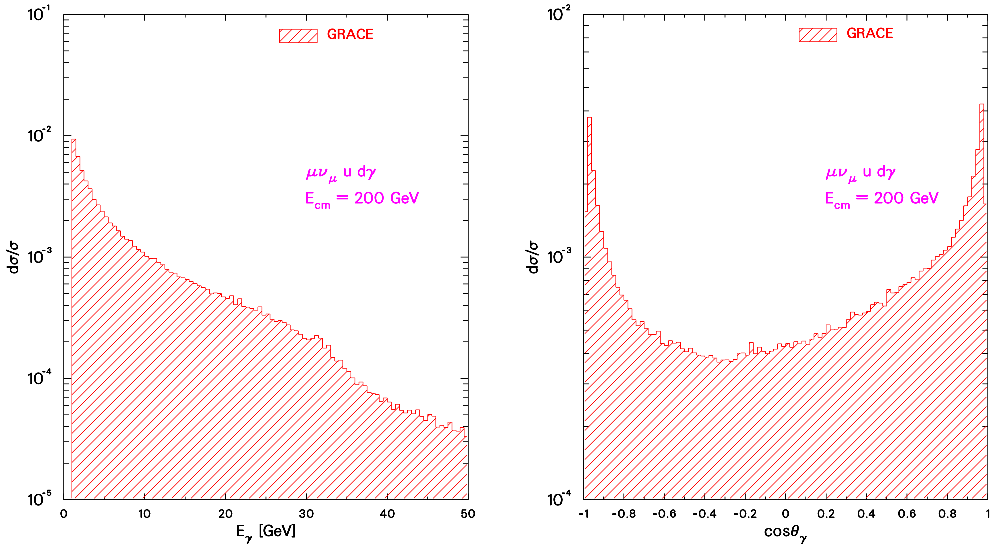

Fig. 35: E_γ and $\cos\theta_\gamma$ distributions for the processe $\mu\nu_\mu ud\gamma$ from GRACE with WW-cuts.

1. Using $4\mathrm{f} + \gamma$ matrix elements with cuts, $10^{-4}\,\mathrm{GeV} < E_\gamma < 10^{-2}\,\mathrm{GeV}$, no angular cut on the photon, $|\cos\theta_\mu| < 0.985$, $E_\mu > 5\,\mathrm{GeV}$, $M(ud) > 10\,\mathrm{GeV}$, giving $\sigma = 0.5105 \pm -0.0002\,\mathrm{pb}$;
2. Using $4\mathrm{f}$ matrix elements with soft-photon function with cuts, $10^{-4}\,\mathrm{GeV} < E_\gamma < 10^{-2}\,\mathrm{GeV}$, no angular cut on the photon, $|\cos\theta_\mu| < 0.985$, $E_\mu > 5\,\mathrm{GeV}$, $M(ud) > 10\,\mathrm{GeV}$ giving $\sigma = 0.5109 \pm 0.0005\,\mathrm{pb}$.

The two methods, therefore, give consistent results.

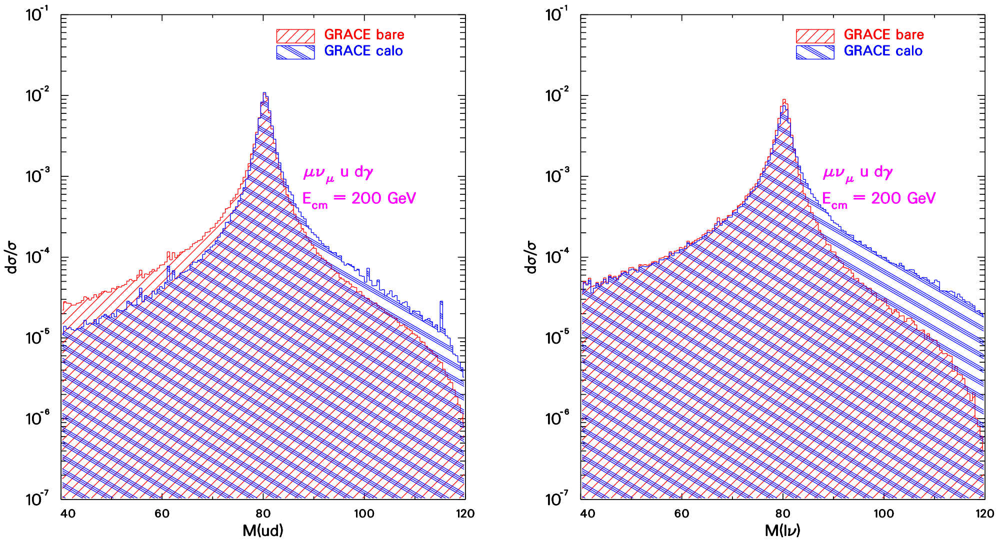

Fig. 36: Bare and calo $M(ud)$ distributions for the processe $\mu\nu_\mu ud\gamma$ from GRACE with WW-cuts.

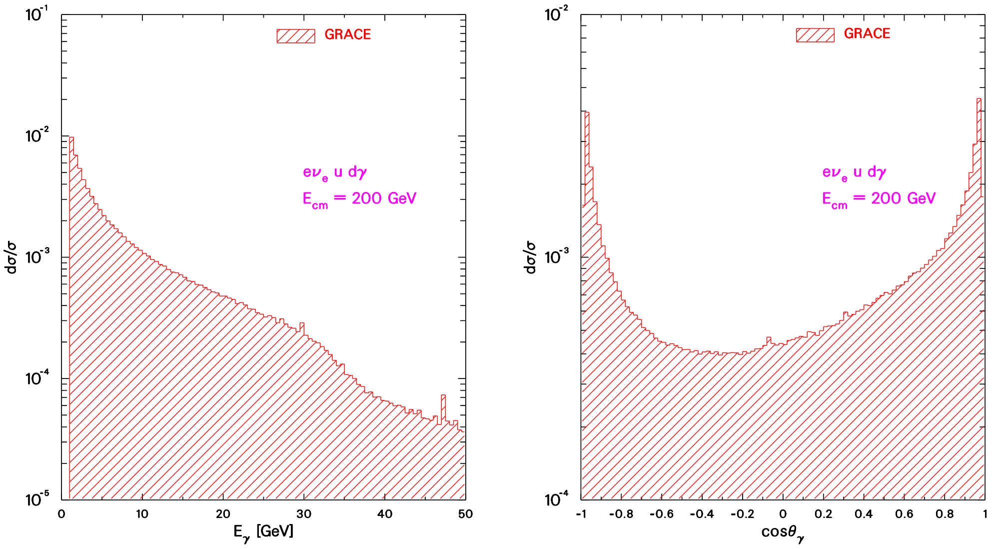

Fig. 37: E_γ and $\cos\theta_\gamma$ distributions for the processe $e\nu_e ud\gamma$ from GRACE with WW-cuts.

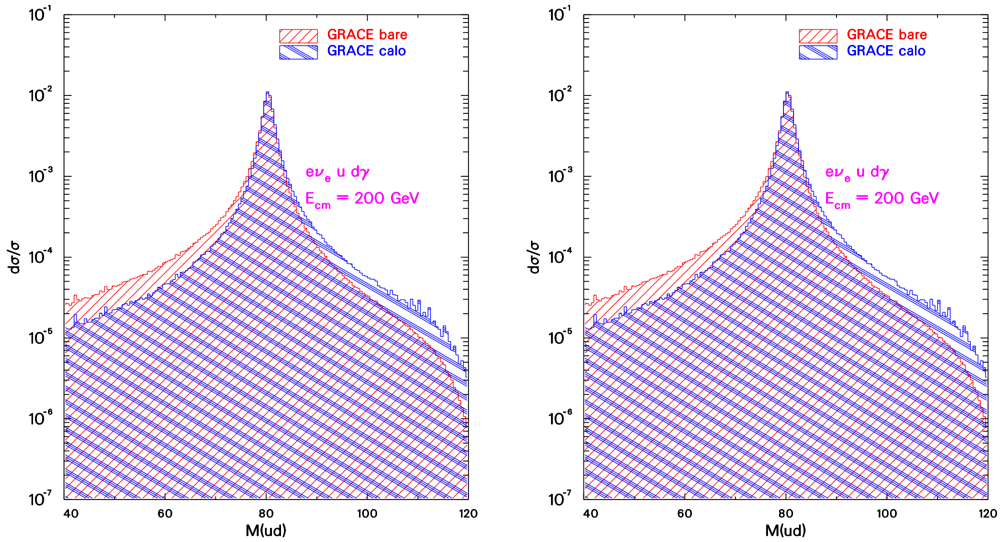

Fig. 38: Bare and calo $M(ud)$ distributions for the processe $e\nu_e ud\gamma$ from GRACE with WW-cuts.

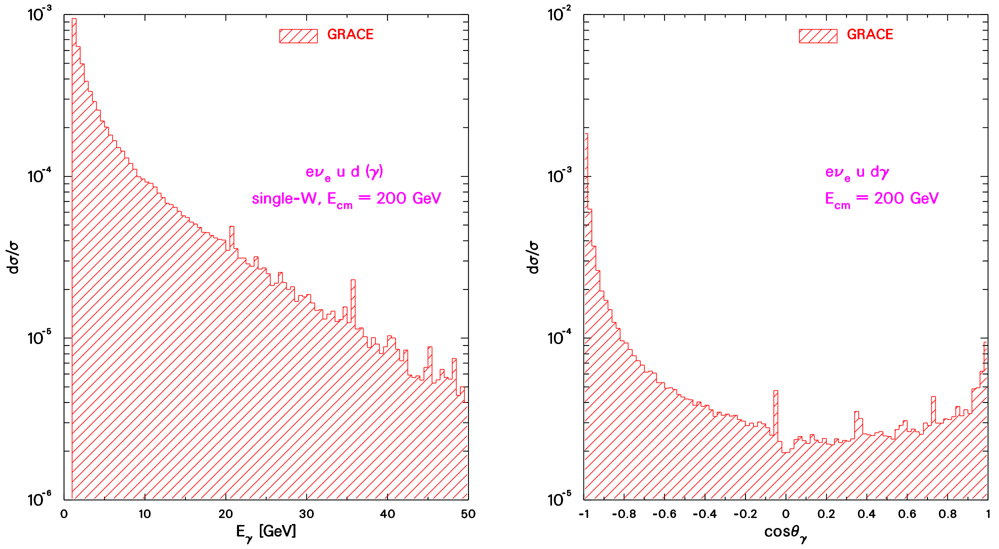

Fig. 39: E_γ and $\cos\theta_\gamma$ distributions for the processe $e\nu_e ud\gamma$ from GRACE with single-W cuts.

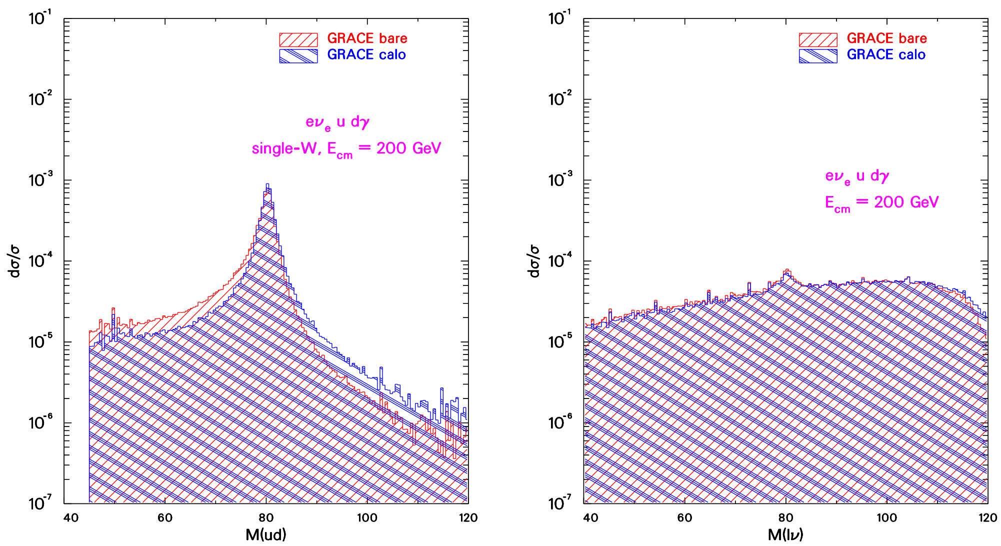

Fig. 40: Bare and calo $M(ud)$ distributions for the processe $e\nu_e ud\gamma$ from `GRACE` with single-W cuts.

11. Single-W

Another interesting process at LEP 2 is the so-called single-W production, $e^+e^- \to W e\nu$ which can be seen as a part of the CC20 process, $e^+e^- \to \overline{q}\,q\,(\mu\,\nu_\mu,\ \tau\,\nu_\tau)\,e\,\nu_e$, or as a part of the Mix56 process, $e^+e^- \to e^+\,e^-\,\nu_e\,\overline{\nu}_e$. For a more detailed theoretical review we refer to [54] and to [55].

All processes in the CC20/Mix56 families are usually considered in two regimes, $|\cos\theta(e^-)| \geq c$ or LA and $|\cos\theta(e^-)| \leq c$ or SA. Strictly speaking the single W production is defined by those events that satisfy $|\cos\theta(e^-)| \geq 0.997$ and, therefore is a SA.

The LA cross-section has been computed by many authors and references can be found in [56]. It represents a contribution to the $e^+e^- \to W^+W^-$ total cross-section, in turn used to derive a value for M_W, the W boson mass. From a theoretical point of view the evaluation of a LA cross-section is free of ambiguity, even in the approximation of massless fermions, as long as a gauge-preserving scheme is applied and $\theta(e^-)$ is not too small.

For SA instead, one cannot employ the massless approximation anymore. In other words, in addition to double-resonant W-pair production with o ne W decaying into $e\nu_e$, there are t-channel diagrams that give a sizeable contribution for small values of the polar scattering angle of the t-channel electron.

Single-W processes are sensitive to the breaking of $U(1)$ gauge invariance in the collinear limit, as described in Ref. [27] (see also [57]). The correct way of handling them is based on the so-called Fermion-Loop (FL)scheme [31], the gauge-invariant treatment of the finite-width effects of W and Z bosons in LEP2 processes. However, till very recently, the Fermion-Loop scheme was available only for the LA-regime.

For $e^+e^- \to e^-\overline{\nu}_e f_1 \overline{f}_2$, the $U(1)$ gauge invariance becomes essential in the region of phase space where the angle between the incoming and outgoing electrons is small, see the work of [27] and also an alternative formulations in [58]. In this limit the superficial $1/Q^4$ divergence of the propagator structure is reduced to $1/Q^2$ by $U(1)$ gauge invariance. In the presence of light fermion masses this gives raise to the familiar $\ln(m_e^2/s)$ large logarithms.

Furthermore, keeping a finite electron mass through the calculation is not enough. One of the main results of [54] was to show that there are remaining subtleties in CC20, associated with the zero mass limit for the remaining fermions.

In Ref. [59] a generalization of the Fermion-Loop scheme has been given (for previous work we refer to [60]). It consists of the re-summation of the fermionic one-loop corrections to the vector-boson propagators and of the inclusion of all remaining fermionic one-loop corrections, in particular those to the Yang–Mills vertices. In the original formulation, the Fermion-Loop scheme requires that vector bosons couple to conserved currents, i.e., that the masses of all external fermions can be neglected. There are several examples where fermion masses must be kept to obtain a reliable prediction. As already stated, this is the case for the single-W production mechanism, where the outgoing electron is collinear, within a small cone, with the incoming electron. Therefore, m_e cannot be neglected.

Furthermore, among the 20 Feynman diagrams that contribute (for $e\overline{\nu}_e u\overline{d}$ final states, up to 56 for $e^+e^-\nu_e\overline{\nu}_e$) there are multi-peripheral ones that require a non-vanishing mass also for the other outgoing fermions. In [59] a generalization of the Fermion-Loop scheme (EFL) is introduced to account for external, non-conserved, currents. Dyson re-summed transitions are introduced without neglecting the $p_\mu p_\nu$-terms and including the contributions from the Higgs-Kibble ghosts in the 't Hooft-Feynman gauge.

The EFL has been implemented within the FORTRAN program `WTO` [61], and in this section we discuss the corresponding numerical results and the comparison, for single-W, between the EFL- scheme and the Fixed-Width (hereafter FW) one.

To be specific the name of Fixed-Width scheme is reserved for the following: the cross-section is computed using the tree-level amplitude. The massive gauge-boson propagators are given by $1/(p^2 + m^2 - i\Gamma)$. This gives an unphysical width for $p^2 > 0$, but retains $U(1)$ gauge invariance in the CC20 process.

The most recent numerical results produced for single-W production are from the following codes [62]: `CompHEP`, `GRC4F`, `NEXTCALIBUR`, `SWAP`, `WPHACT` and `WTO`.

Among these codes, `WPHACT` is the only one to employ the Fermion-Loop scheme in its imaginary version [63], where the full imaginary part of the Fermion-Loop corrections is used (hereafter IFL).

In view of a requested, inclusive cross-section, accuracy of 2% we must include radiative corrections to the best of our knowledge, at least the bulk of any large effect. As we know, the correct scale of the couplings and their differentiation between s and t-channel is connected to the real part of the corrections, so that the imaginary FL is not enough, we need a complete FL for single-W. Having all the parts, the tree-level couplings are replaced by running couplings at the appropriate momenta and the massive gauge-boson propagators are modified accordingly. The vertex coefficients, entering through the Yang–Mills vertex, contain the lowest order couplings as well as the one-loop fermionic vertex corrections.

Each calculation aimed to provide some estimate for single-W production is, at least nominally, a tree level calculation. Among other things it will require the choice of some Input Parameter Set (IPS) and of certain relations among the parameters. Thus, different choices of the basic relations among the input parameters can lead to different results with deviations which, in some case, can be sizeable.

For instance, a possible choice is to fix the coupling constant g as

$$g^2 = \frac{4\pi\alpha}{s^2_{_W}}, \quad s^2_{_W} = \frac{\pi\alpha}{\sqrt{2}G_{_F}M^2_{_W}}, \tag{72}$$

where $G_{_F}$ is the Fermi coupling constant. Another possibility would be to use

$$g^2 = 4\sqrt{2}G_{_F}M^2_{_W}, \tag{73}$$

but, in both cases, we miss the correct running of the coupling. Ad hoc solutions should be avoided, and the running of the parameters must always follow from a fully consistent scheme.

Note that the Fixed-Width scheme behaves properly in the collinear and high-energy regions of phase space, to the contrary of the Running-Width scheme, but it completely misses the running of the couplings, an effect that is expected to be above the requested precision tag of 2%. By considering the impact of the EFL-scheme on the relevant observables we will be able to judge on the goodness of naive rescaling procedures.

Another important issue in dealing with single-W production is connected with the inclusion of QED radiation. It is well known that universal, s-channel structure functions are not adequate enough to include the radiation.

It is quite a known fact that, among the electroweak corrections, QED radiation gives the largest contribution and the needed precision requires a re-summation of the large logarithms. For annihilation processes, $e^+e^- \to \overline{f}f$, initial state radiation is a definable, gauge-invariant concept and we have general tools to deal with it; the structure function approach and also the parton-shower method. However, when we try to apply the algorithm to four-fermion processes that include non-annihilation channels we face a problem: it is still possible to include the large universal logarithms by making use of the standard tools but only as long as the corresponding process is dominated by the annihilation channel.

Unfortunately, the application of the methods for including QED radiation has not received a complete and satisfactory investigation for the non-annihilation components of the processes. The problem, in applying structure functions or parton shower, is related to the question of energy evolution. The choice of the energy scale inside the structure functions is not a trivial matter. The justification of any choice can only be given by comparing the result with a corresponding fixed order calculation. Already from two photon processes we know that a natural scale is t and not s. In principle, once the proper scale is found then the structure functions can reproduce the correct evolution of the soft-photon emission, up to $\mathcal{O}\left(()\,\alpha\right)$. However, a mismatch remains in the constant term that is cured by standard introduction of a K-factor. Even so, we are strongly dependent on the assumption that $-t/m_e^2 \gg 1$ which does not hold for forward scattering, the region relevant for single-W production. Once more, only a fixed-order calculation for single-W could rescue the theoretical prediction.

There is, however, an additional complication in the use of QED structure functions originating from mass effects. The single-W is $s \oplus t$- channels and the t-channel parts look as in Fig. 41.

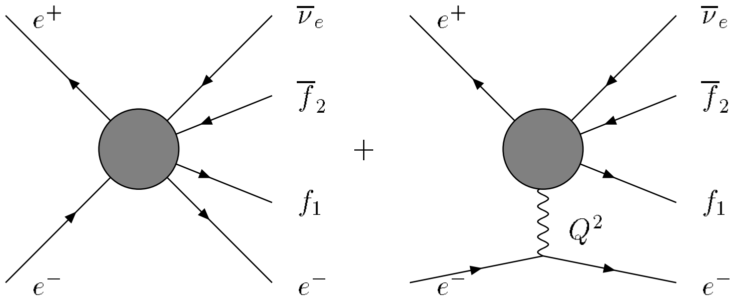

The corresponding cross-section is proportional to

Fig. 41: The CC20 family of diagrams with the explicit component containing a t-channel photon.

$$
\begin{aligned}
\int d\Phi_3 \quad & \frac{1}{\hat{Q}^4}\,\hat{L}_{\mu\nu}\hat{W}_{\mu\nu} \\
\hat{Q} &= \hat{p}_- - q_- \\
\hat{L}_{\mu\nu} &= \frac{1}{2}\,\hat{Q}^2\delta_{\mu\nu} + \hat{p}_\mu\hat{q}_\nu + \hat{q}_{-\mu}\hat{p}_{-\nu}
\end{aligned}
$$

$$
\begin{aligned}
\int d\Phi_3\hat{W}_{\mu\nu} &= \hat{W}_1\,(-\delta_{\mu\nu} + \frac{\hat{Q}_\mu\hat{Q}_\nu}{\hat{Q}^2}) - \frac{\hat{Q}^2}{(\hat{p}_+\cdot\hat{Q})^2}\,\hat{W}_2\,\mathcal{P}_\mu\mathcal{P}_\nu \\
\mathcal{P}^\mu &= \hat{p}_+^\mu - \frac{\hat{p}_+\cdot\hat{Q}}{\hat{Q}^2}\,\hat{Q}^\mu
\end{aligned}
$$

where $\hat{p}$ and $\hat{q}$ denote emission of soft and collinear photons. Usually, $p_-^2 = \hat{p}_-^2 = 0$ and $q_-^2 = \hat{q}_-^2 = 0$, and one writes $\hat{p}_- = x_{\rm in}\,p_-$ and $\hat{q}_- = q_-/x_{\rm out}$ with the kernel cross-section to be weighted with structure functions. Here, however, masses matter should not be neglected and the electrons are in a virtual state, i.e. off their mass-shell. A possible choice is to write

$$
\left(\hat{p}_-\right)^2 = -m_e^2 + \frac{1}{2}\,(1-\beta)\,(1-x_{\rm in})\,s \sim -x_{\rm in}\,m_e^2
$$

The important facts are that $\hat{Q}_\mu\hat{L}_{\mu\nu} = 0$ owing to gauge invariance. Instead we get

$$
\hat{Q}_\mu\hat{L}_{\mu\nu} = 4\,(1-x_{\rm in})\,m_e^2\,q_{-\nu} + 4\,(1-\frac{1}{x_{\rm in}})\,m_e^2\,p_{-\nu}.
$$

Even if we insist in putting $\hat{p}_- = x_{\rm in}p_-$ and $p_-^2 = -m_e^2$, gauge invariance is violated by terms of $\mathcal{O}\left(m_e^2/s\right)$. The effect of constant terms on the Q^2-integrated photon flux-function can be as large as 6%. Gauge-invariance violation affects this term, resulting in some intrinsic theoretical uncertainty.

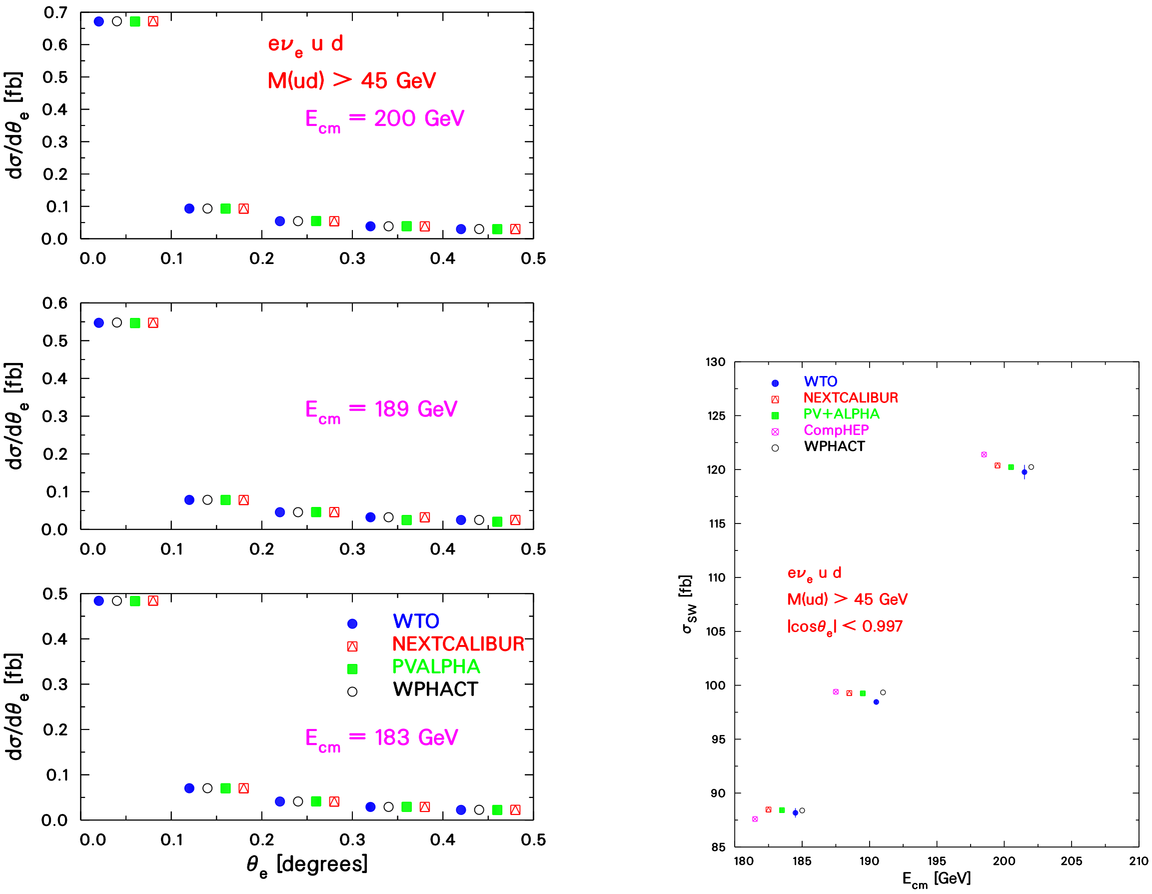

Fig. 42: θ_e distributions for $u\overline{d}\mu^-\overline{\nu}_\mu$ and single-W cross-sections for $u\overline{d}\mu^-\overline{\nu}_\mu$.

11.1 Technical precision in single-W

An old comparison for single-W has been extended to cover

1. $e^+e^- \to q\overline{q}e\nu(\gamma)$, $|\cos\theta_e| > 0.997$, either $M(q\overline{q}) > 45\,$GeV or $E_{q_1}, E_{q_2} > 15\,$GeV, inclusive cross-section accuracy 2%, photon energy and polar angle ($|\cos\theta_\gamma| < 0.997\ (0.9995)$) spectrum
2. $e^+e^- \to e\nu e\nu(\gamma)$, $|\cos\theta_e| > 0.997$, $E_e > 15\,$GeV, $|\cos\theta_e| < 0.7\ (0.95)$, inclusive cross-section accuracy 5%, photon energy and polar angle ($|\cos\theta_\gamma| < 0.997\ (0.9995)$) spectrum.
3. $e^+e^- \to e\nu\mu\nu(\gamma)$ and $e^+e^- \to e\nu\tau\nu(\gamma)$, $|\cos\theta_e| > 0.997$, $E_{\mu/\tau} > 15\,$GeV, $|\cos\theta_{\mu/\tau}| < 0.95$, inclusive cross-section accuracy 5%, photon energy and polar angle ($|\cos\theta_\gamma| < 0.997\ (0.9995)$) spectrum.

With this comparison we want to check a) technical precision at the Born level, b) the correct inclusion of QED radiation, c) QCD corrections, especially in the low-mass region.

The first answer is that technical precision is not a problem anymore, all codes agree on single-W cross-sections and distributions, even for $\theta_e < 0.1^\circ$, even for leptonic final states. On $\sigma_{\rm Born}$ the technical accuracy is 0.1%, the same for $d\sigma/d\theta_e$ for $\theta_e \to 0$. Not only invariant-mass cuts, but also energy-cuts have been tested as shown in Tabs.(17–18).

11.2 Signal definition in single-W

During the last WW99 Crete Workshop a proposal has been made to reach a common *signal* definition for single-W. The persons who participated in the WW99 workshop agreed on some setup to define the single-W production and now this has been formalized in one of the `LEP EWWG` meetings; there, it was decided to have a combination of the single-W cross-section using the signal definitions of Tab.(19) for $e^+e^- \to e^-\overline{\nu}_e f'\overline{f}$: Note that charge-conjugate state should be taken into account and that an asymmetric cut has been introduced for $ee\nu\nu$; the latter is due to the fact that the process itself is CP-even when no cut is applied, but an ambiguity remains if one starts to discuss single-W with e^- in the forward direction. Then we should multiply this process by a factor 2 as well. The goal of this common definition is to be able to combine the different $e\nu\overline{q}q$, $e\nu\mu\nu$, $e\nu\tau\nu$, $e\nu e\nu$ measurements from different experiments so that the new theoretical calculations can be checked with data at a level better than 10%.

Signal definition has a longstanding tradition in LEP physics, the most celebrated being the t-channel subtraction in Bhabha and the most recent being the CC03 cross-section. Here we have a different situation. First of all, nobody has radiative corrections for single-W production, hence the usual argument of the availability of a sophisticated semi-analytical calculation for the signal does not apply. We could avoid a definition of the signal in terms of diagrams and have recourse to a definition in terms of cuts since, in a very narrow cone around the beam axis the single-W family is fully dominated by the t-channel photons. Nevertheless, we want to reach a definition of single-W, all channels, something like $e^+e^- \to e\nu_e + (W \to \mathrm{anything})$. So, in the end, we all agree on the above definition; the core of the question clearly refers to $e\nu_e e\nu_e$. Do we want a *minimal* definition in terms of the number of diagrams or do we prefer the maximal one? In principle, once a diagram-by-diagram separation is introduced one should have a small background $\oplus$ interference. Existing MC can do both ways and most of them can be used to calculate the t-channel cross-section without major rewriting.

12. Assessing the theoretical uncertainty in single-W

In the following sections we present the most recent theoretical developments in single-W and their implementation in the generators. There are common problematic situations with more or less equivalent solutions. One has to assign an error band to the cross-section for lack of t-channel ISR, ISR p_t and uncertainty in the energy scale. As for the energy scale we have an exact calculation based on the Fermion-Loop scheme which, at the Born-level (no QED) is known to be at the 1% level of accuracy. Exact Fermion-Loop, however, is implemented only in one generator while the other offer a wide range of approximations based on the idea of re-scaling the cross-section. If we do not want to use the Fermion-Loop prediction then, by a careful examination of the most plausible re-scaling procedure, we end up with approximately $1\%, 2\%$ and 3% theoretical uncertainty to be assigned to the energy scale in the channels ud, $\mu\nu_\mu$ and $e\nu_e$ respectively. Therefore, a conservative estimate of TU would read as follows:

Energy scale: $\pm 2\%$;

ISR for t-ch, p_t: $\pm 4\%$,

giving a total of $\pm 5\%$.

One should stress that most of the theorists were interested in gauge invariance issues due to unstable particle for CC20. The experimentalists, however, were asking from the beginning for ISR p_t effects, comparison with QEDPSt, SF and YFS. Unfortunately, only few groups have been working on these issues.

One should remember that the experimental situation is different for CC20 than CC03. In CC03, LEP(ADLO) can now test the theory below an uncertainty of $\pm 2\%$. However, ADLO cannot test CC20 better than $\pm 10\%$. One can estimate what CC20 can do by observing that the total cross-section is the order of 1 pb, being 20 times smaller than CC03. In addition, single-W event selection is not easy due to irreducible $WW \to \tau\nu\overline{q}q'$ backgrounds.

	$\sqrt{s} = 183\,\mathrm{GeV}$	$\sqrt{s} = 189\,\mathrm{GeV}$	$\sqrt{s} = 200\,\mathrm{GeV}$
NEXTCALIBUR	26.483 ± 0.041	29.679 ± 0.047	35.893 ± 0.048
PVALPHA	26.47 ± 0.04	29.70 ± 0.04	35.93 ± 0.05

Table 17: Cross-sections [fb] for $e^+e^- \to e^-\overline{\nu}_e\mu^+\overline{\nu}_\mu$.

	$\sqrt{s} = 183\,\mathrm{GeV}$	$\sqrt{s} = 189\,\mathrm{GeV}$	$\sqrt{s} = 200\,\mathrm{GeV}$
NEXTCALIBUR	26.422 ± 0.035	29.655 ± 0.046	35.954 ± 0.052
PVALPHA	26.3 ± 0.2	29.6 ± 0.2	35.92 ± 0.05

Table 18: Cross-sections [fb] for $e^+e^- \to e^-\overline{\nu}_e\tau^+\overline{\nu}_\tau$.

Process	diagrams	cuts
$ee\nu\nu$	t-channel only	$E(e^+) > 20\,\mathrm{GeV}, \lvert\cos\theta(e^+)\rvert < 0.95, \lvert\cos\theta(e-)\rvert > 0.95$
$e\nu\mu\nu$	t-channel only	$E_(\mu^+) > 20\,\mathrm{GeV}$
$e\nu\tau\nu$	t-channel only	$E_(\tau^+) > 20\,\mathrm{GeV}$
$e\nu ud$	t-channel only	$M(ud) > 45GeV$
$e\nu cs$	t-channel only	$M(cs) > 45GeV$

Table 19: Signal definition for single-W processes.

However, the single-Wprocess is a very important (sometimes major) source of backgrounds for searches. Especially, acoplanar two jets with low invariant mass for neutralino search, and in many cases with R-parity violation. In addition, the single-Wprocess will bea major process at LC, not only for TGC but also for the W-boson mass. Thus, we hope that today's theoretical progress is not in vain at all.

In the following few recipes are introduced to improve upon QED ISR; they are all equivalent insofar as they translate into different choices for the scale in the leading-logarithms of the structure functions. Some are very crude approximations with ad hoc cutoff on the scale itself, while other choices are more plausible. However, this problem is far from any satisfactory solution.

12.1 `WTO` and EFL

Authors

G. Passarino

12.11 The ingredients in the Fermion-Loop scheme.

There are several building blocks that enter into the construction of the Fermion-Loop scheme, see for instance [64]. In the 't Hooft–Feynman gauge, the $\delta_{\mu\nu}$ part of the vector–vector transitions can be cast in the following form [64], where $s_\theta(c_\theta)$ is the sine(cosine) of the weak mixing angle:

$$\begin{aligned} S_{\gamma\gamma} &= \frac{g^2 s_\theta^2}{16\,\pi^2}\,\Pi_{\gamma\gamma}(p^2)\,p^2, \quad S_{ZZ} = \frac{g^2}{16\pi^2 c_\theta^2}\,\Sigma_{ZZ}(p^2), \\ S_{Z\gamma} &= \frac{g^2 s_\theta}{16\pi^2 c_\theta}\,\Sigma_{Z\gamma}(p^2), \quad S_{WW} = \frac{g^2}{16\pi^2}\,\Sigma_{WW}(p^2). \end{aligned} \tag{74}$$

Next we have can transform to the $(3,Q)$ basis [64], where one writes

$$\begin{aligned} \Sigma_{ZZ}(p^2) &= \Sigma_{33}(p^2) - 2s_\theta^2\Sigma_{3Q}(p^2) + s_\theta^4\Pi_{\gamma\gamma}(p^2)\,p^2, \\ \Sigma_{Z\gamma}(p^2) &= \Sigma_{3Q}(p^2) - s_\theta^2\Pi_{\gamma\gamma}(p^2)\,p^2. \end{aligned} \tag{75}$$

We now consider three parameters, the e.m. coupling constant e, the $SU(2)$ coupling constant g and the sine of the weak mixing angle s_θ. At the tree level they are not independent, but rather they satisfy the relation $g^2 s_\theta^2 = e^2$. The running of the e.m. coupling constant is easily derived and gives

$$\frac{1}{e^2(s)} = \frac{1}{g^2 s_\theta^2} - \frac{1}{16\,\pi^2}\,\Pi_{\gamma\gamma}(s). \tag{76}$$

However, we have a natural scale to use since at $s = 0$ we have the fine structure constant at our disposal. Therefore, the running of $e^2(s)$ is completely specified in terms of α by

$$\frac{1}{e^2(s)} = \frac{1}{4\,\pi\alpha}\left[1 - \frac{\alpha}{4\,\pi}\,\Pi(s)\right], \qquad \text{with} \quad \Pi(s) = \Pi_{\gamma\gamma}(s) - \Pi_{\gamma\gamma}(0). \tag{77}$$

For the running of g^2 we derive a similar equation:

$$\frac{1}{g^2(s)} = \frac{1}{g^2} - \frac{1}{16\,\pi^2}\,\Pi_{3Q}(s). \tag{78}$$

The running of the third parameter, $s_\theta^2(s)$, is now fixed by

$$s_\theta^2(s) = \frac{e^2(s)}{g^2(s)}. \tag{79}$$

In Fig. 43 we show the running of $e^2(q^2)$ for $q^2 \to 0_+$, compared with the fixed value of e^2 that one would

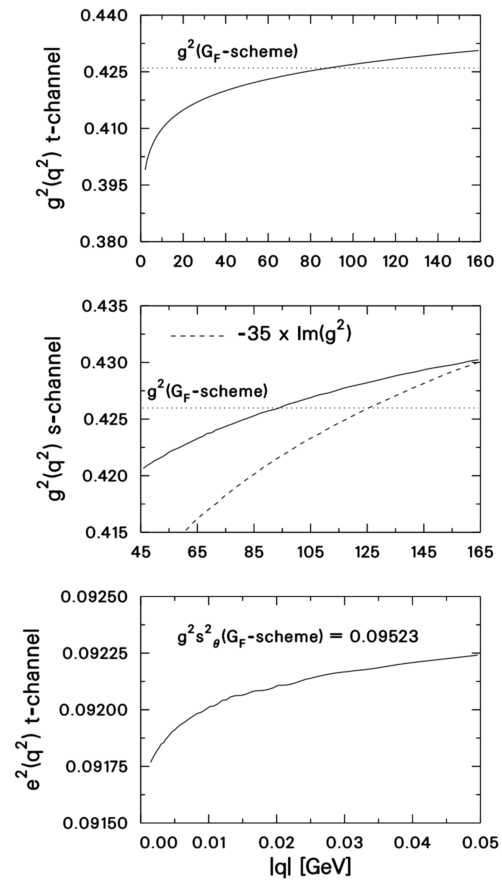

Fig. 43: Running of coupling constants. The sign of $\mathrm{Im}g^2(s)$ is reversed and the corresponding curve is magnified by a factor 35. Here q is the absolute value of the momentum.

use in the G_F-scheme. Furthermore, in the same figure, we show the evolution of $g^2(q^2)$ for q^2 time-like or space-like, again compared with $g^2_{G_F}$. The sizeable difference that one gets between e^2 running in the t-channel and e^2 fixed in the G_F-scheme is expected to be one of the major improvements induced by the EFL-scheme.

The re-summed propagators for the vector bosons are:

$$
\begin{aligned}
G_\gamma(p^2) &= \left\{p^2 - S_{\gamma\gamma}(p^2) - \frac{\left[S_{Z\gamma}(p^2)\right]^2}{p^2 + M_0^2 - S_{ZZ}(p^2)}\right\}^{-1}, \\
G_{Z\gamma}(p^2) &= \frac{S_{Z\gamma}(p^2)}{[p^2 - S_{\gamma\gamma}(p^2)]\,[p^2 + M_0^2 - S_{ZZ}(p^2)] - [S_{Z\gamma}(p^2)]^2}, \\
G_Z(p^2) &= \left\{p^2 + M_0^2 - S_{ZZ} - \frac{\left[S_{Z\gamma}(p^2)\right]^2}{p^2 - S_{\gamma\gamma}(p^2)}\right\}^{-1}, \\
G_W(p^2) &= \left[p^2 + M^2 - S_{WW}(p^2)\right]^{-1}.
\end{aligned} \tag{80}
$$

The quantity $M_0 = M/c_\theta$ is the bare Z mass. An essential ingredient in the construction of the scheme is represented by the location of the complex poles. Substituting the corresponding results into the expressions for the propagators, Eq.(80), we see that all ultraviolet divergences not proportional to p^2 cancel. We obtain

$$
\begin{aligned}
G_Z(s) &= \left[-s + p_Z - Z(s) + Z(p_Z)\right]^{-1}, \\
G_W(s) &= \left[-s + p_W - S_{WW}(s) + S_{WW}(p_W)\right]^{-1}, \\
G_{Z\gamma}(s) &= -\frac{S_{Z\gamma}(s)}{s + S_{\gamma\gamma}(s)}\, G_Z(s), \\
G_\gamma(s) &= -\frac{1}{s + S_{\gamma\gamma}(s)} + \left[\frac{S_{Z\gamma}(s)}{s + S_{\gamma\gamma}(s)}\right]^2 G_Z(s).
\end{aligned} \tag{81}
$$

The vector boson propagators are now expressed as

$$
\begin{aligned}
G_W(s) &= -\frac{g^2(s)}{g^2}\,\frac{\omega_W(s)}{s}, \qquad G_Z(s) = -\frac{c_\theta^2}{g^2}\,\frac{g^2(s)}{c^2(s)}\,\frac{\omega_Z(s)}{s}, \\
G_{Z\gamma}(s) &= \frac{s_\theta}{c_\theta}\left[1 - \frac{s^2(s)}{s_\theta^2}\right] G_Z(s), \\
G_\gamma(s) &= \frac{e^2(s)}{e^2} + \frac{s_\theta^2}{c_\theta^2}\left[1 - \frac{s^2(s)}{s_\theta^2}\right]^2 G_Z(s),
\end{aligned} \tag{82}
$$

where the propagation functions are

$$
\begin{aligned}
\omega_W^{-1}(s) &= 1 - \frac{g^2(s)}{s}\left\{\frac{p_W}{g^2(p_W)} - \frac{1}{16\,\pi^2}\left[f_W(s) - f_W(p_W)\right]\right\}, \\
\omega_Z^{-1}(s) &= 1 - \frac{g^2(s)}{c^2(s)s}\left\{\frac{c^2(p_Z)}{g^2(p_Z)}\,p_Z - \frac{1}{16\,\pi^2}\left[f_Z(s) - f_Z(p_W)\right]\right\}.
\end{aligned} \tag{83}
$$

The explicit form of the $f_{W,Z}$-functions is given in [59]. The complete one-loop re-summation in the 't Hooft-Feynman gauge is equivalent to some *effective* unitary-gauge W-propagator. The whole amplitude can be written in terms of a W-boson exchange diagram, if we make use of the following effective propagator:

$$
\Delta^{\mu\nu}_{\text{eff}} = \frac{1}{p^2 + M^2 - S^0_W}\left[\delta^{\mu\nu} + \frac{p^\mu p^\nu}{M^2(p^2)}\right]. \tag{84}
$$

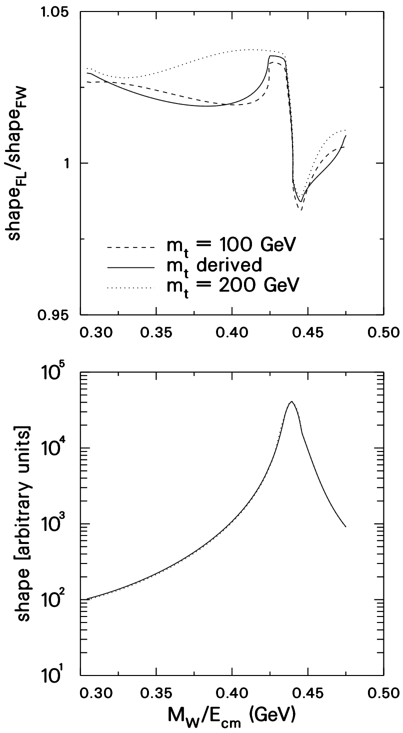

Fig. 44: Comparison between the Fixed-Width and the Fermion-Loop line-shapes, Eq.(85).

The explicit form of $M^2(p^2)$ is, again given in [59]. We now define the following line-shape functions:

$$L_{\rm EFL}(s) = \frac{s^2}{(s-{\rm Re}p_{_W})^2+({\rm Im}p_{_W})^2}\,\frac{1}{|R(s)|^2},$$
$$L_{\rm FW}(s) = \frac{s^2}{\left(s-M^2_{_W}\right)^2+M^2_{_W}\Gamma^2_{_W}}. \tag{85}$$

with a running ρ-factor

$$R(s) = 1+\frac{g^2(s)}{16\,\pi^2}\,\frac{f_W(s)-f_W(p_W)+p_W\left[\Pi_{_{3Q}}(p_W)-\Pi_{_{3Q}}(s)\right]}{s-p_W}. \tag{86}$$

Here $M_{_W}, \Gamma_{_W}$ are the on-shell W mass and total width, respectively. The two line-shapes are compared in Fig. 44 for different values of the top quark mass. We are using complex-mass renormalization but we only include fermionic corrections. Therefore, we can start with the Fermi coupling constant but also with $M_{_W}$ as an input parameter. Equating the corresponding renormalization conditions yields a relation between $M_{_Z}$, $G_{_F}$, ${\rm Re}\{\alpha(M^2_{_Z})^{-1}\}$, $M_{_W}$, and m_t, see [31]. This relation can be solved iteratively for m_t. For the following input parameter set,

$$M_{_W} = 80.350\,{\rm GeV}, \quad M_{_Z} = 91.1867\,{\rm GeV}, \quad G_{_F} = 1.16639\,\times\,10^{-5}\,{\rm GeV}^{-2}, \tag{87}$$

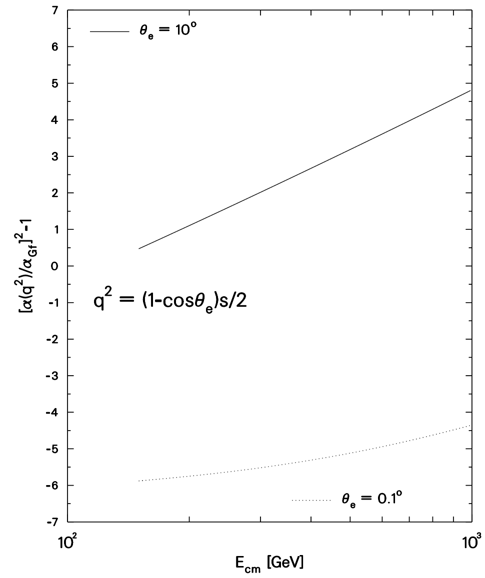

Fig. 45: Running of $\alpha_{\rm QED}(q^2)$ in the t-channel.

we obtain the following solution:

$$\mu_W = \sqrt{{\rm Re}\,(p_W)} = 80.324\,{\rm GeV}, \quad \gamma_W = -\frac{{\rm Im}\,(p_W)}{\mu_W} = 2.0581\,{\rm GeV}, \quad m_t = 148.62\,{\rm GeV}. \tag{88}$$

The $26\,{\rm MeV}$ difference between M_W and μ_W is responsible for the sharp transition around 80 GeV that can be seen in Fig. 44. Apart from that, the Fermion-Loop line-shape can be few percents above the Fixed-Width line shape. The behavior of $e^2(q^2)$ in the t-channel and, to some extent, the ratio between Fermion-Loop and Fixed-Width cross-sections is crucially dependent on which regime we are considering. A careful examination of Fig. 45 shows the following: if we choose

$$< q^2 >= (1- < \cos\theta_e >)\,\frac{s}{2}, \tag{89}$$

and use $10°$ or $0.1°$ as representative for LACC20 or SACC20, we obtain a ratio

$$\begin{aligned} \Big[\frac{\alpha(q^2)}{\alpha_{G_F}}\Big]^2 - 1 \quad &\to \quad -6\% \div -4\%, \quad < \theta_e >= 0.1°, \\ \Big[\frac{\alpha(q^2)}{\alpha_{G_F}}\Big]^2 - 1 \quad &\to \quad +0.5\% \div +5\%, \quad < \theta_e >= 10° \end{aligned} \tag{90}$$

for $\sqrt{s}$ ranging from $150\,{\rm GeV}$ to $1\ \ {\rm TeV}$. Therefore, the effect of a running $\alpha_{\rm QED}$ in the t-channel is to decrease/increase the cross-section, with respect to the Fixed-Width scheme, for SACC20/LACC20.

A final ingredient, existing in the Fermion-Loop scheme, is represented by the inclusion of vertices that are m_t-dependent. The top-quark contributions are particularly important for delayed-unitarity effects. In this respect also terms involving the totally-antisymmetric ε-tensor (originating from vertex corrections) are relevant. While such terms are absent for complete generations of massless fermions owing to the anomaly cancellations, they show up for finite fermion masses.

All details concerning vertices can be found in [59] where one can find the explicit expressions for the vertex form-factors in terms of standard C-functions [65].

12.12 Numerical results.

For the sake of illustration we will consider two examples belonging to the single-W family:

1. $e^+e^- \to u\overline{d}e\nu$, $|\cos\theta_e| > 0.997$, $M(u\overline{d}) > 45\,$GeV;
2. $e^+e^- \to e\nu\mu\nu(\gamma)$, $|\cos\theta_e| > 0.997$, $E_\mu > 15\,$GeV, $|\cos\theta_\mu| < 0.95$.

Our Input Parameter Set is specified by

$$\sqrt{s} = 183/189/200\,\mathrm{GeV}, \quad M_{_W} = 80.350\,\mathrm{GeV}, \quad M_{_Z} = 91.1867\,\mathrm{GeV}, \tag{91}$$

Moreover, we are mostly interested in the variations induced by the Fermion-Loop scheme with respect to the Fixed-Width scheme. Therefore, we will not include other effects that are nevertheless needed in any realistic evaluation of observables:

1. QED Initial State Radiation;
2. QCD naive corrections;
3. Final State Coulomb correction factor;
4. Final State QED radiation
5. Anomalous couplings.

Furthermore, we use trivial CKM matrix element, lepton masses according to PDG [66], light quark masses $5\,\mathrm{MeV}$ (up) and $10\,\mathrm{MeV}$ (down), $G_{_F} = 1.16637\,10^{-5}$ (recent Fermi coupling).

When working in the Fixed-Width approach we use the $G_{_F}$-scheme, that is

$$s^2_\theta = 1 - \frac{M^2_{_W}}{M^2_{_Z}}, \qquad \alpha \equiv \alpha_{G_F} = 4\sqrt{2}\,\frac{G_F M^2_{_W} s^2_\theta}{4\,\pi}, \tag{92}$$

Numerical (integration) errors returned for the cross-section computed with $0 < \theta_e < \theta^{\max}_e$ and $\theta^{\max}_e = 0.1^\circ \div 0.4^\circ$ are, typically, of order $0.05 \div 0.1\%$ for $u\overline{d}$ and $\nu_\mu\mu^+$ final states, respectively. We start in Tab.(20) by comparing EFL and FW cross-sections at $\sqrt{s} = 183\,$GeV. Clearly, the bulk of the cross-section is for very small scattering angle of the electron, dominated by the first bin. The differences between EFL-scheme and FW-scheme are decreasing when $\theta^{\max}_e$ becomes larger and, from the shape of the angular distribution, we infer smaller differences in the higher bins.

To continue our discussion of the numerical results we stay at $\sqrt{s} = 183$ GeV and consider now the angular distribution, $d\sigma/d\theta_e$ for the $u\overline{d}e^-\overline{\nu}_e$ final states. The results are shown in Fig. 46. From Fig. 46 we see that the EFL prediction is lower than the FW one, from -7.46% in the bin $0^\circ - 0.1^\circ$ to -5.56% in the bin $0.3^\circ - 0.4^\circ$. Correspondingly, the first bin is 6.78 higher than the second one, $11.60(16.37)$ than the third(fourth) one. This is not a surprise, since the first bin represents 50% of the total single-W cross-section.

Always in the same figure, we have reported the behavior of $\Big[\alpha(q^2)/\alpha_{G_F} - 1\Big]^2$ as a function of θ_e for three values of y, using the appropriate relation: $q^2 = q^2(\theta_e, y)$. The behavior of EFL/FW-1, when we vary θ_e, is very similar to the one given by the ratio of coupling constants, indicating that the bulk of the effect is in the running of the e.m. coupling constant.

We have repeated the calculation for all the three energies, finding similar results that are shown in Fig. 47. For completeness we have reported the numerical results for the three energies in Tab.(21), where the first entry is Fixed-Width distribution and the second entry is Fermion-Loop one. Only the first four bins are shown, owing to the fact that they are the most significant in the distribution. The third entry in Tab.(21) gives EFL/FW-1 in percent. After discussing the angular distribution we consider the total – single-W – cross-section, defined by an acceptance cut of $|\cos\theta_e| > 0.997$, again for the high-mass case, i.e. $M(u\overline{d}) > 45\,$GeV. It is reported in Tab.(22), where one sees that differences between schemes are of the order of 5% for all energies, supporting the use of some effective $\alpha(< q^2 >)$ with $< q^2 >= (1 - cos < \theta_e >)\, s/2$ where $< \theta_e >\approx 0.1^\circ \div 0.2^\circ$.

	$e^+e^- \to e^-\overline{\nu}_e u\overline{d}$		
$\theta_e^{\max}$ [deg]	EFL	FW	EFL/FW-1 (percent)
$0.1°$	0.04478(3)	0.04841(3)	-7.50(8)
$0.2°$	0.05139(3)	0.05543(3)	-7.29(7)
$0.3°$	0.05525(3)	0.05953(3)	-7.19(7)
$0.4°$	0.05798(3)	0.06243(3)	-7.13(7)
	$e^+e^- \to e^-\overline{\nu}_e \nu_\mu \mu^+$		
$\theta_e^{\max}$ [deg]	EFL	FW	EFL/FW-1 (percent)
$0.1°$	0.01345(3)	0.01415(1)	-4.9(2)
$0.2°$	0.01548(3)	0.01627(2)	-4.9(2)
$0.3°$	0.01667(3)	0.01751(2)	-4.8(2)
$0.4°$	0.01752(3)	0.01839(2)	-4.7(2)

Table 20: σ in pb, from WTO, for the processes $e^+e^- \to e^-\overline{\nu}_e u\overline{d}(\nu_\mu\mu^+)$, for $\sqrt{s} = 183\,\mathrm{GeV}$ and for $\theta_e < \theta_e^{\max}$. Kinematical cuts are as described in the main text. The number in parenthesis shows the statistical error of the numerical integration on the last digit.

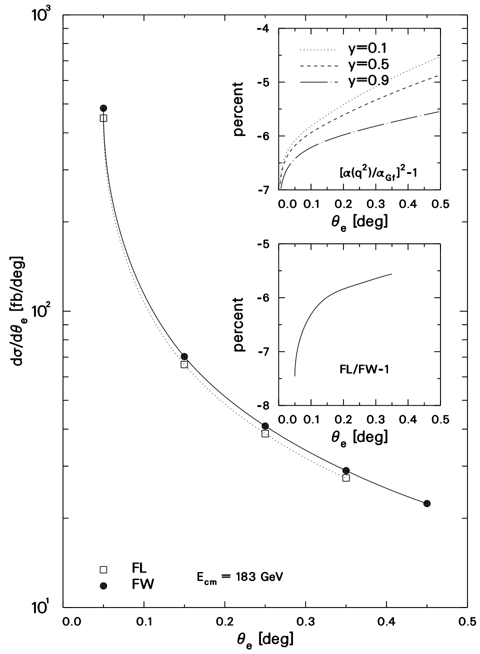

Fig. 46: WTO predictions for $d\sigma/d\cos\theta_e$ [fb/degrees] for $e^+e^- \to u\overline{d}e^-\overline{\nu}_e$ with $M(u\overline{d}) > 45\,\mathrm{GeV}$ and $\sqrt{s} = 183\,\mathrm{GeV}$.

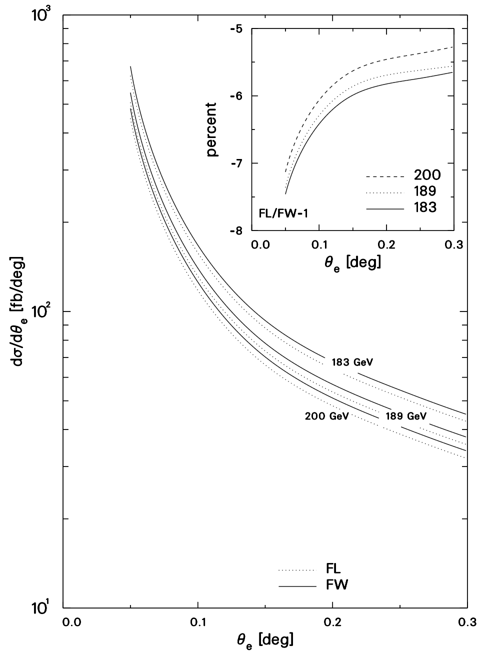

Fig. 47: WTO predictions for $d\sigma/d\cos\theta_e$ [fb/degrees] for $e^+e^- \to u\overline{d}e^-\overline{\nu}_e$ with $M(u\overline{d}) > 45\,\mathrm{GeV}$ and $\sqrt{s} = 183, 189, 200\,\mathrm{GeV}$.

θ_e [Deg]	$\sqrt{s} = 183\,\mathrm{GeV}$	$\sqrt{s} = 189\,\mathrm{GeV}$	$\sqrt{s} = 200\,\mathrm{GeV}$
$0.0° \div 0.1°$	0.48395 0.44784 -7.46	0.54721 0.50695 -7.36	0.67147 0.62357 -7.13
$0.1° \div 0.2°$	0.07026 0.06605 -5.99	0.07815 0.07357 -5.86	0.09323 0.08798 -5.63
$0.2° \div 0.3°$	0.04095 0.03860 -5.74	0.04554 0.04298 -5.62	0.05433 0.05141 -5.37
$0.3° \div 0.4°$	0.02897 0.02736 -5.56	0.03223 0.03045 -5.52	0.03845 0.03646 -5.18

Table 21: $d\sigma/d\theta_e$ in [pb/degrees], from WTO, for the process $e^+e^- \to e^-\overline{\nu}_e u\overline{d}$, for $M(u\overline{d}) > 45$ GeV. First entry is Fixed-Width distribution, second entry is Fermion-Loop one and third entry is EFL/FW-1 in percent.

$\sqrt{s}$	FW	EFL	EFL/FW-1 (percent)
$183\,\mathrm{GeV}$	88.17(44)	83.28(6)	-5.5(5)
$189\,\mathrm{GeV}$	98.45(25)	93.79(7)	-4.7(3)
$200\,\mathrm{GeV}$	119.77(67)	113.67(8)	-5.1(5)

Table 22: Total single-W cross-section in fb, from WTO, for the process $e^+e^- \to e^-\overline{\nu}_e u\overline{d}$, for $M(u\overline{d}) > 45$ GeV and $|\cos\theta_e| > 0.997$. The number in parenthesis shows the statistical error of the numerical integration on the last digit.

We have also computed the single-W cross-sections for a fixed mass of the top quark, $m_t = 173.8\,\mathrm{GeV}$, without finding any significative difference with the previous case where m_t is fixed by a consistency relation: they give $83.29(6)$ fb, $93.80(7)$ fb and $113.68(8)$ fb for $\sqrt{s} = 183\,\mathrm{GeV}, 189\,\mathrm{GeV}$ and $200\,\mathrm{GeV}$.

Next we consider $e^+e^- \to e\nu\mu\nu$, with $|\cos\theta_e| > 0.997$, $E_\mu > 15\,\mathrm{GeV}$, and $|\cos\theta_\mu| < 0.95$. The angular cut on the muon direction is chosen to prevent the logarithmic enhancement that would, otherwise, show up in the multi-peripheral terms. Indeed, when the electron is lost in the beam pipe, and the quasi-massless fermion is emitted parallel to the (quasi-real) photon then the internal fermion propagator will produce an enhancement in the cross section. In Tab.(23) we report the comparison between the EFL distribution and the FW one for $\sqrt{s} = 183\,\mathrm{GeV}$. As before, only the most significant bins are shown $(0.0^\circ \div 0.4^\circ)$.

θ_e [Deg]	FW	EFL	EFL/FW-1 (percent)
$0.0^\circ \div 0.1^\circ$	0.14154	0.13448	-4.99
$0.1^\circ \div 0.2^\circ$	0.02113	0.02031	-3.88
$0.2^\circ \div 0.3^\circ$	0.01238	0.01194	-3.55
$0.3^\circ \div 0.4^\circ$	0.00880	0.00851	-3.30

Table 23: $d\sigma/d\theta_e$ in [pb/degrees], from WTO, for the process $e^+e^- \to e^-\overline{\nu}_e\nu_\mu\mu^+$, for $|\cos\theta_e| > 0.997$, $E_\mu > 15$ GeV, and $|\cos\theta_\mu| < 0.95$. Furthermore, $\sqrt{s} = 183$ GeV.

As for the hadronic case, the EFL prediction is considerably lower than the FW one, although the percentage difference between the two is approximately $2.2\% \div 2.4\%$ smaller than in the previous case.

This fact is reflected in the total single-W cross-section for $e^+e^- \to e^-\overline{\nu}_e\mu^+\nu_\mu$ that we report in Tab.(24).

$\sqrt{s}$	FW	EFL	EFL/FW-1 (percent)
$183\,\mathrm{GeV}$	26.77(14)	25.53(4)	-4.6(5)
$189\,\mathrm{GeV}$	29.73(14)	28.78(4)	-3.2(5)
$200\,\mathrm{GeV}$	36.45(23)	34.97(6)	-4.1(6)

Table 24: Total single-W cross-section in fb for the process $e^+e^- \to e^-\overline{\nu}_e\mu^+\nu_\mu$, for $|\cos\theta_e| > 0.997$, $E_\mu > 15$ GeV, and $|\cos\theta_\mu| < 0.95$, from WTO. The number in parenthesis shows the statistical error of the numerical integration on the last digit.

When we want to improve upon the Fixed-Width scheme, the main accent has to be put on the correct evaluation of the scale in the running of α_{QED}. The latter is particularly important for the t-channel diagrams, dominated by a scale $q^2 \approx 0$ and not $q^2 \approx M_W^2$. However, a consistent implementation of radiative corrections does more than evolving $\alpha_{\rm QED}$ to the correct scale, other couplings are also running, propagators are modified and vertices are included.

We have performed a simple exercise, namely to take the Fixed-Width scheme augmented by a rescaling $[\alpha(q^2)/\alpha_{G_F}]^2$. Since the largest part of the effect is, in any case, confined in the region of very small electron scattering angle we only compute $d\sigma/d\theta_e$ for $0.0^\circ < \theta_e < 0.4^\circ$. Results of our computation are reported in Tab.(25). From Tab.(25) we see that the effective FW-scheme describes considerably well

bin	EFL	FWE	EFL/FWE-1 (percent)	EFL	FWE	EFL/FWE-1 (percent)
$0.0^\circ \div 0.1^\circ$	0.44784	0.45166	+0.85	0.13448	0.13207	-1.79
$0.1^\circ \div 0.2^\circ$	0.06605	0.06615	+0.15	0.02031	0.01989	-2.07
$0.2^\circ \div 0.3^\circ$	0.03860	0.03867	+0.18	0.01194	0.01169	-2.09
$0.3^\circ \div 0.4^\circ$	0.02736	0.02742	+0.22	0.00851	0.00832	-2.23

Table 25: Comparison, with `WTO`, between EFL-scheme and effective FW-scheme, i.e. FW augmented by the running of $\alpha_{\rm QED}$ in the t-channel. First set of results refers to $u\overline{d}$ final states. Second set to the $\mu^+\nu_\mu$ final state. Acceptance cuts are as in the main text and $\sqrt{s} = 183\,{\rm GeV}$.

the hadronic final state with a cut of $M(u\overline{d}) > 45\,$GeV, with a maximal difference of 0.85% in the first bin. However, the diminution induced by $\alpha_{\rm QED}(q^2)$ is too large for the leptonic final state. The latter is a clear sign that other effects are relevant and a naive rescaling does not suffice in reproducing a realistic approximation in all situations, at least not within the 2% level of requested theoretical accuracy.

In order to understand this fact we have computed $d\sigma/d\theta_e$, in the first bin (largest effect), both for $u\overline{d}$ and for $\mu^+\nu_\mu$ final states with varying acceptance cuts. The results of this investigation are shown in Tab.(26) and Tab.(27), respectively. From the numbers in Tab.(26) we see the growth in the cross-section, for all schemes, due to the multi-peripheral peak. The percentage difference between EFL-scheme and FW-scheme decreases, although slowly, for decreasing $M_{\rm min}(u\overline{d})$. There is more, the difference between the two schemes goes from -12.91% for $35\,{\rm GeV} < M(u\overline{d}) < 45\,{\rm GeV}$ to -6.96% for $25\,{\rm GeV} < M(u\overline{d}) < 35\,{\rm GeV}$, to -3.58% for $15\,{\rm GeV} < M(u\overline{d}) < 25\,{\rm GeV}$ and reaches -1.20% for $5\,{\rm GeV} < M(u\overline{d}) < 10\,{\rm GeV}$. With the above cuts we are removing the contribution from the single-resonant W-exchange and the multi-peripheral diagrams start dominating. The same trend is clearly visible in Tab.(27), despite the somewhat larger errors. By increasing $\cos\theta_{\mu,{\rm min}}$ we allow the muon to become more and more collinear to the quasi-real photon, therefore the multi-peripheral contribution counts more and more.

For the multi-peripheral diagrams alone, the inclusion of fermionic corrections changes $\alpha \to \alpha((p-_- q_-)^2)$ in the t-channel photon exchange, $g^2 \to g^2((p_+ - q_+^2)^2)$ in the t-channel W exchange and modifies the t-channel W-propagator. The latter is a large effect. To see it, let us define t-channel line-shape functions,

$$L_{\rm EFL}(t) \quad = \quad \frac{s^2}{(t - {\rm Re}p_W)^2 + ({\rm Im}p_W)^2}\,\frac{1}{|R(t)|^2},$$

$M_{\min}(u\overline{d})$ [GeV]	EFL	FW	EFL/FW-1 (percent)
45	0.04478(3)	0.04841(3)	-7.5(1)
35	0.04711(6)	0.5104(7)	-7.7(1)
25	0.504(1)	0.0546(1)	-7.7(2)
15	0.0552(1)	0.0595(1)	-7.2(2)
10	0.0582(1)	0.0626(1)	-7.0(2)
5	0.0615(1)	0.0659(1)	-6.7(2)
1	0.0637(1)	0.0682(1)	-6.6(2)

Table 26: Comparison, with `WTO`, between EFL-scheme and FW-scheme for the cross-section in pb and $0.0^\circ < \theta_e < 0.1^\circ$. Furthermore, $M(u\overline{d}) \geq M_{\min}$ and $\sqrt{s} = 183\,\mathrm{GeV}$. The number in parenthesis shows the statistical error of the numerical integration on the last digit.

$\cos\theta_{\mu,\min}$	EFL	FW	EFL/FW-1 (percent)
0.95	0.01345(1)	0.01415(1)	-4.9(1)
0.995	0.01485(9)	0.01538(4)	-3.4(6)
0.9995	0.01543(13)	0.01571(9)	-1.8(9)

Table 27: Comparison, with `WTO`, between EFL-scheme and FW-scheme for the cross-section in pb, $0.0^\circ < \theta_e < 0.1^\circ, |\cos\theta_\mu| < \cos\theta_{\mu,\min}$. Furthermore $\sqrt{s} = 183\,GeV$. The number in parenthesis shows the statistical error of the numerical integration on the last digit.

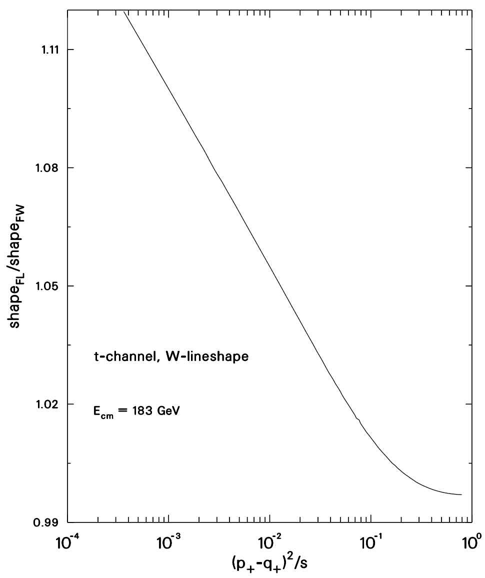

Fig. 48: Comparison between the Fixed-Width and the Fermion-Loop line-shape functions in the t-channel, Eq.(93).

$$L_{\rm FW}(t) \quad = \quad \frac{s^2}{\left(t - M^2_{_W}\right)^2 + M^2_{_W}\Gamma^2_{_W}}. \tag{93}$$

and compare them, as shown in Fig. 48. The EFL t-channel line-shape can be considerably larger than the FW one, due to the ρ-factor, $R(t)$, of Eq.(86). In a circumstance where vertices and s-channel components count very little we can simulate the three effects induced by the EFL-scheme in a simple way. To this end, we compare the following objects:

$$\begin{aligned}
\mathrm{EFL}_{\rm eff}(t,T) &= \alpha^2(T)\,|g^2(t)|^2\,\frac{s^2}{(t-{\rm Re}p_{_W})^2+({\rm Im}p_{_W})^2}\,\frac{1}{|R(t)|^2},\\
\mathrm{FW}_{\rm eff}(t) &= g^8\,s^4_\theta\,\frac{s^2}{\left(t - M^2_{_W}\right)^2 + M^2_{_W}\Gamma^2_{_W}},
\end{aligned} \tag{94}$$

where $T = -(p_- - q_-)^2$ and $t = -(p_+ - q_+)^2$. The comparison is shown, for fixed T and as a function of t, in Fig. 49. The difference, especially for non-vanishing values of t (remember that $M^2_{_W}/s = 0.19$ at $\sqrt{s} = 183\,$GeV), is considerably smaller than the one caused by the running of $\alpha_{\rm QED}$. This confirms our previous findings and gives clear evidence that a naive rescaling of the Fixed-Width results cannot cover all possible cases, with different processes and with kinematical cuts of different kinds, at least not below the threshold of 2% for the theoretical accuracy.

Modifications induced by the fermionic loops are sensitive to the relative weight of single-resonant terms and of multi-peripheral peaks. Furthermore, the effect of radiative corrections inside the W-propagators (ρ-factors) is far from being negligible and tends to compensate the change due to the running of $\alpha_{\rm QED}$.

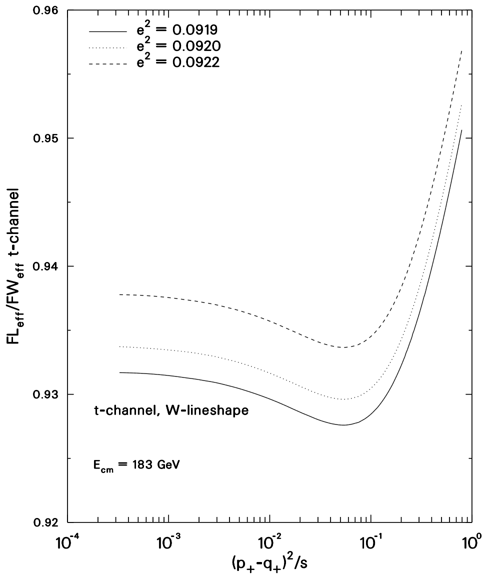

Fig. 49: Comparison between the fixed-width and the fermion-loop line-shape functions in the t-channel, Eq.(94). Three values of $e^2(T)$ are reported.

12.13 Conclusions.

In this Section we have analyzed the numerical impact of introducing the Fermion-Loop scheme for evaluating cross-sections and distributions in single-W production.

A description of single-W processes by means of the Fermion-Loop scheme is mandatory from, at least, two points of view. EFL is the only field-theoretically consistent scheme that preserves gauge invariance in processes including unstable vector-bosons coupled to e.m. currents. Furthermore, single-W production is a process that depends on several scales, the single-resonant s-channel exchange of W-bosons, the exchange of W-bosons in t-channel, the small scattering angle peak of outgoing electrons.

A correct treatment of the multi-scale problem can only be achieved when we include radiative corrections in the calculation, not only one-loop terms but also the re-summation of leading higher-order terms. Recent months have shown that this project can be brought to a very satisfactory level by identifying the correct approximation, process-by-process.

In particular, the $W-W$ configuration, dominated by double-resonant terms, can be treated within the so-called double-pole-approximation or DPA. As a consequence, the theoretical uncertainty associated with the determination of the WW cross-section is sizably decreased. In principle, the same procedure applies to the determination of the ZZ cross-section, where one develops a NC02-DPA approximation instead of the CC03-DPA one.

Within the context of EFL-scheme the theoretical predictions for single-W production become smaller, as compared to other pragmatic, gauge-preserving, schemes. We have found that all the modifications introduced via the Fermion-Loop scheme are relevant: running of the couplings, ρ-factors and vertices, not only the change $\alpha_{\rm QED}(\rm fixed) \to \alpha_{\rm QED}(\rm running)$. Therefore, a naive rescaling cannot reproduce the Fermion-Loop answers for all situations, all kinematical cuts.

The high-energy Input Parameter Set used in all calculations that are presently available – we quote,

Process	$\sqrt{s} = 183\,\mathrm{GeV}$	$\sqrt{s} = 189\,\mathrm{GeV}$	$\sqrt{s} = 200\,\mathrm{GeV}$
$e^+e^- \to e^-\overline{\nu}_e u\overline{d}$	83.237(36)	93.797(75)	113.71(5)
$e^+e^- \to e^-\overline{\nu}_e \nu_\mu \mu^+$	25.476(40)	28.741(44)	34.900(50)
$e^+e^- \to e^-\overline{\nu}_e \nu_\tau \tau^+$	25.442(38)	28.702(41)	34.856(48)

Table 28: WTO single-W cross-sections, in fb, for $\sqrt{s} = 183(189, 200)\,\mathrm{GeV}$ and $|\cos\theta_e| > 0.997$ in the Fermion-Loop scheme. Additional cuts are: $M(u\overline{d}) > 45$ GeV; $E_{\mu(\tau)} > 15$ GeV; $|\cos\theta_{\mu(\tau)}| < 0.95$. The number in parenthesis shows the statistical error of the numerical integration on the last two digits.

among the various schemes, the Fixed-Width scheme, the Overall scheme and the Imaginary Fermion-Loop one – is based on G_F, M_W and M_Z with $\alpha_{\mathrm{QED}}\,(\mathrm{fixed}) = 1/131.95798$. It allows for the inclusion of part of higher order effects in the Born cross-sections but, it fails to give a correct and accurate description of the $q^2 \sim 0$ dominated processes.

A naive, overall, rescaling would lower the single-W cross-section of about 7%. We have found, with the complete Fermion-Loop, that this decrease is process and cut dependent. Moreover, the effect is larger in the first bin for θ_e – $0.0° \div 0.01°$ – in the distribution $d\sigma/d\theta_e$ and tends to become less pronounced for larger scattering angles of the electron. However, the first bin represents almost 50% of the total single-W cross-section, so that, in general, the compensations that occur among several effects never bring the Fl/FW ratio to one. We obtain a maximal decrease of about 7% in the result but, on average, the effect is smaller. We have also found that the effect is rather sensitive to the relative weight of multi-peripheral contributions.

12.14 estimate of TU

A final comment is needed to quantify the theoretical accuracy of single-W production. Bosonic corrections are still missing and, very often, our experience has shown, especially at LEP1, that bosonic corrections may become sizeable [67]. A large part of the bosonic corrections, as e.g. the leading-logarithmic corrections, factorize and can be treated by a convolution. Nevertheless the remaining bosonic corrections can still be non-negligible, i.e., of the order of one percent at LEP2 [68]. For the Born cross-sections 1% should, therefore, be understood as the present limit for the theoretical uncertainty. This will have to be improved, soon or later, since bosonic corrections are even larger at higher energies [69] and the single-W cross-section will cross over the WW one at 500 GeV. Single-W will be one of the major processes at LC to measure not only triple gauge couplings but also the W-mass without color reconnection.

To summarize our findings we present a collection of single-W cross-sections obtained in the Fermion-Loop scheme with WTO in a high precision run. They are shown in Tab.(28) where we also report the $\nu_\tau\tau$ final state. Numerical precision ranges from $0.05\% \div 0.08\%$ for $u\overline{d}$ to $0.14\% \div 0.16\%$ for $\nu_\mu\mu(\nu_\tau\tau)$.

12.2 Single-W and SWAP.

Authors
G. Montagna
M. Moretti
O. Nicrosini
A. Pallavicini
F. Piccinini

12.21 Description of the Method

Contributions of the Pavia/ALPHA group to the subject of single-W production are summarized.

12.22 Hard-scattering matrix element

The exact matrix elements for single-W production are computed by means of the ALPHA algorithm [70] for the automatic evaluation of the Born scattering amplitudes. Fermion masses are exactly accounted for in the kinematics and dynamics. The contribution of anomalous trilinear gauge couplings is also taken into account. The anomalous gauge boson couplings Δk_γ, λ_γ, δ_Z, Δk_Z and λ_Z are implemented according to the parameterization of refs. [135, 72]. The fixed-width scheme is adopted as gauge-restoring approach, as motivated in comparison with other gauge-invariance-preserving schemes in ref. [73].

12.23 Radiative corrections

Leading-log (LL) QED radiative corrections are implemented via the Structure Function (SF) formalism in the collinear approximation [74]. The Q^2-scale entering the SF $D(x, Q^2)$ is fixed by comparing the $O(\alpha)$ expansion of the SF method with the analytic results obtained for the LL photonic corrections as given by soft-photon bremsstrahlung from the external legs, its virtual counterpart and hard-photon radiation collinear to the final-state particles. For example, for the process $e^+e^- \to e^-\bar{\nu}u\bar{d}$, this comparison translates in the following two Q^2-scales: (two initial-state (IS) SFs are assumed: Q^2_- refers to the SF attached to the incoming electron, while Q^2_+ to the SF attached to the incoming positron) [75]

$$Q^2_- = 4E^2\frac{(1-c_-)^2}{\delta^2}\,, \quad Q^2_+ = 2^{\frac{14}{9}}\,E^2\frac{((1-c_{\bar{d}})(1-c_u)^2)^{\frac{2}{3}}}{((1-c_{u\bar{d}})^2\delta^5)^{\frac{2}{9}}} \tag{95}$$

where E is the beam energy, c_- the cosine of the electron scattering angle, c_u and $c_{\bar{d}}$ the cosine of the quark scattering angles with respect to the initial positron, $c_{u\bar{d}}$ the cosine of the relative angle between the quarks, δ the half-opening angle of the electromagnetic jet (calorimetric angular resolution). Also a naive ansatz for the two scales, as motivated by an analysis of the single-W process in terms of the Weizsäcker-Williams approximation, can be given [75] as follows:

$$Q^2_{-,\mathrm{naive}} = |q^2_{\gamma^*}|\,, \quad Q^2_{+,\mathrm{naive}} = M^2_W \tag{96}$$

where $q^2_{\gamma^*}$ is the squared momentum transfer in the $ee\gamma^*$ vertex and M_W is the mass of the W boson.

The effect of vacuum polarization is also taken into account in our calculation, by including the contribution of leptons, heavy quarks and light quarks, the latter according to the standard parameterization of ref. [76].

12.24 Computational tool

The theoretical features sketched above have been implemented into a massive MonteCarlo (MC) program, named SWAP (Single W process with Alpha & Pavia). The multi-channel importance sampling technique is employed to perform the phase-space integration. The code supports realistic event selections and can be employed either as a cross-section calculator or as a true event generator.

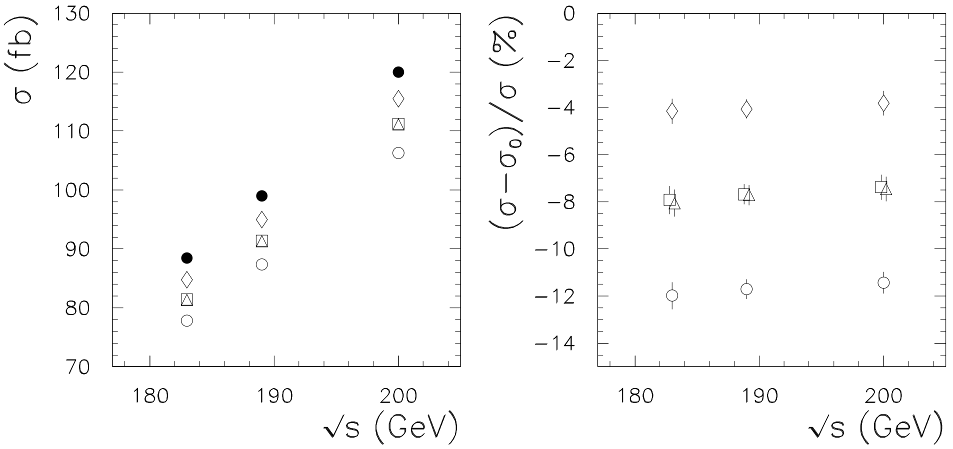

Fig. 50: The effect of LL QED corrections to the cross section of the single-W process $e^+e^- \to e^-\bar{\nu}u\bar{d}$ for different choices of the Q^2-scale in the electron/positron SF. Left: absolute cross section values; Right: relative difference between QED corrected cross sections and the Born one. The marker $\bullet$ represents the Born cross section, $\circ$ represents the correction given by $Q^2_\pm = s$ scale, $\diamond$ represents the correction given by $Q^2_\pm = |q^2_{\gamma^*}|$ scale, $\triangle$ the correction given by the scales of eq. (95), the correction given by the naive scales of eq. (96). The entries correspond to 183, 189, 200 GeV

.

12.25 Results Obtained

The main results obtained in our study can be summarized as follows:

- critical analysis of the energy scale for QED radiation (see Fig. 50);
- evaluation of the effect of running of $\alpha_{\rm QED}$ (see Fig. 51);
- tuned comparisons with other codes (see Sec. 12.26).

Input parameters and cuts used to obtain the numerical results shown in the following are those of the $4f$ proposal for the process $e^+e^- \to e^-\bar{\nu}u\bar{d}$ ($|\cos\vartheta_e| > 0.997, M_{u\bar{d}} > 45$ GeV). For Fig. 50 the value of δ parameter entering eq. (95) is $\delta = 5°$, but it has been checked that the numerical results are very marginally affected by its actual value.

Scales & QED radiation. In Fig. 50 the numerical impact of different choices of the Q^2-scale on the cross section of the single-W process $e^+e^- \to e^-\bar{\nu}u\bar{d}$ is shown. The marker $\bullet$ represents the Born cross section, $\circ$ represents the correction given by $Q^2_\pm = s$ scale for both IS SFs, $\diamond$ represents the correction given by $Q^2_\pm = |q^2_{\gamma^*}|$ scale for both IS SFs, $\triangle$ the correction given by the scales of eq. (95), the correction given by the naive scales of eq. (96). It can be seen that neither the s scale, as implemented in computational tools used for the analysis of the single-W process, nor the $|q^2_{\gamma^*}|$ scale, as recently proposed in ref. [55], are able to reproduce the effects due to the scales of eq. (95) and eq. (96). These two scales are in good agreement and both predict a lowering of the Born cross-section of about 8%, almost independent of the c.m. LEP 2 energy.

Running of $\alpha_{\rm QED}$. Because G_F, M_W and M_Z are the agreed input parameters in the $4f$ proposal, the value of the e.m. coupling constant α is fixed at tree-level to a high energy value as specified by the G_F-scheme. On the other hand, the single-W process is a $q^2_{\gamma^*} \simeq 0$ dominated process and therefore the above high-energy evaluation of α, α_{G_F}, needs to be rescaled to its correct value at small momentum transfer. In order to take into account the effect of the running of α in a gauge invariant way, a *re-weighting* procedure can be adopted, by simply rescaling the differential cross section $d\sigma/dt$ ($t \equiv q^2_{\gamma^*}$) in the following way

$$\frac{d\sigma}{dt} \to \frac{\alpha^2(0)}{\alpha^2_{G_F}}\frac{d\sigma}{dt}\,, \qquad \frac{d\sigma}{dt} \to \frac{\alpha^2(t)}{\alpha^2_{G_F}}\frac{d\sigma}{dt}\,, \tag{97}$$

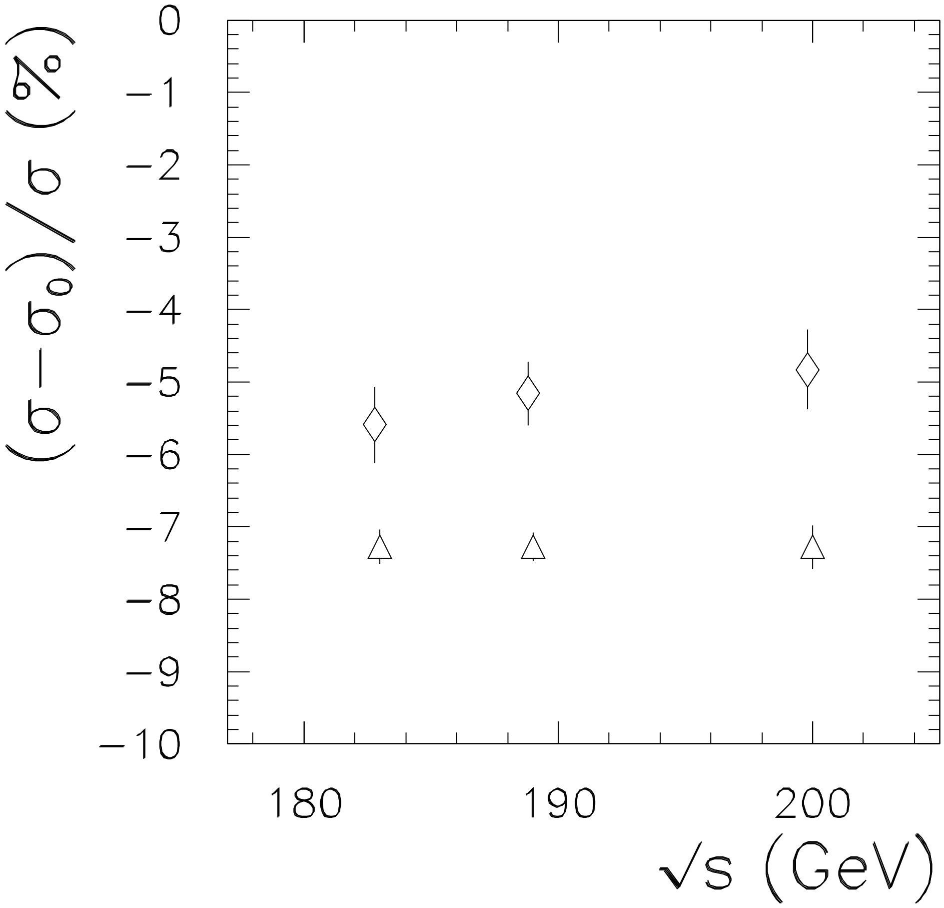

Fig. 51: The effects of the rescaling of $\alpha_{\rm QED}$ from α_{G_F} to $\alpha(q^2_{\gamma^*} = 0)$ ($\triangle$) and $\alpha(q^2_{\gamma^*})$ ($\diamond$) on the integrated cross section of the single-W process $e^+e^- \to e^-\bar{\nu}u\bar{d}$. σ_0 is the cross section computed in terms of α_{G_F}. The entries correspond to 183, 189, 200 GeV.

where $\alpha(0)$, $\alpha(t)$ is the QED running coupling computed at virtuality $q^2_{\gamma^*}$ equal to 0 and t, respectively. Fig. 51 shows the effects of the above re-weighting procedure. The $\triangle$ represent the relative difference between the integrated cross section computed in terms of α_{G_F} and the cross section computed in terms of $\alpha(0)$, while $\diamond$ is the relative difference between the integrated cross section computed in terms of α_{G_F} and the cross section computed in terms of $\alpha(t)$. As can be seen, the rescaling from α_{G_F} to $\alpha(t)$ introduces a negative correction of about $5-6\%$ in the LEP 2 energy range. The difference between $\triangle$ and $\diamond$, which is about $2-3\%$, is a measure of the running of $\alpha_{\rm QED}$ from $q^2_{\gamma^*} = 0$ to $q^2_{\gamma^*} = t$. A detailed numerical analysis of the effect of the running couplings in single-W production has been very recently performed in ref. [59], based on the theoretical results of the massive fermion-loop scheme of ref. [44]. Our results for the running of $\alpha_{\rm QED}$, as shown in Fig. 51, are in agreement with those of ref. [116].

12.26 Available Comparisons

Tuned comparisons between the predictions of `SWAP` and those of other independent codes, namely `CompHEP, NEXTCALIBUR, WPHACT` and `WTO`, are available. These comparison cover single-W Born cross-sections and distributions, including also leptonic final states, and in the presence of both invariant mass and energy cuts.

In order to assess the theoretical uncertainty relative to the treatment of photonic corrections, it would be quite important and certainly useful to compare the predictions of `SWAP`, as given in Sect. 12.25, with those of other codes, based on SF, Parton Shower or YFS method.

12.27 Estimate of TU

The difference shown in Fig. 50 between the predictions given by the two set of Q^2-scales of eq. (95) and eq. (96) is of the order of 1% and it may be considered as a first estimate of the theoretical error in the treatment of QED radiation, which could be corroborated by the comparison with the results of other groups. QED corrections missing in the present approach are beyond the LL approximation.

12.28 Recommendations

The present study shows that the choice $Q^2_\pm = s$ as scale in the IS QED SFs can lead to over-estimate the effect of LL photonic corrections by a factor of 1.5, implying an under-estimate of the QED corrected cross section of about 4%. Also the choice of fixing the scale to $Q^2_\pm = |q^2_{\gamma^*}|$ for both the IS SFs, as recently suggested [55], leads to an under-estimate of the photon correction of about 4%. Since these effects are not negligible in the light of the expected theoretical accuracy, it is recommended to adopt the Q^2-scales as given in eq. (95) or eq. (96), which are motivated by the arguments sketched in Sec. 12.23.

Further, the effect of rescaling $\alpha_{\rm QED}$ from the high-energy value α_{G_F} to $\alpha(q^2_{\gamma^*})$ amounts to a negative correction of about 5-6%, to be taken into account carefully.

12.3 NEXTCALIBUR

Authors

F.A.Berends
C. G. Papadopoulos
R.Pittau

This section describes the features of a new Monte Carlo program NEXTCALIBUR, which aims at keeping the advantages of EXCALIBUR [120], but tries to improve on its shortcomings.

The advantages, which should be kept are the high speed of the program and the applicability to all possible 4-fermion final states. The shortcomings of EXCALIBUR, which are partly related to its assets, are the masslessness of its fermions, the inclusive treatment of ISR QED corrections (no p_t from a photon in an event) and the neglect of any running of coupling constants.

12.31 The strategy of the code

To start with, it should be noted that unless stated otherwise complex gauge boson masses and a complex weak mixing angle are used to ensure gauge invariant matrix elements [121]. This procedure has been shown to work well [122]. The various wanted improvements will now be successively discussed.

12.32 Inclusion of fermion masses

Inside the program a massive matrix element is needed, for the calculation of which a recursive method [123] is used. The larger the number of external particles is, the more competitive this method becomes. It now becomes easy to modify vertices or propagators and to add a photon to the four-fermion production amplitude. So besides the efficiency, the flexibility for future extensions is also an advantage of the method. Of course, the fact that for non-zero masses the number of helicity amplitudes grows exists in every method and increases the computer time. When particular masses are zero the reduced number of helicity amplitudes is used from the start of the recursive calculation.

This massive matrix element now exists in the whole phase space, since the singularities of the massless case are regularized. Nevertheless serious numerical cancellations take place in very specific situations. The most dramatic case is caused by the photonic multi-peripheral diagrams which blow up for forward scattering. When at the same time both electron and positron move in the forward direction, it becomes necessary to perform the calculation in quadruple precision. When only one is moving in the forward direction the usual double precision is sufficient.

The phase space generation is an extension of the treatment in EXCALIBUR, i.e. a self-adjusting multi-channel approach, now including the multi-peripheral situation in an improved form.

With the above mentioned ingredients one indeed has an event generator for any massive four-fermion final state. In particular, for the potentially dangerous kinematical situations events can now be generated , like forward single W-production. Also all channels, where Higgs exchange can take place now indeed contain Higgs exchanges.

12.33 Taking into account the correct scale

As mentioned above, the matrix element calculation can easily be modified. One option is to take into account fermion loop corrections, which becomes relevant when there are different scales in the matrix element, e.g. due to small t-channel scales. A possible solution is the Fermion-Loop approach of refs. [124]-[126], where all fermion corrections are consistently included by introducing running couplings $g(s)$ and $e(s)$, together with the following bosonic propagators

$$P_w(s) = \left(s - \mu_w \frac{g^2(s)}{g^2(\mu_w)} + g^2(s)[T_W(s) - T_W(\mu_w)]\right)^{-1}$$
$$P_z(s) = \left(s - \mu_z \frac{g^2(s)}{c_\theta^2(s)} \frac{c_\theta^2(\mu_z)}{g^2(\mu_z)} + \frac{g^2(s)}{c_\theta^2(s)}[T_Z(s) - T_Z(\mu_z)]\right)^{-1}$$
$$s_\theta^2(s) = \frac{e^2(s)}{g^2(s)}\,,\ c_\theta^2(s) = 1 - s_\theta^2(s)\,, \tag{98}$$

where $T_{W,Z}(s)$ are contributions due to the top quark and $\mu_{w,z}$ the complex poles of the propagators. In presence of the $WW\gamma$ vertex, the above ingredients are not sufficient to ensure gauge invariance, because loop mediated vertices have to be consistently included. On the contrary, when no $WW\gamma$ vertex is present, the neutral gauge boson vertices, induced by the fermion loop contributions, are separately gauge invariant [125].

Instead of explicitly including the loop vertices, we follow a *Modified Fermion-Loop* approach. Namely, we neglect the separately gauge invariant neutral boson vertices, and include only the part of the $WW\gamma$ loop function necessary to renormalize the bare $WW\gamma$ vertex and to insure the $U(1)$ gauge invariance. More details can be found in ref. [127]. Here we just outline the procedure.

As a first step, we take $\mu_{w,z} = M_{W,Z}^2 - i\Gamma_{w,z}M_{W,Z}$, and only consider the real part of the fermion loop corrections, because the contributions responsible of the running of $\alpha_{\rm QED}$ and the leading top terms are confined there. That completely defines our approach for processes mediated by neutral currents only. When the $WW\gamma$ coupling is present, we introduce instead the following effective three gauge boson vertex

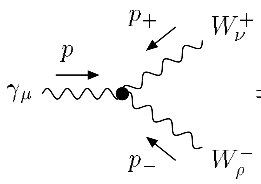

$$= i\, e(s) V_{\mu\nu\rho}(1 + \delta_V)$$

with

$$s = p^2\,,\ s^+ = p_+^2\,,\ s^- = p_-^2$$

$$
\begin{aligned}
V_{\mu\nu\rho} &= g_{\mu\nu}(p-p_+)_\rho + g_{\nu\rho}(p_+ - p_-)_\mu + g_{\rho\mu}(p_- - p)_\nu \\
\delta_V &= \frac{1}{g(s^+)g(s^-)(s^- - s^+)}\Big[g^2(s^+)g^2(s^-)\left[T_W(s^-) - T_W(s^+)\right] \\
&+ \left[g(s^+) - g(s^-)\right]\left[s^- g(s^+) + s^+ g(s^-)\right]\Big] \;.
\end{aligned}
\tag{99}
$$

It is the easy to see that, with the above choice for δ_V, the $U(1)$ gauge invariance - namely current conservation - is preserved, even in presence of complex masses and running couplings.

12.34 Improving the treatment of the QED radiation

Once the matrix element calculation is fixed one can add externally the QED leading logarithmic effects in the Structure Function method [128]. Such a strategy is implemented in most of the programs used for the analysis of the LEP2 data [129] and accurately reproduces the inclusive four-fermion cross sections, at least for s-channel dominated processes. In principle both initial and final state radiation (ISR and FSR) can be treated in this way, as it has been explicitly done originally for Bhabha scattering [130]. Here only the implementation of ISR in `NEXTCALIBUR` is discussed. There are two issues to be discussed. One is the choice of scale q^2 in the leading logarithm

$$
L = \log\left(\frac{q^2}{m_e^2}\right). \tag{100}
$$

Another is the *unfolding* of this leading logarithm in terms of an emitted photon. For the latter issue a particular form of p_t dependent Structure Functions [131] is implemented. These are derived, at the first leading logarithmic order, for small values of p_t. In practice, we replace the quantity

$$
\log\left(\frac{q^2}{m_e^2}\right) \quad \text{by} \quad \frac{1}{1 - c_i + 2\frac{m_e^2}{q^2}}
$$

in the strictly collinear Structure Function for the i^{th} incoming particle, by explicitly generating c_1 and c_2, the cosines (in the Lab frame) of the emitted photons with respect to the incoming particles. Once $c_{1,2}$ are generated, together with the energy fractions $x_{1,2}$, the momenta of two ISR photons are known. The four-fermion event is then generated in the Center-of-Mass frame of the incoming particles *after* QED radiation, and then boosted back to the Lab frame.

We also take into account non leading terms with the substitution [132]

$$
\log\left(\frac{q^2}{m_e^2}\right) - 1 \quad \to \quad \frac{1}{1 - c_i + 2\frac{m_e^2}{q^2}} - 2\frac{m_e^2}{q^2}\frac{1}{(1 - c_i + 2\frac{m_e^2}{q^2})^2}.
$$

The above choice ensures that the residue of the soft-photon pole gets proportional to $\log(\frac{q^2}{m_e^2}) - 1$, after integration over c_i.

As to the scale q^2, for s-channel dominated processes clearly s should be taken. When a process is in fact dominated by small t exchanges and where necessarily -t is much smaller than s, the scale is related to t. This is e.g. the case in small angle Bhabha scattering [133] and the proper scale is chosen as the one which reproduces roughly the exact first order QED correction, which is known for Bhabha scattering. A similar procedure now also exists for the multi-peripheral two photon process [134], since an exact first order calculation is also available [135]. In these t-channel dominated processes it is important to know whether a cross section with angular cuts is wanted, since then the t-related scale will increase and the QED corrections as well. When no exact first order calculations are available the scale occurring in the first order soft corrections is also used as guideline for the scale [134, 136].

In the program `NEXTCALIBUR` one has the option to choose a scale. Since this depends both on the process and the forward kinematical range, when it is a t-channel dominated process, it is at present left as a free choice to the user.

$\sqrt{s}$	BDK	NEXTCALIBUR
20	0.920 ± .011	0.905 ± .011
35	1.070 ± .015	1.079 ± .014
50	1.233 ± .018	1.214 ± .016
100	1.459 ± .025	1.485 ± .020
200	—	1.776 ± .019
200 (all)	—	1.787 ± .030

σ_{tot} *(in nb* $\times 10^7$*) for the process* $e^+e^- \to e^+e^-e^+e^-$. *Only QED diagrams, except in the last entry.*

12.35 Numerical results

In Tabs.(12.35–12.35), we show the total cross sections for the processes $e^+e^- \to e^+e^-\mu^+\mu^-$ and $e^+e^- \to e^+e^-e^+e^-$. Where available, we compare our predictions with the QED numbers published in ref. [137].

$\sqrt{s}$	BDK	NEXTCALIBUR
20	98.9 ± 0.6	99.20 ± 0.98
35	131.4 ± 2.2	131.03 ± 0.88
50	154.4 ± 0.9	152.33 ± 0.83
100	205.9 ± 1.2	204.17 ± 1.73
200	—	263.50 ± 1.31
200 (all)	—	265.58 ± 1.44

σ_{tot} *(in nb) for the process* $e^+e^- \to e^+e^-\mu^+\mu^-$. *Only QED diagrams, except in the last entry.*

NEXTCALIBUR contains all electroweak diagrams, and can therefore be used to compute the electroweak background to the above $\gamma\gamma$ processes. By looking at the last entry of the tables, the latter is found to be less than 1 % at LEP2 energies, at least for totally inclusive quantities.

All numbers have been produced at the Born level, but ISR and running $\alpha_{\rm QED}$ can be included as described in the previous section. Here we mainly want to demonstrate the ability of the program to cover all phase-space regions, without loosing efficiency in the event generation. At the moment, in order to get the necessary numerical accuracy, we run the program in quadruple precision. NEXTCALIBUR has been written in such a way that switching from double to quadruple precision simply implies adding a flag at the compilation time. However, this option is really necessary only when two or more electrons are allowed in the very forward direction. For all the other kinematical configurations, with at most one electron lost in the beam pipe, double precision is sufficient. A version of the program using double precision in all possible situations is currently under study.

In Tabs.(12.35–12.35) we show, as a second example, single-W numbers produced with our Modified Fermion-Loop approach, as discussed in the previous section. Comparisons are made with the exact Fermion-Loop calculation of ref. [124]. The results of the complete Fermion-Loop are reproduced within 2% accuracy for both leptonic and hadronic single-W final states.

It should also be noted that, when neglecting Fermion-Loop corrections, one can directly compare NEXTCALIBUR with other massive Monte Carlo's and one finds excellent agreement for single-W production in the whole phase space [141].

$d\sigma/d\theta_e$	MFL	EFL	MFL/EFL $-$ 1 (percent)
$0.0° \div 0.1°$	0.45382(60)	0.44784	+1.34
$0.1° \div 0.2°$	0.06645(24)	0.06605	+0.61
$0.2° \div 0.3°$	0.03884(19)	0.03860	+0.63
$0.3° \div 0.4°$	0.02779(16)	0.02736	+1.57
σ_{tot}	83.87(9)	83.28(6)	+0.71

$d\sigma/d\theta_e$ [pb/degrees] and σ_{tot} [fb] for the process $e^+e^- \to e^-\bar{\nu}_e u\bar{d}$. The first column is our Modified Fermion-Loop, the second one is the exact Fermion-Loop of ref. [124]. $\sqrt{s} = 183$ GeV, $|\cos\theta_e| > 0.997$, $M(u\bar{d}) > 45$ GeV. QED radiation not included. The number in parenthesis is the integration error on the last digits.

m_H	MFL	EFL	MFL/EFL $-$ 1 (percent)
$0.0° \div 0.1°$	0.13280(21)	0.13448	-1.2
$0.1° \div 0.2°$	0.02003(8)	0.02031	-1.4
$0.2° \div 0.3°$	0.01176(7)	0.01194	-1.5
$0.3° \div 0.4°$	0.00834(6)	0.00851	-1.9
σ_{tot}	25.10(3)	25.53	-1.7

$d\sigma/d\theta_e$ [pb/degrees] and σ_{tot} [fb] for the process $e^+e^- \to e^-\bar{\nu}_e \nu_\mu \mu^+$. The first column is our Modified Fermion-Loop, the second one is the exact Fermion-Loop of ref. [124]. $\sqrt{s} = 183$ GeV, $|\cos\theta_e| > 0.997$, $|\cos\theta_\mu| < 0.95$ and $E_\mu > 15$ GeV. QED radiation not included. The number in parenthesis is the integration error on the last digits.

12.4 `WPHACT`

Authors

E. Accomando
A. Ballestrero
E. Maina

12.41 IFL-scheme

The Imaginary Part Fermion Loop scheme has been generalized to the fully massive case of non conserved weak currents in Ref. [100]. The results obtained have been compared with other possible gauge restoring schemes used in single-W processes computations. The following schemes have been considered in the analysis:

Imaginary-part FL scheme(IFL): The imaginary part of the fermion-loop corrections, as computed in Ref. [100], are used. Fermion masses are neglected only in loops but not in the rest of the diagrams.

Fixed width(FW): The W-boson propagators are given by

$$\left(g^{\mu\nu} - \frac{p^\mu p^\nu}{M_W^2 - i\Gamma_W M_W}\right)\frac{1}{p^2 - M_W^2 + i\Gamma_W M_W} \quad . \tag{101}$$

This gives an unphysical width for $p^2 < 0$, but retains $U(1)$ gauge invariance in the CC20 process [27].

Complex Mass(CM): All weak boson masses squared M_B^2 , $B = W, Z$ are changed to $M_B^2 - i\gamma_B$ [104], including when they appear in the definition of the weak mixing angle. This scheme, which again gives and unphysical width in some cases, has however the advantage of preserving both $U(1)$ and $SU(2)$ Ward identities.

Overall scheme(OA): The diagrams for $e^- e^+ \to e^- \bar{\nu}_e u \bar{d}$ can be split into two sets that are separately gauge invariant under $U(1)$. In the actual implementation of the OA-scheme, t channel diagrams are computed without any width and are then multiplied by $(q^2 - M^2)/(q^2 - M^2 + iM\Gamma)$ where q, M and Γ are the momentum, the mass and the width of the possibly-resonant W-boson. This scheme retains $U(1)$ gauge invariance at the expenses of a mistreatment of the non-resonant terms.

In order to asses the relevance of current non-conservation, the imaginary part of the fermion-loop corrections have also been implemented with the assumption that all currents that couple to the fermion-loop are conserved. In this case the expressions of Ref. [100] reduce to those computed in [27]. Note that the masses of external fermions are nonetheless taken into account in the calculation of the matrix elements. This scheme violates $U(1)$ gauge-invariance by terms which are proportional to the fermion masses squared, as already noted in Ref. [99]. However they are enhanced at high energy by large factors and can be numerically quite relevant. This scheme will be referred to as the imaginary-part FL scheme with conserved currents **(IFLCC)**.

All schemes described above have been implemented in the new version of `WPHACT` [105] in which all fully massive matrix elements have been added to the old massless ones and new phase space mappings have been introduced for dealing with single-W, single-Z and $\gamma\gamma$ contributions.

In Tab.(29) the cross sections for CC20 are given for the different gauge restoring schemes at LEP2 and LC energies. From it, one can immediately deduce that the IFL, FW, CM and the OA schemes agree within $2\,\sigma$ in almost all cases. The IFLCC scheme agrees with the other ones at LEP 2 energies but already at 800 GeV it overestimates the total cross-section by about 6%. At $1.5\ \mathrm{TeV}$ the error is almost a factor of two. On the contrary, even in the presence of non–conserved currents, i.e. of massive external fermions, the FW CM and OA calculations give predictions which are in agreement, within a few per mil, with the IFL scheme. The agreement with the results of a self-consistent approach justifies, from a practical point of view, the ongoing use of the FW, CM and OA schemes.

The possible dependence of this agreement on the particular single-W process considered has been examined and we compare in Tab.(30) the cross-sections obtained in the IFL and FW scheme at $\sqrt{s} = 200$ GeV.

In this case, as in the following ones, the standard cuts have been applied: the electron angle is limited in all processes by $|\cos\theta_e^-| > 0.997$, the other charged lepton by $|\cos\theta_l| < 0.95$, its energy has to be $E_l > 15$ GeV, and $M(u\bar{d}) > 45GeV$.

These results confirm that, at LEP 2, there is no dependence of the cross-sections on the scheme. Distribution of several observables have also been studied with `WPHACT` in the IFL and FW schemes. In most variables like the electron angle and energy no difference has been found. However, the mass spectrum of the $u\bar{d}$ pair shows some scheme dependence, as reported in Fig. 52. The physical motivation for this difference can be traced to the fact that the IFL scheme uses, correctly, a running W-width. In any case, in view of possible discrepancies, the use of IFL has to be preferred among the schemes analyzed in this section.

12.42 Running α. Comparisons with EFL.

The EFL scheme implemented in Ref. [101, 102] for the massive (non-conserved currents) case solves the gauge-invariance problems exactly, as IFL does, but in addition it computes the real part of fermion loop radiative corrections. These terms are known to determine the running of the couplings involved in single-W processes. One may argue, therefore, that considering the running of α_{QED} at an appropriate physical scale might account for the most relevant part of EFL corrections. To test the correctness of this argument, a proper α_{QED} evolution has been introduced as an option in `WPHACT`. For every set of final momenta, α_{QED} is evaluated at the scale t, the virtuality of the photon emitted by the electron line, and used for two vertices in the t-channel contributions only. Computations performed with this choice will be referred to as IFL$_\alpha$. Several comparisons have been performed between the IFL and IFL$_\alpha$ schemes and with the FW/EFL predictions by `WTO`[61].

The good agreement of the two codes as far as FW and IFL schemes are concerned is documented in Tables 31–35 for the cross-sections, the electron angular distribution and the quark invariant mass distribution. However, this has to be considered as a technical agreement more than a physical one.

Whether IFL$_\alpha$ can satisfactory reproduce the EFL complete calculations seems to depend on the process considered. Note, in Tab.(31), the agreement between IFL$_\alpha$ and EFL for the total cross-section of the process $e^-e^+ \to e^-\bar{\nu}_e u\bar{d}$. Only at $200\,$GeV there is a disagreement of less than 0.5% . Moreover, the angular distribution studied in Tab.(32), for the most relevant bins, never shows a higher discrepancy.

The variation of the cross-section of the process at hand with the invariant mass $M(u\bar{d})$ cut is reported in Fig. 53 from which one deduces that the IFL and the IFL$_\alpha$ schemes practically coincide when the cut reaches the mass of the W-boson. In Tab.(33) one sees that, even varying the cuts, the difference between FL and IFL$_\alpha$ is at most of the order of 1%.

The conclusion is, therefore, that at LEP 2 and for $e^-e^+ \to e^-\bar{\nu}_e u\bar{d}$ the IFL$_\alpha$ scheme is reliable at the percent level.

The same does not apply to $e^-e^+ \to e^-\bar{\nu}_e\mu^+\nu_\mu$, as can be verified with the help of Tab.(34) and Tab.(35). From these one sees that the discrepancy is of the order of 2% or worst. This confirms that varying the scale of $\alpha_{\rm QED}$, on an event by event basis, is not completely satisfactory. These numerical results point towards an estimate of about 3% theoretical error for single-W predictions via the IFL$_\alpha$-scheme.

One can try to apply the running of $\alpha_{\rm QED}$ to only one vertex of the t-channel diagrams; the agreement obtained with this approximation (hereafter IFL$_{\alpha 1}$) is much better for $e^-e^+ \to e^-\bar{\nu}_e\mu^+\nu_\mu$. Of course, it becomes worse for $e^-e^+ \to e^-\bar{\nu}_e u\bar{d}$. At $183, 189$ and $200\,$GeV the cross-sections for $e^-e^+ \to e^-\bar{\nu}_e\mu^+\nu_\mu$ are respectively $2565(1), 28.80(2), 34.86(2)$ fb, to be compared with the EFL results of Tab.(34). The first bins of the angular distribution are also very close to EFL. No physical meaning has to be attributed to this fact: there is no theoretical reason for using running $\alpha_{\rm QED}$ just at one vertex. The agreement may be accidental and it is probably due to the fact that with the cuts used for $e^-e^+ \to e^-\bar{\nu}_e\mu^+\nu_\mu$ the contribution of multi-peripheral diagrams is suppressed.

Since the IFL$_\alpha$ and IFL$_{\alpha 1}$ schemes are, in turn, in good agreement with complete EFL for different processes and cuts, the difference between their results will be used as an estimate of the theoretical error for $e^-e^+ \to e^-e^+\nu_e\bar{\nu}_e$ and $e^-e^+ \to e^-e^+\nu_\mu\bar{\nu}_\mu$, where EFL predictions are not available.

The cross-sections for such processes are presented in Tab.(36) and Tab.(37). The angular distributions for the four processes that we have discussed so far are reported in bins of 0.01 degrees in Fig. 54. Note that the relevant part of the cross-section is concentrated in the first three or four bins, also for $e^-e^+ \to e^-e^+\nu_e\bar{\nu}_e$(MIX) and $e^-e^+ \to e^-e^+\nu_\mu\bar{\nu}_\mu$(NC), as well as for the two CC processes.

12.43 Estimate of TU

From the cross-sections of Tables 36 and 37 one deduces that the difference between IFL and IFL$_\alpha$ is of the order of 6%, for both $e^-e^+ \to e^-e^+\nu_e\bar{\nu}_e$ and $e^-e^+ \to e^-e^+\nu_\mu\bar{\nu}_\mu$. The discrepancy between IFL$_\alpha$ and IFL$_{\alpha 1}$ predictions is always of the order of 3% and one has therefore to attribute an estimate of $3 \div 4$ % error to the FL$_\alpha$ calculations for these processes.

Considering all processes together one can conclude that the implementation of a proper running $\alpha_{\rm QED}$ reduces the theoretical uncertainty by about one half with respect to fixed-width or imaginary fermion-loop alone. In some cases this uncertainty is further reduced to less than one percent, but only a comparison with complete fermion loop calculations, as a reference point, may assess whether this is the case. If no comparisons are available for the process and cuts at hand our study points towards a 3% uncertainty of running $\alpha_{\rm QED}$ calculations for both single-W and single-Z. Of course, one should add the uncertainty due to the fact that ISR for annihilation processes is not suited for t-channel contributions.

	190 GeV	800 GeV	1500 GeV
IFL	0.11815 (13)	1.6978 (15)	3.0414 (35)
FW	0.11798 (11)	1.6948 (12)	3.0453 (41)
CM	0.11791 (12)	1.6953 (16)	3.0529 (60)
OA	0.11760 (10)	1.6953 (13)	3.0401 (23)
IFLCC	0.11813 (12)	1.7987 (16)	5.0706 (44)

Table 29: Cross sections for the processes $e^+e^- \rightarrow e^-\bar{\nu}_e u\bar{d}$ for various gauge restoring schemes. No ISR is included and we apply the following cuts: $M(u\bar{d}) > 5\,\mathrm{GeV}$, $E_u > 3\,\mathrm{GeV}, E_{\overline{d}} > 3\,\mathrm{GeV}, \cos(\theta_e) > .997$

	IFL	FW
$e^-e^+ \rightarrow e^-\bar{\nu}_e ud \quad M_{u\bar{d}} > 45$ GeV	0.12043 (10)	0.12041 (11)
$e^-e^+ \rightarrow e^-\bar{\nu}_e ud \quad M_{u\bar{d}} < 45$ GeV	0.028585 (14)	0.028564 (14)
$e^-e^+ \rightarrow e^-\bar{\nu}_e \mu^+\nu_\mu$	0.035926 (34)	0.035886 (32)
$e^-e^+ \rightarrow e^-\bar{\nu}_e e^+\nu_e$	0.050209 (38)	0.050145 (32)

Table 30: Comparison of FW and IFL schemes for different single-W cross sections at 200 GeV. No ISR is included. Cuts are defined in the text.

Some obvious improvements on this point will soon be implemented in `WPHACT`, however a more careful study both for the theoretical uncertainty of these solutions and for a better treatment of t-channel ISR is still needed.

$\sqrt{s}$	FW	IFL	IFL$_\alpha$	EFL	EFL/FW-1 (percent)
$183\,\mathrm{GeV}$	88.17(44)	88.50(4)	83.26(5)	83.28(6)	-5.5(5)
$189\,\mathrm{GeV}$	98.45(25)	99.26(4)	93.60(9)	93.79(7)	-4.7(3)
$200\,\mathrm{GeV}$	119.77(67)	120.43(10)	113.24(8)	113.67(8)	-5.1(5)

Table 31: Total single-W cross-section in fb for the process $e^+e^- \rightarrow e^-\bar{\nu}_e u\overline{d}$, for $M(u\overline{d}) > 45$ GeV and $|\cos\theta_e| > 0.997$. FW and EFL are computed by `WTO`, IFL and IFL$_\alpha$ by `WPHACT`. No ISR. The number in parenthesis shows the statistical error of the numerical integration on the last digit.

13. WW-pairs with `GRACE`

Authors

Y. Kurihara
M. Kuroda
Y. Shimizu

13.1 Introduction

The single-W production processes present an opportunity to study the anomalous triple-gauge-couplings (TGC) at LEP2 experiments. In order to proceed to the precise measurement of them, the inclusion of an

θ_e [Deg]	FW	IFL	IFL$_\alpha$	EFL	EFL/FW-1 (percent)
$0.0^\circ \div 0.1^\circ$	0.67147	0.67077	0.62404	0.62357	-7.13
$0.1^\circ \div 0.2^\circ$	0.09323	0.09321	0.08753	0.08798	-5.63
$0.2^\circ \div 0.3^\circ$	0.05433	0.05455	0.05141	0.05141	-5.37
$0.3^\circ \div 0.4^\circ$	0.03845	0.03867	0.03624	0.03646	-5.18

Table 32: $d\sigma/d\theta_e$ in [pb/degrees] for the process $e^+e^- \to e^-\bar{\nu}_e u\bar{d}$, for $M(u\bar{d}) > 45$ GeV, $\sqrt{s}$=200 GeV. No ISR. FW and EFL are computed by `WTO`, IFL and IFL$_\alpha$ by `WPHACT`.

$M_{\rm min}(u\bar{d})$	FW	IFL	IFL$_\alpha$	EFL	EFL/FW-1 (percent)
45	0.04841(3)	0.04845(3)	0.04510(4)	0.04478(3)	-7.5(1)
35	0.05104(7)	0.05107(1)	0.04754(1)	0.04711(6)	-7.7(1)
25	0.0546(1)	0.05467(2)	0.05090(1)	0.0504(1)	-7.7(2)
15	0.0595(1)	0.05968(2)	0.05555(2)	0.0552(1)	-7.2(2)
10	0.0626(1)	0.06283(2)	0.05847(1)	0.0582(1)	-7.0(2)
5	0.0659(1)	0.06623(2)	0.06164(2)	0.0615(1)	-6.7(2)
1	0.0682(1)	0.06864(1)	0.06388(1)	0.0637(1)	-6.6(2)

Table 33: Cross-sections for the process $e^+e^- \to e^-\bar{\nu}_e u\bar{d}$ in pb for $0.0^\circ < \theta_e < 0.1^\circ$ and $M(u\bar{d}) \geq M_{\rm min}$ (in GeV). $\sqrt{s} = 183\,\mathrm{GeV}$. No ISR. FW and EFL are computed by `WTO`, IFL and IFL$_\alpha$ by `WPHACT`. The number in parenthesis shows the statistical error of the numerical integration on the last digit.

$\sqrt{s}$	FW	IFL	IFL$_\alpha$	EFL	EFL/FW-1 (percent)
$183\,\mathrm{GeV}$	26.77(14)	26.45(1)	24.90(1)	25.53(4)	-4.6(5)
$189\,\mathrm{GeV}$	29.73(14)	29.70(2)	27.98(2)	28.78(4)	-3.2(5)
$200\,\mathrm{GeV}$	36.45(23)	35.93(4)	33.85(4)	34.97(6)	-4.1(6)

Table 34: Total single-W cross-section in fb for the process $e^+e^- \to e^-\bar{\nu}_e\mu^+\nu_\mu$, for $|\cos\theta_e| > 0.997$, $E_\mu > 15\,$GeV, and $|\cos\theta_\mu| < 0.95$. No ISR. FW and EFL are computed by `WTO`, IFL and IFL$_\alpha$ by `WPHACT`. The number in parenthesis shows the statistical error of the numerical integration on the last digit.

θ_e [Deg]	FW	IFL	IFL$_\alpha$	EFL	EFL/FW-1 (percent)
$0.0° \div 0.1°$	0.14154	0.14170	0.1319	0.13448	-4.99
$0.1° \div 0.2°$	0.02113	0.02117	0.01987	0.02031	-3.88
$0.2° \div 0.3°$	0.01238	0.01240	0.01166	0.01194	-3.55
$0.3° \div 0.4°$	0.00880	0.879	0.0830	0.00851	-3.30

Table 35: $d\sigma/d\theta_e$ in [pb/degrees] for the process $e^+e^- \to e^-\bar{\nu}_e\nu_\mu\mu^+$, for $|\cos\theta_e| > 0.997$, $E_\mu > 15$ GeV, and $|\cos\theta_\mu| < 0.95$. $\sqrt{s} = 183$ GeV. No ISR. FW and EFL are computed by `WTO`, IFL and IFL$_\alpha$ by `WPHACT`.

$\sqrt{s}$	final state	IFL	IFL$_\alpha$	IFL$_{\alpha 1}$
$183\,\mathrm{GeV}$	$e^+e^-\nu_e\bar{\nu}_e$ $e^+e^-\nu_\mu\bar{\nu}_\mu$	38.24(1) 12.81(1)	35.99(1) 12.05(1)	37.10(2) 12.42(1)
$189\,\mathrm{GeV}$	$e^+e^-\nu_e\bar{\nu}_e$ $e^+e^-\nu_\mu\bar{\nu}_\mu$	42.38(1) 13.74(1)	39.86(1) 12.92(1)	41.09(2) 13.32(1)
$200\,\mathrm{GeV}$	$e^+e^-\nu_e\bar{\nu}_e$ $e^+e^-\nu_\mu\bar{\nu}_\mu$	50.20(2) 15.37(1)	47.25(2) 14.46(1)	48.70(2) 14.91(1)

Table 36: Total single-W cross-section in fb by `WPHACT` for the processes $e^+e^- \to e^+e^-\nu\bar{\nu}$ for $|\cos\theta_e^-| > 0.997$, $E_{e^+} > 15$ GeV, and $|\cos\theta_{e^+}| < 0.95$. No ISR. The number in parenthesis shows the statistical error of the numerical integration on the last digit.

θ_e [Deg]	final state	IFL	IFL$_\alpha$	IFL$_{\alpha 1}$
$0.0° \div 0.1°$	$e^+e^-\nu_e\bar{\nu}_e$	0.27958	0.260390	0.26990
	$e^+e^-\nu_\mu\bar{\nu}_\mu$	0.09007	0.08386	0.08693
$0.1° \div 0.2°$	$e^+e^-\nu_e\bar{\nu}_e$	0.03890	0.03643	0.03764
	$e^+e^-\nu_\mu\bar{\nu}_\mu$	0.01158	0.01086	0.01123
$0.2° \div 0.3°$	$e^+e^-\nu_e\bar{\nu}_e$	0.02279	0.02146	0.02216
	$e^+e^-\nu_\mu\bar{\nu}_\mu$	0.00680	0.00641	0.00660
$0.3° \div 0.4°$	$e^+e^-\nu_e\bar{\nu}_e$	0.01622	0.01535	0.01573
	$e^+e^-\nu_\mu\bar{\nu}_\mu$	0.00482	0.00456	0.00467

Table 37: $d\sigma/d\theta_e$ in [pb/degrees] by `WPHACT` for the processes $e^+e^- \to e^+e^-\nu\bar{\nu}$ for $|\cos\theta_e^-| > 0.997$, $E_{e^+} > 15$ GeV, and $|\cos\theta_{e^+}| < 0.95$. $\sqrt{s} = 200$ GeV. No ISR.

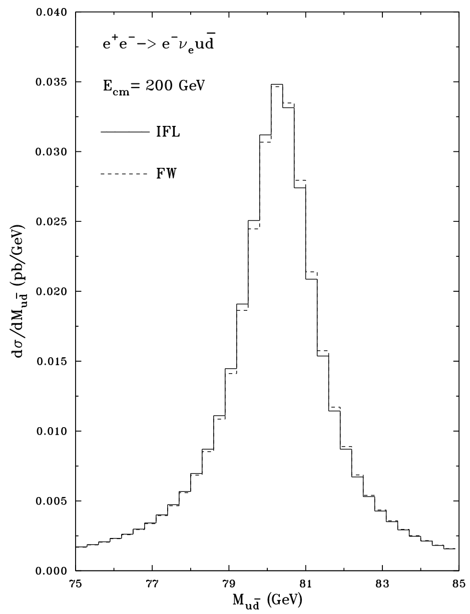

Fig. 52: Mass distribution of the $u\bar{d}$ pair in $e^-e^+ \to e^-\bar{\nu}_e u\bar{d}$ at $\sqrt{s} = 200$ GeV in the IFL and FW schemes. No ISR. $|\cos\theta_e^-| > 0.997$

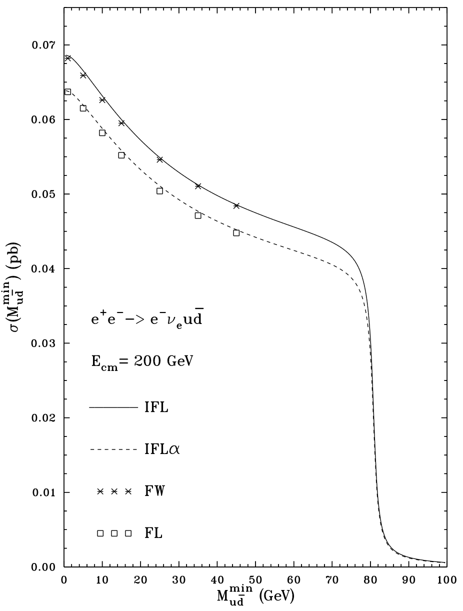

Fig. 53: Total cross section for $e^-e^+ \to e^-\bar{\nu}_e u\bar{d}$ at $\sqrt{s}$ = 200 GeV with $\theta_e < 0.1^\circ$ as a function of the lower cut on $M_{u\bar{d}}$ in IFL and IFLα schemes. The markers give the results of FW and FL by WTO.

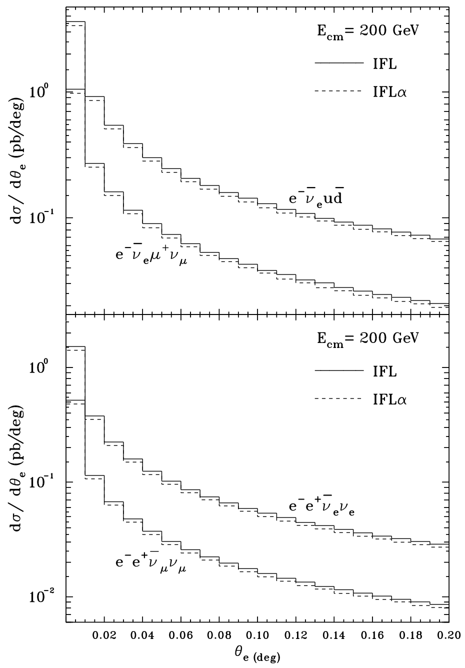

Fig. 54: Angular distributions for different single-W processes at $\sqrt{s}$ = 200 GeV in the IFL and IFLα scheme.

initial state radiative correction (ISR) is inevitable in the generator. As a tool for the ISR the structure function (SF)[166] and the parton shower[167] methods are widely used for the e^+e^- annihilation processes. Since the main contribution, however, comes from the non-annihilation type diagrams for the single-W production processes, the universal factorization method used for the annihilation processes is obviously inappropriate. The main problem lies in the determination of the energy scale of the factorization. According to the study of the two photon process[168], SF and QED parton shower (QEDPS) methods were shown to reproduce the exact $O(\alpha)$ results precisely even for the non-annihilation processes, when the appropriate energy scale is used in those tools.

Here we propose a general method to determine the energy scale to be used in SF and QEDPS. The numerical results of testing SF and QEDPS for the processes of $e^-e^+ \to e^-\bar{\nu}_e u\bar{d}$ and $e^-e^+ \to e^-\bar{\nu}_e\mu^+\nu_\mu$ are given. The systematic errors are also discussed.

13.2 Calculation method

13.21 Energy Scale Determination

The factorization theorem for the QED radiative corrections in the LL approximation is valid independent of the structure of the matrix element of the kernel process. Hence SF and QEDPS must be applicable to *any* e^+e^- scattering processes. However, the choice of the energy scale in SF and QEDPS is not a trivial issue. For simple processes like e^+e^- annihilation and two-photon process with only the multi-peripheral diagrams considered so far, the evolution energy scale could be determined by the exact perturbative calculations. However, this is not always possible for more complicated processes. Hence a way to find a suitable energy scale without knowing the exact loop calculations should be established somehow.

First we look at the general consequence of the soft photon approximation. The soft photon cross section (including both the real and the virtual photon effects) is given by the Born cross section multiplied by the following correction factor in the LL order[169]

$$\begin{aligned}
\frac{d\sigma_{soft}(s)}{d\Omega} &= \frac{d\sigma_0(s)}{d\Omega} \\
&\times \left|\exp\left[-\frac{\alpha}{\pi}\ln\left(\frac{E}{k_c}\right)\sum_{i,j}\frac{e_ie_j\eta_i\eta_j}{\beta_{ij}}\ln\left(\frac{1+\beta_{ij}}{1-\beta_{ij}}\right)\right]\right|^2, \qquad (102)\\
\beta_{ij} &= \left(1-\frac{m_i^2m_j^2}{(p_i\cdot p_j)^2}\right)^{\frac{1}{2}}, \qquad (103)
\end{aligned}$$

where m_j's(p_j's) are the mass(momentum) of j-th charged particle, k_c the maximum energy of the soft photon (boundary between soft- and hard-photons), E the beam energy, and e_j the electric charge in unit of the e^+ charge. The factor η_j is -1 for the initial particles and $+1$ for the final particles. The indices (i, j) run over all the charged particles in the initial and final states.

For the two-photon process, $e^-(p_-) + e^+(p_+) \to e^-(q_-) + e^+(q_+) + \mu^-(k_-) + \mu^+(k_+)$, it is shown in Ref.[168] that the soft-photon factor in Eq.(102) with a $(p_-\cdot q_-)$-term reproduces an exact $O(\alpha)$ correction[170] in the LL approximation. This implies that one is able to read off the possible evolution energy scale in SF from Eq.(102) without explicit loop calculations. However, one may have a question why the energy scale $s = (p_- + p_+)^2$ does not appear in the soft-photon correction even they are included in Eq.(102). When we applied SF to the two-photon process we have ignored those terms which come from the photon bridged between different charged lines. This is because the contributions from the box diagrams with photon exchange between e^+ and e^- is known to be small[171]. Fortunately the infrared part of the loop correction is already included in Eq.(102) and no need to know the full form of the loop diagram. For the two-photon processes if one looks at two terms with, for example $(p_-\cdot p_+)$- and with $(q_-\cdot p_+)$-terms, the momentum of e^- is almost the same before and after the scattering($p_- \approx q_-$). Only the difference appears in $\eta_j\eta_k = +1$ for a (p_-p_+)-term and $\eta_j\eta_k = -1$ for a (q_-p_+)-term. Then these terms compensate each other after summing them up for the forward scattering which is the dominant kinematical region of this process. This is why the energy scale $s = (p_- + p_+)^2$ does not appear in the soft-photon correction despite the fact that it exists in Eq.(102).

When some experimental cuts are imposed, for example the final e^- is tagged in a large angle, this cancellation is not perfect but partial and the energy scale s must appear in the soft-photon correction. In this case the annihilation type diagrams will also contribute to the matrix elements. Then the usual SF and QEDPS for the annihilation processes are justified to be used for the ISR with the energy scale s. One can check which energy scale is dominant under the given experimental cuts by numerically integrating the soft-photon cross section given by Eq.(102) over the allowed kinematical region. Thus in order to determine the energy scale it is sufficient to know the infrared behavior of the radiative process using the soft-photon factor.

Next we determine the energy-scale of the QED radiative corrections to the single-W production process,

$$e^-(p_-) + e^+(p_+) \quad \to \quad e^-(q_-) + \bar{\nu}_e(q_\nu) + u(k_u) + \bar{d}(k_d). \tag{104}$$

The soft-photon correction factor shown in Eq.(102) is numerically integrated with Born matrix element of the process (104) only with t-channel diagrams without any cut on the final fermions. The results are shown in Table38. One can see that the main contribution comes from an electron charged-line (p_-q_--term) and a positron charged-line ($p_+k_uk_d$-term), while all the other contributions are negligibly small. As the same as the two-photon processes, the energy scale of s does not appear in the soft-photon correction. Applying SF or QEDPS for the electron and positron charged-lines individually with energy scale of their

all terms	p_-q_-	$p_+k_uk_d$	all other combinations
1	0.38	0.61	1.9×10^{-3}

Table 38: Soft-photon correction factor from sets of the charged particle combinations for the process of $e^+e^- \to e^-\bar{\nu}_e u\bar{d}$ at the CM energy of 200 GeV. The factor from all terms is normalized to unity.

momentum-transfer squared might be legitimate according to the above results.

13.22 Structure Function Method

The corrected cross section is given by

$$\begin{aligned}\sigma_{total}(s) \quad = \quad & \int dx_{I-} \int dx_{F-} \int dx_{I+} \int dx_u \int dx_d D_{e^-}(x_{I-}, -t_-) D_{e^-}(x_{F-}, -t_-) \\ & D_{e^+}(x_{I+}, p_{Tud}^2) D_u(x_u, m_{ud}^2) D_d(x_d, m_{ud}^2) \sigma_0(\hat{s}),\end{aligned} \tag{105}$$

using the structure function (D_f) with the energy scale of $t_- = (p_- - q_-)^2$, the transverse-momentum squared of the u-$\bar{d}$ system ($p_{Tud}^2 \approx (p_+ - k_u - k_d)^2$), and $m_{ud}^2 = (k_u + k_d)^2$. The energy-scale determination on the positron side is rather ambiguous. The p_{Tu+d} is distributing around $M_W/3$, then the difference between these two energy scales does not give a significant effect on the correction factor. After(before) the photon radiation the initial(final) momenta $p_\pm$ ($q_\pm$) become $\hat{p}_\pm$ ($\hat{q}_\pm$) in the following ways

$$\hat{p}_- \quad = \quad x_{I-} p_-, \quad \hat{q}_- = \frac{1}{x_{F-}} q_-, \ldots \tag{106}$$

respectively. Then the CM energy squared s is scaled as $\hat{s} = x_{I-} x_{I+} s$.

13.23 Parton Shower Method

Instead of the analytic formula of the structure function, a Monte Calro method based on the parton shower algorithm in QED (`QEDPS`) can be used to solve the Altarelli-Parisi equation in the LL approximation[172]. The detailed algorithm of the `QEDPS` is found in Ref.[174] for the e^+e^- annihilation processes, in Ref.[175] for the Bhabha process, and in Ref.[168] for the two-photon process. The same energy scale as SF method is used in `QEDPS` also. One difference between SF and `QEDPS` is that the *ad hoc* replacement of the perturbative expansion coefficient $L(= \ln(Q^2/m_f^2))$ by $L-1$, which was realized by hand for SF, cannot be done for `QEDPS`. Another significant difference between these two is that `QEDPS` can treat the transverse momentum of emitted photons correctly by imposing the exact kinematics at the $e \to e\gamma$ splitting. It does not affect the total cross sections so much when the final e^- have no cut. However, the finite recoiling of the final $e^\pm$ may result a large effect on the tagged cross sections.

In return to the the exact kinematics at the $e \to e\gamma$ splitting, $e^\pm$ are no more on-shell after photon emission. On the other hand the matrix element of the hard scattering process must be calculated with the on-shell external particles. A trick to map the off-shell four-momenta of the initial $e^\pm$ to those at on-shell is needed. Following method is used in the calculations.

1. $\hat{s} = (\hat{p}_- + \hat{p}_+)^2$ is calculated, where $\hat{p}_\pm$ are the four-momenta of the initial $e^\pm$ after the photon emission by `QEDPS`. $\hat{s}$ is mainly positive even for the off-shell $e^\pm$. (When $\hat{s}$ is negative, that event is discarded.)
2. All four-momenta are generated in the rest-frame of the initial $e^\pm$ after the photon emission. Four-momenta of the hard scattering in their rest-frame are $\tilde{p}_\pm$, where $\tilde{p}_\pm^2 = m_e^2$ (on-shell) and $\hat{s} = (\tilde{p}_- + \tilde{p}_+)^2$
3. All four-momenta are rotated and boosted to match the three-momenta of $\tilde{p}_\pm$ with those of $\hat{p}_\pm$.

This method respects the direction of the final $e^\pm$ rather than the CM energy of the collision. The total energy does not conserve because of the virtuarity of the initial $e^\pm$.

13.3 Numerical Calculations

13.31 Total cross sections

Total and differential cross sections of semi-leptonic process of $e^-e^+ \to e^-\bar{\nu}_e u\bar{d}$ and leptonic one, $e^-e^+ \to e^-\bar{\nu}_e\mu^+\nu_\mu$, are calculated with the radiative correction by SF or `QEDPS`. Fortran code to calculate amplitudes of the above processes are produced using `GRACE` system[176]. All fermion-masses are kept finite in calculations. Numerical integrations of the matrix element squared in the four-body phase space are done using `BASES`[177]. For the study of the radiative correction for the single-W productions, only t-channel diagrams(non-annihilation diagrams) are taken into account.

For the total energy of the emitted photons, both methods must give the same spectrum when the same energy scale are used. That is confirmed as shown in Fig.55 at the CM energy of 200 GeV for the semi-leptonic process.

Total cross sections as a function of the CM energies at LEP2 with and without experimental cuts are shown in Fig.56. The experimental cuts applied here are

1. $M_{q\bar{q}} > 45$GeV,
2. $E_l > 20$GeV.

The effect of the QED radiative corrections on the total cross sections are obtained to be 7 to 10% on LEP2 energies.

If one used wrong energy scale s in SF, the ISR effect is overestimated about 4% as shown in Fig.57 both with and without cuts. For the no-cut case SF with a correct energy scale is consistent with `QEDPS` around 0.2%. It may reflect the difference between L and $L-1$ as mentioned in the previous section. On the other hand with the experimental cuts, SF with correct energy-scale gives around 1% deviation from `QEDPS`.

13.32 Hard photon spectrum

Energy and angular distributions of the hard photon from QEDPS are compared with those from the calculations of the exact matrix elements. The cross sections of the process $e^-e^+ \to e^-\bar{\nu}_e u\bar{d}\gamma$ are calculated based on the exact amplitudes generated by GRACE and integrated numerically in five-body phase space using BASES. To compare the distributions, the soft-photon correction for the radiative process must be included. For this purpose QEDPS is implemented into $e^-\bar{\nu}_e u\bar{d}\gamma$ calculations with a careful treatment to avoid a double-counting of the radiation effect. The definition of the hard photon is

1. $E_\gamma > 1GeV$,
2. opening angle between the photon and the nearest final-state charged particles is greater than 5 degree.

The distributions of the hard photons are in good agreement as shown in Fig.58. The total cross section of the hard photon emission agrees each other with 2% level. On the other hand, if the soft-photon correction is not implemented on the radiative process, it gives 30% overestimation.

14. Conclusions

The method to apply the QED radiative correction on the non-annihilation processes are established. The conventional method, SF with energy scale s gives about 4% overestimation for the QED radiative effect on the LEP2 energies. If one wants to look at the hard photon spectrum, the soft-photon correction on these radiative processes are needed.

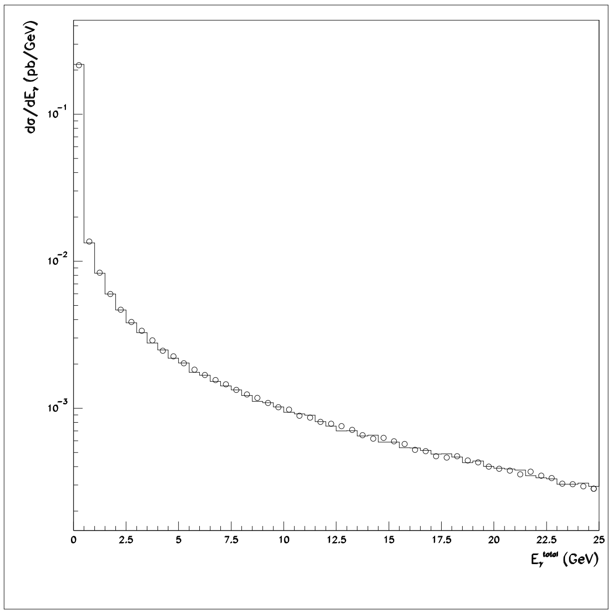

Fig. 55: Differential cross section of the total energy of emitted photon(s) obtained from QEDPS(histogram) and from SF(circle).

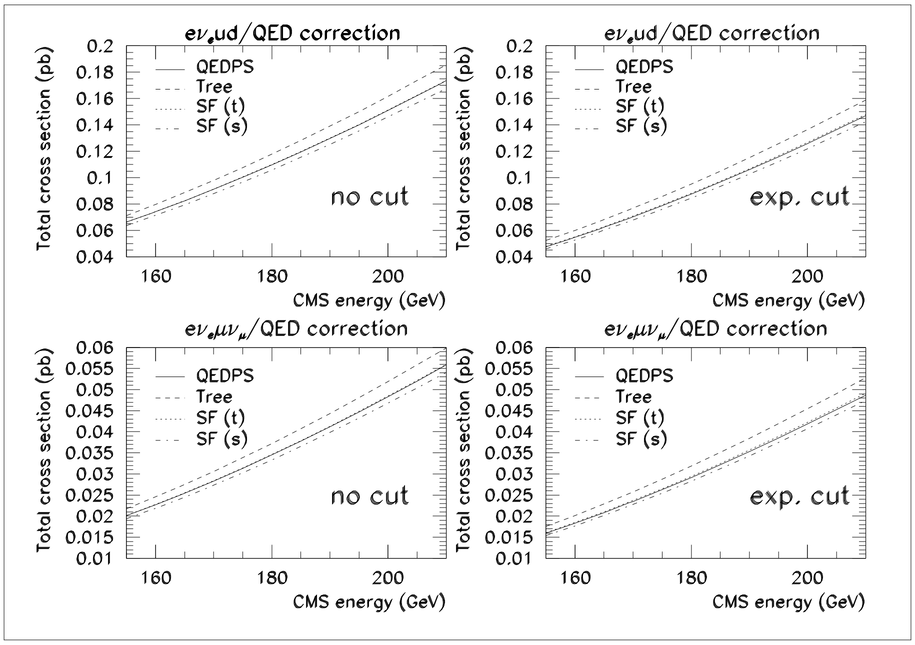

Fig. 56: Total cross sections of $e\nu_e\bar{u}d$ and $e\nu_e\mu\nu_\nu$ processes without and with experimental cuts. SF(t) denotes SF with correct energy scale and SF(s) with wrong energy scale (s).

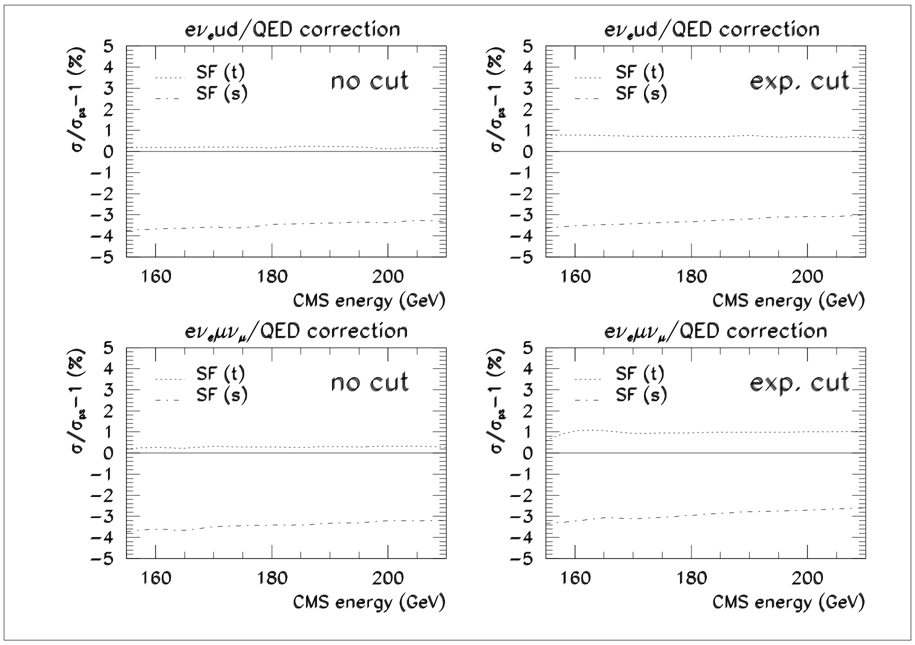

Fig. 57: Total cross sections with SF(s) and SF(t) normalized by those with QEDPS for $e\nu_e\bar{u}d$ and $e\nu_e\mu\nu_\nu$ processes without and with experimental cuts. SF(t) denotes SF with correct energy scale and SF(s) with wrong energy scale (s).

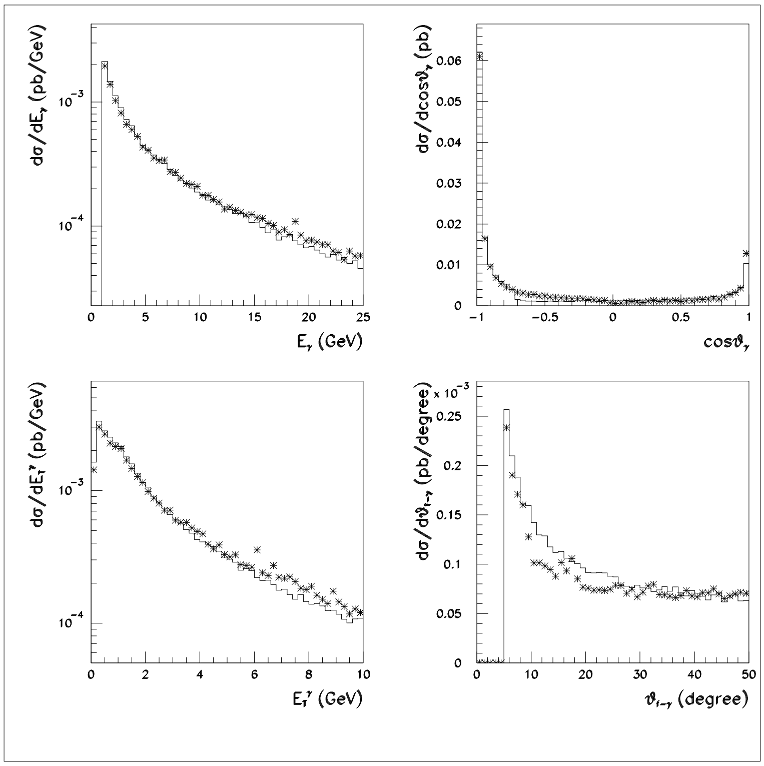

Fig. 58: Differential cross sections of the hard photon; Energy, transverse energy w.r.t. the beam axis, cosine of the polar angle, and opening angle between photon and nearest charged-fermion. A histogram shows the QEDPS result and stars from the matrix element with soft-photon correction.

15. The cross-section σ_{ZZ}.

The cross-section for $e^+e^- \to ZZ$ is defined starting from the NC02 process, very much as $e^+e^- \to W^+W^-$ in terms of CC03, hence we sum over all channels, $e^+e^- \to Z(\to f_1\overline{f}_1)+Z(\to f_2\overline{f}_2)$ including four neutrinos in the final state.

As usual, it is left for the experimenters to evaluate the background, i.e. to define a neutral current cross-section as follows:

$$\sigma_{\rm NC} = \sigma_{\rm NC02}\,\Big(1+\delta^{\rm DPA}_{\rm NC}\Big) + \Big[\sigma_{\rm 4f} - \sigma_{\rm NC02}\Big]. \tag{107}$$

The theoretical prediction, therefore, should concentrate on $\sigma_{\rm NC02}$, with or without $\mathcal{O}\left(\alpha\right)$ radiative correction in DPA-approximation. In particular, the background should account for the Mixed processes (Mix43). There is some important remark to be made. When dealing with $u\bar{u}u\overline{u}$ etc, i.e. with channels containing identical particles, we have to evaluate the unphysical sum of the two diagrams corresponding to $e^+e^- \to Z(\to u_1\overline{u}_1) + Z(\to u_2\overline{u}_2)$, tacitly assuming that there are two u quarks, u of type 1 and u of type 2. The background will take care of all the interferences between the crossings which, however, are not double-resonant. This is a matter of definition, i.e., we could define the ZZ signal to contain all crossings in case of four identical flavors in the final state. That one chooses the first option is largely based on the drawback that, with it,

$$\sigma_{ZZ}\,\times\,{\rm BR}^2(Z->u\overline{u}), \tag{108}$$

is no longer $\sigma_{ZZ\to u\overline{u}u\overline{u}}$. It is certainly true that σ_{ZZ} would be more physical but, for the time being this is the convention.

Bearing this in mind, we should stress that the terminology $\sigma^{\rm NC02}$ is, sometimes, unfaithful, simply because this is not what experiments use in their analysis. A common procedure is to use `EXCALIBUR` and to restrict it to the complete set of double-resonant diagrams. In other words, experiments measure data in some window of invariant mass and extrapolate with some coefficient, evaluated by MC, to what one finally calls the NC02-total cross-section but it represents, instead, the sum of all double-resonant Zdiagrams (for some channel 4 instead of 2).

However, by definition, we select NC02 to be $e^+e^- \to ZZ$, two diagrams (t and u channel), with all Zdecay modes allowed for both Z-bosons. If one computes everything as production $\otimes$ decay then, as long as one remembers to include factors $1/2$, everything is reasonable. The conclusion is based on the following observation. When all diagrams are taken into account we find

$$\begin{aligned}
\sigma(e^+e^- \to \overline{u}u\overline{c}c) &= 208.9\,{\rm fb},\\
\sigma(e^+e^- \to \overline{u}u\overline{s}s) &= 204.4\,{\rm fb},\\
\sigma(e^+e^- \to \overline{d}d\overline{s}s) &= 182.6\,{\rm fb},\\
\sigma(e^+e^- \to \overline{u}u\overline{d}d) &= 1.980\,{\rm pb},\\
\sigma(e^+e^- \to \overline{u}u\overline{u}u) &= 101.4\,{\rm fb},\\
\sigma(e^+e^- \to \overline{d}d\overline{d}d) &= 87.88\,{\rm fb},
\end{aligned} \tag{109}$$

and, as a consequence,

$$R_{uucc/uuuu} = 2.06, \qquad R_{ddss/dddd} = 2.08. \tag{110}$$

In other words, even if we define on-shell and compute off-shell the same result, within few percents, is obtained. Still, one should remember that NC02 is not quite as CC03 where the difference between DPA and full 4f is less than 0.2Eq.(109) we observe that at 189 GeV the $qqqq$ cross-sections with no cut are quite different, NC02 is 324.8 while NC08 is 1718.3 fb and the background is large compared to CC03.

The relative significance of the ZZ cross-section is considerably less than the one attributed to the WW cross-section. Its is smaller and with much larger experimental errors, even at the level of projected ones. As a consequence the NC02 process has received less attention that the CC03 one and, so far, we have no published result on $\mathcal{O}(\alpha)$ DPA calculations for it although, in principle, there is no major obstacle to it.

15.1 YFSZZ

Authors

S. Jadach
W. Placzek
M. Skrzypek
B. Ward
Z. Was

15.11 General Description

The program evaluates the the double resonant process $e^+e^- \to ZZ \to 4f$ in the presence of multiple photon radiation using Monte Carlo event generator techniques. The theoretical formulation is based, in the leading pole approximation (LPA), on $\mathcal{O}(\alpha^2)$ LL YFS exponentiation for the production process, with the possibility of anomalous gauge couplings if the user so desires. The calculation is fully gauge invariant. The Monte Carlo algorithm used to realize the YFS exponentiation is based on the YFS2 algorithm presented in Ref. [152] and in Ref. [153]. In this way, we achieve an event-by-event realization of our calculation in which arbitrary detector cuts are possible and in which infrared singularities are cancelled to all orders in α. A detailed description of our work can be found in Ref. [154].

15.12 Features of the program

The code is a complete Monte Carlo event generator and gives for each event the final particle four-momenta for the entire $4f + n\gamma$ final state over the entire phase space for each final state particle. The events may be weighted or unweighted, as it is more or less convenient for the user accordingly. The code features the realization of the LPA for the NC02 process that is the analog of that given in Ref. [155] for the CC03 process of production and decay of WW pairs. A technical precision check on the program at the level of 2 per mille for the total cross section has been done by comparison with the results in Ref. [156]. The accuracy of the combined result from YFSZZ 1.02 and KoralW 1.42, when the combination is taken in analogy with that presented in Ref. [157] for YFSWW3 1.13 and KoralW 1.42, is expected to be at the level of 2% for the total cross section, due to the missing $O(\alpha)$ pure weak corrections in YFSZZ 1.02, when all tests are finished. These tests are currently in progress.

15.13 How does the code work

The operation of the code is entirely analogous to that of the MC YFS2 in Refs. [152]. A crude distribution based on the primitive Born level distribution and the most dominant part of the YFS form factors that can be treated analytically is used to generate a background population of events. The weight for these events is then computed by standard rejection techniques involving the ratio of the complete distribution and the crude distribution. As the user wishes, these weights may be either used directly with the events, which have the four-momenta of all final state particles available, or they may be accepted/rejected against a maximal weight WTMAX to produce unweighted events via again standard MC methods. Standard final statistics of the run are provided, such as statistical error analysis, total cross sections, etc. The total phase space for the process is always active in the code.

15.14 Description of output

The program prints certain control outputs. The most important output of the program is the series of Monte Carlo events. The total cross section in fb is available for arbitrary cuts in the same standard way as it is for YFS2, i.e. the user may impose arbitrary detector cuts by the usual rejection methods.

Availability

The program is available from the authors via e-mail. The program is currently posted on `WWW` at `http://enigma.phys.utk.edu` as well as on `anonymous ftp` at `enigma.phys.utk.edu` in the form of a `tar.gz` file in the `/pub/YFSZZ/` directory together with all relevant papers and documentation in postscript.

15.2 `ZZTO`

Authors

G. Passarino

15.21 Description.

`ZZTO` is a newly created code for computing σ_{ZZ} which, at the moment, has has universal Initial State QED, Final State QED, Final State QCD, is fully massive with b and c quarks running masses. Fermion-Loop is also implemented.

`ZZTO` is missing non-universal QED ISR and purely weak effects (in DPA); however, it is under construction with the final goal of including those effects.

The code sums over all ZZ decay modes, even $\nu\nu\nu\nu$. However, single channels are available, i.e. $qqqq$, $qq\nu\nu$, qqll, ll$\nu\nu$, llll, $\nu\nu\nu\nu$.

15.3 Comparison between `YFSZZ` and `ZZTO`

In this Section we will compare the NC02 cross-section between `YFSZZ` and the newly created code `ZZTO`. Inside `ZZTO` we have the exact matrix element for $e^+e^- \to ZZ \to 4$f with massive fermions and running masses for the b, c-quarks. The cross-section is without cuts, therefore we can apply final state QCD correction factors beyond the usual *naive* correction. In other words, the total hadronic decay rate of each Z-boson is split into the sum of the vector current induced rate, Γ^V, and of the axial decay rate, Γ^A, which receive different QCD corrections evaluated at the scale equal to the virtuality of the $q\overline{q}$-pair. Non-factorizable QCD corrections are neglected. Final state QED corrections are also included, again evaluated at the virtuality of the pair, i.e. with $\alpha(M^2_{\rm pair})$. Initial state QED corrections include, so far, only the universal part of the structure functions evaluated at the scale s.

We now come to the comparison with `YFSZZ`. Here, $\sqrt{s} = 188.6\,GeV$ and QCD is not included. The result is shown in Tab.(39). From Tab.(39) we see a remarkable agreement, further quantified in Tab.(40). Furthermore, for σ_{ZZ} with Born+ISR+QCD the uncertainty related to the IPS (Input Parameter Set) is approximately 1%. This doesn't mean, yet, that the total, true, theoretical uncertainty is 1%. The ZZ line-shape, as predicted by `ZZTO` and including QCD corrections is shown in Tab.(42) where the results refer to the α-scheme. Finally, in Fig. 59 we present the NC02 line-shape for a wide range of energy, comparing the α-scheme with the G_F-scheme. Our recommendation is to use the G_F-scheme since it allows us to include part of higher order effects in the Born cross-sections.

It looks plausible to have a $\pm 2\%$ of theoretical uncertainty assigned to the NC02 cross section, although this value could be underestimating the real error; there are partial indications, coming from a Fermion-Loop analysis, that show larger deviations and the Fermion-Loop is usually accurate at the 1% level.

channel	YFSZZ	ZZTO G_F-scheme	ZZTO α-scheme
$qqqq$	294.6794(490)	298.4411(60)	294.5715(59)
$qq\nu\nu$	175.4404(302)	175.5622(35)	174.9855(35)
qqll	88.1805(134)	88.7146(18)	87.9881(18)
ll$\nu\nu$	26.2530(463)	26.0940(5)	26.1342(5)
llll	6.5983(15)	6.5929(1)	6.5706(1)
$\nu\nu\nu\nu$	26.1080(71)	25.8192(5)	25.9868(5)
total	617.2596(755)	621.2241(124)	616.2366(123)

Table 39: Comparison for the NC02 cross-section between YFSZZ and ZZTO at $\sqrt{s} = 188.6$ GeV. The cross sections are in fb.

channel	ZZTO(G_F)/YFSZZ - 1	ZZTO(α)/YFSZZ - 1
$qqqq$	+1.28	-0.04
$qq\nu\nu$	+0.07	-0.26
qqll	+0.61	-0.22
ll$\nu\nu$	-0.61	-0.45
llll	-0.08	-0.42
$\nu\nu\nu\nu$	-1.11	-0.46
total	+0.64	-0.17

Table 40: Differences YFSZZ/ZZTO for the NC02 cross-section in percent.

channel	ZZTO $G_F/\alpha - 1$
$qqqq$	+1.31
$qq\nu\nu$	+0.33
qqll	+0.83
ll$\nu\nu$	-0.15
llll	+0.34
$\nu\nu\nu\nu$	-0.64
total	+0.81

Table 41: Scheme differences in percent according to ZZTO.

$\sqrt{s}$ [GeV]	σ_{α}^{ZZ} [pb] with QCD	$\sigma_{G_F}^{ZZ}$ [pb] with QCD
180	0.12465(1)	0.12568(1)
181	0.16027(2)	0.16160(2)
182	0.21113(2)	0.21287(2)
183	0.27741(2)	0.27970(2)
184	0.35187(1)	0.35477(1)
185	0.42599(1)	0.42950(1)
186	0.49527(1)	0.49936(1)
187	0.55838(1)	0.56299(1)
188	0.61531(1)	0.62039(1)
189	0.66652(1)	0.67203(1)
190	0.71260(1)	0.71848(1)
191	0.75407(1)	0.76030(1)
192	0.79141(1)	0.79794(1)
193	0.82509(1)	0.83190(1)
194	0.85552(2)	0.86258(2)
195	0.88300(2)	0.89028(2)
196	0.90779(1)	0.91528(1)
197	0.93020(1)	0.93787(1)
198	0.95046(1)	0.95830(1)
199	0.96877(1)	0.97677(1)
200	0.98530(2)	0.99343(2)
201	1.00017(2)	1.00843(2)
202	1.01353(2)	1.02189(2)
203	1.02551(1)	1.03397(1)
204	1.03626(1)	1.04481(1)
205	1.04589(1)	1.05452(1)
206	1.05450(1)	1.06320(1)
207	1.06214(1)	1.07090(1)
208	1.06888(1)	1.07770(1)
209	1.07480(2)	1.08367(2)
210	1.07996(2)	1.08888(2)

Table 42: ZZ line-shape from `ZZTO`.

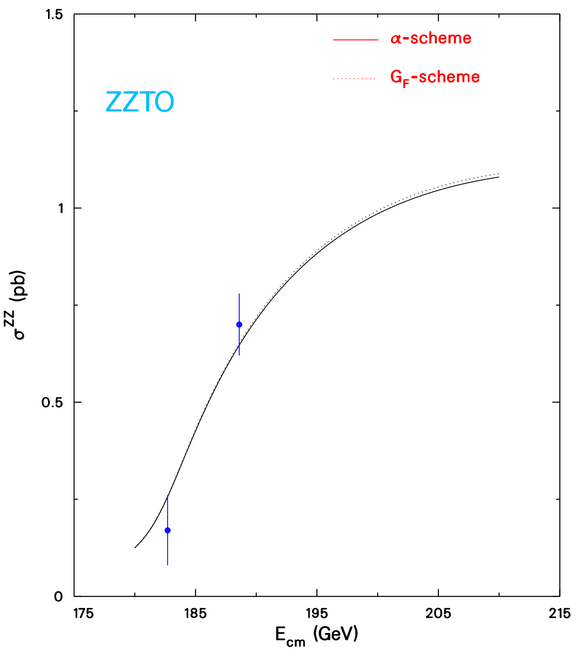

Fig. 59: ZZ line-shape from ZZTO

References

[1] M. Steinhauser, Phys. Lett. B429 (1998) 158.

[2] S. Eidelman and F. Jegerlehner, Z. Phys. C67 (1995) 585.

[3] B. Kniehl, Nucl. Phys. B347 (1990) 86.

[4] D. Bardin et al., Report on *Event Generators for WW Physics* in Vol.1, *Report of the Workshop in Physics at LEP2*, Altarelli, G. et al., eds., 1996, CERN-96-01.

[5] J. Fujimoto et al., *Nucl. Phys. (Proc. Suppl.)* **37B** (94) 169;
F. Caravaglios and M. Moretti, *Z. Phys.* **C74** (97) 291;
F. Jegerlehner and K. Kolodziej, hep-ph/9907229.

[6] A. Denner, S. Dittmaier, M. Roth and D. Wackeroth, *Nucl. Phys.* **B560** (99) 33.

[7] PVALPHA reference for $\mathrm{e}^+\mathrm{e}^- \to 4f\gamma$ complete

[8] A. Aeppli, G.J. van Oldenborgh and D. Wyler, *Nucl. Phys.* **B428** (94) 126.

[9] M. Böhm et al., *Nucl. Phys.* **B304** (88) 463.

[10] J. Fleischer, F. Jegerlehner and M. Zrałek, *Z. Phys.* **C42** (89) 409.

[11] D.Yu. Bardin, S. Riemann and T. Riemann, *Z. Phys.* **C32** (86) 121;
F. Jegerlehner, *Z. Phys.* **C32** (86) 425.

[12] A. Denner and T. Sack, *Z. Phys.* **C46** (90) 653.

[13] F. Berends and R. Kleiss, *Z. Phys.* **C27** (85) 365.

[14] W. Beenakker, K. Kołodziej and T. Sack, *Phys. Lett.* **B258** (91) 469;
W. Beenakker, F.A. Berends and T. Sack, *Nucl. Phys.* **B367** (91) 287;
K. Kołodziej and M. Zrałek, *Phys. Rev.* **D43** (91) 3619;
J. Fleischer, F. Jegerlehner and K. Kołodziej, *Phys. Rev.* **D47** (93) 830.

[15] K. Melnikov and O. Yakovlev, *Nucl. Phys.* **B471** (1996) 90.

[16] W. Beenakker, F.A. Berends and A.P. Chapovsky, *Phys. Lett.* **B411** (97) 203 and *Nucl. Phys.* **B508** (97) 17.

[17] A. Denner, S. Dittmaier and M. Roth, *Nucl. Phys.* **B519** (98) 39 and *Phys. Lett.* **B429** (98) 145.

[18] A. Denner, S. Dittmaier, M. Roth and D. Wackeroth, BI-TP 2000/06, in preparation.

[19] V.S. Fadin, V.A. Khoze and A.D. Martin, *Phys. Rev.* **D49** (94) 2247;
K. Melnikov and O. Yakovlev, *Phys. Lett.* **B324** (94) 217.

[20] A.P. Chapovsky and V.A. Khoze, *Eur. Phys. J.* **C9** (1999) 449.

[21] Y. Kurihara, M. Kuroda and D. Schildknecht, hep-ph/9908486.

[22] W. Beenakker, F.A. Berends and A.P. Chapovsky, *Nucl. Phys.* **B548** (99) 3.

[23] S. Jadach et al., *Phys. Lett.* **B417** (98) 326.

[24] S. Jadach et al., hep-ph/9907436.

[25] A. Denner, S. Dittmaier, M. Roth and D. Wackeroth, hep-ph/9912261; hep-ph/9912447.

[26] W. Beenakker and A. Denner, *Int. J. Mod. Phys.* **A9** (94) 4837.

[27] E.N. Argyres *et al.*, *Phys. Lett.* **B358** (1995) 339.

[28] R.G. Stuart, *Phys. Lett.* **B262** (1991) 113;
A. Aeppli, G.J. van Oldenborgh and D. Wyler, *Nucl. Phys.* **B428** (1994) 126.

[29] W. Beenakker, F.A. Berends and A.P. Chapovsky, *Nucl. Phys.* **B548** (1999) 3.

[30] U. Baur and D. Zeppenfeld, *Phys. Rev. Lett.* **75** (1995) 1002.

[31] W. Beenakker *et al.*, *Nucl. Phys.* **B500** (1997) 255.

[32] M. Beuthe, R. Gonzalez Felipe, G. Lopez Castro and J. Pestieau, *Nucl. Phys.* **B498** (1997) 55;
G. Passarino, *hep–ph/*9911482;
E. Accomando, A. Ballestrero, E. Maina, *hep–ph/*9911489.

[33] W. Beenakker, F.A. Berends and A.P. Chapovsky, *hep–ph/*9909472.

[34] A. Kanaki and C.G. Papadopoulos, *hep–ph/*0002082.

[35] K. Melnikov and O. Yakovlev, *Phys. Lett.* **B324** (1994) 217;
V.S. Fadin, V.A. Khoze and A.D. Martin, *Phys. Rev.* **D49** (1994) 2247.

[36] A. Denner, S. Dittmaier, M. Roth and D. Wackeroth, *hep–ph/*9904472.

[37] M. Böhm *et al.*, *Nucl. Phys.* **B304** (1988) 463;
W. Beenakker, K. Kołodziej and T. Sack, *Phys. Lett.* **B258** (1991) 469.

[38] A. Denner and T. Sack, *Z. Phys.* **C46** (1990) 653 and papers quoted therein.

[39] A. Denner, S. Dittmaier and M. Roth, *Nucl. Phys.* **B519** (1998) 39 and *Phys. Lett.* **B429** (1998) 145.

[40] W. Beenakker, A.P. Chapovsky and F.A. Berends, *Phys. Lett.* **B411** (1997) 203 and *Nucl. Phys.* **B508** (1997) 17.

[41] V.S. Fadin and V.A. Khoze, *Sov. J. Nucl. Phys.* **48** (1988) 309;
V.S. Fadin, V.A. Khoze and A.D. Martin, *Phys. Lett.* **B311** (1993) 311;
D. Bardin, W. Beenakker and A. Denner, *Phys. Lett.* **B317** (1993) 213;
V.S. Fadin et al., *Phys. Rev.* **D52** (1995) 1377.

[42] W. Beenakker, F.A. Berends and A.P. Chapovsky, *Phys. Lett.* **B435** (1998) 233.

[43] S. Jadach et al., *hep–ph/*9907436.

[44] G. Passarino, Unstable particles and non-conserved currents: a generalization of the fermion-loop scheme, hep-ph/9911482.

[45] A. Denner, S. Dittmaier, M. Roth and D. Wackeroth, in preparation.

[46] M. Böhm et al., *Nucl. Phys.* **B304** (1988) 463;
A. Denner and T. Sack, *Z. Phys.* **C46** (1990) 653.

[47] A. Denner, S. Dittmaier and M. Roth, *Nucl. Phys.* **B519** (1998) 39.

[48] A. Denner, S. Dittmaier, M. Roth and D. Wackeroth, *Nucl. Phys.* **B560** (1999) 33.

[49] W. Beenakker et al., in *Physics at LEP2*, eds. G. Altarelli, T. Sjöstrand and F. Zwirner (Report CERN 96-01, Geneva, 1996), p. 79, hep-ph/9602351.

[50] S. Dittmaier, *Nucl. Phys.* **B565** (2000) 69;
M. Roth, dissertation ETH Zürich No. 13363, 1999.

[51] M. Böhm, A. Denner and S. Dittmaier, *Nucl. Phys.* **B376** (1992) 29; E: **B391** (1993) 483.

[52] F.A. Berends, R. Pittau and R. Kleiss, *Nucl. Phys.* **B424** (1994) 308;
F.A. Berends, P.H. Daverveldt and R. Kleiss, *Nucl. Phys.* **B253** (1985) 441 and *Comput. Phys. Commun.* **40** (1986) 285;
J. Hilgart, R. Kleiss and F. Le Diberder, *Comput. Phys. Commun.* **75** (1993) 191.

[53] R. Kleiss and R. Pittau, *Comput. Phys. Commun.* **83** (1994) 141.

[54] G. Passarino, The Single W Production Case, hep-ph/9810416.

[55] E.E. Boos and M.N. Dubinin, Single W-boson production at Linear Colliders, hep-ph/9909214.

[56] D. Bardin et al. Report on *Event Generators for WW Physics* in Vol.1, 'Report of the Workshop in Physics at LEP2', G. Altarelli et. al., CERN-96-01.

[57] Y. Kurihara, D. Perret-Gallix and Y. Shimizu, Phys. Lett. B349(1995) 367.

[58] U. Baur and D. Zeppenfeld, Phys. Rev. Lett. 75(1995)1002.

[59] G. Passarino, Unstable Particles and Non-Conserved Currents: A Generalization of the Fermion-Loop Scheme, hep-ph/9911482, to appear in Nuclear Physics B.

[60] J. Hoogland and G. J. van Oldenborgh, Phys. Lett. B402(1197)379.

[61] G. Passarino, Comp. Phys. Comm. 97(1996)261.

[62] F. Berends, R. Kleiss and R. Pittau, Comp. Phys. Comm. 85(1995)437;
F. Caravaglios and M. Moretti, Phys. Lett. B308(1995)332;
G. Passarino, Comp. Phys. Comm. 97(1996)261;
J. Fujimoto et al., Comp. Phys. Comm. 100(1997)128;
D. G. Charlton et al., Comp. Phys. Comm. 99(1997)335;
E. Accomando and A. Ballestrero, Comp. Phys. Comm. 99(1997)270;
A. Pukhov et al, INP-MSU-98-41-542, hep-ph/9908288;
E. Boos et al., in Dubna 1990, Standard model and beyond 265-269;
S. Jadach et al., Comp. Phys. Comm. 119(1999)272.

[63] E. Accomando, A. Ballestrero and E. Maina, hep-ph/9911489.

[64] D. Bardin and G. Passarino, The Standard Model in the Making, Clarendon Press - Oxford, 1999.

[65] G. Passarino and M. Veltman, Nucl. Phys. B160(1979)151.

[66] C. Caso et al., Euro. Phys. Jour. C3(1998)1.

[67] D. Bardin, W. Hollik and G. Passarino (eds.), *Reports of the working group on precision calculations for the Z resonance* (CERN 95-03, Genève, 1995).

[68] W. Beenakker et al., in *Physics at LEP2*, eds. G. Altarelli, T. Sjöstrand and F. Zwirner, (CERN 96-01, Genève, 1996) Vol. 1, p. 79, hep-ph/9602351.

[69] P.M. Zerwas (ed.), *e^+e^- collisions at 500 GeV: The physics potential* (DESY 93-123C, Hamburg, 1993);
W. Beenakker and A. Denner, Int. J. Mod. Phys. A9 (1994) 4837.

[70] F. Caravaglios and M. Moretti, Phys. Lett. B358 (1995) 332.

[71] K. Gaemers and G. Gounaris, Z. Phys. C1 (1979) 259.

[72] K. Hagiwara, K. Hikasa, R.D. Peccei and D. Zeppenfeld, Nucl. Phys. B282 (1987) 253.

[73] E. Accomando, A. Ballestrero and E. Maina, Non-conserved currents and gauge-restoring schemes in single-W production, hep-ph/9911489

[74] E.A. Kuraev and V. Fadin, Sov. J. Nucl. Phys. 41 (1985) 466;
G. Altarelli and G. Martinelli, in *Physics at LEP*, J. Ellis and R. Peccei eds., CERN 86-02, Geneva, 1986), Vol. 1 p. 47;
O. Nicrosini and L. Trentadue, Phys. Lett. B196 (1987) 551, Z. Phys. C39 (1998) 479; F.A. Berends, G. Burgers and W.L. van Neerven, Nucl. Phys. B297 (1988) 429;
S. Jadach and M. Skrzypek, Z. Phys. C49 (1991) 577; M. Skrzypek, Acta Phys. Pol. B23 (1992) 135;
M. Cacciari, A. Deandrea, G. Montagna and O. Nicrosini, Europhys. Lett. 17 (1992) 123.

[75] A. Pallavicini, On photon radiation in single-W process, talk given at CERN meeting on 12/10/99;
G. Montagna, M. Moretti, O. Nicrosini, A. Pallavicini, F. Piccinini, paper in preparation.

[76] S. Eidelman and F. Jegerlehner, Z. Phys. C67 (1995) 585.

[77] F. A. Berends, R. Pittau and R. Kleiss, Comput. Phys. Commun. **85**, 437 (1995).

[78] A. Denner, S. Dittmaier, M. Roth and D. Wackeroth, Nucl. Phys. **B560**, 33 (1999).

[79] E. Accomando, A. Ballestrero and E. Maina, hep-ph/9911489.

[80] A. Kanaki and C .G. Papadopoulos, hep-ph/0002082.

[81] G. Passarino, hep-ph/0001212 and hep-ph/9911482.

[82] W. Beenakker et al., Nucl. Phys. **B500**, 255 (1997).

[83] E. Argyres et al., Phys. Lett. **B358**, 339 (1995).

[84] R. Pittau, in preparation.

[85] E. A. Kuraev and V. S. Fadin, Yad. Fiz. **41**, 753 (1985) [Sov. J. Nucl. Phys. **41**, 466 (1985)];
G. Altarelli and G. Martinelli, in Physics al LEP, CERN-Yellow Report 86-06, eds. J. Ellis and R. Peccei (CERN, Geneva, February 1986);
O. Nicrosini and L. Trentadue, Phys. Lett. **B196**, 551 (1987);
F. A. Berends, G. Burgers and W. L. van Neerven, Nucl. Phys. **B297**, 429 (1988) and **B304**, 921E (1988).

[86] W. Beenakker, F. A. Berends, S. C. van der Marck, Nucl. Phys. **B349**, 323 (1991).

[87] G. Montagna, M. Moretti, O. Nicrosini and F. Piccinini, Nucl. Phys. **B541**, 31 (1999);
O. Nicrosini and L. Trentadue, Nucl. Phys. **B318**, 1 (1989) and Phys. Lett. **B231**, 487 (1989).

[88] F. A. Berends and R. Kleiss, Nucl. Phys. **B260**, 32 (1985) and **B178**, 141 (1981).

[89] W. Beenakker, F. A. Berends, S. C. van der Marck, Nucl. Phys. **B355**, 381 (1991).

[90] Y. Kurihara, J. Fujimoto, Y. Shimizu, K. Kato, K. Tobimatsu and T. Munehisa, hep-ph/9912520.

[91] F. A. Berends, P. H. Daverveldt and R. Kleiss, Nucl. Phys. **B253**, 412 (1985).

[92] G. Montagna, M. Moretti, O. Nicrosini, A. Pallavicini and F. Piccinini, paper in preparation and in *On photon radiation in single-W process*, talk at the LEP2 Monte Carlo Workshop [141], Oct. 12 1999.

[93] F. A. Berends, R. Pittau and R. Kleiss, Nucl. Phys. **B424**, 308 (1994).

[94] M. L. Mangano et al., in Physics at LEP2, CERN 96-01 (1996), eds. G. Altarelli, T. Sjöstrand and F. Zwirner, Vol 2, p. 299.

[95] D. Bardin et al., in Physics at LEP2, CERN 96-01 (1996), eds. G. Altarelli, T. Sjöstrand and F. Zwirner, Vol 2, p. 3.

[96] E. Accomando and A. Ballestrero, Comput. Phys. Commun. **99**, 270 (1997).

[97] `http://www.to.infn.it/~giampier/lep2.html`.

[98] U. Baur and D. Zeppenfeld, Phys. Rev. Lett. **75** (1995) 1002.

[99] J. Hoogland and G. J. van Oldenborgh, Phys. Lett. **B402** (1997) 379.

[100] E. Accomando, A. Ballestrero and E. Maina, hep-ph/9911489.

[101] G. Passarino, hep-ph/9911482.

[102] G. Passarino, hep-ph/0001212.

[103] W. Beenakker, F.A. Berends and A.P. Chapovsky, hep-ph/9909472.

[104] A. Denner, S. Dittmaier, M. Roth and D. Wackeroth, BI-TP 99/10, PSI–PR–99–12, hep-ph/9904472.

[105] E. Accomando and A. Ballestrero, Comp. Phys. Comm. **99** (1997) 270.

[106] J. Fleischer, F. Jegerlehner and M. Zrałek, *Z. Phys.* **C42** (1989) 409;
K. Kołodziej and M. Zrałek, *Phys. Rev.* **D43** (1991) 3619;
J. Fleischer, F. Jegerlehner and K. Kołodziej, *Phys. Rev.* **D47** (1993) 830.

[107] W. Beenakker, F.A. Berends and T. Sack, *Nucl. Phys.* **B367** (1991) 287.

[108] K. Melnikov and O. Yakovlev, *Nucl. Phys.* **B471** (96) 90.

[109] A. Denner, S. Dittmaier, M. Roth and D. Wackeroth, hep-ph/9912261; hep-ph/9912447.

[110] M. Böhm et al., *Nucl. Phys.* **B304** (88) 463;
A. Denner and T. Sack, *Z. Phys.* **C46** (90) 653.

[111] G. Belanger, F. Boudjema, Y. Kurihara, D. Perret-Gallix and A. Semenov, Bosonic quartic couplings at LEP2, hep-ph/9908254 and references therein.

[112] A. Denner, S. Dittmaier, M. Roth, D. Wackeroth, Nucl. Phys. B560 (1999) 33.

[113] G. Montagna, O. Nicrosini, F. Piccinini, Comput. Phys. Commun. 98 (1996) 206.

[114] G. Montagna, M. Moretti, O. Nicrosini, F. Piccinini, Nucl. Phys. B541 (1999) 31.

[115] M. Osmo, Four fermions plus gamma at LEP2, talk given at CERN meeting on 25/06/99;
G. Montagna, M. Moretti, O. Nicrosini, M. Osmo, F. Piccinini, paper in preparation.

[116] G. Passarino, Single-W production and Fermion-Loop scheme: numerical results, hep-ph/0001212.

[117] D.R. Yennie, S.C. Frautschi and H. Suura, *Ann. Phys.* **13** (1961) 379.

[118] E. Boos, M. Dubinin, V. Ilyin, A. Pukhov, V. Savrin, preprint INP MSU 94-36/358, 1994 (hep-ph/9503280);
P.Baikov et.al, in: *Proc.of X Workshop on High Energy Physics and Quantum Field Theory*, ed.by B.Levtchenko, V.Savrin, Moscow, 1996, p.101;
A. Pukhov et.al., hep-ph/9908288;
see also `http://theory.npi.msu.su/~comphep`.

[119] T. Sjoestrand, Comput.Phys.Commun., 82 (1994) 74

[120] F. A. Berends, R. Pittau and R. Kleiss, Comput. Phys. Commun. **85**, 437 (1995) and Nucl. Phys. **B424**, 308 (1994).

[121] A. Denner, S. Dittmaier, M. Roth and D. Wackeroth, Nucl. Phys. **B560**, 33 (1999).

[122] E. Accomando, A. Ballestrero and E. Maina, hep-ph/9911489.

[123] A. Kanaki and C .G. Papadopoulos, hep-ph/0002082.

[124] G. Passarino, hep-ph/0001212 and hep-ph/9911482.

[125] W. Beenakker et al., Nucl. Phys. **B500**, 255 (1997).

[126] E. Argyres et al., Phys. Lett. **B358**, 339 (1995).

[127] R. Pittau, in preparation.

[128] E. A. Kuraev and V. S. Fadin, Yad. Fiz. **41**, 753 (1985) [Sov. J. Nucl. Phys. **41**, 466 (1985)];
G. Altarelli and G. Martinelli, in Physics al LEP, CERN-Yellow Report 86-06, eds. J. Ellis and R. Peccei (CERN, Geneva, February 1986);
O. Nicrosini and L. Trentadue, Phys. Lett. **B196**, 551 (1987);
F. A. Berends, G. Burgers and W. L. van Neerven, Nucl. Phys. **B297**, 429 (1988) and **B304**, 921E (1988).

[129] See, for example, F. A. Berends, R. Pittau and R. Kleiss, Nucl. Phys. **B426**, 344 (1994).

[130] W. Beenakker, F. A. Berends, S. C. van der Marck, Nucl. Phys. **B349**, 323 (1991).

[131] G. Montagna, M. Moretti, O. Nicrosini and F. Piccinini, Nucl. Phys. **B541**, 31 (1999);
O. Nicrosini and L. Trentadue, Nucl. Phys. **B318**, 1 (1989) and Phys. Lett. **B231**, 487 (1989).

[132] F. A. Berends and R. Kleiss, Nucl. Phys. **B260**, 32 (1985) and **B178**, 141 (1981).

[133] W. Beenakker, F. A. Berends, S. C. van der Marck, Nucl. Phys. **B355**, 381 (1991).

[134] Y. Kurihara, J. Fujimoto, Y. Shimizu, K. Kato, K. Tobimatsu and T. Munehisa, hep-ph/9912520.

[135] F. A. Berends, P. H. Daverveldt and R. Kleiss, Nucl. Phys. **B253**, 421 (1985).

[136] G. Montagna, M. Moretti, O. Nicrosini, A. Pallavicini and F. Piccinini, paper in preparation and in *On photon radiation in single-W process*, talk at the LEP2 Monte Carlo Workshop [141], Oct. 12 1999.

[137] F. A. Berends, P. H. Daverveldt and R. Kleiss, Phys. Lett. **B148**, 489 (1984) and Nucl. Phys. **B253**, 441 (1985).

[138] M. L. Mangano et al., in Physics at LEP2, CERN 96-01 (1996), eds. G. Altarelli, T. Sjöstrand and F. Zwirner, Vol 2, p. 299.

[139] D. Bardin et al., in Physics at LEP2, CERN 96-01 (1996), eds. G. Altarelli, T. Sjöstrand and F. Zwirner, Vol 2, p. 3.

[140] E. Accomando and A. Ballestrero, Comput. Phys. Commun. **99**, 270 (1997).

[141] `http://www.to.infn.it/~giampier/lep2.html`.

[142] J. Fleischer, F. Jegerlehner and M. Zrałek, Z. Phys. **C42** (1989) 409;
M. Zrałek and K. Kołodziej, Phys. Rev. **D43** (1991) 43;
J. Fleischer, K. Kołodziej and F. Jegerlehner, Phys. Rev. **D47** (1993) 830;
J. Fleischer *et al.*, Comput. Phys. Commun. **85** (1995) 29 and references therein.

[143] E. Barberio and Z. Wąs, Comput. Phys. Commun. **79** (1994) 291 and references therein.

[144] S. Jadach and B.F.L. Ward, Phys. Lett. B**274** (1992) 470.

[145] S. Jadach, B.F.L. Ward and Z. Wąs, Comp. Phys. Commun. **79** (1994) 503; *ibid.* (2000), in press.

[146] S. Jadach, B.F.L. Ward and Z. Wąs, preprint UTHEP-99-0901, Sept., 1999, to appear.

[147] S. Jadach, W. Płaczek, M. Skrzypek, B.F.L. Ward and Z. Wąs, Phys. Lett. **B417** (1998) 326.

[148] S. Jadach, W. Płaczek, M. Skrzypek, B.F.L. Ward and Z. Wąs, CERN-TH-99-222, UTHEP-98-0502, Phys. Rev. D, 2000, in press.

[149] S. Jadach, W. Płaczek, M. Skrzypek, B.F.L. Ward and Z. Wąs, preprint UTHEP-00-0101, Jan., 2000, to appear.

[150] S. Jadach, W. Płaczek, M. Skrzypek, B.F.L. Ward and Z. Wąs, Comp. Phys. Commun. **119** (1999) 272.

[151] S. Jadach and B.F.L. Ward, Comput. Phys. Commun. **56** (1990) 351.

[152] S. Jadach and B.F.L. Ward, Comput. Phys. Commun. **56** (1990) 351.

[153] S. Jadach, B.F.L. Ward and Z. Wąs, Comput. Phys. Commun. **66** (1991) 276.

[154] S. Jadach, W. Płaczek and B.F.L. Ward, Phys. Rev. **D56** (1997) 6939.

[155] S. Jadach, W. Płaczek M. Skrzypek, B.F.L. Ward and Z. Wąs, Phys. Lett. B**417** (1998) 326.

[156] D. Bardin *et al.*, Nucl. Phys. B**477** (1996) 27.

[157] S. Jadach, W. Płaczek, M. Skrzypek, B.F.L. Ward and Z. Wąs, preprint UTHEP-00-0101, to appear.

[158] W. Beenakker and F.A. Berends, in Physics at LEP2, ed. G. Altarelli et al. (CERN 96-01, Geneva 1996), Vol. I, p. 79, hep-ph/9602351.

[159] S. Dittmaier, hep-ph/9811434.

[160] A. Denner, S. Dittmaier, M. Roth, D. Wackeroth, hep-ph/9904472.

[161] W. Beenakker, F.A. Berends and A.P. Chapovski, DTP/98/90, hep-ph/9811481.

[162] Y.Kurihara, K.Kuroda and D. Schildknecht, in preparation.

[163] T. Ishikawa, T. Kaneko, K. Kato, S. Kawabata, Y. Shimizu, H. Tanaka. `GRACE` manual, KEK report 92-19, 1993.

[164] Y.Kurihara, K.Kuroda and D. Schildknecht, BI-TP 99/30, hep-ph/9908486 v2.

[165] A.Denner, S.Dittmaier, M.Roth and D. Wackeroth, BI-TP 99/45, hep-ph/9912261.

[166] E.A. Kuraev, V.S. Fadin, Sov. J. Nucl. Phys. **41** (1985) 466,
G. Altarelli, G. Martinelli, in *"Physics at LEP"* J. Ellis, R. Peccei eds. CERN 86-02 (CERN, Geneva, 1986),
O. Nicrosini, L. Trentadue, Phys. Lett. **B196** (1987) 551; Z. Phys. **C39** (1988) 479,
F.A. Berends, G. Burgers, W.L. van Neerven, Nucl. Physc **B297** (1988) 429.

[167] G. Marchesini, B.R. Webber, Nucl. Phys. **B238** (1984) 1,
R. Odorico, Nucl. Phys. **B172** (1980) 157,
T. Sjöstrand, Comput. Phys. Commun. **79** (1994) 503.

[168] Y. Kurihara, J. Fujimoto, Y. Shimizu, K. Kato, K. Tobimatsu, T. Munehisa, hep-ph/9912520.

[169] F. Bloch, A. Nordsieck, Phys. Rev. **37** (1937) 54,
D. R. Yennie, S. C. Frautschi, H. Suura, Ann. Phys. **13** (1961) 379.
See also S. Weinberg, "The Quantum Theory of Fields" (Cambridge University Press, New York, 1995), Section 13.

[170] F.A. Berends, P.H. Daverveldt, R. Kleiss, Nucl. Phys. **B253** (1985) 412.

[171] W.L. van Neerven, J.A.M Vermaseren, Nucl. Phys. **B238** (1984) 73,
W.L. van Neerven, J.A.M Vermaseren, Phys. Lett. **B137** (1984) 241,
W.L. van Neerven, J.A.M Vermaseren, NIKHEF Amsterdam preprint 84-2 (1984).

[172] R. Odorico, Nucl. Phys. **B172** (1980) 157,
G. Marchesini, B.R. Webber, Nucl. Phys. **B238** (1984) 1.

[173] W. Beenakker, F.A. Berends, W.L. van Neerven, Proceedings of *"Radiative Correction for e^+e^- Collisions"*, Ed. J.H. Kühn, Springer-Verlag, Heidelberg 1989, p.3.

[174] T. Munehisa, J. Fujimoto, Y. Kurihara, Y. Shimizu, Prog. Theor. Phys. **95** (1996) 375.

[175] J. Fujimoto, Y. Shimizu, T. Munehisa, Prog. Theor. Phys. **91** (1994) 333,
K. Tobimatu, in preparation.

[176] T. Ishikawa, T. Kaneko, K. Kato, S. Kawabata, Y. Shimizu and H. Tanaka, KEK Report 92-19, 1993, The GRACE manual Ver. 1.0
and see also H. Tanaka, Comput. Phys. Commun. **58** (1990) 153
H. Tanaka, T. Kaneko and Y. Shimizu, Comput. Phys. Commun. **64**(1991) 149.

[177] S. Kawabata, Comp. Phys. Commun. **41** (1986) 127; *ibid.,* **88** (1995) 309.

[178] J. Fujimoto, M. Igarashi, N. Nakazawa, Y. Shimizu, K. Tobimatsu, Prog. Theor. Phys. Suppl. No.100 (1990), 1. Formulae used in the present work are given in Chapter 11.